

UC San Diego

UC San Diego Electronic Theses and Dissertations

Title

Simulated diurnal rainfall physics in a multi-scale global climate model with embedded explicit convection

Permalink

<https://escholarship.org/uc/item/1067h3fc>

Author

Pritchard, Michael Stephen

Publication Date

2011

Peer reviewed|Thesis/dissertation

UNIVERSITY OF CALIFORNIA, SAN DIEGO

**Simulated diurnal rainfall physics in a multi-scale global climate model
with embedded explicit convection**

A dissertation submitted in partial satisfaction of the
requirements for the degree
Doctor of Philosophy

in

Oceanography

by

Michael S. Pritchard

Committee in charge:

Richard Somerville, Chair
Joel Norris, Co-Chair
John Helly
Lynn Russell
Jeff Severinghaus
Guang Zhang
Joanna McKittrick

2011

Copyright
Michael S. Pritchard, 2011
All rights reserved.

The dissertation of Michael S. Pritchard is approved, and it is acceptable in quality and form for publication on microfilm:

Co-Chair

Chair

University of California, San Diego

2011

DEDICATION

This dissertation is dedicated to my beautiful, brilliant wife, and
offered in memory of John O. Roads.

EPIGRAPH

*Diurnal rainfall variability is not a simple process
and defies simple explanations.*
— Yang and Smith (2006)

TABLE OF CONTENTS

	Signature Page	iii
	Dedication	iv
	Epigraph	v
	Table of Contents	vi
	List of Figures	viii
	Acknowledgements	xxii
	Vita and Publications	xxiii
	Abstract	xxiv
Chapter 1	Overview	1
Chapter 2	Literature Review	4
	2.1 The diurnal rainfall cycle	4
	2.1.1 Global observations	4
	2.1.2 Physical mechanisms	15
	2.1.3 Central US nocturnal rainfall	23
	2.1.4 A controversial aspect of Central US nocturnal rainfall	40
	2.2 Distortions of diurnal rainfall in global climate models . .	42
	2.2.1 An integrative constraint on global model physics	43
	2.2.2 The Arakawa-Schubert cumulus parameterization	45
	2.2.3 Distortions of the diurnal rainfall mode in the Community Atmosphere Model	52
	2.3 Next generation multi-scale climate modeling	58
	2.3.1 Concept	59
	2.3.2 History	61
	2.3.3 SP-CAM's simulated climate	70
	2.3.4 SP-CAM's diurnal rainfall cycle	77

Chapter 3	Statement of the problems addressed	84
	3.1 Optimally evaluating the effect of super-parameterization on the simulated global diurnal rainfall cycle.	86
	3.2 Non-local control of the marine diurnal rainfall cycle by land	89
	3.3 Evidence for slow-manifold control of the Central US nocturnal rainfall maximum	91
Chapter 4	Evaluating the effect of super-parameterization on the simulated global diurnal rainfall cycle.	95
	4.1 Empirical orthogonal function analysis of diurnal rainfall	97
	4.2 Holistic diurnal rainfall diagnostics	108
	4.3 Conclusions	135
Chapter 5	Non-local control of the marine diurnal rainfall cycle by land	143
	5.1 Climate model representation of tropical diurnal subsidence waves	144
	5.2 Effects of super-parameterization on the tropical ocean diurnal water budget	151
	5.3 A model-informed explanation for the Gulf Stream diurnal rainfall pattern	156
Chapter 6	Evidence for slow-manifold control of the Central US nocturnal rainfall maximum	173
	6.1 Models, observations and simulation design	176
	6.2 Propagating diurnal convection	177
	6.3 Regional flows, thermodynamics, and synoptics	181
	6.4 Genesis and multi-scale structure of a propagating event	192
	6.5 Discussion	196
	6.6 Conclusion	208
Chapter 7	Summary	212
Appendix A	Model nomenclature	216

LIST OF FIGURES

Figure 2.1:	Local solar time $T_{max}(h)$ when the diurnal harmonic ($S1$) of (left) DJF and (right) JJA mean frequency of occurrence peaks for nondrizzle precipitation gauge data from 1976-1997. Adapted from Figure 5 of Dai (2001).	6
Figure 2.2:	Percentage of the mean daily variance explained by the (left) diurnal and (right) semidiurnal harmonics for JJA mean frequency occurrence for nondrizzle precipitation gauge data. Values over 50% and 30% are hatched in the left and right columns, respectively. Adapted from Figure 4 of Dai (2001).	6
Figure 2.3:	Representative distribution of rain gauge data. Reproduced from Figure 1 of Kidd (2001).	7
Figure 2.4:	Fitted boreal summer (JJA) composite diurnal precipitation harmonic a) amplitude and b) phase, as inferred from two decades of infrared cloud top temperature retrievals. Adapted from Figures 2 and 3 of Yang and Slingo (2001).	9
Figure 2.5:	Peak local time of maximum rain rate derived from Tropical Rainfall Measuring Mission precipitation radar (upper) and total microwave imager (middle), and peak local time of minimum brightness temperature at 10.8 microns (lower) for JJA 1998–2003. The pixels where rain rate (infrared brightness temperature) within 1 hour of the local time of maximum rain rate (minimum brightness temperature) are above (below) mean rain rate (brightness temperature) for radar and microwave (infrared) data, where rain frequency is more than 1%, and where the rain rate is more than 10 mm mon ⁻¹ (the mean brightness temperature is less than 280 K) are colored. Reproduced from Figure 1 of Yamamoto et al. (2008).	13
Figure 2.6:	Combined microwave precipitation estimate for the 3-h period centered at 0000 UTC 25 May 2004 in mm/hr. Blacked-out areas denote regions that lack reliable estimates, while the zero values in the remaining areas are color-coded to depict the coverage by the various sensors. The order of precedence for display and corresponding zero color are TMI (white), SSM/I (light gray), AMSR-E (medium gray), and AMSU-B (dark gray). Reproduced from Figure 1 of Huffman et al. (2007).	14

Figure 2.7:	“Normalized amplitude and phase of the diurnal cycle in the total frequency of precipitation, including trace events for the summer season (June-August [1951-1960])” from rain gauge station data. The number of barbs denotes the amplitude of the 24-hour harmonic, and the phase is indicated by the orientation of the arrows. “An arrow pointing from the north indicates a midnight maximum (local time); one pointing from the east indicates a 0600 maximum, etc.”. The Central US nocturnal maximum is evident as a region of anomalously high amplitude, with arrows directed from the north. Reproduced from Wallace (1975).	24
Figure 2.8:	Relationship among mesoscale convective complex (MCC) population centers, elevated terrain, and prevailing flow, showing the Central US hotspot of organized convection activity as part of a more general phenomenon. Reproduced from Laing and Fritsch (1997) (their Figure 4).	26
Figure 2.9:	“Diurnal radar echo frequency of occurrence, in JJA, expressed as percent of days within a given hour that precipitation echo is present: (a) 2100, (b) 0200, (c) 0700, and (d) 1300 UTC. Readers are referred to the supplementary animation, which provides a superior visualization of the continental diurnal cycle (online at http://dx.doi.org/10.1175/2008JCLI2275.s1).” Reproduced from Carbone and Tuttle (2008)	27
Figure 2.10:	(Left) West to east cross section of mesoscale height (solid lines, in m) and zonal wind (dashed lines, in m/s) perturbations at the time of the MCC. (Right) West to east cross section of mesoscale temperature (dashed lines in ° C) and moisture (solid lines, in g/kg) perturbations at the time of the MCC. Reproduced from Maddox (1981); Tripoli and Cotton (1989b).	30
Figure 2.11:	“(a) Idealized profiles of net heating associated with convective and stratiform precipitation in a mesoscale convective system. The x axis is nondimensional until precipitation amounts are specified for the convective and stratiform regions. (b) Profiles of net heating by a mesoscale convective system with different fractions of stratiform precipitation. Adapted from Schumacher et al. (2004).” Reproduced from Houze (2004).	32

Figure 2.12: “Schematic diagram showing the airflow relative to a two-dimensional, steady state mesoscale convective system in a large-scale environment of given wind shear. The environmental air entering the updraft is potentially unstable, and there is a pressure decrease across the system from right to left at middle levels. The streamlines are those required by conservation of mass, momentum, entropy, and vorticity. Adapted from Moncrieff (1992).” Reproduced from Houze (2004).	33
Figure 2.13: “Postulated structure of potential vorticity anomalies produced by a region of convection and the associated changes in temperature and wind structure. The circulation is cyclonic around the lower, positive anomaly, and anticyclonic around the upper anomaly as shown by the arrows.” Reproduced from Raymond and Jiang (1990).	35
Figure 2.14: “Schematic illustration of the [height-longitude] structure of the idealized Rocky Mountain-Great Plains daytime circulation.” Reproduced from Cotton and Anthes (1989) (their Figure 9.39). Originally from Dirks (1969).	37
Figure 2.15: Conceptual schematic of major physical processes involved in the 2D structure of an idealized mountain-plains solenoidal circulation in the lee of the Rockies. Reproduced from Wolyn and McKee (1994) (their Figure 12).	37
Figure 2.16: “A schematic diagram showing interactions between resolved processes in a model and (the unresolved component of) moist convection. The formulation of the right half of the loop represents the cumulus parameterization problem.” Reproduced from Arakawa (2004) (Figure 3a).	47
Figure 2.17: Conceptual schematic of the assumed geometry of hot towers in Arakawa-Schubert-type moist convection parameterizations. Reproduced from Arakawa and Schubert (1974) (their Figure 1).	48
Figure 2.18: Representative example of the stability adjustment incurred on a forecast or climate model due to the influence of an Arakawa-Schubert type convection parameterization. Reproduced from (UCAR, 2009).	50

Figure 2.19: “(left) The [local solar time (hours)] of the [maximum] of the [fitted 24-hour] harmonic of .. observed ... JJA ... total precipitation. (right) Same as (left) but for [Community Climate System Model v.2]-simulated ... total precipitation.” Reproduced from Dai and Trenberth (2004) Figure 12.	53
Figure 2.20: The composite 1984 JJA diurnal rainfall cycle a) time of maximum rainfall (local hour), and b) amplitude (mm/day), as simulated by (bottom) CAM3.0 and (top) CAM3.5 (which added an entrainment dilution assumption to the Arakawa-Schubert cumulus closure scheme). c) The simulated diurnal rainfall cycle in CAM3.0 (red line) over two regional diurnal amplitude hot spots, compared against two modern climatological observational products - a microwave rainfall product (TMI; blue lines) and a merged multi-satellite product (3B42 TRMM; black line). Adapted from Neale (2007).	54
Figure 2.21: Height-dependent relative frequency of occurrence (colors, percentage) of a deep heavily precipitating objective statistical cluster regime of convection comparing (a) joint spaceborne lidar and radar measurements against (b,c) two current versions of the Community Atmosphere Model run through instrument simulators. The higher frequency of occurrence of this regime overall in the models (33% and 27%) compared to observations (13%), and especially at high reflectivity values, is statistical evidence that CAM rains too intensely, too frequently. Adapted from (Zhang et al., 2010) (their Figures 3, 5 and 7).	55
Figure 2.22: “Schematic view of the diurnal cycle of [continental locally forced] precipitating convection, as simulated by [an ensemble of 2D cloud resolving models] and several [GCMs run in single column model mode]. The boundary layer convection (thermals) is represented by the dotted curves on both schemes, as it partly relies on the turbulence in the CRMs with a two-kilometer horizontal resolution”. Reproduced from Guichard et al. (2004). . .	57

Figure 2.23: Schematic showing the typical configuration of the two resolved scales in the superparameterization approach to representing clouds in climate models. The outer box represents a single grid column of the host exterior model. The inner boxes represent the interior grid points of the embedded explicit convection model, arranged conventionally in two dimensions, and with a “cloud system resolving model” (CSRМ) horizontal resolution of several kilometers. The lateral boundaries of the interior model are periodic. Reproduced from (Ovtchinnikov et al., 2006) (their Figure 1).	59
Figure 2.24: “Hovmöller ([longitude-time]) diagrams of the [north-south] averaged surface precipitation rate from (a) the experiment using [the cloud super-parameterization] approach and b) the experiment using the 3D cloud resolving model. Precipitation intensity larger than 0.2 and 1 mm/h is shown using light and dark shading, respectively”. Reproduced from Grabowski and Smolarkiewicz (1999) Figure 3.	62
Figure 2.25: Climatological JJA precipitation simulated in response to prescribed sea surface temperatures by a) conventional CAM3.0, b) SP-CAM3.0 with a 2D zonally oriented CRM, showing the simulated “Great Red Spot” precipitation bias in the white box, compared to c) observations and d)-e) SP-CAM3.0 with a 3D embedded CRM d) without versus e) with interactive momentum coupling across the two resolved scales. Adapted from Khairoutdinov et al. (2005) (their Figures 3 and 16).	68
Figure 2.26: Number of hits from peer reviewed articles or conference papers containing the word “superparameterization”, by year, as indicated by a Google Scholar search initiated on June 1, 2011	69
Figure 2.27: “... daily mean rainfall rate distributions for GPCP [observations] (green), CAM (blue), and MMF (red) [showing rainfall rate expressed as a] contribution to seasonal rainfall total as a function of rainfall rate” for a) the Amazon Basin, b) the Central United States and c) the Western Pacific. The embedded explicit convection approach to climate simulation tends to improve the intermittency and intensity statistics of rainfall. Adapted from DeMott et al. (2007) (their Figures 2-4).	71

Figure 2.28: “The symmetric raw spectral power divided over the background power (signal-to-noise ratio spectrum) for the ... [outgoing longwave radiation (OLR)] ... as (left) simulated by [SP-CAM3.0], (middle) derived from observations, and (right) simulated by [CAM3.0]. Superimposed are the theoretical shallow-water dispersion curves for the equatorial Rossby and Kelvin waves for the equivalent depths of 12, 25, and 50 m. Contour interval is 0.1, with contours beginning at 1. Observations are 1979–2004 NOAA Advanced Very High Resolution Radiometer-interpolated OLR data (Liebmann and Smith, 1996)”. SP-CAM3.0 was integrated from 1986-2003 and configured with 30 vertical levels, a spectral semi-Lagrangian dynamical core (T42 truncation) with a 30-minute timestep in the external resolved scale, and 32 interior grid CSRM columns arranged in a meridional 2D periodic array with a 20 s timestep. Reproduced from (Khairoutdinov et al., 2008) (their Figures 8 and 9) 72

Figure 2.29: “Frequency distributions of in-cloud [cloud water content (CWC)] at Manus from (a) ARM retrievals, (b) CAM model, [and] (c) [SP-CAM3.0] model. The shading represents the percentage of radar retrievals or model gridboxes at each level that fall within the given CWC bin. The frequency distributions are normalized such that the sum of each level is 100%. Clear layers are included in the normalization although not shown in the plot. The median CWC of the cloudy points at each level is also indicated by the solid lines. The dashed line in (b) represents the median of the grid-box average CWC in the CAM. The ARM median CWC is also [super-imposed on the model plots] for comparison purposes”. Adapted from McFarlane et al. (2007) (their Figure 4). 74

Figure 2.30: “Intensity plots of seasonal zonal profiles of radar hydrometeor fraction (dBZe > -27.5) [showing a) CloudSat observations, b) SP-CAM] ... simulated radar output, and [c) the] difference (model simulation - observation). Vertical axis is height above mean sea level (in km), and horizontal axis is latitude. Cloud-Sat is a near-nadir-pointing instrument and so does not obtain full pole-to-pole coverage. The radar also suffers from ground clutter effects and is unable to detect most cloud with in 1.2 km of the surface... Missing detections near the surface due to surface clutter are accounted for in the radar simulation process.” Adapted from Marchand et al. (2009b) Figure 1.	75
Figure 2.31: “JJA geographical distribution of (left) the local time of non-drizzle precipitation frequency maximum and (right) the percent of days with nondrizzle precipitation, as simulated with (upper) the standard CAM, (middle) SP-CAM, and (lower) from the dataset by Dai (2001)”. This is the first evidence that super-parameterization improves the simulated diurnal rainfall cycle over land. Reproduced from Khairoutdinov et al. (2005) Figure 13.	78
Figure 2.32: “Diurnal composite of net all-sky minus clear-sky heating rate at Manus for (a) ARM, (b) MMF (with precipitation), (c) [SP-CAM3.0] (without precipitation) and (d) [CAM3.0].” The blue feature near 15 km in SP-CAM is associated with intermittent nocturnal cirrus longwave cooling, an important dynamical ingredient to the tropical diurnal cycle that is absent in conventional CAM. Despite being exaggerated in SP-CAM (due to overly frequent simulated tropical deep convection) the existence of a nocturnal cirrus cooling feature is an improvement in simulated tropical diurnal cycle dynamics. Reproduced from McFarlane et al. (2007) Figure 22.	79
Figure 4.1: (Left panel) Eigenvalue spectrum for the composite JJA diurnal cycle of precipitation as simulated by CAM and MMF, and as observed in TRMM 3B42. (Right panels) Normalized histograms of the percent variance attributable in the 2000-member bootstrapping ensemble of EOF calculations, for each model; error bars in the eigenvalue spectrum are computed from these distributions.	103

Figure 4.2:	(a) Principle component (PC) time series of the leading EOF of the composite boreal summer diurnal cycle of precipitation as simulated by CAM (red) and MMF (blue), compared to TRMM observations (black). Solid lines and shading denote the mean \pm one standard deviation of a 2000 member ensemble of randomly undersampled bootstrap EOF calculations. (b)-(d) Ensemble mean spatial projection of EOF ₁ for (b) TRMM data, (c) the MMF, and (d) CAM.	104
Figure 4.3:	As in Figure 4.2, but for EOF ₂	106
Figure 4.4:	JJA (left) and DJF (right) precipitation for (top) one year simulation of SP-CAM3.0, compared to (middle) 7 years of a merged multi-satellite, multi-instrument observational product (TRMM 3B42) and (bottom) CAM3.0. The contouring interval is 1 mm/day for precipitation rates below 3 mm/day (unshaded contours) and 3 mm/day for precipitation rates greater than or equal to 3 mm/day (shaded contours). Root-mean-squared difference and pattern correlation coefficient relative to the observations are shown for the two models.	112
Figure 4.5:	Amplitude of (color hue; mm/day), and variance attributable to (color saturation; fraction) the least squared fitted 24-hour harmonic of precipitation for (top) the SP-CAM, (middle) satellite observations and (bottom) standard CAM, during (left) JJA and (right) DJF. RMS difference and pattern correlation relative to the observations are shown for the two models.	116
Figure 4.6:	As in Figure 4.5, but for the phase, or peak timing (color hue; local hour) of the fitted 24-hour sinusoid of precipitation.	117
Figure 4.7:	CT08 metric of the broadness of the composite day's precipitation peak (color hue) for (top) the SP-CAM, (middle) satellite observations and (bottom) standard CAM, during (left) JJA and (right) DJF. For the two models, the absolute bias in the time of peak precipitation (color saturation) is also shown. The CT08 broadness quantity is the number of hours that must be marched forward and backward from the time of maximum precipitation in order to encompass 68 % of the total area under the mean summer day precipitation time series. Cool color hues correspond to regions with tightly peaked diurnal cycles, and warm hues correspond to broad or multiply peaked composite diurnal variability.	119

Figure 4.8:	(Left) CT08 metric of the broadness of the mean JJA day's maximum precipitation, shown in a zonal transect domain of interest over the US eastern seaboard and Gulf Stream, comparing the model simulations and the satellite observations, bin-averaged to the model grid. The along-transect structure of the time evolution in the cross-track-averaged mean summer day is shown for comparison to the right.	122
Figure 4.9:	As in Figure 4.8, but for a DJF zonal transect straddling equatorial South America.	123
Figure 4.10:	As in Figure 4.9, but for a DJF meridional transect straddling equatorial Africa.	124
Figure 4.11:	Evolution of the composite JJA day's precipitation over North America, comparing the two climate models against the satellite observations. Snapshots of the 3-hourly average precipitation rate are shown. Local solar time at the longitude axis limits is superimposed at the bottom of each subpanel in text. Note the model-observation-model comparison shown here is more intuitively absorbed in animation format; viewing the auxilliary animation file is recommended.	127
Figure 4.12:	Height-longitude section contrasting the diurnal chronology of convective heating and convective moistening in the SP-CAM and the CAM, along a zonal transect straddling the Gulf Stream and eastern United States (Transect 1 in Figure 4.7). The quantities shown are tendencies exerted by convection in the physics package, i.e. by nudging towards the nested CRM in the SP-CAM and as diagnosed by conventional parameterization in CAM. The vertical coordinate is normalized pressure ($\sigma = p/1000$ hPa), and the land component at the western edge of the transect is identifiable as a blanked out region at the base of the domain. This is easiest viewed in the auxiliary animation file, Video S2 [CONVTEND.MOV].	132
Figure 4.13:	Amplitude of the fitted 24-hour diurnal harmonic of JJA composite rainfall in a) observations compared to b)-h) an ensemble of conventional and superparameterized global climate model simulations in various configurations. See text for details. . . .	139
Figure 4.14:	As in Figure 4.13 but for the phase (local time of maximum rainfall) of the 24-hour rainfall harmonic.	140

Figure 5.1:	“Diurnal amplitude (a), and local time of maximum diurnal surface divergence (b) for April-September 2003 from the tandem SeaWinds data (left panels).” Reproduced from Wood et al. (2009) Figure 1.	145
Figure 5.2:	(Left) simulated JJA vs. (right) observed MJJAS composite diurnal cycle of surface divergence, contrasting an ensemble of coarse resolution climate models. The observational panel is reproduced from Wood et al. (2009).	147
Figure 5.3:	As in Figure 5.2 but for the phase of the fitted 24-hour harmonic.	148
Figure 5.4:	As in Figure 5.2 but for the amplitude of the fitted 24-hour harmonic.	150
Figure 5.5:	Composite DJF diurnal cycle of all components of the vertically integrated moisture budget, averaged over ocean points only within a latitude band from 10 S to 10 N, comparing (left) CAM3.0 to (right) SPCAM3.0.	153
Figure 5.6:	As in Figure 5.5 but unfolding the zonal variability in the composite budget, and including land points. Each descending subplot shows the local time - longitude structure for each of the four terms in the water budget, comparing (left) CAM3.0 and (right) SPCAM3.0. The composite diurnal cycle is repeated twice for clarity.	154
Figure 5.7:	a) JJA mean 2000-2006 rainfall rate from the TRMM 3B42 observations bin averaged to a 1.9×2.5 model grid, defining coastal land and Gulf stream regions of interest (grid points marked ‘O’ and ‘X’, respectively). b) Horizontally averaged composite rainfall cycle in the Gulf stream region. c) As in b) but retaining the zonal variability in the composite and focusing only on the nocturnal (rainiest) times. The dashed line corresponds to constant local solar time.	158
Figure 5.8:	Multi-model comparison of the observed (solid black line) and simulated (colored lines) horizontal mean Gulf Stream JJA composite diurnal rainfall variability in the transect defined in Figure 5.7a, for an ensemble of models that treat sub-grid convection differently.	160
Figure 5.9:	As in 5.8 but showing the zonal structure of the a) observed versus b)-f) simulated diurnal anomalous rainfall.	160

Figure 5.10: The simulated Gulf Stream diurnal cycle of JJA precipitation (blue line), expressed as a sink to the column water budget, compared to two balancing source terms, latent fluxes (black line) and vertically integrated moisture convergence (red line). The dashed red line shows the effect of diurnal wind variations on the vertically integrated moisture convergence (see text for details). The only model that does not simulate realistic Gulf Stream rainfall a) has a dominant balance between precipitation and latent heat fluxes whereas the other models b)-f) suggest diurnal variations of moisture convergence play an important role in balancing the Gulf Stream rainfall cycle.	162
Figure 5.11: Height-time section unfolding the vertical structure of the diurnal moisture convergence column water budget term (red line in Figure 5.10) expressed as a layer mass-weighted contribution to the total column tendency.	164
Figure 5.12: Amplitude of the fitted JJA composite 24-hour diurnal harmonic of (left) zonal versus (right) meridional wind on the lowest model level, for the ensemble of climate models in Appendix A.	165
Figure 5.13: As in Figure 5.13, but for the phase (local time of maximum diurnal anomaly).	167
Figure 5.14: Comparison of the (a) coastal land versus (b) Gulf Stream horizontal average column (dashed lines) radiative heating, (dotted lines) convective heating and (solid lines) their sum. The right panel c) shows that the land-ocean contrast in radiative heating (dashed lines) is amplified by the convective heating (solid lines; radiative plus convective heating).	168
Figure 5.15: Pressure-time sections comparing the structure of the simulated composite diurnal cycle of convective heating over the coastal land horizontal averaging region (gridpoints marked ‘o’ in Figure 5.7a).	169

Figure 6.1:	Reduced transect comparison of the time-longitude structure of warm season diurnal convective activity in the lee of the Rocky Mountains between 35-45N a) as observed in 2005 from spaceborne infrared imagers, and b) as diagnosed from the total physics package temperature tendency averaged between 350 hPa and 750 hPa in the free-running CAM3.5 and c) SP-CAM3.5 simulations.	178
Figure 6.2:	Time-longitude section showing the standard deviation across tropospheric model levels of the physics package temperature tendency (a storm location proxy) and fitted zonal phase speed (overlain line) for 12 of 13 propagating convective events simulated by SP-CAM3.5 in the lee of the Rockies.	180
Figure 6.3:	Histograms across the ensemble of simulated propagating convection events showing a.) the distribution of c_x , the fitted zonal phase speed from Figure 6.2, b.) the implied storm propagation speed relative to the mean mass-weighted background flow, $c_x - \bar{u}$, and c.) the implied storm steering level.	182
Figure 6.4:	JJA climatological precipitable water anomaly at 0000 UTC (shading; mm) for the single-season a) SP-CAM3.5 and b.) CAM3.5 simulations, relative to the Rapid Update Cycle 2003 analysis (contours; interval of 5 mm)	184
Figure 6.5:	3-hour average vertical pressure velocity centered at (left) 22Z and (right) 8Z comparing the upward branch of the Central US solenoidal diurnal mountain-plains circulation in (top) the Rapid Update Cycle analysis during JJA 2003, to JJA averages of the single-season (middle) SP-CAM3.5 and (bottom) CAM3.5 simulations. Local time of day is depicted on 24-hour clock icons.	185
Figure 6.6:	Pressure-longitude section showing JJA climatological static stability ($\partial\theta/\partial z$) averaged from 35-45N in the lee of the Rockies for a) CAM3.5, b.) SP-CAM3.5 and c.) a year of ECMWF interim reanalysis. Surface topography is shown in black.	187
Figure 6.7:	Maps over the central United States comparing the nocturnal evolution of the 850 hPa vapor transport (vector field; $q\mathbf{V}_H$) showing the Great Plains Low Level Jet (LLJ) and its associated moisture convergence (shading; $\nabla \cdot (q\mathbf{V}_H)$) in (top) the 2003 Rapid Update Cycle analysis, compared to global simulations using (middle) CAM3.5 and (bottom) SP-CAM3.5.	188

Figure 6.8: As in Figure 6.7 but showing the diurnal anomaly of low-level wind shear magnitude (700 hPa minus 950 hPa) associated with the Great Plains Low Level Jet (LLJ) in (top) the 2003 Rapid Update Cycle analysis, (middle) CAM3.5 and (bottom) SP-CAM3.5.	190
Figure 6.9: Composite anomaly maps over the central US showing the deviation of surface pressure (shading; hPa), positive column water vapor mass anomalies (contour interval of 4 g/m ²) and column water vapor transport (vector field) during 12 propagating convection events in SP-CAM3.5, relative to its simulated seasonal JJA climatology.	191
Figure 6.10: SP-CAM3.5 500 hPa geopotential height (km) showing the synoptic state during a simulated 3-day packet of consecutive diurnal orogenic convection propagation.	193
Figure 6.11: Height-longitude structure at 40 N showing the time evolution of (left) zonal and (right) meridional wind during Event A. Condensate concentration contours are superimposed for values of (0.005, 0.01, 0.1, 1) g/kg.	194
Figure 6.12: As in Figure 6.11, but for (left) vertical pressure velocity and (right) $d\theta/dz$	195
Figure 6.13: Time-longitude matrix of height-longitude sections showing snapshots of condensate within adjacent cloud resolving models at 40N in SP-CAM3.5 during a simulated organized propagation episode, at five hour intervals from top to bottom. Shaded transparent contours outline the 0.01 g/kg threshold for non-precipitating cloud water (red; QC), non-precipitating cloud ice (yellow; QI), precipitating cloud water (blue; QPC) and precipitating cloud ice (green; QPI) within the embedded explicit convection model subdomains shown above. Surface orography is shown in black.	197
Figure 6.14: Pressure-longitude sections at 2am local time, showing storm-relative zonal flow (solid streamlines) atop the convective heating structure (temperature tendency due to the embedded CRM; thin contours at 10 K/day increments, negative contours dotted; light shading for $\partial T/\partial t > +15$ K/day, dark shading for $\partial T/\partial t < -15$ K/day) for 12 separate instances of MCS propagation in the lee of the Rockies in SP-CAM3.5.	199

Figure 6.15: Conceptual schematic illustrating how multi-grid propagation of convective signals can occur across the two resolved scales, (top) interior Cloud Resolving Model (CRM) and (bottom) exterior Large Scale (LS), contained in SP-CAM3.5. A sequence of events is shown at adjacent LS grid columns x_1 (left) and x_2 (right), straddling the transition from (above dashed line) LS timestep t_1 to the subsequent LS timestep t_2 . Since the CRMs are laterally periodic, convective propagation can only occur as mediated by the LS model. 202

Figure 6.16: Schematic illustrating how the scale interface in (top) GCMs is re-engineered in (bottom) the Multi-scale Modeling Framework (MMF) approach to global climate modeling. Light grey arrows define the code flow, and the vertical dashed line separates the resolved and sub-grid scales. In the MMF approach, “memory” at the inner resolved scale plays a role in the sub-grid response to large-scale forcing. 204

Figure 6.17: a) A snapshot showing the horizontal extent of the 400 hPa SP-CAM3.5 heating signature during a nocturnal propagating convective event on its $1.9^\circ \times 2.5^\circ$ finite volume horizontal grid. b) Diffuse representation of the same field after spectral horizontal interpolation to triangular truncation at T85. 207

ACKNOWLEDGEMENTS

This work has been enabled by funding from the Center for Multiscale Modeling of Atmospheric Processes (CMMAP), a multi-institutional National Science Foundation (NSF) science and technology center based at Colorado State University, funding from the Department of Energy, and supercomputer support from the NSF distributed network of Teragrid resources.

Section 4.1, in part, is a reprint of material as it appears in Empirical orthogonal function analysis of the diurnal cycle precipitation in a multi-scale climate model 2009. Pritchard, Michael S., Somerville, R. C. J., *Geophysical Research Letters*, 35 (5), L05812. The dissertation author was the primary investigator and author of this paper.

Section 4.2, in part, is a reprint of material as it appears in Assessing the diurnal cycle or precipitation in a multi-scale climate model 2009. Pritchard, Michael S., Somerville, R. C. J., *Journal of Advances in Modeling Earth Systems*, Vol. 1, Article No. 16, 2009. The dissertation author was the primary investigator and author of this paper.

Chapter 6, in part, is a reprint of material as it appears in Orographic propagating precipitation systems over the US in a global climate model with embedded explicit convection 2011. Pritchard, Michael S., Moncrieff, M. W. and Somerville, R. C. J., *Journal of the Atmospheric Sciences*, in press. The dissertation author was the primary investigator and author of this paper.

VITA

- 2004 B. Sc. in Physics and Mathematics, University of Toronto, Toronto, Canada
- 2006 M. Sc. in Earth Science, University of Alberta, Edmonton, Canada
- 2011 Ph. D. in Oceanography, University of California, San Diego

PUBLICATIONS

Pritchard, M. S., M. W. Moncrieff and R. C. J. Somerville. Orographic propagating precipitation systems over the US in a global climate model with embedded explicit convection. *Journal of the Atmospheric Sciences*, 68, 1821-1840, 2011.

Pritchard, M. S. and R. C. J. Somerville. Assessing the diurnal cycle of precipitation in a multi-scale climate model. *Journal of Advances in Modeling Earth Systems*, 1, Art. No. 12, 2009.

Pritchard, M. S. and R. C. J. Somerville. Empirical orthogonal function analysis of the diurnal cycle of precipitation in a multi-scale climate model. *Geophysical Research Letters*, 36 (5), L05812, 2009.

Pritchard, M. S., A. B. G. Bush and S. J. Marshall. Interannual atmospheric variability affects continental ice sheet simulations on millennial time scales. *Journal of Climate*, 21 (22), 5976-5992, 2008.

Pendlebury, D., T. G. Shepherd, M. S. Pritchard, and C. McLandress. Normal mode Rossby waves and their effects on chemical composition in the late summer stratosphere. *Atmospheric Chemistry and Physics* 8(7), 1925-1935, 2008.

Pritchard, M. S., A. B. G. Bush and S. J. Marshall. Neglecting ice-atmosphere interactions underestimates ice sheet melt in millennial-scale deglaciation simulations. *Geophysical Research Letters*, 35 (1), L01503, 2008.

ABSTRACT OF THE DISSERTATION

**Simulated diurnal rainfall physics in a multi-scale global climate model
with embedded explicit convection**

by

Michael S. Pritchard

Doctor of Philosophy in Oceanography

University of California San Diego, 2011

Richard Somerville, Chair

Joel Norris, Co-Chair

It is well known that the statistical methods (“parameterizations”) used to represent cloud processes for climate prediction distort the simulated diurnal rainfall cycle. In this study, the “superparameterization” technique (embedding explicit models of convection) is investigated as a method of improving diurnal rainfall in order to study the mechanisms supporting it and to reduce uncertainties in climate prediction.

Analysis of the effect of superparameterization on the simulated global diurnal rainfall cycle uncovers several unappreciated benefits of the technique: Diurnal rainfall becomes less well fit by a 24-hour sinusoid, more horizontally inhomogeneous within continents and oceans, and conforms better to transitions straddling coastlines. While these effects are robust to arbitrary configuration choices in the application of superparameterization, a favorable shift in the peak timing of continental rainfall is not. Regional deficiencies are documented associated with the Andean topography, and the Asian monsoon.

Like conventional parameterizations that account for dilution, superparameterization favorably reduces the amplitude of the tropical land latent heating diurnal cycle. This removes an unrealistic deep barotropic subsidence wave that otherwise exerts undue remote control by land on the simulated diurnal cycle over the tropical ocean. The level of remote control of marine surface divergence is otherwise found to be undersimulated such that the tropical surface divergence signature of land-sea remote control does not validate well against scatterometer observations.

Over the Gulf Stream, the pattern of warm season diurnal rainfall variability is captured in several simulations. Analysis suggests a giant sea breeze circulation fueled by convectively amplified cross-coastal radiative imbalances, may help explain the observed change in local rainfall timing with distance offshore.

In the Central US warm season, the superparameterization approach is shown to capture packets of eastward traveling organized convection that underly a regional nocturnal convection maximum. The simulated rate and range of eastward travel validates against ground based radar data despite the fact that small scale storm propagation mechanisms (gust fronts and density currents) are artificially restricted to have only local effects under superparameterization. This is interpreted as evidence in support of an alternative “slow manifold” view that these systems are primarily propagated by large-scale dynamics.

Chapter 1

Overview

This dissertation is situated in the context of a broad problem facing the climate science community – the fact that cloud processes are not well represented in the numerical tools that are used to project future climate change. As a consequence, important questions facing society, like “are cloud feedbacks likely to amplify or damp global warming?” or “how should farmers expect precipitation to change in future climate?” cannot yet be reliably answered by climate science.

One striking symptom of this unsatisfactory state of affairs is an unrealistic distortion of simulated *diurnal rainfall* in conventional global climate models (GCMs). The diurnal rainfall cycle is one of the most simply forced modes of convective variability in the atmosphere, and capturing it is a zero-order litmus test for the fidelity of simulated cloud-atmosphere interactions.

As supercomputing capacity grows, new atmospheric simulation technologies are being developed that offer hope for improvement. However the optimal tool - a fully global cloud resolving model - is currently far too computationally expensive to apply to the problem of long term global climate projection, and is expected to remain so for decades (Khairoutdinov and Randall, 2003).

This dissertation focuses on an interim prototype tool (“superparameterized”

climate simulation) that has emerged this decade, which retains some of the benefits of resolving convection explicitly while making unique tradeoffs to remain computationally affordable for the problem of long-term global climate projection. Unlike conventional GCMs, which represent cloud processes using simple statistical models that distort certain modes of atmospheric variability, superparameterized climate simulations (also called Multiscale Modeling Frameworks; MMFs) use thousands of embedded cloud-resolving models (CRMs)¹. Little is known about the prototype MMF approach to climate modeling, which introduces substantial physical idealizations of its own.

In this dissertation, analysis of the diurnal rainfall mode in superparameterized simulations serves two scientific purposes.

The first is to contribute to the community assessment of the potential that this new technology may offer for improving the representation of cloud physics for the problem of future climate projection. In this context, the fact that the diurnal rainfall mode is the most simply forced convective regime in the atmosphere, and that a rich history of literature exists explaining its physics in many parts of the world, is useful.

The second purpose is to seek new insight into the mechanisms that support diurnal rainfall in nature, in two regions of interest where superparameterized simulations offer a useful vantage point:

1. **Over the ocean:** Here, trustworthy satellite constraints on the space-time structure of rainfall have only recently provided adequate sampling of diurnal rainfall. The physical mechanisms behind the observed pattern – which

¹Also, unlike continuously explicit convection resolving models, MMFs can be run on global domains and integrated for multiple decades with existing computers.

involve large scale circulations set up by convective heating over land – are not completely understood. This is also not well suited to analysis with ultra-high resolution models, for which representing large horizontal scales for multi-month integrations remains a computational challenge. Since superparameterized simulations permit the representation of large horizontal scales without requiring a statistical treatment of convection, they provide a useful perspective from which to investigate these mechanisms numerically.

2. **In the Central US:** In this region, the role of fast- vs. slow-manifold controls on diurnal organized convection is in debate in the current literature. A unique feature of super-parameterized models – artificial restriction of the spatial range over which fast-manifold physics can operate – provides a useful new perspective to this discussion.

The following literature review introduces some relevant background to motivate the three specific problems that are stated in Chapter 3 and addressed in Chapters 4 to 6. Conclusions are summarized in Chapter 7.

Chapter 2

Literature Review

2.1 The diurnal rainfall cycle

2.1.1 Global observations

Since the dawn of the satellite and computer age, the instrumental record of the composite global diurnal rainfall mode has been progressively refined, to a point where today we have good confidence in its structure over most of the world. The inherently patchy record initially provided by in situ surface rain gauges has been augmented with remotely sensed signatures of rainfall, at first from infrared detectors, and now with more accurate microwave sensors. Interdisciplinary work and data sharing for climate science have further led to “best estimate” precipitation products, in which multiple inter-calibrated satellite detectors’ information content have been patched together, and fused with ground based gauge and radar data.

There is a rich scientific history of measuring daily rainfall variations using rain gauges. Wallace (1975) describe early research dating back to the mid-nineteenth century. By the dawn of the twentieth century, the major difference between conti-

mental (afternoon maximum) and marine (nocturnal maximum) diurnal rain cycles was well documented (Hann, 1901). Regions that bucked this general trend were an early scientific curiosity, such as the central US summertime nocturnal rainfall maximum (Kincer, 1916). At the national scale, the development of standardized weather observations during the twentieth century spawned a series of diurnal rainfall studies from countries around the world, summarized in Table 1 of Wallace (1975).

International coordination and systematic digitalization of decades worth of international rain gauge data on land and aboard ships refined the observed composite diurnal rainfall cycle in the 1990s. In landmark studies, Dai et al. (1999) and Dai (2001) analyzed the diurnal and semi-diurnal modes in a large United States dataset (Higgins et al., 1996) and globally, in an international dataset coordinated by the World Meteorological Organization (Woodruff et al., 1993). Their summary of the significance of the diurnal rainfall mode is authoritative:

Except for winter mid- and high-latitudes, diurnal variations in the precipitation and thunderstorm frequencies are significant (especially over land areas and during summer), with diurnal amplitudes generally exceeding 20% of the daily mean values. The diurnal harmonic explains about 40% to 80% of the total daily variance over land areas, while it accounts for about 40 % of the variance over the oceans. The semidiurnal harmonic accounts for about 15%-25% (20%-40%) of the daily variance over land (ocean) areas. [Dai (2001), pp. 1126-1127]

Figure 2.1 shows the global distribution of rainfall timing from the 24-hour diurnal rainfall harmonic from the rain gauge record (Dai, 2001). This metric is meaningfully significant where the 24-hour harmonic explains significant variance in the actual diurnal composite rainfall time series, i.e. in the hatched regions shown in the left panel of Figure 2.2. Key features include the predominant afternoon timing over summer hemisphere land masses, nocturnal oceanic maxima, shifting to morning near coastal oceans, and the rich geographic complexity within continents, including the Central US nocturnal maximum.

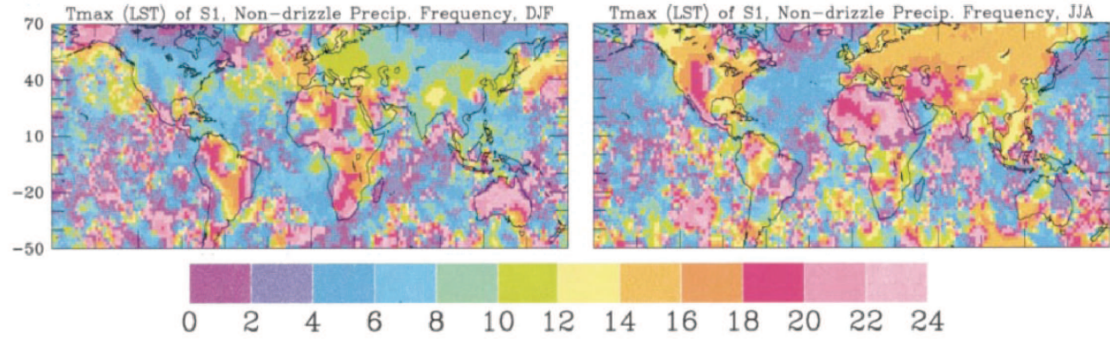


Figure 2.1: Local solar time $T_{max}(h)$ when the diurnal harmonic ($S1$) of (left) DJF and (right) JJA mean frequency of occurrence peaks for nondrizzle precipitation gauge data from 1976-1997. Adapted from Figure 5 of Dai (2001).

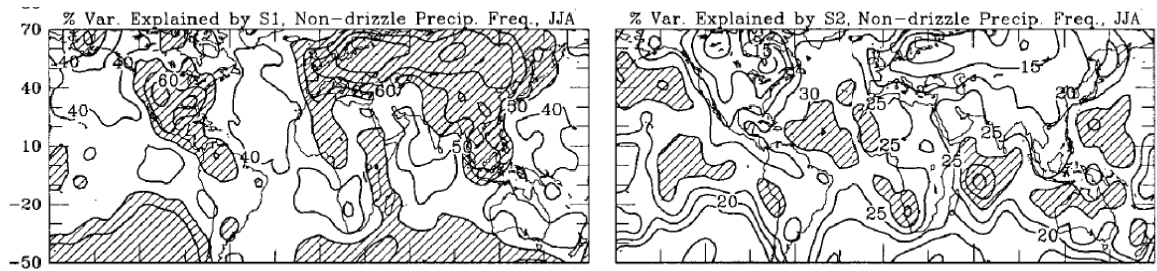


Figure 2.2: Percentage of the mean daily variance explained by the (left) diurnal and (right) semidiurnal harmonics for JJA mean frequency occurrence for nondrizzle precipitation gauge data. Values over 50% and 30% are hatched in the left and right columns, respectively. Adapted from Figure 4 of Dai (2001).

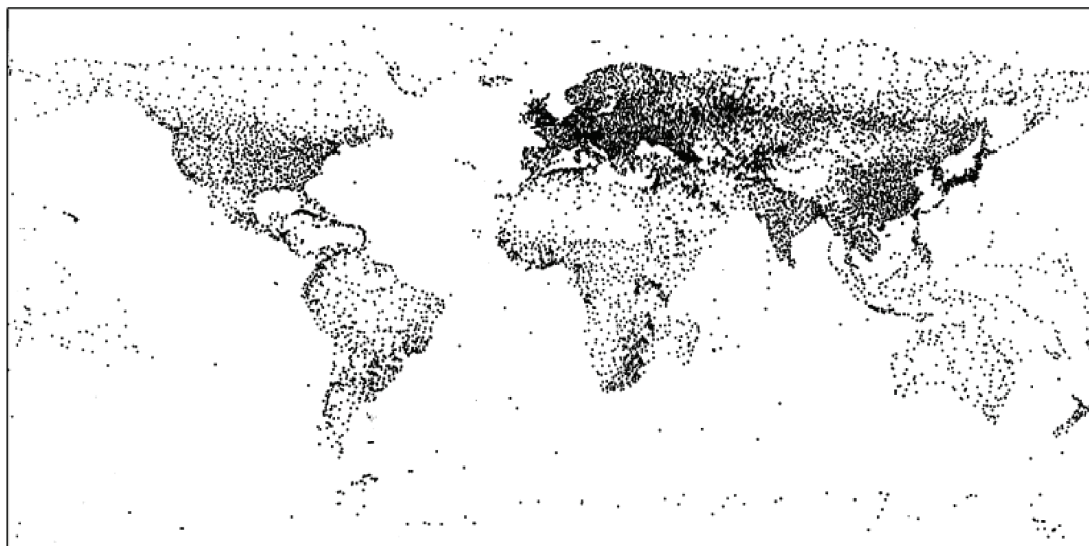


Figure 2.3: Representative distribution of rain gauge data. Reproduced from Figure 1 of Kidd (2001).

Rain gauges provide a simple, direct measure of rainfall that is unambiguous. But gauge measurements also suffer from sampling issues. Although the map from Dai (2001) in Figure 2.1 appears to show global data coverage, in fact rain gauge sampling is biased strongly toward northern hemispheric land (Figure 2.3). Over oceans, Dai (2001) acknowledge that the statistical significance of the diurnal composite timing from the gauge record in Figure 2.1 is highly uncertain. Even over heavily populated industrial areas, the modern rain gauge network is neither dense enough nor reported frequently enough to adequately characterize rainfall structures, which are notoriously small scale and statistically non-Gaussian.

Remote sensing satellite observations have become increasingly important for filling the gaps in the rain gauge record. The benefit of high spatial and temporal coverage has proved to outweigh drawbacks associated with the complex inverse estimation algorithms (so-called “retrievals”) required to infer rainfall from indirect

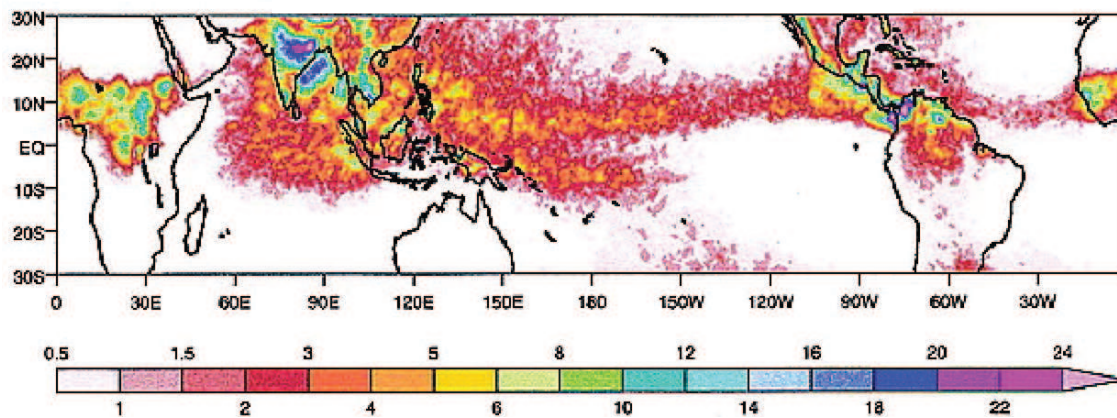
radiometric signatures of convection.

In the seventies and eighties, infrared radiometers on board constellations of geostationary weather satellites provided the lion's share of radiometric measurements used to remotely infer characteristics of diurnal precipitation (e.g. Albright et al. (1985)). Elevated cloud tops and upper tropospheric water vapor anomalies frequently accompany rainfall, and they are highly emissive in the infrared. Observations of infrared brightness temperatures at $11\ \mu\text{m}$ (atmospheric window) and $6.7\ \mu\text{m}$ (water vapor) can be combined to detect such high clouds (Fu et al., 1990) and upper tropospheric water vapor (Soden and Bretherton, 1993). On diurnal timescales, the separable cloud and vapor infrared signatures are phase lagged with respect to precipitation, consistent with gross aspects of the diurnal convective lifecycle (Soden, 2000; Tian et al., 2004).

On coarse space/time scales (2.5° , 24 hours) a "precipitation index" can be derived from infrared radiometer measurements of cold cloud cover, which shows some correlation skill against ground based radar measurements (Arkin and Meisner, 1987). In its essence, the infrared precipitation index rainfall retrieval approach is based on simple geometric relationships between clouds and rainfall; the physical premise being that deeper (colder, brighter) cloud tops imply stronger (more) rainfall (Kidd, 2001). This idea works better for unorganized tropical deep convection but breaks down when convection is orographically organized or frontal. Readers may refer to Joyce and Arkin (1997) for a brief review of the early history of the infrared precipitation index.

Recognizing its importance in validating climate model physics, Yang and Slingo (2001) published the first climatological composite diurnal cycle of cloud top brightness temperature and an inferred precipitation index. These data were derived from two decades of infrared observations obtained on multiple satellite platforms, inter-calibrated by the International Satellite Cloud Climatology Project (ISCCP), providing excellent statistics. The 24-hour harmonic's ampli-

a) Amplitude (mm/day)



b) Phase (local hour)

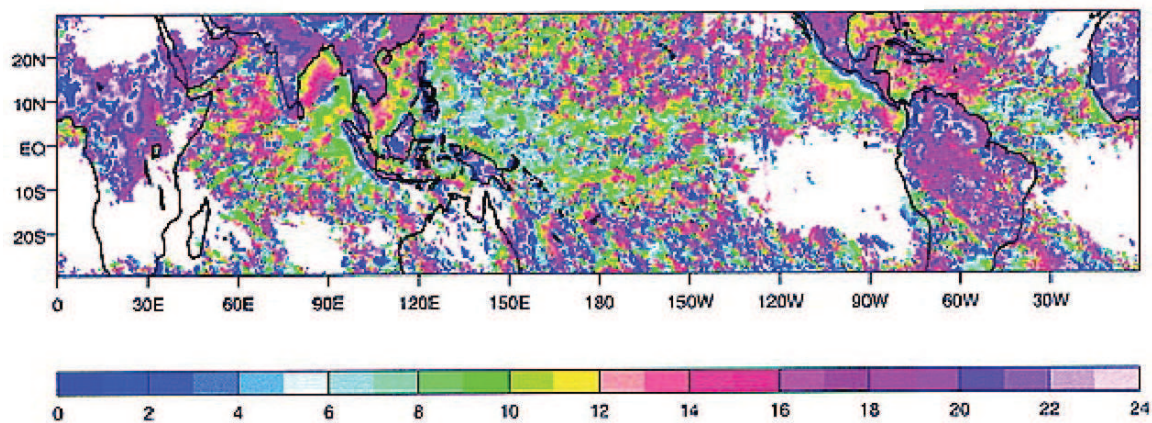


Figure 2.4: Fitted boreal summer (JJA) composite diurnal precipitation harmonic a) amplitude and b) phase, as inferred from two decades of infrared cloud top temperature retrievals. Adapted from Figures 2 and 3 of Yang and Slingo (2001).

tude and phase of boreal summer composite diurnal brightness temperature from their analysis are reproduced in Figure 2.4. One of the most remarkable features is the richness in the structure of diurnal rainfall within land masses, near coastlines, and even within vast open ocean basins. This rich structure is apparent despite heavy temporal averaging in the composite, emphasizing that the physics of diurnal rainfall are highly regional, modulated by topography and coastlines, and inherently complex.

In the past decade, microwave estimates of precipitation have practically obsoleted infrared rainfall proxies. A key disadvantage of all infrared-based rainfall retrievals is that the fundamental measurement is of cloud top brightness temperature, not rainfall. Modern precipitation remote sensing methods avoid the associated pitfalls of vapor and cloud top height mis-estimation in the infrared by instead measuring microwave radiometric signals. Microwaves interact strongly with raindrops and are not substantially obscured by overlying clouds (Kidd, 2001). Operational microwave rainfall remote sensing technologies in orbit today include passive microwave imagers (e.g. the Special Sensor Microwave / Imager (SSM/I) on defense meteorological satellites), high spectral resolution microwave sounders (e.g. the Advanced Microwave Sounding Unit (AMSU) on board NOAA weather satellites) and even active microwave (spaceborne radar) on research satellites (e.g. the Tropical Rainfall Measurement Mission and CloudSAT).

Microwave rainfall retrievals from passive sensors are highest quality over the ocean, where brightening in thermal microwave emission bands (e.g. at 50.3 GHz) due to elevated rain drops contrasts strongly against the homogenous background sea surface thermal emission. Over land, retrievals based on thermal emission do not work well, because the background land surface emissivity varies strongly in space and time at these wavelengths. An alternate but less accurate retrieval approach can be used over land based on higher wavelength microwave signals in the raindrop scattering – as opposed to thermal emission – regime (e.g. 90 GHz)

(Kidd and Barrett, 1990; Kidd, 2001). At these wavelengths, the presence of rainfall can be inferred due to dimming at the top of the atmosphere when underlying hydrometeors scatter microwave photons out of the column below (Petty, 1995). Passive microwave sounders - as opposed to imagers - further resolve coarse vertical distributions of rainfall rate, and atmospheric liquid water content profiles, by combining information from multiple detector channels arranged at high spectral resolution across individual spectral lines. More recent technologies provide enhanced vertical information from the backscatter return from active microwave (spaceborne radar; Kummerow et al. (1998); Stephens et al. (2002)).

Although they are crucial for filling gaps in the patchy gauge record, remote sensing observations from space come with problematic sampling challenges of their own. Satellite measurements are collected along orbits that introduce significant space-time biasing of the diurnal cycle. Distant geosynchronous orbits provide large fields of view, but limited, static spatial coverage whereas low-earth orbits trace out near-complete global coverage but measurements are collected on relatively small fields of view and often biased to sample certain phases of the diurnal cycle. An extreme example is the NASA “A-Train”, in which a series of overlapping detectors including space-borne precipitation radar chase each other along an orbit that is rigidly locked at each latitude to a specific local time of day, providing no sampling of the local diurnal cycle at any location. As a result of these orbital issues, no one satellite platform can sufficiently characterize the global daily mode of rainfall.

One landmark satellite recently bucked this general trend, achieving for the first time statistically significant sampling of the diurnal rainfall composite from a single remote sensing platform. The Tropical Rainfall Measurement Mission (TRMM), launched in 1997, combines microwave imaging, infrared sounding, and active microwave (radar) instruments on a satellite that is in a unique precessing, tropics-oriented orbit (Kummerow et al., 1998). As a result, TRMM has a pro-

nounced (especially in midlatitudes) but slowly drifting local time sampling bias, (Hirose and Nakamura, 2005). Eight years' of observations have proved sufficient to alias this drift through the diurnal mode and statistically characterize the composite diurnal rainfall cycle as a whole from the raw sensors on this single platform (Hirose et al., 2008).

Figure 2.5 shows an intercomparison of the composite diurnal rainfall cycle as detected by each of the three rainfall sensors on board the TRMM platform (Yamamoto et al., 2008). This remotely sensed perspective on diurnal rainfall complements the patchy gauge record shown previously in Figure 2.1. That the independent sensors agree on the structure of the diurnal composite is encouraging. The top panel shows the state of the art, highest quality remotely sensed precipitation radar return data. In this 8-year composite the gross features of the gauge data (Dai, 2001) in Figure 2.1 are reproduced: Local time of peak rain over the ocean is in the middle of the night, progressing closer to the early morning for coastal ocean, while over land it is in the mid- to late-afternoon. The infrared data show a subtle phase delay relative to the radar and microwave data, emphasizing the point made earlier, that infrared signals are associated with a later phase of the convective lifecycle (high-altitude cloud and vapor signatures generally occur after rainout in deep convection) (Yamamoto et al., 2008).

Although the majority of microwave rainfall measurements take place on satellites with non-precessing orbits that do not sample the diurnal cycle adequately, there are enough microwave instruments in orbit today with sufficiently overlapping footprints that 80% of the world's surface is sampled within a typical three hour interval (Figure 2.6; Huffman et al. (2007)). Appropriate inter-calibration methods have been devised so that microwave data from multiple platforms can be used in combination with each other as well as with infrared retrievals and rain gauge networks to produce a "best estimate" of global rainfall. Early global multisensor precipitation climatologies were at coarse spatial and temporal resolution

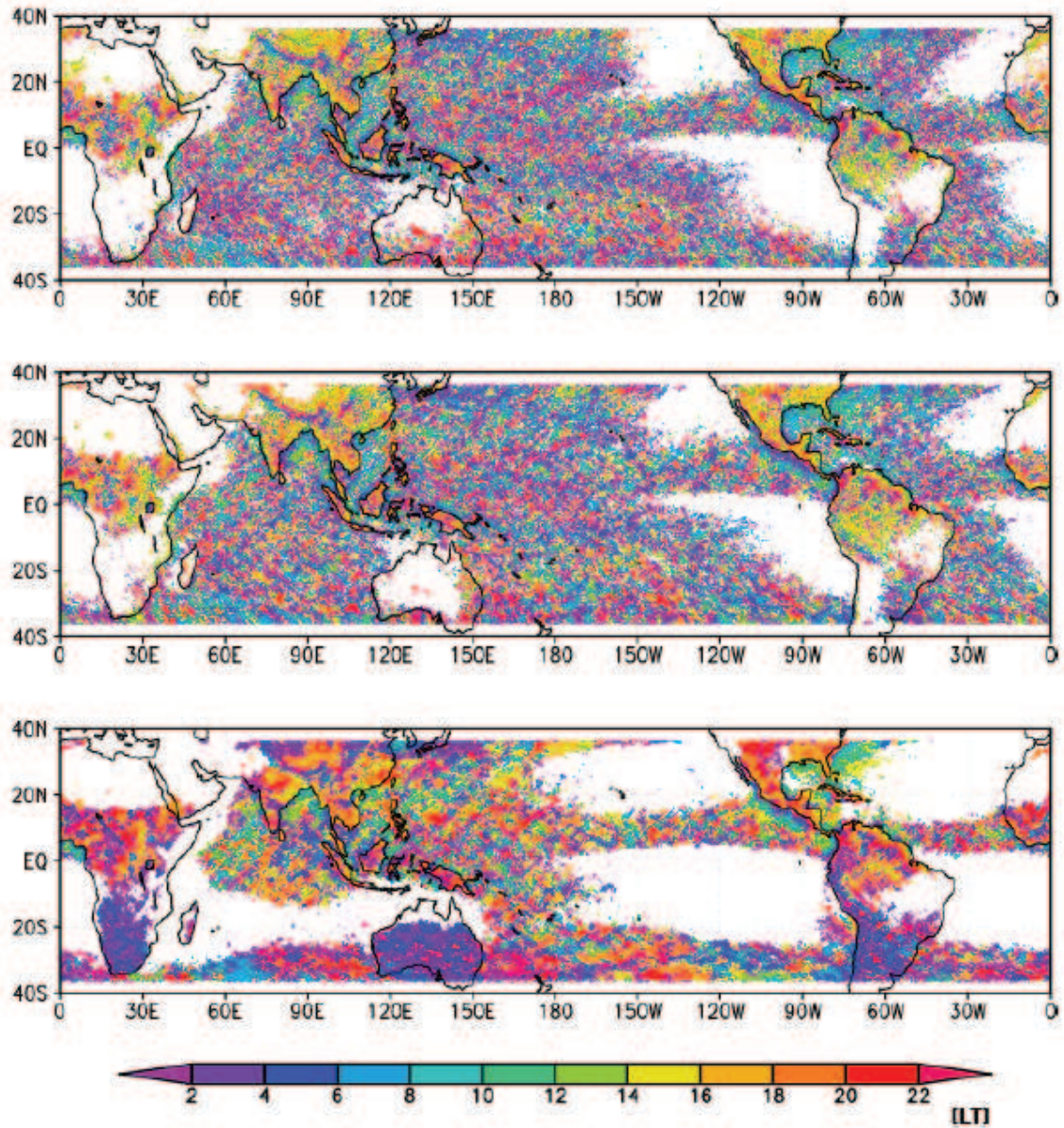


Figure 2.5: Peak local time of maximum rain rate derived from Tropical Rainfall Measuring Mission precipitation radar (upper) and total microwave imager (middle), and peak local time of minimum brightness temperature at 10.8 microns (lower) for JJA 1998–2003. The pixels where rain rate (infrared brightness temperature) within 1 hour of the local time of maximum rain rate (minimum brightness temperature) are above (below) mean rain rate (brightness temperature) for radar and microwave (infrared) data, where rain frequency is more than 1%, and where the rain rate is more than 10 mm mon^{-1} (the mean brightness temperature is less than 280 K) are colored. Reproduced from Figure 1 of Yamamoto et al. (2008).

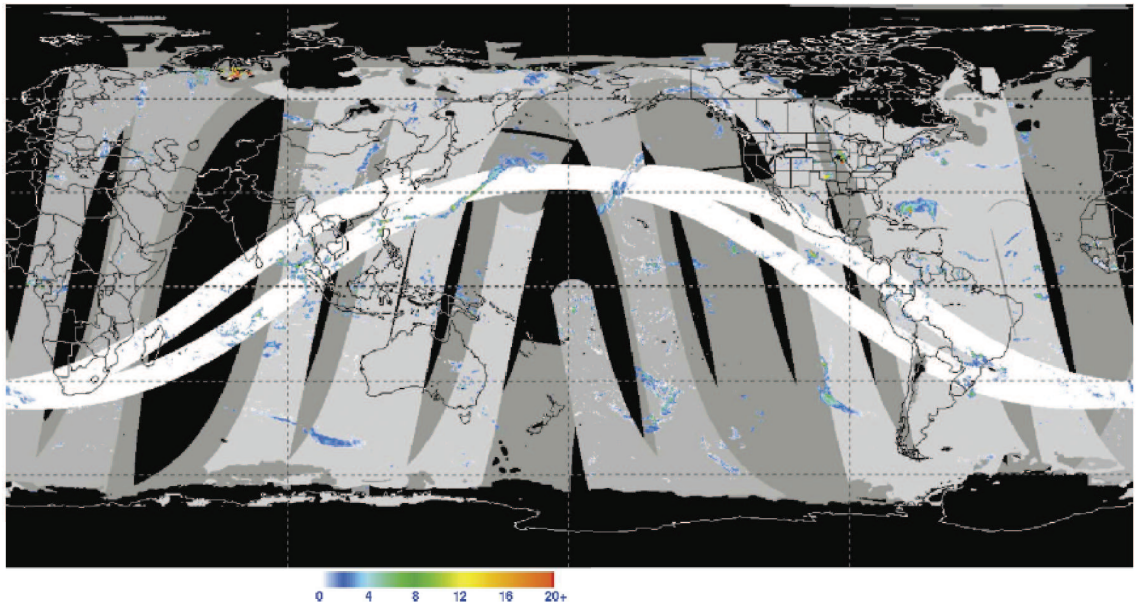


Figure 2.6: Combined microwave precipitation estimate for the 3-h period centered at 0000 UTC 25 May 2004 in mm/hr. Blacked-out areas denote regions that lack reliable estimates, while the zero values in the remaining areas are color-coded to depict the coverage by the various sensors. The order of precedence for display and corresponding zero color are TMI (white), SSM/I (light gray), AMSR-E (medium gray), and AMSU-B (dark gray). Reproduced from Figure 1 of Huffman et al. (2007).

(1-2.5 °, monthly; (Huffman et al., 1995; Xie and Arkin, 1995, 1997). As a recent legacy effort of the Tropical Rainfall Measurement Mission, multisensor techniques have since been refined to much higher space-time resolution (0.25 °, 3 hourly) in a new gridded rainfall data product called TRMM 3B42 (Huffman et al., 2007). Since the climatological composite diurnal cycle of precipitation in 3B42 has been well-studied and appears to be in good agreement with independent precipitation products and surface data, its practical advantages for the purpose of model evaluation are compelling (Dai et al., 2007). This state of the art “best estimate” of global rainfall is thus the primary data ground truth employed in this dissertation.

2.1.2 Physical mechanisms

Unlike the simple sinusoidal daily solar cycle of radiation that drives it, the daily cycle of rainfall is richly structured. Recall Figures 2.4 and 2.5, which showed heavily composited observations of the diurnal harmonic of precipitation inferred from infrared brightness temperatures, microwave imagers, and spaceborne radar. On the one hand, over many land regions the fact that diurnal rainfall peaks in the mid-afternoon is suggestive of an intuitive lagged response of boundary layer destabilization to local solar heating and evapo-transpiration. On the other hand, the observations clearly show that over just as many regions, the structure of the climatological composite daily rainfall cycle is nothing like the solar cycle that drives it. Extreme examples include the central United States, and the open ocean, where peak rainfall tends to happen in the middle of the night, a full 180 degrees out of phase with the solar cycle.

Diurnal convective physics are complicated by the fact that the daily cycle of solar heating excites many atmospheric modes of variability that conspire to influence convection in a complex manner. For instance, over extra-tropical mountain ridges, the diurnal cycle of elevated boundary layer heating and cooling creates

horizontal pressure anomalies in the atmosphere, causing lagged semi-geostrophic adjustment accelerations in widespread regional orographic circulations (Holton, 1967). The low level aspects of these and other (frictional) circulation responses to diurnal heating in turn modulate meridional fluxes and convergence of vapor, resulting in complex, counter-intuitive phase lags in the diurnal convective response such as the Central United States nocturnal maximum (see Section 2.1.3). Another prominent example of non-local diurnal control occurs in the coastal oceans of the tropics, where energetic continental daytime convection sparks deep gravity wave disturbances that exert control on convection over waters hundreds of kilometers away (Mapes et al., 2003). This phenomenon can be seen in the extended halos of anomalously high diurnal rainfall amplitude and concentric phase striations surrounding the Indonesian islands, off the western coast of equatorial South America, and down the Bay of Bengal in Figure 2.4 (Yang and Slingo, 2001).

Yang and Smith (2006) sum up the complexity of the physics behind the observed composite diurnal cycle:

In essence, diurnal variability [of rainfall] over planet Earth is heterogeneous but regionally coherent and arising from multiple mechanisms competing for dominance. At no time in seeking to decipher the cause of diurnal signals can the elements of “time to fruition,” “downstream propagation,” “available moisture,” and “radiative-dynamic interactions” be overlooked because all ... underlie the specific amplitude and exact timing of a phase peak. Diurnal rainfall variability is not a simple process and defies simple explanations. [Yang and Smith (2006)]

Despite this inherent complexity, several worthwhile and insightful historical attempts have been made to explain the physical character of gross aspects of diurnal rainfall using simple theory. The following discussion draws heavily on contemporary historical reviews and secondary references from Yang and Slingo (2001) and Yang and Smith (2006), who consider the problem from the climate scale, as well as from texts by Pielke (2002) and Li (2004), who discuss insights gained from explicit simulation with limited domain convection resolving models.

The afternoon rain maximum over most land

The predominant afternoon rainfall maximum over land has long been explained as a lagged response to the local noon-peaking land surface heating and evapotranspiration cycles (Yang and Smith, 2006). The rainfall phase delay of several hours is due in part to the time-scale for dry convective boundary layer deepening (the driving sensible and latent heat transport that precondition deep convective rainout being limited by the timescale of dry eddy overturning and lifetime of unorganized shallow convection), and partly by the physics of organized thunderstorm convection in the (frequent) presence of vertical wind shear (Byers and Battan, 1949; Newton, 1950). Rotunno et al. (1988b) discuss the essential physics of shear organization, showing how density currents at the edges of evaporatively cooled rain-shafts can interact with low-level shear to favor enhanced storm longevity (and thus later, more intense rainout). The actual dynamics of organization are inherently nonlinear and three dimensional, involving upscale cascades of energy and momentum through eddy and cloud interaction, often mediated by convectively generated and ducted gravity waves (Pandya and Durran, 1996; Kuang and Bretherton, 2006; Khairoutdinov and Randall, 2006; Wu et al., 2009). The emergent self-sustaining balanced organized convective “system” behavior on the mesoscale allows for rainout many hours after peak surface heating has come and gone.

Although fundamentally this system behavior is considered as a lagged response, with the ultimate forcing understood to be surface heating of the land (Yang and Smith, 2006), controversies exist in the current literature regarding the relative roles of several competing physical processes in setting the timing. For instance, explicit simulations implicate mesoscale cold pool organization (Khairoutdinov and Randall, 2006), bulk entrainment humidification preconditioning (Kuang

and Bretherton, 2006), in the timing of land rainfall.

The coastal region

Near coastlines, the diurnal rainfall cycle is influenced by diurnally reversing solenoidal circulations set up by the differential heating and cooling of land vs. ocean. The structure of coastal diurnal circulations changes fundamentally across a critical latitude of 30° where the Coriolis and diurnal frequencies are equal. Poleward of this critical latitude “Coriolis effects can make the land breeze an inertial continuation of the sea breeze” (Mapes et al., 2003). Simple models provide insight into the structure of isolated coastal solenoids in these two regimes. Rotunno (1983) show that, poleward of 30° , the horizontal scale of an inviscid, linear atmosphere to a diurnally varying heat sources is confined to $\Delta x = \frac{Nh}{\sqrt{f^2 - \Omega^2}}$, whereas equatorward of 30° inertial gravity wave dynamics allow the effects to extend indefinitely, “along ray paths extending upward and outward from the coast”. Including surface friction and nonlinearity produces similar isolated circulation structures in the two regimes (Yan and Anthes, 1987). In explicit simulations, convective feedbacks, wave interactions with various synoptic background flows, coastal orography, and surface vegetation all conspire to produce a wide range of solenoidal sea breeze circulation structure and scale from region to region (Pielke, 2002). A common thread is the setup of sharp, propagating land surface fronts (a.k.a. sea breeze fronts) that mechanically favor daytime deep convection over land and simultaneous (through continuity) daytime subsidence over adjacent ocean. Indeed, convecting sea breeze fronts are routinely observed propagating inland from (and oriented parallel to) coastlines during the day (Simpson et al., 1977; Wakimoto and Atkins, 1994, e.g).

The reverse solenoidal circulation is often invoked to explain nocturnal rainfall

maxima over coastal ocean (Yang and Smith, 2006). From this perspective, the strong diurnal radiative heating and convection over coastal land thermally drives large scale circulations that remotely control aspects of the adjacent coastal ocean diurnal rainfall cycle, where local radiative diurnal heating is weaker (Dai and Deser, 1999; Dai, 2001; Randall et al., 1991). In an analysis of the large scale phase of surface wind divergence inferred from sparse marine weather station data Dai (2001) suggested that an early morning oceanic rainfall maximum is associated with “a large-scale diurnal circulation in which surface air converges and rises over continents (except for the innermost parts) and diverges and sinks over large nearby oceanic areas in the afternoon and early evening and the opposite occurs in the early morning.” (Dai and Deser, 1999; Dai, 2001). This sort of effect is strikingly apparent off the western coast of Colombia, where the steep slopes of the Andes extend the coastal land diurnal heating signature deep into the atmosphere, exciting long range gravity wave mediated vacillations in the diurnal hydrological cycle offshore (Mapes et al., 2003). Diurnally resolving satellite scatterometer measurements have only recently begun to reveal the rich structure of these sorts of land-ocean diurnal remote control mechanisms, via their global surface wind divergence (i.e. subsidence) signature (Gille et al., 2003, 2005; Wood et al., 2009). Especially in the tropics and subtropics, long-range remote control is thought to have implications for diurnal cloud properties and rainfall (Munoz, 2008; Wood et al., 2009), a topic which will be revisited in Section 5.1.

The open ocean

In remote regions of the tropical ocean, a nocturnal to mid-morning rainfall maximum is observed (Albright et al., 1985; Hendon and Woodbery, 1993; Janowiak et al., 1994) but the underlying physics are an ongoing topic of debate.

Historically, theories linking open ocean diurnal rainfall to planetary pressure tides were briefly popular. On planetary scales, resonant normal modes of the atmosphere excited primarily by diurnal solar ozone heating in the stratosphere and thermosphere produce diurnal surface pressure signatures. Where solar tide pressure anomalies cannot be converted into geostrophic motions (i.e. in the tropics) and surface solar heating cycles are weak (over the high heat capacity oceans), mechanical lifting of moist air due to low-level convergence associated with solar tide pressure anomalies can be thought of as a causative control on diurnal rainfall. This idea has however fallen out of favor:

Although Malkus (1964) and Brier and Simpson (1969) suggested that daily variations in precipitation are forced by the tides, the idea has been met with skepticism (Lindzen, 1978) on the grounds that the tidal moisture convergences are not strong enough to produce significant fluctuations of precipitation. [Randall et al. (1991)]

Today, two flavors of radiation-convection feedbacks are usually invoked to explain the open ocean rainfall cycle (Yang and Smith, 2006), as described below. Sui et al. (1997) trace the underlying conceptual connection as far back as Kraus (1963).

A major substantive physical theory for the open ocean nocturnal/morning maximum stemmed from surface observations collected during the 1974 Global Atmospheric Research Program (GARP) Atlantic Tropical Experiment (GATE). Using GATE observations, Gray and Jacobson (1977) proposed a mechanism to explain why intense rain over the open ocean is often maximized in the early morning hours, colloquially called the “Dynamic-Radiation-Convection (DRC)” mechanism in the classification scheme of Yang and Smith (2006). The idea was supported by some early observational (McBride and Gray, 1980) and numerical modeling results (Fingerhut, 1978). It posits the pre-existence of a tropical cloud cluster, a form of organized convection that is responsible for much of the intense rainfall in

the tropical open ocean and thus assumed to dominate climatological composites of diurnal rainfall variability there. Since such organized convective systems are long-lived, the enhancement of nocturnal cloud-top radiative cooling at sunset is sustained long enough to produce anomalous nocturnal large-scale clear air subsidence surrounding the system. Through mass balance, this subsidence drives low-level convergence beneath the system, favoring additional mechanical uplift and rainout. The early morning open ocean rainfall maximum is thus explained through the above chain of events, as a lagged dynamic response to radiative effects:

...the convergence cycle typically follows the radiational forcing with a time lag of 3-6 hours... We believe this to be a natural consequence of the hourly accumulation of the disturbance minus surrounding region radiational energy differences. Thus, the maximum accumulated nighttime radiational cooling effects should occur 1-2 hours after sunrise and a maximum in solar warming effects near sunset.[Gray and Jacobson (1977)]

Randall et al. (1991) present a complementary theory involving radiation-convection interactions, based on analysis of an early GCM simulation of the tropical open ocean diurnal rainfall cycle. Their theory cast the problem locally (without involving non-local subsidence or convergence feedbacks) whereby the accumulated day-night differences in cloud top radiative heating imbalances affect convection *directly* through their influence on local thermodynamic stability. For example, the cumulative effect of enhanced nocturnal cloud top cooling exerts a destabilizing effect on GCM cloudy columns. Yang and Smith (2006) tag the Randall et al. (1991) mechanism and its variants the “Static-Dynamic-Radiation (SRC)” mechanism. A key difference with respect to the above is that whereas Gray and Jacobson (1977) invoke vertical velocity as part of the causative chain of events that drive the early morning maximum, Randall et al. (1991) explain it as fundamentally an *effect* of diabatic and radiative effects:

The observed [open-ocean] diurnal [rainfall] cycle can be qualitatively accounted for by direct radiation-convection interactions, although indirect radiative-convective interactions mediated by the large scale dynamics and the remote influence of the continents also play a part. Specifically, the absorption of solar radiation by clouds leads to a reduction of the precipitation rate in the afternoon (near the end of the daylight hours), relative to the early morning (near the end of the night). The observed diurnally varying large-scale vertical motion field is apparently *forced by* the diurnal cycles of radiative and latent heating; it is not a critical forcing agency for the observed diurnal cycle of precipitation over the oceans. [Randall et al. (1991), p. 60]

Two decades after GATE, the DRC and SRC mechanisms described above came to be viewed as secondary effects after a subsequent intensive observing field campaign in the tropical western Pacific led researchers to a more fundamental theoretical understanding of open ocean nocturnal rainfall. During the 1992-1993 Tropical Ocean Global Atmosphere Coupled Atmosphere Response Experiment (TOGA-COARE), diurnal variations of the vertical energy and moisture budgets within a patch of convecting atmosphere were constrained using an intensive array of soundings. These observations, combined with substantial developments in explicit cloud simulation, allowed the DRC and SRC mechanisms to be tested. In a pair of papers, Sui et al. (1997) and Sui et al. (1998) argued that neither the TOGA-COARE budget observations themselves, nor numerical sensitivity experiments driven by them, could support DRC or SRC as the fundamental mechanism driving the dominant nocturnal oceanic peak. Instead, they suggest these are second order effects, and that a simpler thermodynamic process is at work, in which clear sky cooling at night simply humidifies the tropical atmosphere via the Clausius-Clapeyron relation. Explicit deep convection modeling efforts by Liu and Moncrieff (1998) reached similar conclusions - nocturnal maxima of tropical rainfall could be achieved even when cloud-radiation interactions were disabled in numerical models. In a recent text on numerical cloud simulation, Li (2004)

attribute the Sui et al. insight to earlier work by Tao et al. (1996), and affirm the basic mechanism using additional scale analysis diagnostics of explicit cloud-resolving TOGA-COARE simulations. They argue causation from such analysis is conclusive, and that:

colder temperatures cause lower saturated mixing ratios making it easier for water vapor to be condensed and deposited into precipitation. Therefore, nocturnal radiative cooling leads to colder air temperatures that make it easier for clouds to develop and hence rainfall. [Li (2004), p. 214]

Another finding emphasized during and since TOGA-COARE was the frequent presence of a secondary tropical oceanic diurnal rainfall maximum in the afternoon. This secondary maximum was linked to local surface forcing, whereby undisturbed large-scale conditions were associated with sustained low wind conditions leading to abnormally large sea surface skin temperatures in the absence of wind-driven surface layer mixing (Sui et al., 1997, 1998; Yang and Smith, 2008).

2.1.3 Central US nocturnal rainfall

Observed nocturnal rainfall maximum

The US national network of rain gauges show a pronounced nocturnal rainfall maximum over the Central US during boreal summer. Figure 2.7 shows the Fourier decomposed 24-hour harmonic in a climatological composite of weather station data (Wallace, 1975). A region of anomalously high amplitude (more wind barbs) and nocturnal phase (vectors pointing from the north) dominates the Central United states.

The vigorous Central US nocturnal maximum of rainfall is co-located with an anomalous population center of Mesoscale Convective Systems (MCSs). MCSs constitute a form of convection that was discovered at the dawn of satellite mete-

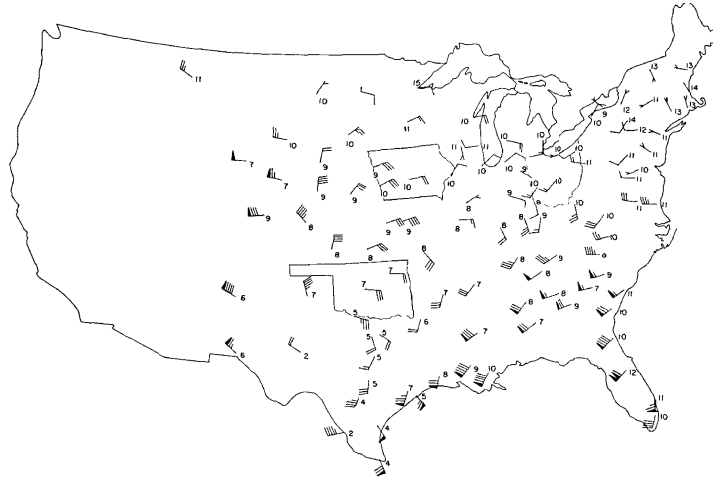


Figure 2.7: “Normalized amplitude and phase of the diurnal cycle in the total frequency of precipitation, including trace events for the summer season (June-August [1951-1960])” from rain gauge station data. The number of barbs denotes the amplitude of the 24-hour harmonic, and the phase is indicated by the orientation of the arrows. “An arrow pointing from the north indicates a midnight maximum (local time); one pointing from the east indicates a 0600 maximum, etc.”. The Central US nocturnal maximum is evident as a region of anomalously high amplitude, with arrows directed from the north. Reproduced from Wallace (1975).

orology to be organized on scales larger than previously thought possible at mid-latitudes (Maddox, 1980; Houze, 2004; Carbone and Tuttle, 2008). MCSs show up as bright ellipsoids on orbital infrared imagers, due to their horizontally expansive and highly emissive “cloud shield” anvils. The self-similar morphology of MCSs in the Central US allows automatic identification and statistical analysis of their population centers. Maddox (1980) defined the following ruleset for an IR feature to be counted as one of these especially large, circular forms of MCS¹:

- There has to be a continuous area of IR brightness temperature below -32 degrees Celsius, larger than 100,000 km².
- There also has to be within that a smaller “shield” colder than -52 C (area must be bigger than 50,000 km²)
- The above conditions must hold for at least 6 hours.
- The shape of an ellipse fitted to the above contours must have eccentricity bigger than 0.7 at the time of its maximum extent (these are rather elliptical features).

Statistical analysis of the population centers of MCS events, based on the objective identification algorithm above, revealed the Central US as a hot spot for MCS activity. An analysis of data from 1982 and 1983 suggest that MCS rain is responsible for 30%-70% of total warm season rainfall in the region (Fritsch et al., 1986). Figure 2.8 shows a schematic constructed from many years’ satellite imagery by Laing and Fritsch (1997). Laing and Fritsch (1997) emphasize that enhanced organized convection populations tend to occur in the lee of many mountain chains worldwide, especially where equatorward sources of moisture are supplied by low-level jet circulations. In this sense, the Central US nocturnal maximum is

¹Maddox originally coined this specific, large class of MCS as a “Mesoscale Convective Complex (MCC)”. The more general, modern nomenclature of MCS is used in this dissertation.

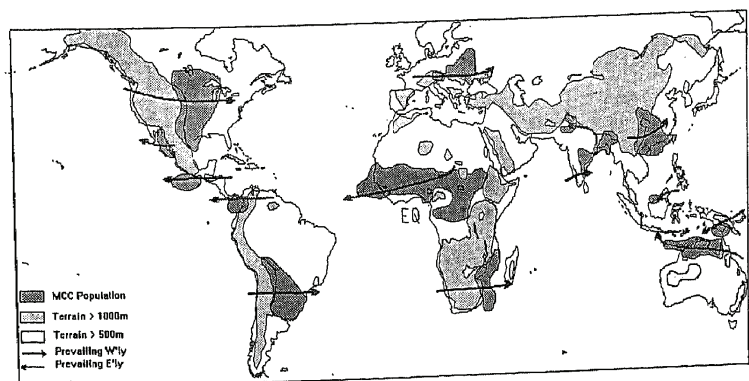


Figure 2.8: Relationship among mesoscale convective complex (MCC) population centers, elevated terrain, and prevailing flow, showing the Central US hotspot of organized convection activity as part of a more general phenomenon. Reproduced from Laing and Fritsch (1997) (their Figure 4).

an example of a more general phenomenon of the continental diurnal rainfall cycle near mountain ridges.

Many of the MCSs that deliver nocturnal warm season rainfall to the Central US are generated nonlocally, upstream over the Rockies, during the preceding afternoon. Maddox (1981) analyzed two years of satellite infrared imager data over the Central US and estimated that almost half of the cases were linked to orographic convection upstream. The number of storms generated non-locally fluctuates from year to year; for instance, Lin (1986) found only 25% MCCs to be orogenic (non-locally generated over topography) based on analysis of one year's data (Tripoli and Cotton, 1989a). Nocturnal destabilization due to favorable meteorological conditions at night is also important for maintaining and enhancing MCSs that propagate into the Central US (Trier and Parsons, 1993). A contemporary reanalysis built around a high resolution regional model (the North American Regional Reanalysis; NARR) suggests that 50 % of total Central US summertime rainfall is due to the eastward propagating mode (Jiang et al., 2006).

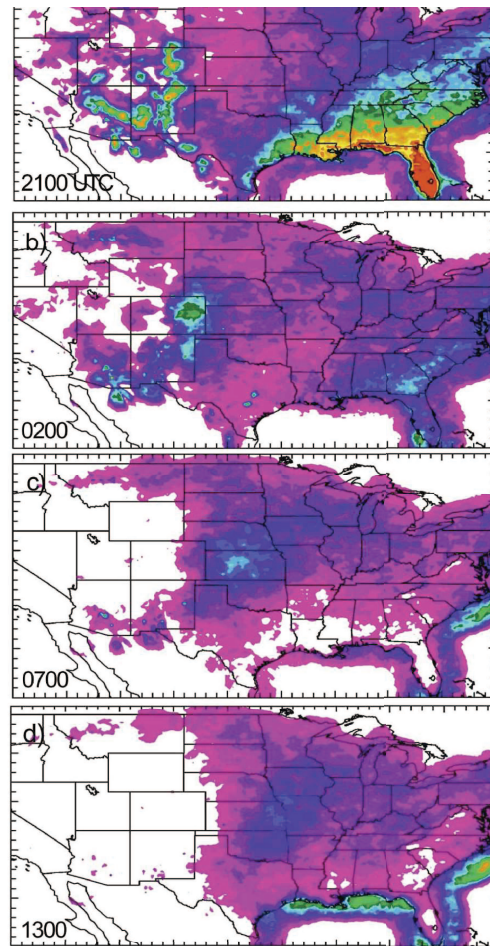


Figure 2.9: “Diurnal radar echo frequency of occurrence, in JJA, expressed as percent of days within a given hour that precipitation echo is present: (a) 2100, (b) 0200, (c) 0700, and (d) 1300 UTC. Readers are referred to the supplementary animation, which provides a superior visualization of the continental diurnal cycle (online at <http://dx.doi.org/10.1175/2008JCLI2275.s1>).” Reproduced from Carbone and Tuttle (2008)

The modern national network of ground based rainfall radars constitutes the best available observational constraint on the basic structure of the eastward propagating Central US MCS convection mode. Although quantitative rain rate retrievals are inherently uncertain, radars provide an excellent data constraint on rainfall occurrence (i.e. backscatter above an assigned threshold). Binned by time of day, composited radar exceedence thresholds track major diurnal rainfall phenomena. Carbone and Tuttle (2008) published a twelve year climatology of radar data from the US warm season, which clearly captures the fine-scale climatological composite structure of the Central US eastward propagating convection mode. Figure 2.9 (and the equivalent animation at <http://dx.doi.org/10.1175/2008JCLI2275.s1>) demonstrates its space-time structure. A north-south line of orographic convection, roughly following the Rockies, is the initiating event at 2100 UTC (2pm mountain time). Subsequently, a large feature of enhanced averaged reflectivity travels eastward, representing the climatological average of eight years' propagating MCS rainfall².

Central US physical mechanisms

The nocturnal maximum of Central US, MCS-mediated rainfall is currently understood to result from a complex interplay of several competing physical processes, many unique to the regional continental circulations set up by elevated daytime (nighttime) heating (cooling) over the Rockies.

Maddox (1981) derived the first MCS thermodynamic composite by lining up measurements from the synoptic sounding network during an ensemble of satellite detected mature MCS events. Figure 2.10 shows the geopotential height, zonal wind, moisture, and temperature anomalies associated with this climatological

²Other notable features of US rainfall climatology in Figure 2.9 are the dramatic sea breeze rainfall cycles straddling the northern coast of the Gulf of Mexico and along the eastern Seaboard, as well as the very high amplitude afternoon rainfall maximum in the US Southeast.

MCS composite.

In the following discussion, three key features in Maddox’s composite (labeled A through C) are discussed through the lens of hindsight from three decades of theoretical, numerical and field campaign studies into MCS dynamics. The first (Feature A) is a low level moisture anomaly, a hallmark of a southerly low-level atmospheric jet that is now understood to be the most important moisture/energy source feeding Central US MCSs. The second (Feature B) is a thermal anomaly - upper level heating - associated with a characteristic MCS diabatic heating pattern that links MCS morphology to a mesoscale relative flow pattern that supports long-lived convection. The third (Feature C) is a set of upper level wind anomalies that highlight the equally important role of quasi-geostrophic dynamics in supporting MCS convection on larger scales.

The nocturnal Low Level Jet (LLJ)

Feature A in Figure 2.10 highlights a moist anomaly in Maddox’s MCS composite between 800 hPa to 600 hPa. The position of this moist anomaly coincides with the location of a climatological southerly low level jet (LLJ; not shown) to the east of the Rockies. The LLJ is a feature of mean summer US climate, steered geostrophically by the persistent summertime Bermuda high and oriented northward due to the blocking effect of the Rocky Mountains to the west (Wexler, 1961). The LLJ is rich with Gulf of Mexico humidity and where it terminates, horizontal moisture convergence provides a fuel source for observed organized convection (Maddox, 1983; Trier et al., 2006, 2010). The LLJ signature in Maddox’s MCS anomaly composite provided an early hint that anomalous moisture and temperature advection due to fluctuations of the LLJ were important to Central US MCS formation. Follow-on work by Maddox (1983), restricted to a subset of ten mature storm systems, confirmed this notion, finding that “strong low-level convergence, warm advection, and ascending motion are present within the LLJ region in the

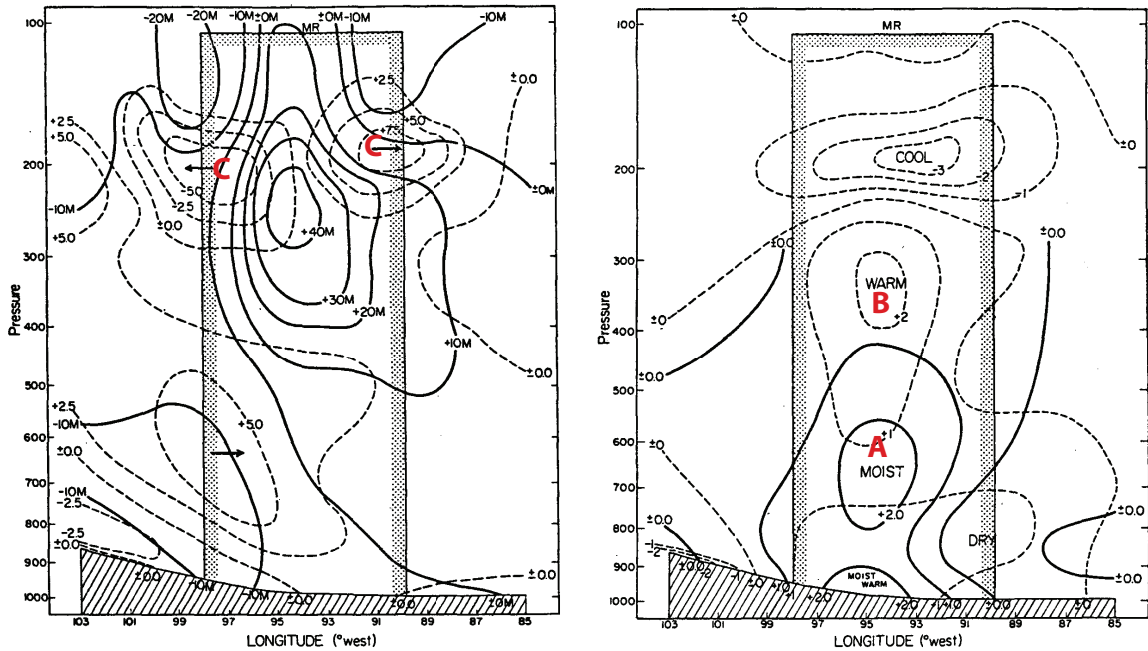


Figure 2.10: (Left) West to east cross section of mesoscale height (solid lines, in m) and zonal wind (dashed lines, in m/s) perturbations at the time of the MCC. (Right) West to east cross section of mesoscale temperature (dashed lines in °C) and moisture (solid lines, in g/kg) perturbations at the time of the MCC. Reproduced from Maddox (1981); Tripoli and Cotton (1989b).

environment prior to MCS development” (Stensrud, 1996).

The LLJ direction and speed fluctuate diurnally in a manner that converges more moisture at night. This is now thought to be a fundamental reason for the nocturnal phase of the Central US diurnal rainfall cycle (Stensrud, 1996). These LLJ fluctuations are in part a lagged semi-geostrophic wind response to the diurnally reversing horizontal pressure gradient anomaly caused by elevated daytime heating (nighttime cooling) over the Rockies (Holton, 1967). Inertial accelerations also kick in when surface turbulent boundary layer friction shuts off at sunset (Blackadar, 1957; Buajatti and Blackadar, 1957). The net effect of the accelerations associated with these diurnal changes in force balance is that the LLJ is most intense and most southerly (and hence most potential buoyancy laden with Gulf Stream humidity) in the middle of the night. The fundamental importance of the LLJ in supplying moisture preferentially at night to fuel Central US nocturnal MCS is a matter of record (Trier and Parsons, 1993; Stensrud, 1996; Trier et al., 2006).

Diabatic heating and balanced MCS mesoscale slantwise relative flow

Feature B in Figure 2.10 highlights a mid-to-upper tropospheric warm anomaly between 500 hPa and 250 hPa, to emphasize the importance of diabatic heating in MCS dynamics. The upper tropospheric warm anomaly is due to latent heat release (dominated by ice fusion aloft) during deep MCS convection. Beneath the warm anomaly, a lower tropospheric dry anomaly is the signature of substantial stratiform rainout, which is in turn associated with evaporative drying and cooling. Combined, these two features emphasize a fundamental aspect of MCS morphology inherent to their mesoscale dynamics - the combination of large scale stratiform anvil convection with a smaller scale deep convection zone embedded within it (Houze, 2004). The superposition of a convective diabatic heating vertical mode within a large scale high-level precipitating stratiform anvil mode results in a

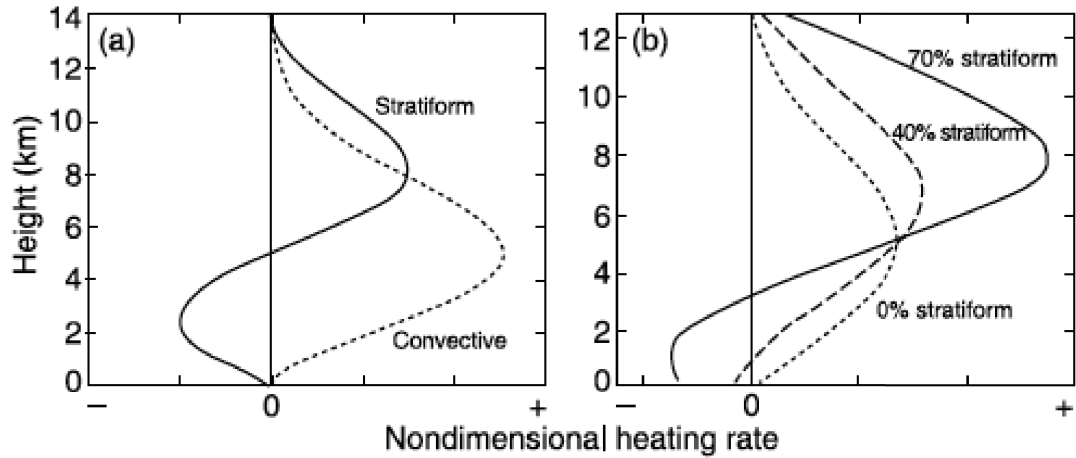


Figure 2.11: “(a) Idealized profiles of net heating associated with convective and stratiform precipitation in a mesoscale convective system. The x axis is nondimensional until precipitation amounts are specified for the convective and stratiform regions. (b) Profiles of net heating by a mesoscale convective system with different fractions of stratiform precipitation. Adapted from Schumacher et al. (2004).” Reproduced from Houze (2004).

characteristic “loaded gun” pattern of MCS diabatic heating on the environment. This net profile of diabatic heating is shown conceptually in Figure 2.12, where the solid line in panel b) shows the classic “loaded gun” profile of organized convection.

The “loaded gun” diabatic heating profile associated with MCS convection excites a spectrum of atmospheric waves that perturb the mean flow in the vicinity of an MCS in a fashion that helps sustain convection on timescales longer than the lifetime of individual convective cells (Houze, 2004). Pandya and Durran (1996) have shown with explicit linear gravity wave modeling that a characteristic storm-relative circulation, involving far-field (order hundreds of kilometers) slantwise ascending and descending motions, develops as a result of convectively generated gravity waves in response to the deep convective component of diabatic heating. Figure 2.12 schematically shows this characteristic MCS relative circulation struc-

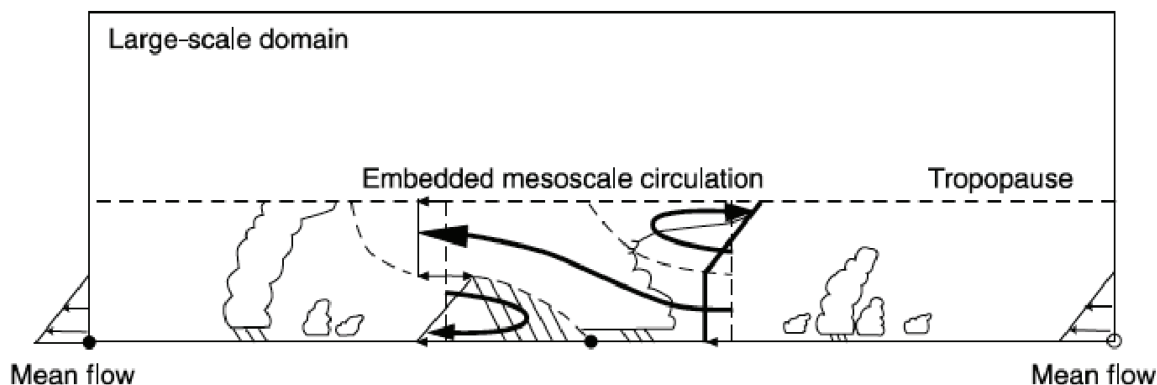


Figure 2.12: “Schematic diagram showing the airflow relative to a two-dimensional, steady state mesoscale convective system in a large-scale environment of given wind shear. The environmental air entering the updraft is potentially unstable, and there is a pressure decrease across the system from right to left at middle levels. The streamlines are those required by conservation of mass, momentum, entropy, and vorticity. Adapted from Moncrieff (1992).” Reproduced from Houze (2004).

ture. Such slantwise ascending mesoscale relative inflow ahead of, and slantwise descending inflow behind, has long been observed in the MCS environment (Houze, 2004). This relative flow regime emerges analytically from conserving mass, momentum, entropy and vorticity in the context of 2D steady-state balanced non-hydrostatic flow for an assumed propagating pressure disturbance (Thorpe et al., 1980; Moncrieff, 1981). This is compelling proof that slantwise relative mesoscale flow is fundamental to long-lived MCS convection³.

Balanced large scale flow and potential vorticity MCS dynamics

Feature C in Figure 2.10 highlights a pair of large-scale upper tropospheric zonal wind anomalies at 300 hPa. The corresponding meridional velocity anomalies (not shown) belie a large scale rotation that emphasize the importance of

³Interested readers can refer to a distilled theory by Moncrieff and colleagues, who present an archetypal dynamical model of this phenomenon (Moncrieff, 1992).

geostrophic adjustment to MCS diabatic heating for these disturbances. Tripoli and Cotton (1989a,b) point out the interesting fact that MCS processes transcend the critical length scale of the Rossby deformation radius L_R ,

$$L_R \approx \frac{c_g}{f}. \quad (2.1)$$

L_R describes how far a disturbance may spread out horizontally in steady-state (e.g. due to small scale dynamics like gravity waves) before achieving inertial balance on large scales. Here,

$$c_g = N/m \quad (2.2)$$

is the gravity wave phase speed in a stably stratified atmosphere with Brunt-Väisälä frequency N and vertical wavenumber m (Bretherton and Smolarkjewicz, 1989), and f is the Coriolis parameter. Tripoli and Cotton (1989b) point out that $L_R \approx 300$ km at 40 N, which falls in the middle of the MCS scale range. This has important dynamical implications:

For scales larger than L_R , the inertial restoring forces dominate the [convectively generated] gravity wave dynamics and this causes the wind to come into adjustment with the mass (or temperature) field. For scales smaller than L_R , the vertical stability of the atmosphere dominates the wave dynamics and so the mass field adjusts to the wind, or transient gravity oscillations are produced. [Tripoli and Cotton (1989a)]

Thus, in addition to the convectively generated gravity waves discussed previously, which are responsible for setting up slantwise relative flow on the mesoscale, the broader aggregate MCS diabatic heating pattern also projects onto large scale inertial dynamical modes. This provides a source of slow manifold memory on large scales that can play a role in sustaining MCS disturbances as they travel over large distances. From the perspective of potential vorticity dynamics, a sustained MCS convective heating generates changes in Ertel potential vorticity (P),

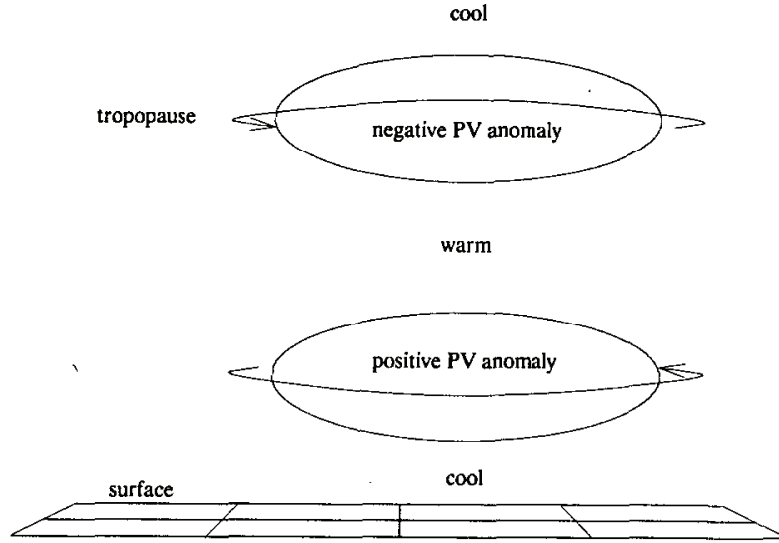


Figure 2.13: “Postulated structure of potential vorticity anomalies produced by a region of convection and the associated changes in temperature and wind structure. The circulation is cyclonic around the lower, positive anomaly, and anticyclonic around the upper anomaly as shown by the arrows.” Reproduced from Raymond and Jiang (1990).

$$P \equiv -g \frac{\partial \theta}{\partial p} (\zeta_{\theta} + f), \quad (2.3)$$

which are subsequently remembered by the flow and advected or distorted along with it (Raymond and Jiang, 1990; Li and Smith, 2010). Here g is gravitational acceleration, θ is potential temperature, and ζ_{θ} is the relative vorticity on a surface of constant θ . MCS latent heating initially influences P through changes in $\frac{\partial \theta}{\partial p}$. The sorts of relative circulations associated with a P anomaly generated by MCS latent heating in this fashion are illustrated schematically in Figure 2.13.

In a zonally sheared wind environment, isentropic surfaces are tilted in the height-latitude plane (due to the thermal wind relation) in such a way that cyclonic flow around the positive P anomaly causes motion upward along isentropes on the

eastern flank of the disturbance, due to northward motion, and subsidence behind it (Raymond and Jiang, 1990; Li and Smith, 2010). In this fashion, the balanced flow associated with convectively generated MCS potential vorticity anomalies produce lifting ahead of an MCS as it advects eastward. This is one proposed mechanism for large scale propagation (Raymond and Jiang, 1990).

The mountain-plains solenoidal circulation

Many of the wave-related MCS processes discussed above must be interpreted in light of a complicated, diurnally reversing, basic state solenoidal circulation in the lee of the Rockies. This circulation results fundamentally from the slope heating of the Continental divide and the front range of the Rockies, and is referred to as the “mountain-plains solenoid” (Carbone and Tuttle, 2008). Dirks (1969) first examined it numerically in a 2-D non-hydrostatic model with a sloping surface and an imposed diurnally oscillating surface potential temperature forcing. The characteristic daytime phase of this flow is shown in Figure 2.14. The thermally driven solenoidal flow reverses nocturnally, and is generally enhanced by stronger ambient shear and diminished by stronger ambient stability. Cotton and Anthes (1989) describe this circulation as follows:

At the juncture between the steep mountain slope and the more gentle sloping plains, two solenoidal circulations interact. Associated with the heated steep mountain slope, an intense deep solenoidal circulation develops with its upward branch focused over the mountain peaks and its downward branch centered over the transition between the mountain slope and the plains slope. Associated with the gentle sloping plains is another solenoidal circulation with its ascending branch just east of the sinking branch of the mountain solenoid and its subsidence branch located much farther east.[Cotton and Anthes (1989)]

In reality, the MPS is quite complex. Wolyn and McKee (1994) investigated the structure and dynamics of an idealized 2D mountain-plains solenoid in detail,

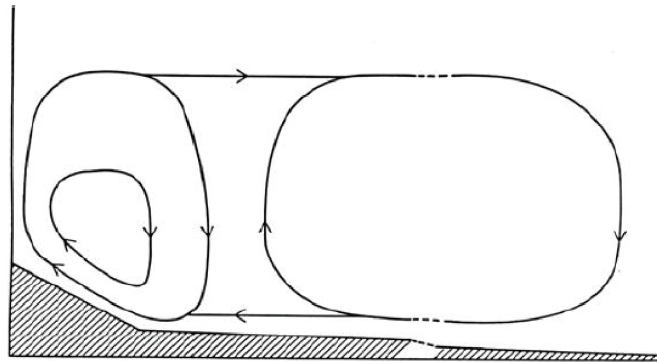


Figure 2.14: “Schematic illustration of the [height-longitude] structure of the idealized Rocky Mountain-Great Plains daytime circulation.” Reproduced from Cotton and Anthes (1989) (their Figure 9.39). Originally from Dirks (1969).

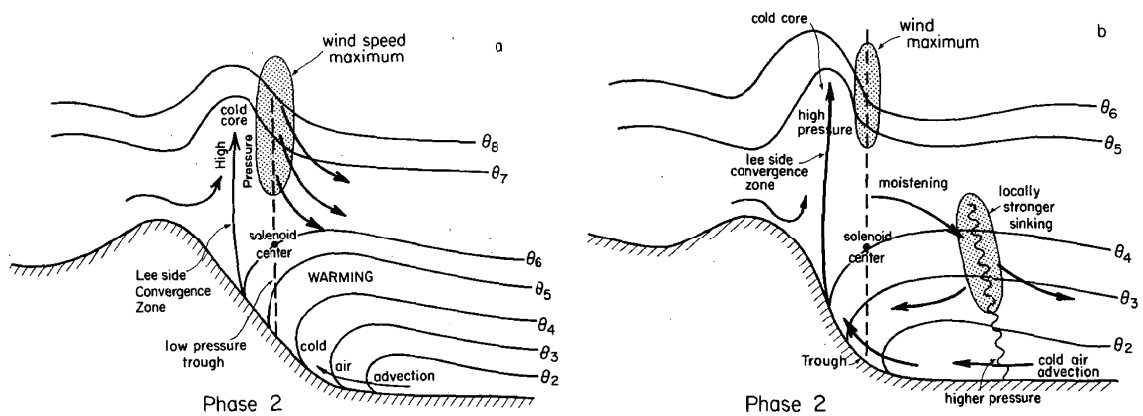


FIG. 12. Conceptual diagrams for phase 2: (a) stage 1, and (b) stage 2.

Figure 2.15: Conceptual schematic of major physical processes involved in the 2D structure of an idealized mountain-plains solenoidal circulation in the lee of the Rockies. Reproduced from Wolyn and McKee (1994) (their Figure 12).

using radiosonde observations in the Central US as boundary and initial conditions for a state of the art cloud resolving model. Figure 2.15 shows their conceptual model of the MPS, emphasizing an interplay between several competing physical processes. Chimney slope flows interact with the stationary mountain wave flow, resulting in a leeside convergence zone linked to upward motion, mass convergence aloft and compensating adiabatic subsidence warming at midlevels to the east.

The eastern daytime subsidence component of the MPS circulation over the Great Plains is especially important for the physics of the Central US nocturnal rainfall maximum. It is associated with a subsidence inversion (barrier to vertical motion), which traps daytime boundary layer surface buoyancy over a vast area (Carbone and Tuttle, 2008). The CAPE generated by daytime solar insolation thus accumulates and is focused into a narrow leeside zone by upslope surface density flows (Dirks, 1969; Tripoli and Cotton, 1989a) where it has the capacity to be rapidly injected to mountain convection, occasionally (in conditions of conducive wind shear) resulting in long-lived nocturnal MCS events.

Summary of Central US nocturnal MCS chronology

The current understanding of the nocturnal summer rainfall maximum in the Central United States is that it results from several competing physical mechanisms that conspire to phase lag rainfall 180 degrees relative to the solar insolation cycle. A contemporary conceptual chronology follows:

- Two regional circulations focus CAPE generated from daytime insolation over the Great Plains into a narrow leeside zone adjacent to the Rockies. First, large-scale daytime subsidence associated with the “Mountain Plains Solenoid” (MPS) circulation produces a subsidence inversion (barrier to vertical motion) over the Great Plains, trapping daytime surface buoyancy over a vast area (Carbone and Tuttle, 2008). Second, this CAPE accumulates

and is focused into a narrow leeside zone by upslope surface density flows (Dirks, 1969; Tripoli and Cotton, 1989a).

- Meanwhile, afternoon cumuli are initiated by chimney convergence (gravitational density flows) over small scale peaks in the Rockies (Dirks, 1969). The mountain cumuli move east where they sometimes intercept and tap the narrow leeside reservoir of accumulated Plains buoyancy (Tripoli and Cotton, 1989a). When embedded in a large scale zonal wind basic state that is vertically sheared and conducive to organized convection, this occasionally leads to upscale growth and organization into MCSs (Tripoli and Cotton, 1989a).
- The mesoscale dynamics of organized convective systems prolong and intensify convection in a coherent ensemble that continues to move east, both through advection by the mean zonal westerlies, and through the action of convectively generated gravity waves and/or density currents associated with evaporative rainshafts, constrained by background slope flow circulations (Bernardet and Cotton, 1998; Tripoli and Cotton, 1989a,b).
- As the MCS moves east of the leeside convergence zone, access to the surface reservoir of accumulated daytime buoyancy decreases and eventually shuts off when it encounters the Plains capping inversion (Tripoli and Cotton, 1989a).
- In the event that the MCS is at a special latitude zone, it can encounter a new fuel source to draw on at the terminus of a potential energy rich long-range southerly low-level jet (LLJ) overlying the capping inversion (Tuttle and Davis, 2006; Trier et al., 2010).
- Three main factors in turn favor nocturnal intensification for such organized convective systems:

1. The LLJ direction and speed fluctuate diurnally in a manner that converges more moisture at night.
2. The Mountain-Plains solenoidal circulation reverses at night; over the Plains, daytime descent reverses to large scale ascent at night, removing the subsidence barrier to convection for MCSs that survive into the night (Carbone and Tuttle, 2008).
3. During the day, convectively generated gravity waves (CGWs) emanating from MCSs escape to deposit their energy in the stratosphere. But at night, these gravity waves are instead ducted horizontally by a refractivity layer associated with efficient nocturnal cloud top radiative cooling of MCS anvil clouds (Tripoli and Cotton, 1989a). Propagating outward horizontally, these CGWs can seed new convective cells, expanding the MCS convective heating structure to large horizontal scales, where it can accelerate self-sustaining geostrophic wind and potential vorticity anomalies (Tripoli and Cotton, 1989b; Raymond and Jiang, 1990).

2.1.4 A controversial aspect of Central US nocturnal rainfall

What mechanisms primarily underly the climatological eastward rate of MCS motion in the Central US, which situates the climatological nocturnal rainfall maximum where it is observed?

Carbone et al. (2002) were the first to clearly pose this question as a challenge for the community, in which they set up a dialectic that has had a lasting impact on recent literature. In it, they pointed out that the phase speed of the observed eastward moving radar composite backscatter signal (Figure 2.9) contains a propagating component relative to the mass weighted vertically integrated background tropospheric flow. Interestingly, the apparent propagation speed could equally well

be explained by appealing to gravity wave dynamics as it could be by appealing to density current dynamics. Indeed, both density currents and gravity waves are known to play a role in observed and explicitly simulated organized convection propagation at the level of individual systems.

Carbone et al. (2002) asked the interesting question of which mechanism (gravity waves, or cold pools) is primarily responsible for the observed nocturnal rainfall phase speed in the Central US climatological composite. Researchers in numerical weather prediction and the cloud resolving modeling community have since argued extensively on opposite sides of Carbone’s debate (Tuttle and Carbone, 2004; Schumacher and Johnson, 2005; Tian et al., 2005; Wilson and Roberts, 2006; Trier et al., 2006; Weckwerth and Parsons, 2006; Ashley et al., 2007; Lang et al., 2007). Recently, Matsui et al. (2010) claimed that only the gravity wave mechanism could consistently explain new observations of zonal variations in the phase speed of composite US rainfall propagation, but the controversy continues.

An alternative school of thought attributes the apparent rate of eastward Central US rainfall propagation primarily to “slow manifold” processes. From this perspective, sustained MCS diabatic heating excites potential vorticity anomalies that, owing to the characteristic vertical structure of organized convective heating, are maximized in the mid-troposphere. As a result the mid-level zonal winds primarily control the system eastward motion simply through zonal potential vorticity advection. From this perspective, the apparent system propagation relative to the mass weighted vertically integrated background flow discussed above is just an illusion. Evidence supporting this viewpoint includes the fact that some MCS events have been observed to switch intermittently back and forth from a gravity wave- vs. a density current-dominated propagation regime (William Cotton; personal communication). Other observations show systems disappearing and then reappearing or regenerating farther east (Tuttle and Carbone, 2004).

One interpretation of these findings is that there is a more fundamental “glue”

holding things together on larger scales, i.e. that fast manifold processes like density currents and gravity waves operate within a broader dynamical envelope. This mechanism was advocated in the 2D explicit convection study of Tripoli and Cotton (1989a) and formalized in terms of potential vorticity dynamics by Raymond and Jiang (1990). Recently, Li and Smith (2010) presented an observational argument for this slow-manifold mechanism based on seasonal differences in the relationships between the diurnal phase structure of NARR PV, and a high density network of raw surface pressure and surface temperature observations. Remarkably, they claim an eastward drifting PV anomaly and pressure signal is present in all seasons, but just doesn't drive precipitation in the winter season.

In some sense, the answer to Carbone's debate almost certainly lies somewhere in the middle. Gravity waves and cold pools both modulate convection and interact with broader modes of slow-manifold dynamics in the atmosphere. However, the debate is not entirely a false one - it is a constructive way to think about cumulus parameterization and focusing on deficiencies in the representation of rainfall processes in numerical weather and climate models, which need improving (see next section). The debate is worth reviewing here, since **a major result of this dissertation will be a new contribution to it**, via the discovery of a propagating nocturnal convection signal within a global modeling framework that limits the scale over which fast manifold processes can operate in a new way.

2.2 Distortions of diurnal rainfall in global climate models

A robust diurnal rainfall cycle is an important test of a GCM's model physics and thus the reliability of climate change projections, but current generation models do not capture the diurnal rainfall cycle (IPCC, 2007). The utility of the diurnal

rainfall mode as a strong constraint on physical approximations used in GCMs is described in Section 2.2.1. This is followed by a review of the most widely used cumulus parameterization in current GCMs (Section 2.2.2) and the distortions produced in the global and central US simulated diurnal rainfall cycle when this type parameterization is deployed in a climate model (Section 2.2.3).

2.2.1 An integrative constraint on global model physics

Diagnostics of the global diurnal cycle of precipitation and cloud cover provide an excellent integrative litmus test for the fidelity of the many interactive cloud, land surface, radiative transfer, and boundary layer parameterizations in GCMs and weather prediction models (Knievel et al., 2004). The diagnostic utility of the diurnal rainfall cycle is reviewed above because **a major contribution of this dissertation is the discovery of several improvements in simulated diurnal rainfall in a prototype next generation GCM that represents sub-grid convection in a new way.**

Yang and Slingo (2001) sum up the philosophy behind focusing on diurnal rainfall as an important GCM diagnostic:

The most fundamental modes of variability of the global climate system are the diurnal and seasonal cycles, which are associated with large and well-defined variations in the solar forcing. As basic, forced modes of the climate system, the ability of [GCMs] to represent these cycles should be a key test of the correctness of any model.... an accurate representation of the diurnal cycle over land and ocean provides a key test of many aspects of the physical parameterizations in a climate model, from radiative transfer and surface exchanges through to boundary layer, convective, and cloud processes. [Yang and Slingo (2001)]

As described in Section 2.1.1, despite being driven by a simple forcing, the observed diurnal rainfall response is complex because there are a wide variety of

cloud-atmosphere-surface interactions operating differently in different parts of the world. Designing a suite of parameterizations that gets these inter-relationships correct in all regimes is an enormous challenge. Proof that it has not been solved is evident in the common practice within the regional high resolution atmospheric modeling community, of switching convection parameterizations based on the location of a limited domain simulation, in accordance with known locally dominant controls on convection. This is a luxury that cannot be afforded in global climate change simulations, which inherently require a “one size fits all” approach to treating sub-grid physics. As an example, Dai et al. (1999) enumerate some of the physics that must be accurately simulated by the sub-grid models in a GCM to capture diurnal rainfall physics:

...for a climate model to correctly simulate the diurnal cycle in summer precipitation, it has to:

1. properly simulate the regional and large-scale circulations, especially the low-level convergence field;
2. produce realistic cloud cover evolution and cloud optical thickness so that the diurnal cycle at the surface can be captured correctly; and
3. generate subgrid moist convection at the proper frequency and intensity so that the model atmosphere can maintain the correct [convective available potential energy]. [Dai et al. (1999)]

Importantly, distortions of the simulated diurnal rainfall cycle can have far-reaching and counter-intuitive consequences on other aspects of climate simulated by GCMs. For instance, surface rainfall is associated with clouds, which strongly affect atmospheric radiation, and release latent heat of condensation or fusion in the atmospheric column. Thus distortions in the daily timing of peak rainfall are a symptom of accompanying distortions in other components of the energy budget, with consequences for the mechanisms supporting simulated mean climate and thus its sensitivity to external forcing. Wilson and Mitchell (1986) provide one clear example:

...diurnal variations affect surface and atmospheric fluxes of energy (Bergman and Salby, 1997), water (Trenberth et al., 2003), and momentum (Dai and Deser, 1999). For example, because surface solar heating typically has a sharp midday peak, precipitation that occurs during the day evaporates from the surface more rapidly than that at night. This changes the fraction of rainfall involved in runoff versus evaporation and the partitioning of surface energy into latent and sensible heat fluxes. Climate models without a diurnal cycle cannot simulate these nonlinear processes, resulting in degraded model simulations [Wilson and Mitchell (1986).]

Many more pathways could be envisioned in which biases in diurnal rainfall could nonlinearly “cascade” onto mean climate energetics and adversely distort simulations of climate sensitivity. Getting the diurnal rainfall cycle correct is clearly an important test for a GCM to pass.

2.2.2 The Arakawa-Schubert cumulus parameterization

How are the many unresolved physical processes that result in rainfall represented in a climate model? This is the classic “cumulus parameterization problem,” which is illustrated conceptually in Figure 2.16, and formally defined as a quest to

... [formulate] the statistical effects of moist convection to obtain **a closed system for predicting weather and climate**. [Arakawa (2004)]

The **closure** process, i.e. formulating the statistical effects of sub-grid moist convection in terms of resolved large-scale variables, is a crucial, but not necessarily well-posed part of the problem. The various closure assumptions introduced in the cumulus parameterization process can have a large impact on the overall simulation. This is evident in the fact that much of the spread in the ensemble of GCM projections reviewed in the latest IPCC synthesis can be traced to differences in the way they approximate the effects of sub-grid convection (Bony and Dufresne, 2005).

Many modern moist convection parameterizations in GCMs mimic an approach originated by Arakawa and Schubert (1974) (Arakawa, 2004). This approach uses a “quasi-equilibrium” (hereafter QE) closure, i.e. it assumes that an ensemble of detraining clouds exists in statistical, thermodynamic near-equilibrium with a **local** measure of large-scale potential instability, such as convective available potential energy (CAPE). While early observational campaigns in the tropics suggested QE was a reasonable approximation for unorganized tropical deep convection on sufficiently long timescales (Arakawa and Schubert, 1974), more recent work has shown that local QE breaks down in midlatitudes (Zhang, 2002). It is easy to imagine how a concept like QE ought to break down conceptually as computers become faster and grid scales become smaller (i.e. part of the statistical effects of convection occur non-locally) and as timesteps decrease (i.e. non-equilibrium characteristics of convection become important to its interaction with resolved dynamics). Indeed, Jones and Randall (2011) quantitatively show through explicit simulation that the approach in general breaks down for spatial scales less than about 250 km and timescales less than about 30 hours. Nonetheless, most modern climate models still use a QE-based convective closure to handle deep convection, based on the Arakawa and Schubert (1974) scheme, and as such the approach is reviewed here. In practice, a triggering threshold CAPE value is required before the scheme becomes active, such that it is not called to represent extremely shallow convective regimes.

Randall et al. (1997), summarized the key elements of the Arakawa-Schubert parameterization algorithm below. Interested readers may refer to their distilled contemporary description of the interior workings and design philosophy of the approach, some of which will be reviewed here.

[Arakawa and Schubert] used a very simple cumulus cloud model to formulate the eddy fluxes ... in terms of **a convective mass flux and the differences between the in-cloud and environmental soundings**. [They] allowed the possibility that many different “types”

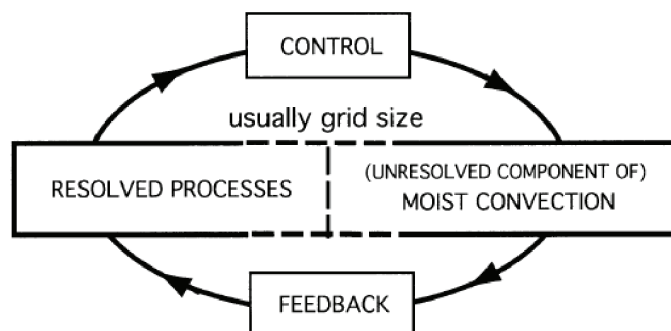


Figure 2.16: “A schematic diagram showing interactions between resolved processes in a model and (the unresolved component of) moist convection. The formulation of the right half of the loop represents the cumulus parameterization problem.” Reproduced from Arakawa (2004) (Figure 3a).

[i.e. size categories] and they **considered the contribution of each cloud type to the eddy fluxes, the convective net condensation rate, and the convective precipitation rate.** They introduced a **highly idealized but explicit model for the interactions of the cumuli with the sub-cloud layer.** Finally, they proposed a **closure assumption to determine the intensity of convective activity, as measured by the cloud-base mass fluxes for each of the cloud [size categories].** [Randall et al. (1997) p. 285]

A sub-grid cloud parameterization necessarily makes some assumptions about the geometry of the ensemble of clouds that are not being resolved. One novelty of the Arakawa-Schubert approach is that the assumed ensemble is a spectrum of hot towers of varying heights, representing in total a small fraction of the total grid box cell area. This idea is visualized in Figure 2.17, and basically is inspired by unorganized deep tropical convection over the ocean. The inclusion of the degree of freedom of varying cloud heights within the ensemble is an advantage of the Arakawa scheme that gives it flexibility, allowing for a wider spectrum of possible

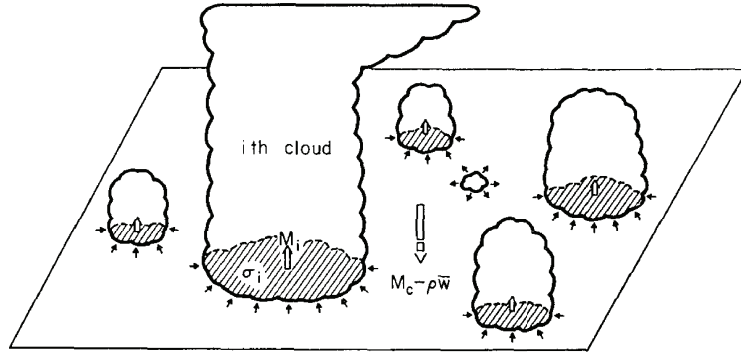


Figure 2.17: Conceptual schematic of the assumed geometry of hot towers in Arakawa-Schubert-type moist convection parameterizations. Reproduced from Arakawa and Schubert (1974) (their Figure 1).

sub-grid convective feedbacks than other convective schemes, but which comes at the cost of slightly more computational overhead (UCAR, 2009).

The specific formulation of a deep convection parameterization inherently restricts possible interactions of sub-grid cloud effects with the environment to a subset of predefined pathways. The behavior of the parameterization, and the diabatic forcing that it incurs on the resolved scale dynamics, are strongly sensitive to the degrees of freedom in these assumptions (UCAR, 2009). Within the physical assumptions in the classical Arakawa-Schubert scheme:

- the environment between the clouds is assumed to be instantaneously subsiding (warming and drying) to balance the vertical convective mass fluxes in the clouds.
- All cloud bases are assumed to originate at the top of the planetary boundary layer and inherit its properties at cloud base.
- The temperature profile in the cloud is assumed identical to the environ-

ment⁴.

- Environmental air is assumed to be entrained into clouds through their lateral boundaries; equivalently, all clouds have a convective vertical mass flux profile that decays exponentially with height.
- Cloudy air is detrained only at a cloud top location that is diagnosed for each ensemble member at its level of neutral buoyancy based on a one dimensional undilute⁵ buoyant parcel model.

The ensemble solution is closed by an iterative numerical solution under the constraint that the combined effect of the ensemble members must deplete CAPE at a specified timescale according to local QE. This becomes an implicit problem that can be solved with numerical methods (Zhang and McFarlane, 1995).

From the perspective of this dissertation, a key concern is the net heating and moistening effect that a sub-grid convection package induces on the host GCM in response to a potentially unstable resolved large scale tendency⁶. Figure 2.18 illustrates an example of the sort of thermal and moisture anomalies that a conventional Arakawa-Schubert type of convection scheme induces on the large scale host model in response to deep convective instability. Overall stabilization is typically small in amplitude, due to many compensating effects within the clouds versus the environment, which allows the large scale resolved forcing to continually destabilize and precipitate under appropriate circumstances (UCAR, 2009). Compensating

⁴This concept is also inspired by tropical dynamics. As the Coriolis parameter vanishes, the Rossby deformation radius becomes very large. In other words, unlike the midlatitudes, fast manifold processes in the tropics rapidly spread convective thermal anomalies in clouds throughout the inter-cloud environment, such that in-cloud temperature profiles are similar to the environment (Sobel et al., 2001)

⁵The assumption of undilute ascent in the diagnosis of the level of neutral buoyancy produces some unrealistic effects, making the amount of convective adjustment in some sense too sensitive to planetary boundary layer properties, and not sensitive enough to the humidity of environmental air in the mid-troposphere (Christopher Bretherton, personal communication)

⁶As we will see, this effect can change dramatically if the sub-grid parameterization is replaced with an explicit embedded model of convection

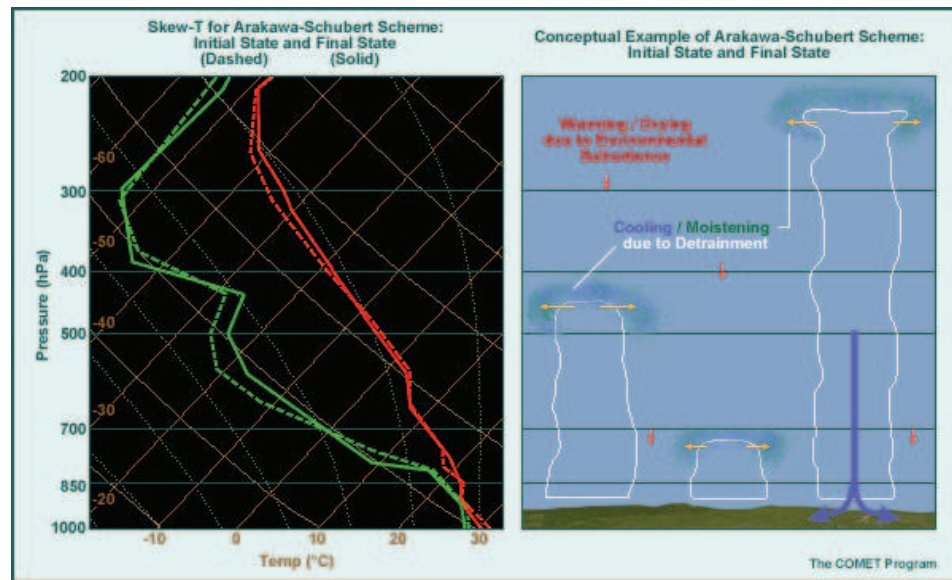


Figure 2.18: Representative example of the stability adjustment incurred on a forecast or climate model due to the influence of an Arakawa-Schubert type convection parameterization. Reproduced from (UCAR, 2009).

subsidence in the environment dominates the overall mid-tropospheric response to convection, through warming and drying. Moistening occurs in the upper atmosphere where the clouds are assumed to detrain at their cloud tops.

Implementation in the Community Atmosphere Model

This dissertation will involve several new analyses of a widely used, well-characterized, mature GCM called the Community Atmosphere Model (CAM) version 3.0. It will also involve analysis of several unofficial prototype versions of CAM, one of which is based on a new CAM development version (NCAR software version tag 3.5.32; hereafter CAM3.5) created in January of 2008. Some relevant specifics of the deep convection parameterization details in these two versions of CAM are therefore reviewed here.

In CAM3.0, Zhang and McFarlane (1995) (hereafter ZM95) implemented a modified version⁷ of the Arakawa-Schubert deep convection parameterization. In addition to the basic features reviewed above this implementation also included a representation of restabilization of boundary layer air by convective downdrafts. In this implementation, clouds detrain moisture only “above a mid-tropospheric minimum of moist static energy... ensuring that the cloud top detrainment is confined to the conditionally stable portion of the atmospheric column” (Collins et al., 2004). The QE closure assumption requires CAPE to be removed by deep convection with a 2 hour timescale. The scheme is only activated if local CAPE is greater than a threshold value of 70 J/kg.

In CAM3.5, the deep convection scheme was updated to relax an approximation that was recognized to make deep convection too insensitive to the environmental humidity in the mid-troposphere (Zhang et al., 2010). The one-dimensional buoyant parcel model in the deep convection parameterization in CAM3.0 unreal-

⁷Interested readers may refer to Section 4.1 of Collins et al. (2004) for a full description of the ZM95 scheme used in CAM3.0.

istically assumed undilute ascent inside the cloud. To account for the influences of environmental entrainment on cloud detrainment height, as of April of 2007 (CAM development version 3.4.11) a modification to ZM95 was merged onto the main code trunk of CAM by Richard Neale at the National Center for Atmospheric Research. This involved the addition of a dilution assumption to the buoyancy calculation in the one-dimensional parcel model. Dilute ascent was modeled based on the stochastic mixing model of Raymond and Blyth (1992). This modification provided a missing pathway for resolved dry anomalies to inhibit the vigor (depth) of sub-grid convective towers through entrainment mixing at their lateral boundaries. One improvement that resulted was a decrease in overly simulated deep convection, and an increase in infrequently simulated congestus convection (Zhang et al., 2010). As discussed below, this had consequences for simulated diurnal rainfall.

In the following section, several known distortions of the diurnal rainfall cycle in CAM3.0 and CAM3.5 are reviewed. It is worth mentioning that in June of 2010, a new version of CAM was released, which employs new methods for dealing with cumulus parameterization. However, due to its recent release and the fact that its simulated diurnal cycle has not yet been systematically investigated (Rich Neale, personal communication) this version is beyond the scope of this dissertation.

2.2.3 Distortions of the diurnal rainfall mode in the Community Atmosphere Model

Figure 2.19 demonstrates a classic diurnal rainfall problem that happens in climate models that use QE-based cumulus parameterizations. The figure is reproduced from Dai and Trenberth (2004), who compared the local time of maximum JJA precipitation simulated by the Community Climate System Model v. 2 (right) against observations (left). Attention should be limited to land masses in the tropics and the northern hemisphere (summer) portion of this plot, over land,

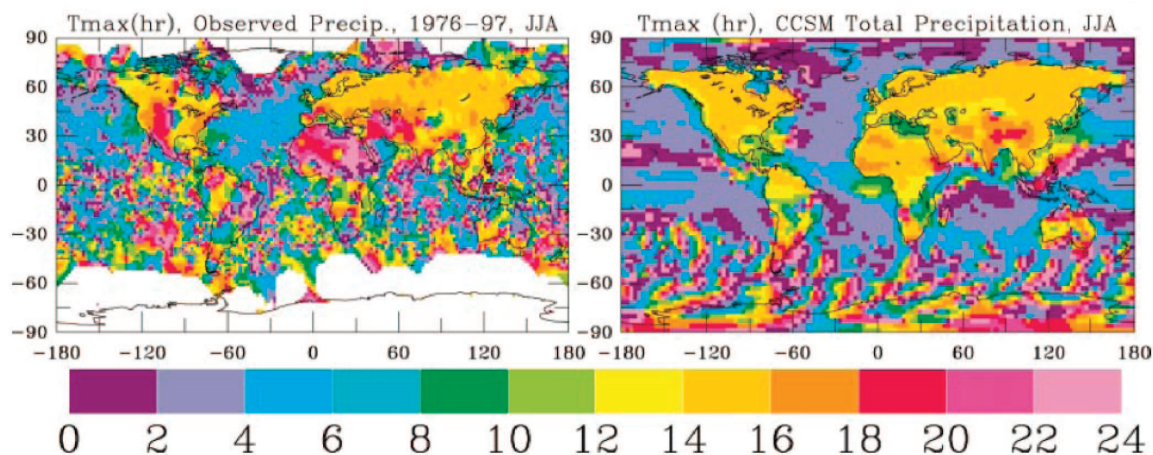


Figure 2.19: “(left) The [local solar time (hours)] of the [maximum] of the [fitted 24-hour] harmonic of .. observed ... JJA ... total precipitation. (right) Same as (left) but for [Community Climate System Model v.2]-simulated ... total precipitation.” Reproduced from Dai and Trenberth (2004) Figure 12.

where the diurnal mode is a strong contributor to the total rainfall variance (not shown). Whereas observations indicate a late afternoon to evening maximum in rainfall, with substantial regional variability, the climate model simulates a diurnal rainfall cycle that is nearly sun-synchronous (peaks at local noon) everywhere.

Figure 2.20 shows the same erroneously sun-synchronous simulated continental rainfall timing documented from CCSM2 above persists in contemporary CAM3.0 and CAM3.5 simulations today. In addition to the premature timing of continental convection, current versions of the Community Atmosphere Model have too high an amplitude of diurnal rainfall (Figure 2.20b,c). This can be seen in the African and South American observational comparisons (Figure 2.20c). The high amplitude bias has been partially corrected by the dilution assumption introduced in the convection modifications in CAM3.5, but the rainfall local timing bias persists.

Distortions in the diurnal rainfall cycle in CAM are linked to broader biases in the frequency and intensity of surface rainfall in atmospheric models that use

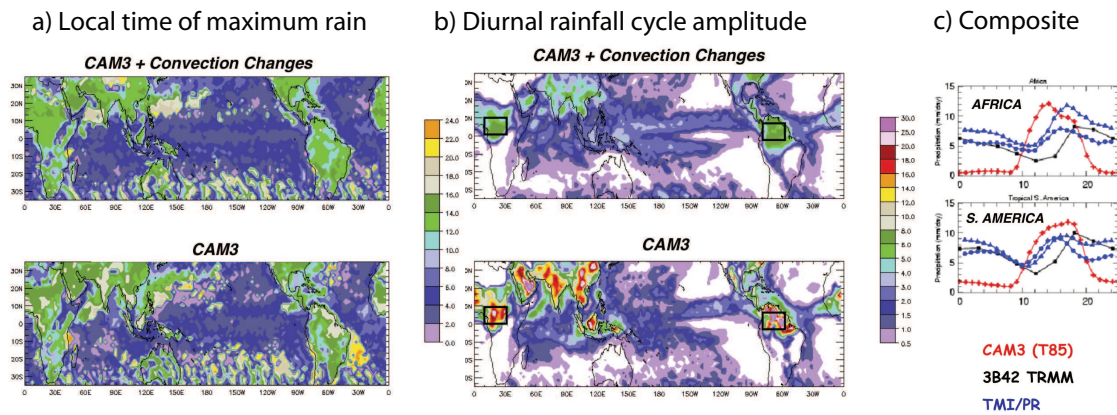


Figure 2.20: The composite 1984 JJA diurnal rainfall cycle a) time of maximum rainfall (local hour), and b) amplitude (mm/day), as simulated by (bottom) CAM3.0 and (top) CAM3.5 (which added an entrainment dilution assumption to the Arakawa-Schubert cumulus closure scheme). c) The simulated diurnal rainfall cycle in CAM3.0 (red line) over two regional diurnal amplitude hot spots, compared against two modern climatological observational products - a microwave rainfall product (TMI; blue lines) and a merged multi-satellite product (3B42 TRMM; black line). Adapted from Neale (2007).

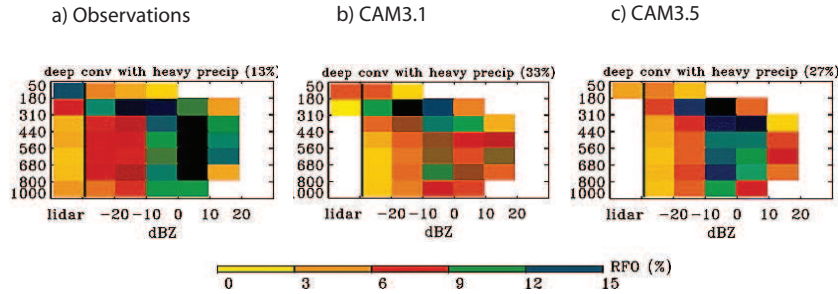


Figure 2.21: Height-dependent relative frequency of occurrence (colors, percentage) of a deep heavily precipitating objective statistical cluster regime of convection comparing (a) joint spaceborne lidar and radar measurements against (b,c) two current versions of the Community Atmosphere Model run through instrument simulators. The higher frequency of occurrence of this regime overall in the models (33% and 27%) compared to observations (13%), and especially at high reflectivity values, is statistical evidence that CAM rains too intensely, too frequently. Adapted from (Zhang et al., 2010) (their Figures 3, 5 and 7).

cumulus parameterization. Such models are well known to produce deep, heavily raining precipitation too infrequently (Guichard et al., 2004; Sun et al., 2006; Grabowski et al., 2006). There is a colloquial adage that GCMs rain “too frequently, too weakly”. Figure 2.21 illustrates this deficiency in the Community Atmosphere Model from a recent cluster analysis of convective statistics relative to two modern spaceborne active sensing rainfall datasets. Zhang et al. (2010) show the relative frequency of occurrence of a deep convective regime that occurs in both nature and the model but with different frequency. Whereas this regime of heavily precipitating convection accounts for only 13% of total convection in nature (Fig. 2.21a), in CAM3.0 it occurs three times as often (Fig. 2.21b). The addition of the dilute buoyancy assumption in the Arakawa-Schubert deep convection parameterization in CAM3.5 produces a modest improvement from this perspective.

Distortions of the statistics of rainfall intensity and frequency, and the structure

of diurnal rainfall, are not unique to CAM, but exhibited by many modern GCMs used for climate projection, as indicated in the latest synthesis report of the IPCC,

Sun et al. (2006) investigated the intensity of daily precipitation simulated by 18 [Atmosphere-Ocean coupled] GCMs, including several used in [the 2007 IPCC Fourth Assessment] report. They found that most of the models produce light precipitation ([less than] 10 mm/day) more often than observed, too few heavy precipitation events and too little precipitation in heavy events ([greater than] 10 mm/day). [IPCC AR4 Section 8.5.2],

and in a recent synthesis study of the diurnal cycle:

...it is difficult for ... GCMs to capture the diurnal cycle of deep convection, in terms of both magnitude and phase, over the land as well as over the ocean (Dai et al., 1999; Lin et al., 2000; Yang and Slingo, 2001; Betts and Jakob, 2002). Interestingly, all these studies detected a time lag in the diurnal cycle of deep convection simulated by large-scale models, with convective rainfall occurring too early during daytime compared with observations. [Guichard et al. (2004)]

Guichard et al. (2004) led a European community effort to understand the reasons for the premature timing of deep convection in several European GCMs that use cumulus parameterization. Their strategy was to drive single column model (SCM) versions of multiple GCMs using different cumulus parameterizations with lateral advection and surface flux forcings derived from an intensive field campaign during conditions of locally forced convection observed at the Atmospheric Radiation Measurement (ARM) site in the Central US. By focusing on a time period in which the diurnal cycle at ARM was forced primarily by local surface fluxes, they avoided the many complications (e.g. non-local, non-equilibrium thermodynamics) associated with Central US MCS. By comparing the SCM convection simulations (which consistently rained too early) to explicit cloud resolving models forced identically (which rained more realistically in the afternoon) they distilled

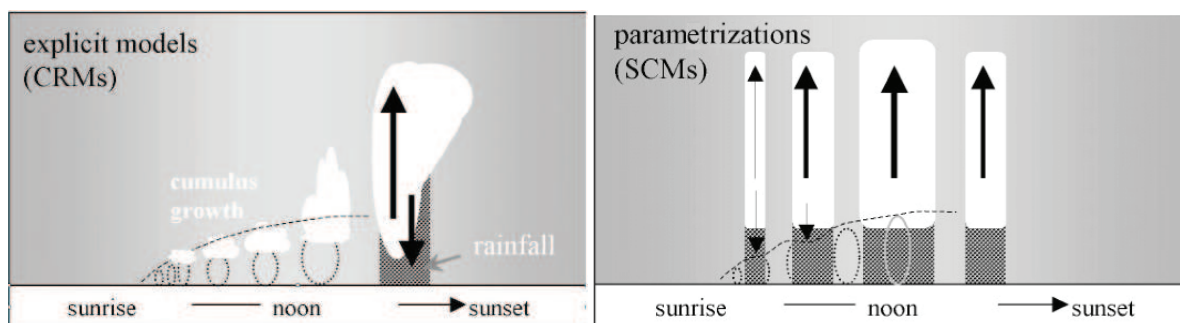


Figure 2.22: “Schematic view of the diurnal cycle of [continental locally forced] precipitating convection, as simulated by [an ensemble of 2D cloud resolving models] and several [GCMs run in single column model mode]. The boundary layer convection (thermals) is represented by the dotted curves on both schemes, as it partly relies on the turbulence in the CRMs with a two-kilometer horizontal resolution”. Reproduced from Guichard et al. (2004).

several lessons regarding the deficiency of the cumulus parameterizations in representing locally forced continental convection in the presence of high CAPE.

Figure 2.22 demonstrates the most important conceptual schematic that arose from the Guichard et al. (2004) model intercomparison experiment. Despite high ambient CAPE, the CRMs tended to convect very modestly in the early morning, producing a shallow layer that deepened as local surface heating ramped up near local noon, gradually eliminating convective inhibition. A phase lag of several hours for deep precipitating convection in the CRM simulations appeared to be related to entrainment preconditioning, i.e. moisture detrained from shallow convective thermals would thermodynamically pave the way for successive generations of thermals to reach higher levels, until ultimately attaining their lifted condensation level and accessing the overlying CAPE. In contrast, the GCM behavior was to begin raining early in the morning, and intermittently firing very deeply, often “attaining the level of neutral buoyancy within a single timestep”. Guichard et al. (2004) emphasized that, while the GCM deep convection parameterization was

designed to represent a specific regime of convection (tropical unorganized deep hot towers) to successfully simulate the continental diurnal cycle it would need to actually represent:

... a succession of [convective] regimes, from dry to moist non-precipitating to precipitating convection... [all of which] equally play a part in this complex transitory phenomenon [and whose]... representation involves an ensemble of parameterizations, and how they interact together. Concerning deep convection [parameterizations] more precisely, one might expect improvements from:

- the introduction of triggering factors relying more on the boundary layer convective activity than simply on low-level convective instability criteria,
- stronger sensitivity of convection to the moisture field
- a better treatment of convective downdrafts, and
- the representation of the finite time of cloud development.

[Guichard et al. (2004)]

2.3 Next generation multi-scale climate modeling

In this section, a candidate prototype next generation global modeling technique is discussed, which alters the way that clouds are represented in global models, in an attempt to meet many of the challenges facing conventional cumulus parameterization identified above. The technique is called “cloud superparameterization (SP)”, and the global models that employ it are called “Multi-scale Modeling Frameworks (MMFs)” (Randall et al., 2003). In many ways, this dissertation is concerned with the potential opportunities that this new strategy offers for improving diurnal rainfall physics for global climate projection.

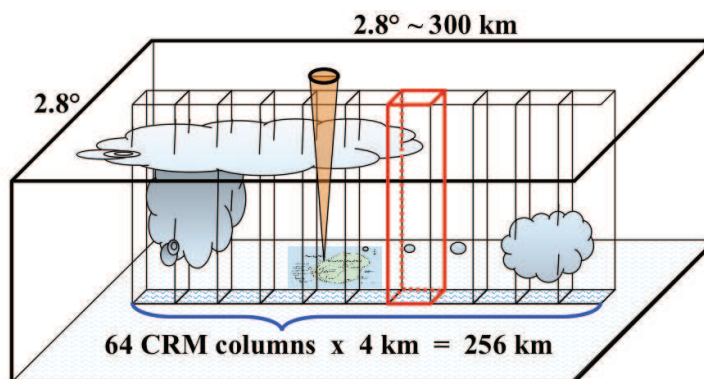


Figure 2.23: Schematic showing the typical configuration of the two resolved scales in the superparameterization approach to representing clouds in climate models. The outer box represents a single grid column of the host exterior model. The inner boxes represent the interior grid points of the embedded explicit convection model, arranged conventionally in two dimensions, and with a “cloud system resolving model” (CSRM) horizontal resolution of several kilometers. The lateral boundaries of the interior model are periodic. Reproduced from (Ovtchinnikov et al., 2006) (their Figure 1).

2.3.1 Concept

Multi-scale Modeling Frameworks (MMFs) are GCMs that use thousands of embedded idealized 2D cloud process resolving model arrays to calculate sub-grid cloud and boundary layer adjustments to resolved dynamics, instead of conventional statistical parameterizations like the Arakawa-Schubert algorithm (Randall et al., 2003).

Figure 2.23 shows the grid design philosophy in a single column of a multi-scale climate model. The outer resolved scale (exterior wire frame box) has a horizontal resolution typical of current generation climate prediction models, on the order of 100 to 200 km. As in GCMs, at the outer resolved scale of MMFs, the predicted variables like temperature, water vapor, pressure, etc. represent averages on 100-200 km scales. In GCMs, the “sub-grid” is handled using statistical param-

eterizations to represent the unresolved effects of boundary layer turbulence and clouds. In MMFs, the sub-grid is instead handled using “super-parameterization”, i.e. by embedding an interior high resolution model as represented by the interior wire frame boxes in the figure. The embedded model is driven by the resolved scale tendencies of the outer model, and statistics harvested from its convective response replace the conventional quasi-equilibrium parameterizations for estimating sub-grid fluxes of heat and moisture due to clouds used in conventional GCMs (Grabowski and Smolarkiewicz, 1999).

In keeping with common practice in the literature, in this dissertation the interior model will be referred to as a “Cloud Resolving Model” (CRM) though in reality it does not resolve all of the important eddies important to cloud-scale dynamics. Although the governing equations admit such motions, in practice the interior model is run with a “coarse” (from the perspective of cloud modelers) horizontal resolution on the order of 1 to 4 km. In other words, the “CRM” explicitly predicts the evolution of the largest of mesoscale updrafts and downdrafts, but itself parameterizes the effects of small scale updrafts and downdrafts, and the eddies that typically mediate cloud-environment mixing. Alternately the interior model is called a “Cloud System Resolving Model” (CSRМ) or more vaguely a model of “explicit convection”. Typical applications of MMFs arrange the interior grid columns in a straight line, oriented either in the east-west direction or the north-south direction, such that the interior domain is two dimensional. The governing equations of the interior model contain terms that do not exist in the scaled hydrostatic primitive equations of the exterior model, representing explicit non-hydrostatic meso-scale dynamics.

One of the most practical advantages of MMFs is that, despite being hundreds of times more expensive to run than GCMs, they are thousands of times less computationally expensive to run than fully global “cloud resolving” models. They are also much more scaleable than GCMs (Khairoutdinov et al., 2005) on parallel

computers, a technical necessity for such an expensive model. Parallel scalability is won at the expense of arguably severe physical idealizations in the interior CRM:

1. under-sampling space (reducing dimensionality) and
2. enforcing periodic lateral boundary conditions (resolved clouds that drift out the edge of a CRM array re-appear upstream).

As a result of 2, the additional calculations incurred by solving cloud-scale dynamics are self-contained in each grid column of the outer model, such that they can be carried out in parallel on different processors, with no cloud-scale information transmitted between adjacent CRMs. Distributing the calculation in this fashion is key to the technical success of the MMF approach (Grabowski and Smolarkiewicz, 1999). Thanks to this scalability, MMFs can already achieve climate-scale integrations in an affordable wall clock time using hundreds to thousands of modern processors. MMFs are envisioned as an interim research tool for the next two to three decades before global cloud resolving models are affordable (Randall et al., 2003).

2.3.2 History

The cloud super-parameterization idea was originated in a mesoscale simulation of a tropical squall line by Grabowski and Smolarkiewicz (1999). In this initial implementation, the exterior model was configured in a limited domain of 400×400 km with 40 km horizontal resolution and 25 km vertical resolution, and driven by large scale forcings derived from radiosonde array observations during the GATE field campaign in the tropical Atlantic. The interior model was arranged in a 2D $x - z$ plane, with 1 km horizontal resolution, and 1/3 km vertical resolution. Remarkably, as shown in Figure 2.24, the technique successfully simulated the propagation of a precipitating squall line that transcended adjacent CRM arrays.

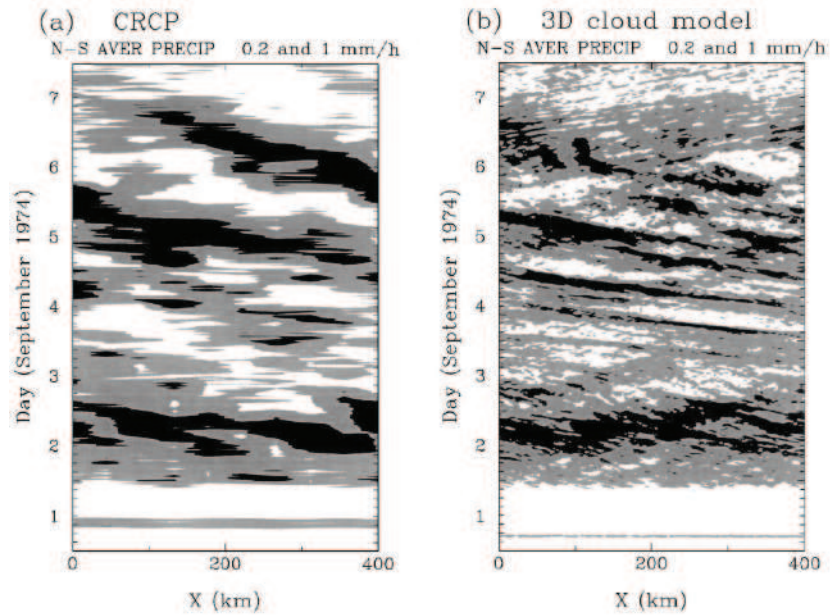


Figure 2.24: “Hovmöller ([longitude-time]) diagrams of the [north-south] averaged surface precipitation rate from (a) the experiment using [the cloud superparameterization] approach and b) the experiment using the 3D cloud resolving model. Precipitation intensity larger than 0.2 and 1 mm/h is shown using light and dark shading, respectively”. Reproduced from Grabowski and Smolarkiewicz (1999) Figure 3.

The super-parameterization approach was re-visited in the context of larger scale simulations in Grabowski (2001), who explored the sensitivity of an idealized 2D zonal Walker cell flow to the horizontal resolution of the outer model. They emphasized that the representation of organized convection in the 2D Walker cell, and of 3D tropical squall lines, was strongly sensitive to the horizontal resolution of the exterior model (alternatively, the interior model’s zonal extent), and did not converge cleanly to the explicit CRM answer. However, the average properties of mean large scale ascent and descent regime thermodynamics in the 2D Walker cell flow did appear to converge. Based on this resolution sensitivity analysis, Grabowski advocated that the super-parameterization approach might be most realistically applied when the host model uses a coarse (order 100 km) resolution, such that the interior domains are large enough to admit convective organization.

Grabowski (2001) was also the first to attempt a global MMF simulation, on an idealized aqua-planet with grossly simplified radiative transfer, in which he discovered the potential of the super-parameterization approach to admit more realistic convectively coupled tropical wave dynamics than current GCMs. He discovered a curiously robust intra-seasonal signal reminiscent of the Madden Julian Oscillation (MJO)⁸. This would be a turning point in the atmospheric modeling community’s interest in the super-parameterization approach.

Super-parameterization took a first step towards becoming a community research tool when Khairoutdinov and Randall (2001) embedded a 2D version of their cloud resolving model into the National Center for Atmospheric Researchs (NCAR) Community Atmosphere Model (CAM) v3.0, a widely used climate model with a sophisticated land-surface model, realistic sea surface temperatures, continents, topography, and vegetation. This new MMF was named SP-CAM3.0⁹, for

⁸The Madden-Julian Oscillation is a pulse of precipitating tropical deep convection, representing the largest mode of natural intraseasonal variability in the tropical atmosphere. The rainfall and intrinsic persistence of the MJO are poorly simulated in most modern global climate and weather models.

⁹CAM currently has several alternative formulations of its atmospheric dynamical core, but

Super-Parameterized CAM, and will be the subject of considerable analysis in this dissertation.

The cloud resolving model embedded in SP-CAM3.0 is described in Khairoutdinov and Randall (2003). Briefly, it solves the non-hydrostatic momentum equations of fluid dynamics using the anelastic approximation (i.e. filtering sound waves from the governing equations to allow a longer time step). Prognostic thermodynamic variables include the liquid/ice water moist static energy, total precipitating and total non-precipitating water. The model tracks precipitating water partitioned using a thermal condition into snow, graupel, and rain water categories, but with simple bulk microphysics. The lateral boundary conditions of the CRM domain are periodic. The embedded model operates in a nested time integration with a time step 50 to 100 times shorter than the host model's outer time step, depending on model configuration¹⁰. The CRM stores its state between successive iterations. Vertical fluxes of heat, moisture and precipitation are fed back to the host model, and drive large scale dynamical tendencies, which are applied as persistent boundary conditions that force the following steps cloud-resolving integration.

CRM momentum transport is not coupled to the large-scale model in almost all published applications of the MMF, including SP-CAM3.0, purportedly due to the unrealism¹¹ of 2D turbulent momentum transport. It can be argued that this choice of approach is somewhat unsatisfactory. On this view, one may note that organized convection, notably MCS, transports horizontal momentum counter-gradient (mean-flow acceleration) in certain atmospheric layers and down-gradient (mean-flow deceleration) in other layers. Then the two-dimensional organized convective momentum transport as formulated by Moncrieff (1992) is consistent with

SP-CAM3.0 was built around the semi-Lagrangian, spectral scheme.

¹⁰For example, in a typical application with the outer model configured at T42 triangular spectral truncation (400-700 km effective resolution) and 32 horizontal CRM points spaced 4 km apart, the inner CRM time step is 20 seconds and the outer GCM time step is 30 minutes.

¹¹In 2D, or geostrophic turbulence, similarity theory suggests the enstrophy, or momentum, transport is upscale, rather than downscale as is the case in 3D.

the quasi-linear geometry typical of an MCS. In support of this view, it can be pointed out that Kingsmill and Houze (1999) examined the momentum fields in all MCSs observed by airborne Doppler radar in TOGA-COARE. They showed that even though MCSs in nature are three-dimensional, the fundamental properties of 2D vertical momentum transport remain. Surely further research will be needed to settle this point conclusively and to establish all the advantages and disadvantages of the choice of not allowing the embedded CRM to transmit momentum effects upscale in the MMF. At the present early state of development of MMFs, this and many other tentative model architecture decisions may need to be revisited in light of future experience.

Unlike Grabowski's original work, in which the exterior model represented an atmospheric toy model with severe approximations for surface and radiative processes, the creation of SP-CAM marked the first time the super-parameterization technique was deployed in a modern GCM with realistic radiation and surface models. Flagship results presented in Khairoutdinov and Randall (2001) were a stable simulated climate, with improved representation of the climatological rainfall in the south Pacific convergence zone, a notorious challenge for conventional CAM3.0. At this early stage of development, the prognostic boundary layer parameterization in CAM was left untouched, and the radiative transfer calculations were not linked to the new information of sub-grid cloud variability and overlap in the CRM.

By 2003, it was apparent that SP-CAM admitted much improved MJO variability in the tropics (Randall et al., 2003). At this point David Randall from Colorado State University led an effort to rally community support to explore the super-parameterization in more detail. Among the many persuasive justifications emphasized in this "advocacy" piece were the following:

[Unlike, conventional climate models, super-parameterized climate models..]

- ... explicitly simulate deep convection, including mesoscale organization (e.g., squall lines), downdrafts, anvils, etc.
- ... explicitly simulate fractional cloudiness, down to a scale of a few kilometers.
- ... explicitly simulate cloud overlap in [both] the radiative ... [and] microphysical sense
- ... explicitly simulate the convective enhancement of the surface fluxes...
- ... explicitly simulate convectively generated gravity waves.
- ... can provide global simulations of the statistics of mesoscale and microscale cloud organization

[Randall et al. (2003)]

One year later (by 2005), development of SP-CAM had progressed to the point where the climate model's radiation code was explicitly linked to the sub-grid information content in the embedded CRM. As a result, SP-CAM became the first model with the computational potential to explicitly simulate cloud radiative feedbacks to climate change on long timescales, a critical unsolved problem in climate science. A series of offline sensitivity experiments by Cole et al. (2005a) demonstrated that separately calculating radiative effects on each column of the CRM independently gave a substantially different domain average result than calculating radiative effects on the CRM domain average cloud profile¹². Their offline tests also indicated that, at least at the nominal 4 km horizontal resolution of the CRM, fully 2D Monte-Carlo ray-tracing radiative transfer (i.e. accounting for multi-dimensional radiative transfer effects) did not add much additional benefit to the radiative transfer simulation results¹³. Ever since, the computationally

¹²This was to demonstrate that making the sorts of assumptions about sub-grid cloud geometry commonly used in GCMs, such as maximal random cloud overlap, is an inferior strategy compared to the MMF approach of explicitly simulating sub-grid cloud geometry and its response to large scale forcings.

¹³Cole et al. (2005a) cautioned that 2D radiative transfer would likely become increasingly important if the embedded CRM's horizontal resolution was increased substantially

costly radiative transfer calculations have been done using the independent column approximation in SP-CAM's embedded CRM fields (i.e. computing radiative transfer through each column of the CRM independently). Cole et al. (2005b) discussed several sensitivity experiments that varied the way in which radiation was interactively coupled to the CRM in online SP-CAM experiments, emphasizing the superior potential of the super-parameterization approach to represent cloud-radiative feedbacks on a seasonal scale, relative to conventional methods:

This ... raises the bar for conventional radiative transfer parameterizations: not only must they yield unbiased domain-average radiative fluxes (which almost all parameterizations fail to do...), they must also represent local interactions between radiation and clouds. This is a tremendous challenge because it implies that in conventional GCMs the parameterizations of cloud amount, radiative transfer, and cloud-scale dynamics must be coupled, and their equations solved simultaneously. [Cole et al. (2005b)]

In July of 2006, the National Science Foundation began funding a new ten-year Science and Technology Center called the Center for Multiscale Modeling of Atmospheric Processes (CMMAP), led by David Randall at Colorado State University. The Center funds two dozen graduate students¹⁴ and about a hundred researchers from multiple US institutions, to explore and develop a variety of promising next generation prototype climate simulation technology. Since its inception, interest and publications about the super-parameterization approach to atmospheric modeling has grown dramatically (see Figure 2.26). As a result of CMMAP research, SP-CAM's simulated climate has now been scrutinized on several timescales and under several configurations (see next section). The results have been encouraging enough that NCAR is now internally exploring strategies to incorporate super-parameterization into future versions of their Community Earth System Model (Richard Neale, personal communication).

¹⁴Most of this dissertation research was funded by CMMAP, and shares the spirit of a broader

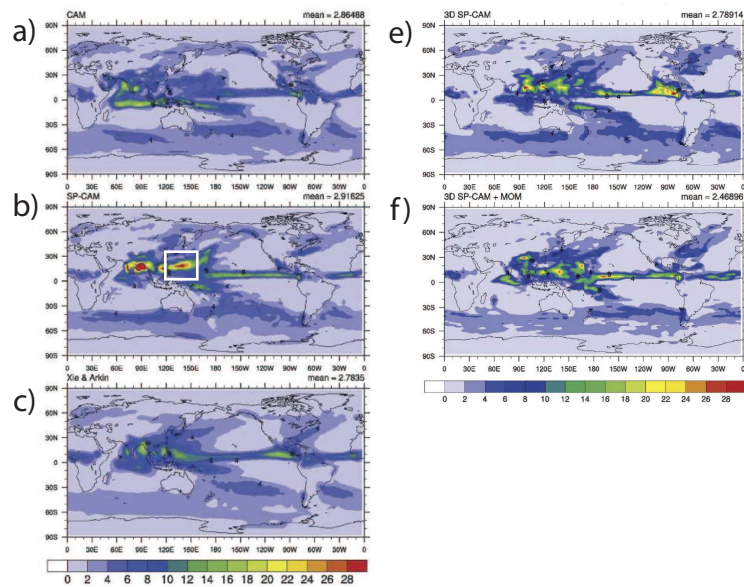


Figure 2.25: Climatological JJA precipitation simulated in response to prescribed sea surface temperatures by a) conventional CAM3.0, b) SP-CAM3.0 with a 2D zonally oriented CRM, showing the simulated “Great Red Spot” precipitation bias in the white box, compared to c) observations and d)-e) SP-CAM3.0 with a 3D embedded CRM d) without versus e) with interactive momentum coupling across the two resolved scales. Adapted from Khairoutdinov et al. (2005) (their Figures 3 and 16).

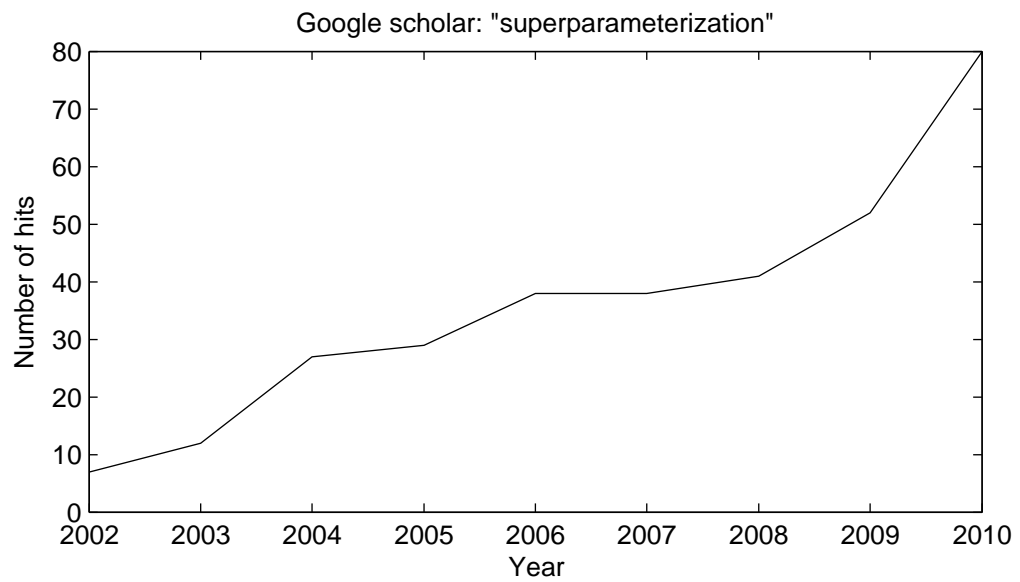


Figure 2.26: Number of hits from peer reviewed articles or conference papers containing the word “superparameterization”, by year, as indicated by a Google Scholar search initiated on June 1, 2011

2.3.3 SP-CAM’s simulated climate

SP-CAM3.0 simulates a stable climate with mean state thermodynamic biases on the same order as conventional CAM3.0. The first publication showing detailed aspects of SP-CAM3.0’s simulated climate was by Khairoutdinov et al. (2005), as calculated from a short (from the climate perspective) preliminary 500-day simulation with prescribed sea surface temperatures¹⁵. The authors emphasized that in many ways, the simulated climate in SP-CAM3.0 looked surprisingly reasonable, especially considering that they had dramatically overhauled the way sub-grid convection was handled without significant re-“tuning” of unconstrained model parameters thereafter (Khairoutdinov et al., 2005). Top of the atmosphere radiative balances were shown to be in approximate balance, and the patterns of simulated mean relative humidity and rainfall looked overall no less reasonable than they had in conventional CAM3.0. Simulated temperature and relative humidity biases in the climatological mean state were of the same order in the two models.

One promising aspect of SP-CAM3.0’s climatology was an improvement in the intermittency and intensity statistics of simulated rainfall. This was particularly evident in diagnostics of the climatological probability distribution function of simulated rainfall rate as a function of intensity, which were compared against baseline climate-quality records at three well instrumented field sites (DeMott et al. (2007); see Figure 2.27).

Khairoutdinov et al. (2008) later showed dramatic evidence that cloud super-parameterization robustly improves the spectrum of simulated tropical convectively coupled atmospheric wave motions¹⁶. By organizing two decades of simulated out-

initiative of the Center to explore the potential and limitations of the super-parameterization concept, in this case focusing on diurnal timescales.

¹⁵This baseline SP-CAM3.0 climatology has since been superseded by an 18-year climatology with a meridionally oriented 2D CRM in Khairoutdinov et al. (2008)

¹⁶In this new 18-year baseline climatology simulation, as with almost all SP-CAM simulations

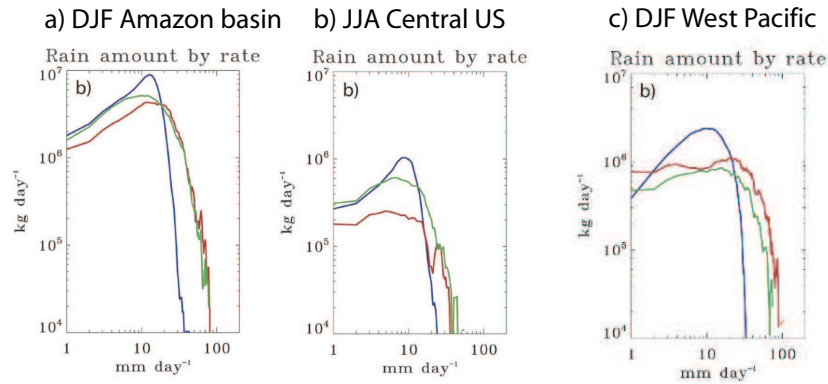


Figure 2.27: “... daily mean rainfall rate distributions for GPCP [observations] (green), CAM (blue), and MMF (red) [showing rainfall rate expressed as a] contribution to seasonal rainfall total as a function of rainfall rate” for a) the Amazon Basin, b) the Central United States and c) the Western Pacific. The embedded explicit convection approach to climate simulation tends to improve the intermittency and intensity statistics of rainfall. Adapted from DeMott et al. (2007) (their Figures 2-4).

going long-wave radiation (OLR; a deep convection proxy) fluctuations into its temporal variance binned by space- and time-scale, the authors achieved a compact vantage point from which to evaluate the climate model’s internal tropical large scale convective variability against satellite observations. The results of this analysis were striking, and are reproduced in Figure 2.28¹⁷. Remarkably, distortions in the convectively coupled tropical Kelvin wave speed due to the cumulus parameterizations in CAM (right panel) appear to be corrected by the cloud super-parameterization approach. Missing OLR intraseasonal variance in the MJO regime (low positive wavenumber, low positive time frequency) in the conventional GCM appears when super-parameterization is employed.

since it, the embedded 2D CRM was oriented meridionally, as it was argued that this mitigated to some degree the Great Red Spot JJA rainfall bias

¹⁷It should be noted that because it shows only the signal-to-noise ratio, this figure masks the fact that SP-CAM’s MJO OLR variance itself is somewhat over-simulated (not shown)

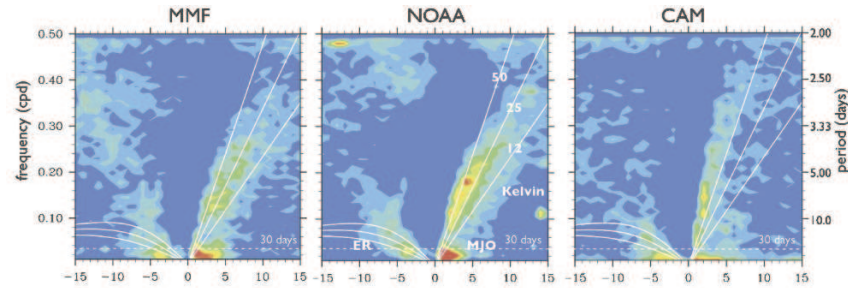


Figure 2.28: “The symmetric raw spectral power divided over the background power (signal-to-noise ratio spectrum) for the ... [outgoing longwave radiation (OLR)] ... as (left) simulated by [SPCAM3.0], (middle) derived from observations, and (right) simulated by [CAM3.0]. Superimposed are the theoretical shallow-water dispersion curves for the equatorial Rossby and Kelvin waves for the equivalent depths of 12, 25, and 50 m. Contour interval is 0.1, with contours beginning at 1. Observations are 1979–2004 NOAA Advanced Very High Resolution Radiometer-interpolated OLR data (Liebmann and Smith, 1996)”. SPCAM3.0 was integrated from 1986–2003 and configured with 30 vertical levels, a spectral semi-Lagrangian dynamical core (T42 truncation) with a 30-minute timestep in the external resolved scale, and 32 interior grid CSRM columns arranged in a meridional 2D periodic array with a 20 s timestep. Reproduced from (Khairoutdinov et al., 2008) (their Figures 8 and 9)

The improvements in rainfall statistics, and tropical wave motions in SP-CAM were also accompanied by some perplexing new problems in its simulated climate. The most notable, emphasized by Khairoutdinov et al. (2005), are regional precipitation biases in SP-CAM’s tropical rainfall climatology during boreal summer (JJA). The most extreme of these has become known to CMMAP as the “Great Red Spot¹⁸”. Basically, it is an anomalous blob of simulated precipitation in the northwestern tropical Pacific that occurs for mysterious reasons during JJA (see Figure 2.25). Khairoutdinov et al. (2005) has shown that this bias structure is quite sensitive to the orientation and configuration of the embedded CRMs. In their follow-on 18 year simulation, Khairoutdinov et al. (2008) confirmed the existence of the Great Red Spot and further showed through analysis of the simulated annual cycle harmonic that SP-CAM contains a distorted “super-monsoon” in south Asia overall. In general, the Western Pacific, Bay of Bengal, and Asian monsoon rainfall during JJA are a weak point of SP-CAM simulations forced by prescribed SSTs¹⁹.

Important biases have also been documented in the microphysical and radiative properties of SP-CAM3.0’s simulated tropical cloud fields. An early evaluation of simulated cloud fraction histograms against ARM data in the Tropical Western Pacific hinted that high clouds are simulated too frequently in SP-CAM3.0, but cautioned that the scale representativeness of the observations versus the embedded

¹⁸The causes of the Great Red Spot and super-monsoon JJA precipitation bias structures in superparameterized climate simulations are still unresolved and an area of active research. Luo and Stephens (2006) initially hypothesized that they might be caused by a superactive convection-evaporation-wind feedback that allows precipitation to get out of control, perhaps due to local recycling of large convective events caused by the use of cyclic boundary conditions in regions of mean horizontal convergence. Khairoutdinov et al. (2005) showed that the Great Red Spot bias is quite sensitive to the configuration of the embedded CRM grid array (zonal 2D, meridional 2D, versus fully 3D with or without momentum super-parameterization; see Figure 2.25). Stan et al. (2010) showed that the bias is mitigated to some degree through coupling to an interactive ocean model.

¹⁹Interestingly, these are also regions where prototype global cloud system resolving models (i.e. atmospheric models with uniform 1-4 km resolution) contain systematic, mysteriously overactive mean rainfall biases.

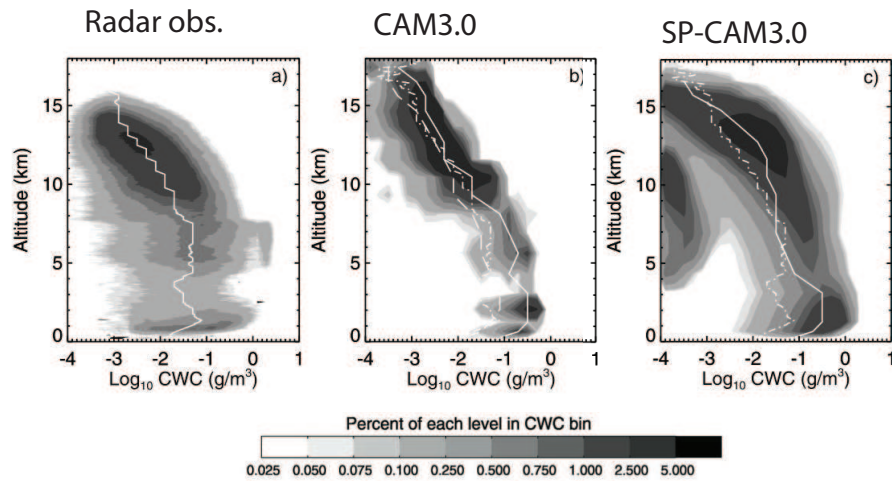


Figure 2.29: “Frequency distributions of in-cloud [cloud water content (CWC)] at Manus from (a) ARM retrievals, (b) CAM model, [and] (c) [SP-CAM3.0] model. The shading represents the percentage of radar retrievals or model gridboxes at each level that fall within the given CWC bin. The frequency distributions are normalized such that the sum of each level is 100%. Clear layers are included in the normalization although not shown in the plot. The median CWC of the cloudy points at each level is also indicated by the solid lines. The dashed line in (b) represents the median of the grid-box average CWC in the CAM. The ARM median CWC is also [super-imposed on the model plots] for comparison purposes”. Adapted from McFarlane et al. (2007) (their Figure 4).

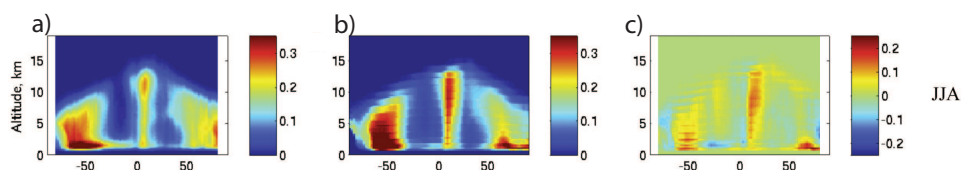


Figure 2.30: “Intensity plots of seasonal zonal profiles of radar hydrometeor fraction ($\text{dBZe} > -27.5$) [showing a) CloudSat observations, b) SP-CAM] ... simulated radar output, and [c) the] difference (model simulation - observation). Vertical axis is height above mean sea level (in km), and horizontal axis is latitude. CloudSat is a near-nadir-pointing instrument and so does not obtain full pole-to-pole coverage. The radar also suffers from ground clutter effects and is unable to detect most cloud with in 1.2 km of the surface... Missing detections near the surface due to surface clutter are accounted for in the radar simulation process.” Adapted from Marchand et al. (2009b) Figure 1.

CRM were not equivalent (Ovtchinnikov et al., 2006). Subsequently, McFarlane et al. (2007) used height-resolved cloud water content retrievals from a vertically pointing radar at a tropical ARM station as a baseline for SP-CAM validation. Figure 2.29 shows the probability density of the cloud water content in the observations and simulations from their analysis. On the one hand, improvements due to cloud super-parameterization were evident in that SP-CAM3.0’s cloud population appeared less unrealistically bi-modal than CAM. On the other hand, this analysis confirmed that both tropical high clouds and tropical boundary layer clouds extended too high in SP-CAM3.0’s atmosphere and with too much condensate. McFarlane et al. (2007) showed that these climatological cloud property biases in the tropics were associated with severe distortions in the tropical cloud-related radiative heating balance, relative to inferred heating rate profiles from ARM observations (see their Figure 13).

Biases in the simulated cloudiness of SP-CAM’s embedded CRM have since been characterized in detail by researchers affiliated with CMAP using instrument simulator techniques to handle problems like scale representativeness in com-

paring to observations (Zhang et al., 2008; Marchand et al., 2009a,b; Marchand and Ackerman, 2010). This approach emphasizes a secondary advantage of the MMF approach, which is that the interior cloud resolving model contains *small-scale information* that opens new doors for doing meaningful satellite intercomparison²⁰. It is now well recognized that SP-CAM3.0 “produces too much high and thin cloud, especially above 10 km [as a] common feature of the model in convective regions” (Marchand et al., 2009a) and, in many cases, low clouds that are too optically thick and too close to the ground (Marchand and Ackerman, 2010). In a validation of SP-CAM against the emerging high quality CloudSat space-borne radar climatological record of global cloudiness, Marchand et al. (2009b) provide a spectacular perspective on these characteristic simulated cloud biases in SP-CAM3.0. Figure 2.30 illustrates the results; the bias anomaly on the right panel clearly shows the preponderance of high clouds that are too thick and high in convecting regions, and dense optically thick low clouds in the subtropics. In summarizing their analysis, the authors also provide the following excellent contemporary review of the state of simulated clouds in SP-CAM3.0:

[SP-CAM] does a good job of reproducing the broad [radar reflectivity] pattern of tropical convergence zones, subtropical belts, and midlatitude storm tracks, as well as their changes in position with the annual solar cycle. Nonetheless, the comparison also reveals a number of model shortfalls including (1) excessive hydrometeor coverage at all altitudes over many convectively active regions, (2) a lack of low-level hydrometeors over all subtropical oceanic basins, (3) excessive low-level hydrometeor coverage (principally precipitating hydrometeors) in the

²⁰In contrast, GCM comparisons to satellite data using instrument simulator techniques require sub-grid “generators”—algorithms that assume unresolved distributions of hydrometeor occurrence that are important to account for in the net radiative transfer calculation. Whereas in conventional models these must be rigidly prescribed, in the MMF approach such distributions are harvested from the embedded CRM. Interestingly, the embedded CRM also contains useful additional *dynamical* information about 2D mesoscale convective organization, which has not traditionally been analyzed in MMF diagnostic studies. Chapter 6 will break new ground on this front.

midlatitude storm tracks of both hemispheres during the summer season (in each hemisphere), and (4) a thin band of low-level hydrometeors in the Southern Hemisphere of the central (and at times eastern and western) Pacific in the MMF, which is not observed by CloudSat. This band resembles a second much weaker ITCZ but is restricted to low levels. [Marchand et al. (2009b)]

2.3.4 SP-CAM’s diurnal rainfall cycle

Excluding (including) the work in this dissertation, six (nine) papers have been published documenting aspects of the simulated diurnal rainfall cycle using the multi-scale modeling framework approach to climate simulation (Khairoutdinov et al., 2005; McFarlane et al., 2007; DeMott et al., 2007; Khairoutdinov et al., 2008; Zhang et al., 2008; Tao et al., 2009; Pritchard and Somerville, 2009b,a; Pritchard et al., 2011). To put the research in this dissertation in appropriate context, a review of the pre-existing extent of understanding of the robustness of the MMF diurnal cycle structure, and the physical mechanisms supporting and distinguishing it from conventional climate simulations, follows.

The first hint of improved diurnal rainfall variability using the MMF approach to climate simulation was demonstrated by Khairoutdinov et al. (2005). Figure 2.31 (left panel) shows their comparison of the simulated seasonal (JJA) local time of maximum precipitation in CAM3.0 and SP-CAM3.0 against the baseline rain gauge observational record of Dai (2001)²¹. Beyond remarking on the improved timing of rainfall over land in SP-CAM3.0, in this study the authors did not explore or discuss which aspects of cloud super-parameterization were responsible for the improvement.

McFarlane et al. (2007) subsequently analyzed the diurnal cycles of cloudiness, precipitation, and cloud radiative heating rate profiles at a single tropical

²¹Recall Figure 2.1 and the associated discussion in Section 2.1.1 regarding this observational product.

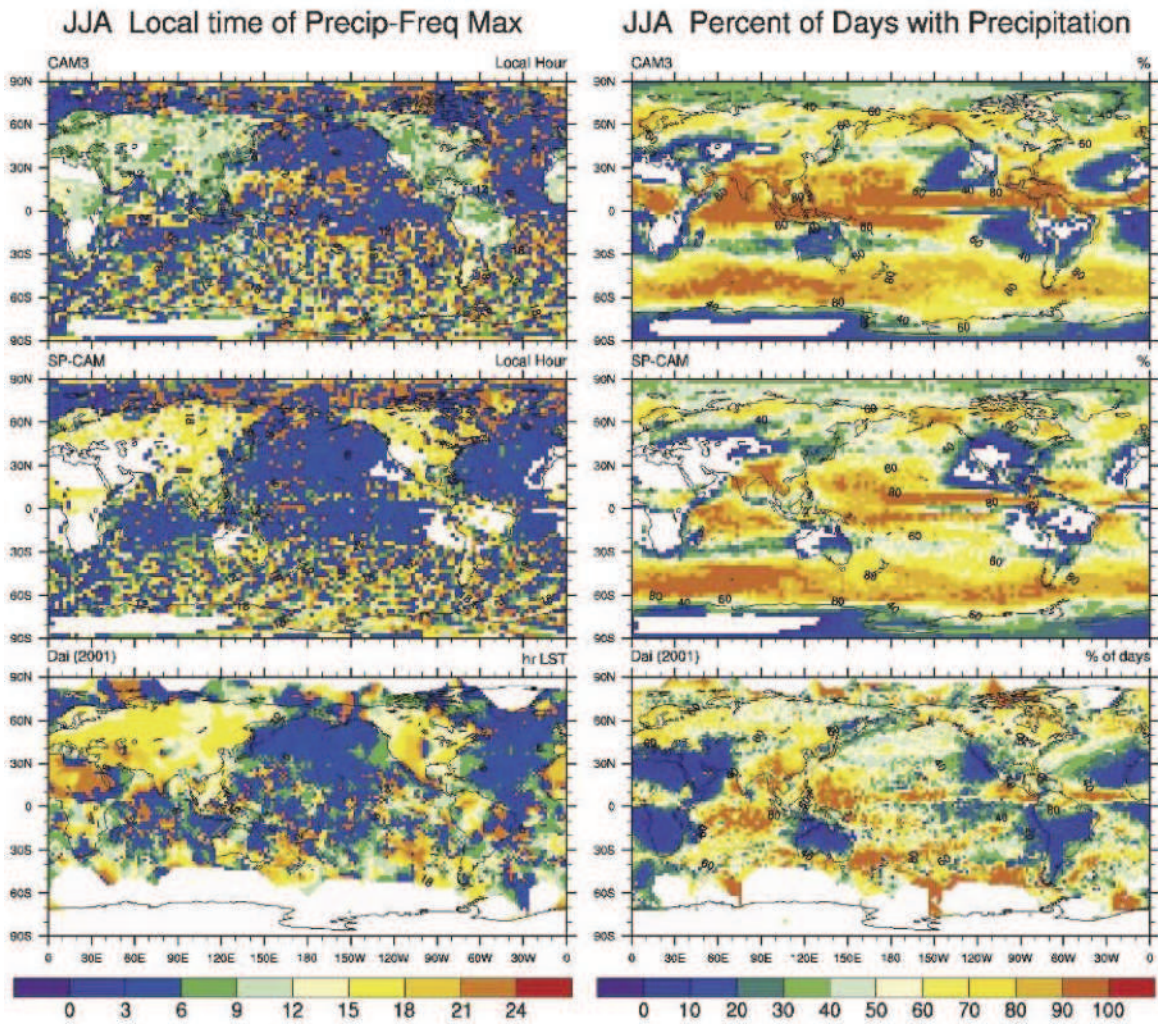


Figure 2.31: “JJA geographical distribution of (left) the local time of nondrizzle precipitation frequency maximum and (right) the percent of days with nondrizzle precipitation, as simulated with (upper) the standard CAM, (middle) SP-CAM, and (lower) from the dataset by Dai (2001)”. This is the first evidence that superparameterization improves the simulated diurnal rainfall cycle over land. Reproduced from Khairoutdinov et al. (2005) Figure 13.

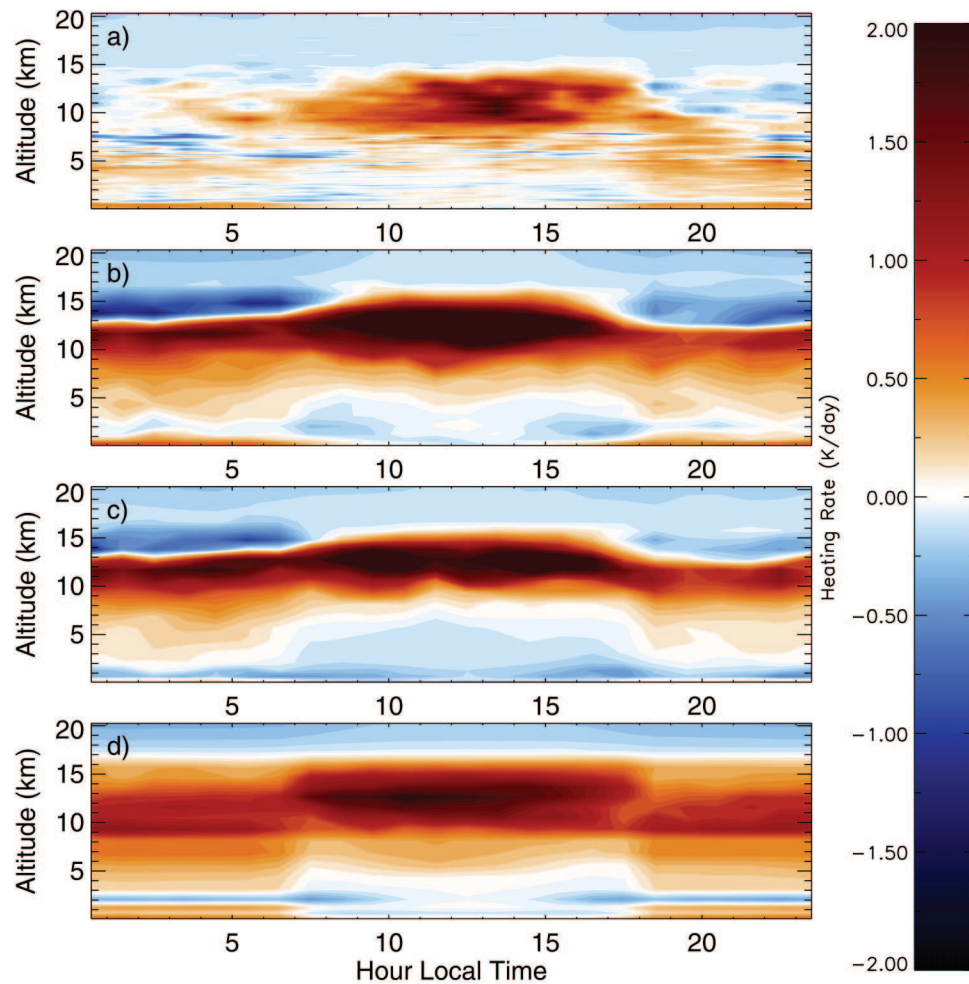


Figure 2.32: “Diurnal composite of net all-sky minus clear-sky heating rate at Manus for (a) ARM, (b) MMF (with precipitation), (c) [SPCAM3.0] (without precipitation) and (d) [CAM3.0].” The blue feature near 15 km in SP-CAM is associated with intermittent nocturnal cirrus longwave cooling, an important dynamical ingredient to the tropical diurnal cycle that is absent in conventional CAM. Despite being exaggerated in SP-CAM (due to overly frequent simulated tropical deep convection) the existence of a nocturnal cirrus cooling feature is an improvement in simulated tropical diurnal cycle dynamics. Reproduced from McFarlane et al. (2007) Figure 22.

grid point in the same SP-CAM and CAM simulations. The authors compared the simulation climatology at this single grid-point against baseline retrievals from ARM millimeter radar observations, focusing on the radiative properties of the simulated clouds²². Their analysis (see Figure 2.32) showed that although SP-CAM over-predicted the frequency of deep tropical precipitation, and contained far too much high cirrus clouds relative to the observations, the radiation-cloud interactions harvested from its embedded CRM nonetheless produced an improvement in the realism of simulated diurnal cloud-radiative feedbacks resulting from intermittent ice cloud effects:

Due to the nonlinear nature of radiative transfer, [CAM3.0] cannot produce the full range of radiative heating responses seen in the ARM [observations], which has important implications for the climate sensitivity of the model. In particular, due to the low frequency of optically thick ice clouds, the frequency of LW cooling at cloud top is greatly reduced. The lack of optically thick ice clouds and high frequency of optically thin, high altitude ice cloud resulted in a significantly different LW heating distribution in [CAM3.0] than in [SPCAM3.0]. [McFar-MatAck07]

DeMott et al. (2007) are responsible for the most in-depth analysis of the physics supporting the improved simulated diurnal rainfall statistics in SP-CAM, using ARM rain gauge and thermodynamic sounding climatology data in three sub-regions as a baseline. Based on an analysis of the statistical relationships²³ between simulated convection and mean thermodynamics in the regions, they arrived at the following conclusion:

In [CAM3.0], there is little or no lag between boundary layer energy buildup and rainfall, whereas [SP-CAM3.0] successfully simulates the observed increase (decrease) in boundary layer [moist static energy]

²²The authors emphasized that intermittent nocturnal cloud top cooling of elevated cirrus is an important diurnal ingredient to the tropical composite diurnal rainfall cycle at this site.

²³The authors inferred causality from lag-correlation analysis of composite diurnal rainfall time series of rainfall vs. CAPE, CIN and boundary layer moist static energy.

prior to (following) a rain event. [CAM3.0] simulates a pervasive decoupling between upper- and lower-level relative humidity maxima, while no such decoupling is observed, or simulated by the MMF. [DeMott et al. (2007)]

DeMott et al. (2007) showed that the statistical relationship between free tropospheric relative humidity and rainfall is distorted in CAM3.0 but improved in SP-CAM3.0²⁴. The authors argue that the formulation of the ZM95 implementation of the Arakawa-Schubert cumulus parameterization in CAM3.0 is responsible for these deficiencies, particularly through the assumption that all plumes in ZM95 are assumed to detrain their moisture only above the (usually quite high) level of minimum entropy in the troposphere. They emphasize, as in the review study of Guichard et al. (2004) discussed previously, that the observations bely a progression of events, from shallow to deep convection, that is inconsistent with this parameterization formulation, suggesting the improvement in SP-CAM’s diurnal timing over land occurs for the same reasons seen in offline CRMs:

The boundary layer energizes, producing a positive buoyancy profile, and supports development of initial convective plumes. These initial plumes detrain before attaining significant depth and deepen the low-level moist layer, allowing subsequent plumes to attain greater heights before detraining. Each successive “wave” of plumes consumes boundary layer [energy]. Eventually, the lower troposphere moistens enough to support deep convection and heavy rainfall. The remnants of the deep convective clouds moisten the upper troposphere ... Our analysis shows that this progression is realistically simulated by the MMF when sufficient low-level moisture is available, but [CAM3.0] does not simulate the observed lags.[DeMott et al. (2007)]

Zhang et al. (2008) moved beyond analyzing rainfall variability at individual grid points and sub-regions, instead leveraging orbital data to examine the complex

²⁴See e.g. their Figure 9 d)-f).

space-time structure of the simulated tropical diurnal cycle in a four year simulation using a new version of the prototype model, SP-CAM3.5²⁵. Their strategy was to fly virtual instrument simulators, representing the Tropical Rainfall Measuring Mission (TRMM) payload of simultaneous passive microwave and infrared imagers/sounders, and active microwave (radar), within the SP-CAM simulated environment. The instrument simulators sample the atmosphere along consistent orbital paths, and emulate forward radiative transfer physics directly from the model predicted fields, producing modeled radiometric signatures that are directly comparable to satellite data.

Unfortunately, the instrument simulator evaluation strategy in Zhang et al. (2008) convolved the information about SP-CAM’s rainfall diurnal cycle with its representation of diurnal cloudiness. Previously documented model biases in tropical cloudiness (too much high cloud) had a very deleterious effect on emulated infrared radiances at the top of the atmosphere. As a result, viewed from the perspective of traditional satellite derived proxies for precipitation in the infrared (precipitation index, upper tropospheric relative humidity) the SP-CAM diurnal rainfall cycle appeared to be very poorly simulated. Interestingly, when viewed from a more “raw” detection of rainfall (precipitation radar emulation), the SP-CAM3.5 appeared to have a much more reasonable space-time structure in its tropical diurnal rainfall cycle, especially in boreal winter²⁶. This is significant, since it can be argued that the actual precipitation rate produced by the CRMs is “more thermodynamically important” in terms of the effects induced on the host model (Khairoutdinov and Randall, 2001).

Khairoutdinov et al. (2008) also analyzed the dynamics of the simulated diur-

²⁵Unlike the SP-CAM3.0, which was built around the spectral dynamical core of CAM3.0, SP-CAM3.5 was built around the finite-volume dynamical core of modern versions of CAM. Zhang et al. (2008) ran the model at an outer resolution of $2^\circ \times 2.5^\circ$.

²⁶i.e. when the seasonal mean pattern was not distorted by regional precipitation bias structures like the Great Red Spot

nal cycle at a stratocumulus grid point in the Eastern Pacific in SPCAM3.0. The authors emphasized that - despite the coarse 4 km resolution of the CRM array - a realistic progression of diurnal interactions was captured, with maximum IR cooling and cloud water content at nighttime, and downdraft-driven²⁷ cloud breakup during the day.

Finally, a new independently developed superparameterized climate model was unveiled by NASA in 2009, in which their finite-volume general circulation model (fvGCM) was coupled to their cloud resolving model, the Goddard Cumulus Ensemble (GCE) model. Results from a diurnal rainfall analysis in Tao et al. (2009) confirmed the basic finding from diurnal timescales in SP-CAM3.0 (see their Figure 6). The third operational superparameterized global climate model was announced by a group at the Department of Energy this year, but its behavior has not yet been analyzed on diurnal timescales.

²⁷Downdrafts were diagnosed by the characteristically negative skewness of below-cloud vertical velocity

Chapter 3

Statement of the problems addressed

Despite being the most simply forced mode of rainfall variability in the climate system, the physics controlling the global diurnal rainfall cycle are not completely understood. For instance, controversies exist in the literature regarding what controls the usual late afternoon maximum rainfall timing observed over continents, versus the highly unusual regional nocturnal maximum in the Central US. Over the oceans, the observational record of diurnal rainfall is less mature, and some questions have correspondingly not even been addressed in detail - for instance, what controls the apparent pattern of the diurnal rainfall cycle over the Gulf Stream, and what is its connection to land forcing?

In the global climate modeling literature, the diurnal cycle of rainfall, as well as clouds and convection in general, are notoriously distorted in the models that were applied to project future climate in the latest IPCC assessment report. This casts unsatisfactory doubt on the reliability of long-term projections of the future hydrologic response to externally forced climate change.

The above literature review has emphasized that a new computationally inten-

sive prototype climate simulation technology, super-parameterized (or multi-scale) climate modeling, appears to do a better job at representing some critical aspects of the observed diurnal rainfall cycle. Given this development, this dissertation is concerned with a simple over-arching question:

What do super-parameterized climate simulations enable us to find out about how the diurnal rainfall cycle works?

The following chapters provide some incremental new work on this front, and are aimed at the following three questions,

- **Chapter 4: To what extent does cloud super-parameterization improve the diurnal rainfall mode in global climate simulations?**
- **Chapter 5: Can super-parameterized simulations help inform the problem of remote control of the marine diurnal rainfall cycle by land?**
- **Chapter 6: What does artificially restricting the scale of fast manifold processes in super-parameterized simulations imply about the mechanisms supporting the Central US nocturnal rainfall maximum?**

An underlying theme of discussion will be lessons from model intercomparison that contribute to the ongoing debate about how to fix existing biases at diurnal timescales in conventional global climate projection models. Since it is simply forced, well observed, and efficient to simulate, progress in fixing the distorted diurnal convection mode in next generation GCMs is a logical first step towards improving the representation of simulated cloud and convection statistics on other

time scales. This is in turn necessary to improve confidence in global climate model projections of how cloud and rainfall feedbacks may interact with continued externally forced climate change.

The following preamble expands briefly on each of the above questions, emphasizing in advance how the work in each chapter is aimed at a gap in the current literature, for context.

3.1 Optimally evaluating the effect of super-parameterization on the simulated global diurnal rainfall cycle.

The effect of super-parameterization on the simulated global diurnal rainfall cycle has not been adequately characterized. To address the following shortcomings in the existing published record, the work in Chapter 4 **refines the documentation of the diurnal rainfall cycle in a super-parameterized climate simulation** (Pritchard and Somerville, 2009b,a).

Best practices in the observational literature emphasize that, because of regional eccentricities of its space-time variability, single diagnostics or single grid-points are insufficient to gain a holistic view of the structure of the diurnal rainfall cycle (Carbone et al., 2002; Carbone and Tuttle, 2008; Kikuchi and Wang, 2008). From this perspective, the existing literature documenting diurnal variability in super-parameterized climate models was incomplete. Prior studies have either evaluated only a single diurnal rainfall diagnostic¹ as a function of location/season,

¹Khairoutdinov et al. (2005) and Tao et al. (2009) evaluated the horizontal structure of the daily timing of maximum precipitation against rain gauge data, and Zhang et al. (2008) compared the horizontal structure of the fitted 24-hour harmonic of top-of-the atmosphere radiation against a satellite

or multiple diagnostics but only at a single model grid-point².

Two examples from the observational literature provide inspiration for how to better characterize the diurnal rainfall cycle for global model evaluation. The first is Carbone and Tuttle (2008), who synergistically combined multiple complementary diurnal cycle diagnostics to describe the character of the US diurnal rainfall cycle as captured by the national weather radar network. The second is Kikuchi and Wang (2008) who simultaneously analyzed both spatial and temporal variability in a climatological global diurnal rainfall data set using statistical techniques. By linearly decomposing the composite diurnal rainfall data into the two spatial patterns responsible for the most diurnal variance (eigenmode decomposition), they demonstrated the many physical processes, including diurnal propagation and differences between continental and marine diurnal cycles, that this procedure allows to be compactly evaluated. Kikuchi and Wang (2008) also emphasized the important role that contemporary gauge-calibrated, satellite-derived rainfall best estimates³ should play for evaluating climate models. In prior publications, such multi-satellite rainfall data had not been adequately applied to evaluating the space-time variability of diurnal rainfall in super-parameterized climate models. To update the existing literature on the representation of diurnal rainfall variability in super-parameterized simulations, Chapter 4 employs both the techniques of Kikuchi and Wang (2008) (eigenmode decomposition; Section 4.1) and Carbone and Tuttle (2008) (multiple complementary diagnostics; Section 4.2), and leverages a multi-satellite precipitation “best estimate” for a more refined model evaluation of diurnal rainfall.

It is important to distinguish the work in Chapter 4 from the only previous

²DeMott et al. (2007) explored the relationship between rainfall, relative humidity, and boundary layer properties at three well-instrumented field sites, while Khairoutdinov et al. (2008) analyzed the simulated co-variability of cloud liquid water, radiative cooling, and vertical velocity at a stratocumulus grid point in the subtropical Pacific.

³This method merges superior information from multiple modern microwave radiometers on an international ensemble of weather satellites (see Section 2.1.1.)

study, Zhang et al. (2008), that has also brought satellite data to bear on evaluating diurnal convective variability in a super-parameterized climate model. In this work the intercomparison strategy obscured the nature of the simulated surface rainfall cycle. In order to compare simulation output against satellite data, the authors emulated forward radiative transfer through the model’s hydrometeor fields, sampling the atmosphere on a consistent orbital path as the satellite⁴. On the one hand it can be argued that this “instrument simulator” technique provides a more faithful model comparison against the fundamental satellite measurement (radiance). But on the other hand, the approach also unfortunately obscures the true structure of the simulated diurnal rainfall cycle, conflating it with biases in the height, optical thickness, and sub-grid distribution of clouds and their diurnal variability. As a result, Zhang et al. (2008) made an important contribution of emphasizing the effect of cloud biases on the diurnal variability of simulated radiances at the top of the atmosphere. But they did not characterize the simulated diurnal rainfall cycle itself to the extent that will be contributed in this dissertation. It is important to untangle the rainfall cycle independently, since it can be argued to be more “thermodynamically important” than the diurnal cycle of cloud position and water content (Khairoutdinov and Randall, 2001).

Finally, the work in Chapter 4 extends on all prior studies by also including a concluding intercomparison of the simulated diurnal rainfall cycle amongst several variants of SP-CAM, CAM and a new MMF developed at PNNL. This is to discover and document the unknown sensitivity of the MMF simulated diurnal rainfall signal to what are arguably arbitrary model configuration choices (e.g. resolution, degree of microphysics, CRM orientation) at this early stage of MMF development. The intent here is to distinguish true improvements due to the additional physics within super-parameterization from the sort of fortuitous coincidences that are

⁴The alternative strategy used in this dissertation is to leverage multiple satellites to solve the sampling problem

sometimes possible in a single model run's parameter space.

3.2 Non-local control of the marine diurnal rainfall cycle by land

The fact that the diurnal cycles of solar and latent heating are much more vigorous over land than over ocean dictates that part of the oceanic diurnal rainfall cycle is a remote response to circulations induced by energetic diurnal land processes (Dai and Deser, 1999; Dai, 2001). **Chapter 5 asks three related questions:**

1. **Can coarse resolution climate projection models capture observed tropical diurnal subsidence waves over the ocean?** Equatorward of the diurnal-inertial resonant latitude (30 degrees), part of the marine diurnal cycle has long been argued to be remotely controlled by land (Meisner and Arkin, 1987; Alliss and Raman, 1995b; Dai and Deser, 1999). This effect has become a topic of increasing interest due to new diurnally resolving orbital data characterizing surface winds from multiple scatterometer satellites. The climatology derived from this satellite record belies a strikingly coherent pattern of diurnal surface winds and convergence that clearly links nearby land to far-field marine processes on diurnal timescales (Gille et al., 2003, 2005; Wood et al., 2009). Long-range remote subsidence waves, especially apparent in the eastern subtropical Pacific, are thought to have implications for diurnal cloud properties and rainfall (Munoz, 2008; Wood et al., 2009). Wood et al. (2009) advocate that the structure of these subsidence waves as captured by scatterometers provides a useful constraint on the representation of diurnal convective processes in global climate models.

Section 5.1 brings this new data constraint to bear in evaluating subsi-

dence waves in the tropics and subtropics in super-parameterized and conventional climate simulations. Prior to this work, the only application of this scatterometer data to evaluate the representation of oceanic surface divergence waves in a global atmospheric model has been in the context of a very high resolution operational weather forecast model (Robert Wood, personal communication). However, numerical weather prediction and climate projection are very different problems. The ultra high resolution and sophisticated physics packages in weather models are not luxuries affordable to climate projection models, which must be integrated for decades, not days. Hence, the realism of subsidence waves in climate models must be separately evaluated. New work therefore documents the representation of long-range subtropical and tropical diurnal subsidence waves in a conventional vs. super-parameterized climate model.

2. **Does super-parameterization alter remote control of the marine diurnal rainfall cycle by land?** Section 5.2 views the effects of subsidence waves emanating from land masses in the tropics from the perspective of the vertically integrated water budget, to explore potential connections to modulations of diurnal rainfall.
3. **How do land-sea control mechanisms relate to the observed Gulf Stream diurnal rainfall pattern?** In the extra-tropics, diurnal rainfall variance stands out relative to surrounding areas over the Gulf Stream and Kuroshio regions during JJA. Although this has been remarked upon in satellite and radar data analyses, it has been a topic of limited research⁵(Alliss and Raman, 1995b; Carbone and Tuttle, 2008). Although the possible dynamics linking Gulf Stream diurnal rainfall with remote dynamics forced by

⁵This is in part due to the reasonable fact that the diurnal signal-to-noise ratio is very small in the extratropics, since synoptic eddies account for much more variance than diurnal processes.

diurnal processes over land are more limited in spatial scale (due to inertial effects), there are nonetheless reasons to believe long-range remote control can have an important effect (Wood et al., 2009). A change in local timing of peak precipitation with distance offshore over the Gulf Stream suggests that remote land influences may play a role (Janowiak et al., 2007). This effect may be purely advective (Alliss and Raman, 1995b) or more complex (Janowiak et al., 2007; Ruane, 2010). **Section 5.3** makes a contribution to this issue via a multi-model intercomparison documenting sensitivity of the composite simulated diurnal rainfall pattern over the Gulf Stream to the method of representing sub-grid convection. The simulated diurnal precipitation pattern is examined, both to document its realism, and to evaluate the land-sea diurnal connection mechanism. In reconciling the results, a case is made that a viable long-range control mechanism may indeed explain the Gulf Stream diurnal rainfall cycle, and that sufficient sensitivity of the convection module to free tropospheric relative humidity perturbations is integral to the mechanism.

3.3 Evidence for slow-manifold control of the Central US nocturnal rainfall maximum

Chapter 6 asks the question: **Can a super-parameterized climate model simulate realistic nocturnal convection over the Central US?**

A large fraction of the summer rainfall feeding the growing season in the Central US Plains (and other heavily populated continental interior regions near mountain ridges) comes from long-lived, organized nocturnal mesoscale convective systems (see Section 2.1.3). Historically, the problem has been that the statistical parameterizations used to represent unresolved cloud processes in conventional global

climate models do not admit the necessary physics of organized convection to simulate such systems.

All prior studies of the simulated diurnal rainfall cycle, including the work in Chapter 4 of this dissertation, suggest that super-parameterized global climate models *cannot* capture the physics of the Central US nocturnal rainfall maximum zone. A US nocturnal maximum is not evident in the JJA diurnal composite of Khairoutdinov et al. (2005) (Figure 2.31) nor in the analysis of Central US cloudiness statistics by Ovtchinnikov et al. (2006). DeMott et al. (2007) found no evidence of the observed strong nocturnal maximum in their analysis of the Southern Great Plains grid point’s rainfall statistics. Instead, their results indicated a very weak diurnal rainfall signal with indeterminate local time of maximum⁶. Zhang et al. (2008) excluded extratropical latitudes from their analysis against spaceborne data.

The ability or disability of superparameterized GCMs to capture the physics of the nocturnal maximum of Central US rainfall is relevant to a controversy in the literature about “fast-manifold” versus “slow-manifold” control of the underlying propagation of organized convection in the region (see Section 2.1.4 for background). Chapter 6 adds a new dimension to this debate from the vantage point of super-parameterized simulations, in which the horizontal scale over which fast manifold propagation mechanisms can operate is artificially restricted.

In the discussion section of Ovtchinnikov et al. (2006), a “fast manifold” interpretation was invoked to explain the apparent inability of superparameterized GCMs to capture Central US MCS as *inherent*:

Given the fact that the CRMs have periodic lateral boundary conditions and cannot maintain large-scale horizontal gradients (and hence

⁶The authors attributed this primarily to a regional mean-state humidity bias of unknown origin in SP-CAM3.0, showing that the lower atmosphere in the region, below 700 hPa in SP-CAM3.0, was “astonishingly warm and dry”. They did not explore the causes of this simulated dry bias.

baroclinicity) and that the exchange among CRMs is handled through tendencies of large-scale variables, the MMF ability to propagate synoptic-scale disturbances, such as fronts or mesoscale convective systems, may not be much different from that of the CAM. [(Ovtchinnikov et al., 2006)]

On the one hand, it is logical to think that the MMF assumption of periodic boundary conditions⁷ in the embedded CRMs might preclude simulation of the physics supporting the Central US nocturnal rainfall maximum. Conventional wisdom in the current mesoscale and weather literature argues that “fast-manifold” processes such as convective cold pools, small-scale gravity waves and gust fronts are key to the long-range propagation of organized convection and hence the nocturnal rainfall maximum in the Central US (Carbone and Tuttle, 2008). By design of the MMF approach, simulated cold pools and gust fronts cannot have a long-range effect.

On the other hand, another school of thought suggests “slow-manifold” mechanisms may be more important for the propagating nocturnal rainfall in the Central US, such as semi-geostrophic adjustment (Tripoli and Cotton, 1989b), large scale advection of convectively generated potential vorticity anomalies (Raymond and Jiang, 1990; Li and Smith, 2010), and large scale gravity waves excited with the convection (Pandya and Durran, 1996; Moncrieff and Liu, 2006).

In this context, Chapter 6 documents the discovery of a robust nocturnal organized propagating Central US convection signal in a revisited super-parameterized climate model simulation. The signal emerges when resolution is increased modestly at both resolved scales, and diagnostic attention is broadened from just *surface precipitation* to *convective heating structures* (i.e. precipitation within the column). Several analysis techniques are pursued to evaluate the realism of the

⁷Recall that this assumption is inescapable since it is fundamental to the motivation for the MMF approach in terms of its unique *computational affordability* for the climate projection problem.

nocturnal convection signal and its physical consistency: How well do the simulated phase and propagation speeds of the storms agree with ground-based radar climatology? Are they generated under appropriate synoptic forcing? Is the genesis mechanism in line with the field campaign informed conceptual model of Tripoli and Cotton (1989a)? What is the impact of cloud super-parameterization on the regional circulations that are known to support Central US nocturnal convection in nature?

Since the signal is shown in many ways to be realistic, it is argued to constitute new numerical evidence consistent with a dominant “slow-manifold” interpretation of Central US nocturnal rainfall propagation.

Chapter 4

Evaluating the effect of super-parameterization on the simulated global diurnal rainfall cycle.

Section 3.1 motivated the need to document the effect of super-parameterization on the simulated diurnal rainfall cycle in more detail than has otherwise been published. Two strategies for improved diagnosis of the simulated global diurnal rainfall were highlighted, based on observational literature best practices by Kikuchi and Wang (2008) and Carbone and Tuttle (2008). In this chapter, each is applied in turn to document the structure of, and effect of super-parameterization on, the simulated diurnal rainfall cycle in global climate model simulations. The goal is a holistic evaluation of the diurnal rainfall mode.

Section 4.1 applies the approach of Kikuchi and Wang (2008). Results from empirical orthogonal function (EOF) decomposition of the simulated boreal summer climatological composite diurnal cycle of precipitation in an MMF and a conven-

tional GCM are compared to a multi-satellite data product developed as a part of the Tropical Rainfall Measuring Mission. The eigenspectrum, principal component time series, and the projection of leading precipitation EOFs in a 2000-member bootstrap ensemble eigenmode decomposition of the MMF composite day are a better match to observations than the GCM. Analysis shows that regional deficiencies in the MMF diurnal cycle are manifest as localized anomalies in the spatial projections of EOF₁ and EOF₂.

Section 4.2 adopts the philosophy of Carbone and Tuttle (2008), applying multiple complementary diagnostics of the diurnal rainfall cycle to gain a more complete view of its space-time structure. These include traditional harmonic analysis, and non-traditional diagnostics such as the broadness of the peak precipitation in the mean summer day, reduced dimension transect analysis, and animations of the full spatial and temporal variability of the composite mean summer day. Precipitation in SPCAM3.0 is evaluated against multi-satellite merged satellite data and a control simulation with a climate model that employs conventional cloud and boundary layer parameterizations. This analysis highlights several improved features of the diurnal cycle of precipitation in the multi-scale climate model that have not previously been remarked on: It is less sinusoidal over the most energetic diurnal rainfall regimes, more horizontally inhomogeneous within continents and oceans, and more faithful to observed structural transitions in the composite diurnal cycle chronology straddling coastlines than the conventional climate model. A regional focus on North America suggests that SPCAM3.0 at T42 resolution is unable to capture diurnally propagating precipitation signals associated with organized convection in the lee of the Rockies¹. The chronology of precipitation events elsewhere in the vicinity of North America is improved due to super-parameterization, especially over sea breeze circulation regions along the eastern seaboard and the Gulf of Mexico, as well as over the entirety of the Gulf Stream.

¹This issue is revisited in Chapter 6

As a baseline against which to compare simulated precipitation, a rain gauge-scaled, multi-satellite, gridded 3-hourly, high resolution (0.25° by 0.25°) precipitation product called TRMM 3B42 is used. This product is a best estimate that combines high quality microwave radiometer and precipitation radar data from the Tropical Rainfall Measuring Mission (TRMM) satellite with complementary but lower quality (but more abundant) infrared and microwave radiometer measurements from other platforms (see Huffman et al. (2007) for details). Of course, it would be more philosophically appealing to use as a ground truth only raw, direct observations of precipitation as are available from dense networks of rain gauges, or perhaps from TRMM's precipitation radar alone. But the sampling biases that would be incurred by this strategy - in the case of the TRMM radar as a result of its narrow swath width (Hirose and Nakamura, 2005), and in the case of gauge data from inhomogeneities in the spatial distribution of weather stations - would unnecessarily complicate a large-scale analyses of the diurnal cycle. Since the climatological composite JJA diurnal cycle of precipitation in 3B42 has been well-studied and appears to be in good agreement with independent precipitation products and surface data (Dai et al., 2007), its practical advantages for the purpose of model comparison and evaluation are compelling.

4.1 Empirical orthogonal function analysis of diurnal rainfall

As is well known, the usual tools for climate forecasting, global climate models (GCMs), do not simulate realistic diurnal hydrologic variability (Collier and Bowman, 2004). Diurnal precipitation in GCMs is too sinusoidal, peaks too early over continents and is too horizontally homogenous over large regions where spatial variations are observed in nature. Biases at diurnal time scales have the capacity

to distort hydrologic variability on longer time scales in GCMs, casting doubt on projections of future hydrologic variability.

A new approach to climate modeling, multi-scale modeling, offers improvement in the simulation of diurnal hydrologic variability in several regions. Previous exploration of the diurnal cycle in MMFs has revealed:

- Improved timing of maximum precipitation over continents (Khairoutdinov et al., 2005).
- Realistic relationships between the diurnal variability of cloud liquid water, longwave cooling, vertical velocity variance, inversion height and sub-cloud vertical velocity skewness, along a transect displaying a range of cloud types (Khairoutdinov et al., 2008).
- Biases in the diurnal variability of outgoing longwave radiation products used as operational precipitation proxies (Zhang et al., 2008).

In this study new results are presented demonstrating a *global* improvement in the diurnal cycle of precipitation in an MMF relative to a conventional GCM, as diagnosed by empirical orthogonal function (EOF) decomposition of the climatological mean summer day. This EOF approach was recently advocated as a benchmark test for evaluating simulated hydrologic diurnal variability against new space-borne precipitation climatological observations (Kikuchi and Wang, 2008). The results indicate that the MMF appears to pass this test; the eigenstructure of the mean summer day's precipitation in the MMF is much more faithful to the observations than the conventional GCM.

Background

The MMF used in this study is a prototype under development at the Center

for Multiscale Modeling of Atmospheric Processes (CMMAP), and is described in Khairoutdinov et al. (2005). It is identical to the National Center for Atmospheric Research Community Atmosphere Model v3.0 (CAM3; Collins et al. (2006)) except that the parameterizations for deep and shallow sub-grid convection have been replaced with a nested integration of a two dimensional ($x - z$) realization of the CRM described in Khairoutdinov and Randall (2003), with periodic lateral boundary conditions. The CRM solves the non-hydrostatic momentum equations of fluid dynamics subject to the anelastic approximation, using bulk microphysics to track conversions between multiple categories of interactive precipitating and non-precipitating prognostic water condensate variables, including ice, snow, liquid water, and graupel (Khairoutdinov and Randall, 2003).

The simulations analyzed are four month (MJJA) boreal summer integrations of the MMF and CAM; the first month is considered spin-up so only results from JJA are shown. In the MMF, the CRM time step is 20 seconds, and multi-scale coupling to the large-scale atmosphere and land surface model occurs on the 15 minute time step of the host GCM. We run the host GCM at T42 horizontal resolution ($2.8^\circ \times 2.8^\circ$) and configure the CRM to run on 32 nested grid columns spaced horizontally 4 km apart and on 26 vertical levels co-located with the interior of the GCM vertical grid. At this horizontal resolution the majority of vertical moisture transport in the CRM is explicitly resolved, with sub-grid transport responsible for less than 10 % of zonal mean moisture fluxes (Khairoutdinov et al., 2008).

As in Kikuchi and Wang (2008), TRMM 3B42 is used as an observational baseline for EOF analysis of the mean summer day's precipitation. TRMM 3B42 is a gridded ($0.25^\circ \times 0.25^\circ \times 3$ hours) "best estimate" of precipitation that combines observations from several space-borne instruments, including the precipitation radar and microwave radiometer on board the Tropical Rainfall Measuring Mission (TRMM) as well as infrared and microwave radiometers from other orbiting platforms (Huffman et al., 2007). The climatological composite diurnal cycle

in TRMM 3B42 is in good agreement with independent surface radar and rain gauge data (Dai et al., 2007).

Methods

Independent patterns of variability in the mean summer day’s precipitation that account for high amounts of statistical variance can be identified using empirical orthogonal function (EOF) decomposition.

EOF decomposition is applied to a regularly gridded local solar time- (LST-) space matrix of the diurnal precipitation anomaly about its daily mean. Construction of this matrix is complicated by the fact that both the model output and observations are discretized at regular intervals in universal time (UTC), which means that discretization in local solar time (LST) varies as a function of longitude. Following Kikuchi and Wang (2008), Fourier interpolation is applied along the periodic local solar time dimension after conversion from UTC, to re-discretize LST consistently at each longitude and construct a regularly gridded matrix conducive to EOF analysis.

Special attention must be paid to estimating uncertainty in the eigenvalue spectrum, since EOF patterns and their corresponding principle component (PC) time series provide meaningful information only where the uncertainty in their associated eigenvalues is sufficiently small so that adjacent EOFs are not at risk of statistical degeneracy with each other (North et al., 1982). A common approach to calculating this sort of uncertainty in the eigenvalue spectrum is to apply the “significance test” posed by North et al. (1982). However this technique requires some knowledge of the degrees of freedom (DOF) in the space-time dataset (Wallace et al., 1992) and introduces some questionable assumptions about the linearity of error propagation. As Kikuchi and Wang (2008) point out, estimating the DOF in

a climatological composite mean summer day of precipitation is not at all straightforward: There are likely at least as many DOF as there are independent time samples in the composite mean summer day, but surely fewer DOF than there are total time samples in all of the days that went into the composite (92 for the model observations, 644 for the satellite data). In their EOF analysis of the composite annual mean summer day’s precipitation from TRMM 3B42, Kikuchi and Wang (2008) chose to apply North’s significance rule assuming 50 DOF, arguing this was a conservative choice between the former (8 time samples in the composite day) and the latter (many thousand time samples behind the composite mean).

Here a different technique is chosen. Uncertainties in the eigenvalue spectra of the mean summer day are estimated instead using a custom statistical resampling technique. This approach combines random re-sampling (bootstrapping) and under-sampling (jackknifing) of the composite diurnal cycle of precipitation. Repeated EOF decomposition operations are carried out on 2000 randomly populated subsets of the full mean summer day space-time matrix, and standard errors are estimated based on the resulting ensemble of eigenvalue spectra. This method is faithful to the nonlinearity of sampling error propagation through the sequence of EOF matrix operations. The full space-time matrix is *undersampled* because there is significant correlation between spatially adjacent grid points’ diurnal variability. The spatial dimension of each randomly populated bootstrap ensemble member’s time-space matrix is thus limited to a fraction f of the N spatial grid points x_i in the full space-time matrix. The degree of undersampling is estimated as

$$f = 1/N \sum_1^N f_i(R_i) \quad (4.1)$$

where R_i is the cross-correlation map of the x_i -th point’s mean summer day time series with every other point in space, and f_i is defined as the fractional area occupied by the $R_i = 0.8$ contour that encloses the x_i -th point in space. Based on correlation analysis of TRMM data bin-averaged to the climate models’ T42 grid,

it is estimated that $f \approx 7\%$.

Results

Figure 4.1 shows that the bootstrap ensemble eigenvalue spectrum of the MMF composite boreal summer day's precipitation is improved relative to CAM. In the observations, two primary EOFs are statistically distinguishable in the bootstrap ensemble, accounting for $63.0 \pm 10.4\%$ and $26.1 \pm 8.5\%$ of the variance in the TRMM 3B42 composite boreal summer day, respectively. This is consistent with the findings of Kikuchi and Wang (2008). The eigenspectrum in the MMF mean summer day is remarkably similar to the observations, with $61.7 \pm 8.6\%$ of the variance in EOF₁, and $24.1 \pm 7.2\%$ in EOF₂. But in CAM the eigenstructure of diurnal precipitation is distorted - the leading EOF explains over 85% of the variance, and higher modes are statistically indistinguishable in the randomly undersampled bootstrapping ensemble.

Figure 4.2 (a) shows corresponding improvement in the structure and amplitude of the MMF bootstrap ensemble mean principle component (PC) time series for EOF₁ and EOF₂ relative to CAM. Both the MMF and TRMM PC1 time series are sinusoidal in structure, and each having a minimum around 0900 LST; the maximum of PC1 occurs at 2100 LST in the MMF, compared to 1800 LST in TRMM. In contrast, the PC1 time series of the leading EOF in CAM has a very different structure.

Figure 4.2 (b)-(d) compares the spatial projection of the leading EOF in the two climate models and the observations. In the TRMM data, EOF₁ is mostly positive over land and negative over the oceans. This mode captures the phase difference of marine vs. continental diurnal precipitation cycles, with a tendency for higher amplitudes in the wetter tropics due to higher diurnal ranges there (Kikuchi and

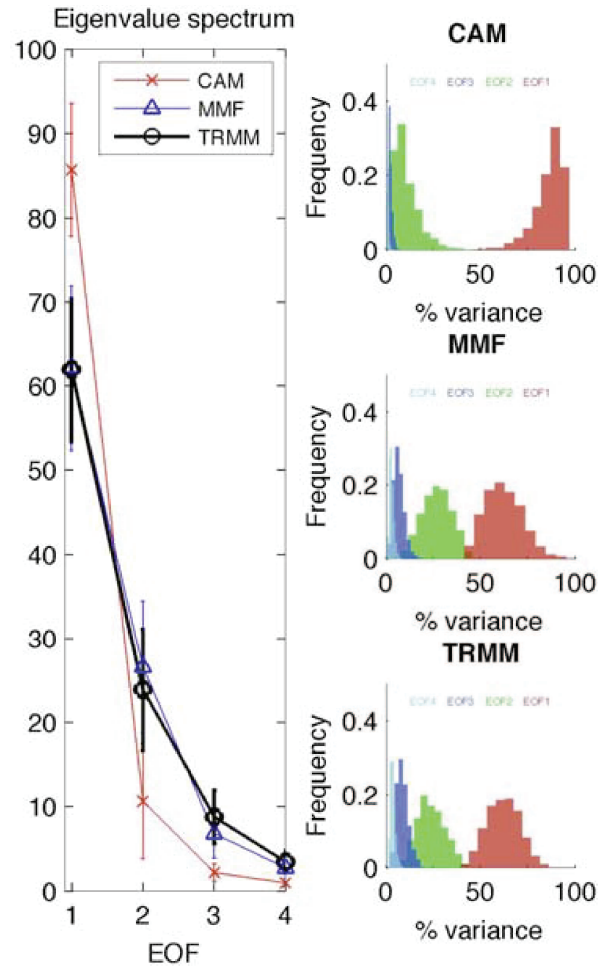


Figure 4.1: (Left panel) Eigenvalue spectrum for the composite JJA diurnal cycle of precipitation as simulated by CAM and MMF, and as observed in TRMM 3B42. (Right panels) Normalized histograms of the percent variance attributable in the 2000-member bootstrapping ensemble of EOF calculations, for each model; error bars in the eigenvalue spectrum are computed from these distributions.

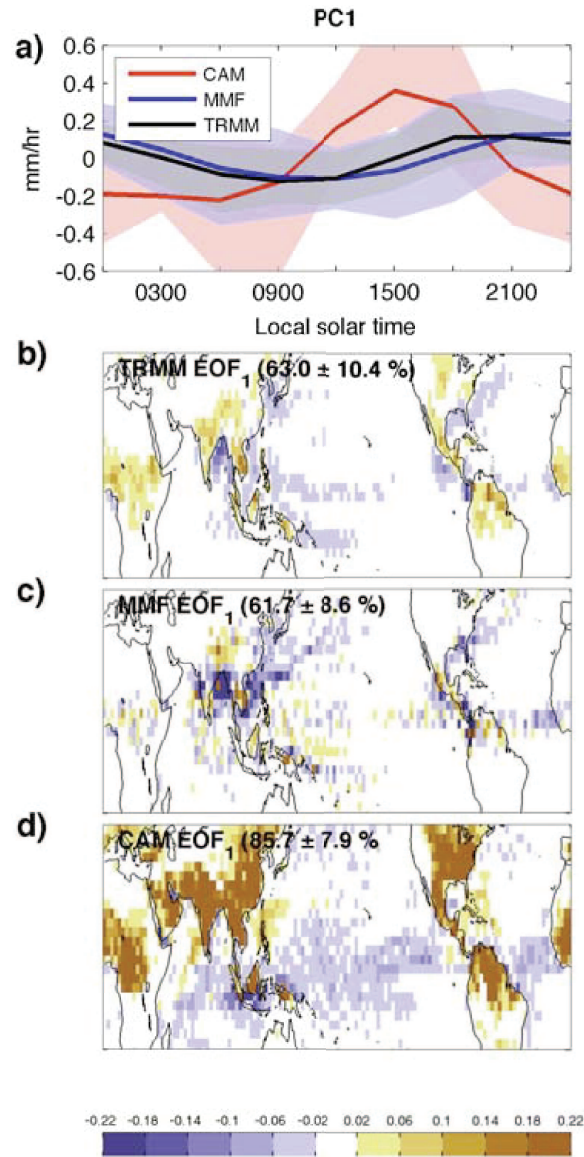


Figure 4.2: (a) Principle component (PC) time series of the leading EOF of the composite boreal summer diurnal cycle of precipitation as simulated by CAM (red) and MMF (blue), compared to TRMM observations (black). Solid lines and shading denote the mean \pm one standard deviation of a 2000 member ensemble of randomly undersampled bootstrap EOF calculations. (b)-(d) Ensemble mean spatial projection of EOF₁ for (b) TRMM data, (c) the MMF, and (d) CAM.

Wang, 2008). Although this broad structure is also present in EOF₁ for both MMF and CAM, the amplitude of EOF₁ is dramatically improved in the MMF. The MMF captures observed continental maxima in EOF₁ over northeastern Brazil, Central America, central Africa, and Thailand as well as oceanic minima in the tropics, over the Atlantic and Pacific storm tracks, and the South Pacific Convergence Zone (SPCZ). But the MMF EOF₁ is not perfect: the (positive) magnitude of EOF₁ is underestimated over the central United States, western equatorial Africa, and central Brazil and the (negative) magnitude of EOF₁ is overestimated over the oceans. The MMF also exhibits excessive EOF₁ amplitude in the vicinity of the Indian monsoon and over the Western Pacific. But in comparison to CAM, which has excessive EOF₁ amplitude over all continental land masses, the global structure of the leading diurnal EOF in the MMF is significantly improved.

Figure 4.3 (a) shows corresponding improvement in the MMF EOF₂ principal component time series (PC2). As in TRMM 3B42, PC2 in the MMF has a broad local maximum peaking at 1500 LST, and a minimum from 0000-0300 LST. The PC2 time series in CAM is not shown, since the second EOF in CAM explains little variance and is difficult to distinguish from subsequent EOFs (Figure 4.1).

Figure 4.3 (b)-(d) shows that the spatial structure of EOF₂ in the MMF compares reasonably well to the observations, but is far from perfect. Local maxima in EOF₂ over the southeastern United States, northeastern South America, and northeastern Asia are reasonably well reproduced by the MMF. However, the MMF does not capture observed minima in the spatial projection of EOF₂ over the central United States and equatorial Africa. As was the case for EOF₁, the amplitude of oceanic minima in EOF₂ is exaggerated in the MMF, as is the EOF₂ amplitude over the Western Pacific and Indian monsoon region.

Taken together, Figures 4.1 to 4.3 are compelling evidence of improved diurnal hydrologic variability in the MMF relative to CAM. The correspondence of a realistic eigenspectrum and PC time series in the MMF with spatial projections of

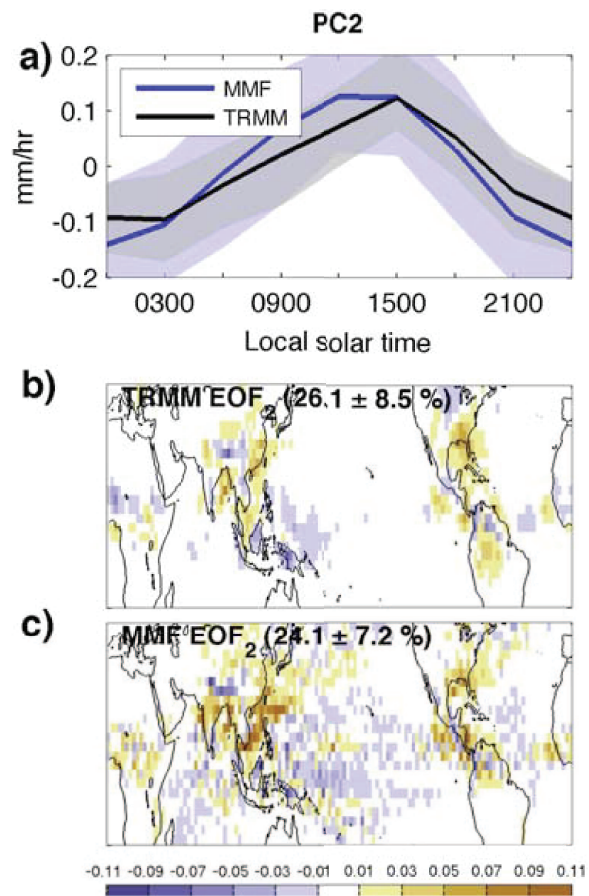


Figure 4.3: As in Figure 4.2, but for EOF₂.

the leading EOFs that are in broad agreement with observations strongly suggests overall improved performance at diurnal time scales. However regional biases in the spatial projections of EOF₁ and EOF₂ suggest that in certain parts of the globe, the MMF diurnal cycle needs improvement.

Discussion and Conclusions

The development of Earth system models capable of reproducing observed hydrologic variability on diurnal time scales is a high priority and an important step towards making important projections about hydrologic variability on longer time scales. Empirical orthogonal function (EOF) decomposition of the climatological composite boreal summer diurnal cycle of rainfall demonstrates that a prototype multi-scale modeling framework (MMF) vastly outperforms its conventional global climate model (GCM) counterpart at simulating the diurnal cycle of precipitation.

The eigenspectrum for the MMF mean summer day, as well as the principle component time series of its two leading EOFs, are a remarkable match to observations. This is very promising. The spatial projection of EOF₁ and EOF₂ in the MMF are in broad agreement with observations, but also exhibit several regional biases consistent with areas of known diurnal variability in the model. MMFs are still in their infancy, and further work is needed to correct these regional biases, which occur at both diurnal and seasonal time scales (not shown).

EOF decomposition is found to provide a meaningful and compact way to appraise the overall space-time variability of simulated climatological diurnal rainfall variability in climate models. This is an endorsement of the recent recommendation of Kikuchi and Wang (2008) that this approach be used as a litmus test to evaluate the simulated diurnal cycle of precipitation in climate models against gridded precipitation products.

Section 4.1, in part, is a reprint of material as it appears in Empirical orthogonal function analysis of the diurnal cycle precipitation in a multi-scale climate model 2009. Pritchard, Michael S., Somerville, R. C. J., *Geophysical Research Letters*, 35 (5), L05812. The dissertation author was the primary investigator and author of this paper.

4.2 Holistic diurnal rainfall diagnostics

Traditionally, a global view of diurnal variability is obtained by constructing spatial maps of some scalar metric that describes the time evolution of the climatological composite summer day time series (transformed to Local Solar Time, LST). There are many conceivable scalar descriptors of a composite day's time evolution; the most commonly scrutinized are the phase and amplitude of the least-squares-fitted 24-hour (S1; diurnal) and 12-hour (S2; semi-diurnal) harmonics (Chang et al., 1995; Collier and Bowman, 2004; Dai and Trenberth, 2004) and the (unfitted) local time of peak precipitation. Less commonly employed, but important and complementary diagnostics of the composite diurnal cycle include the unfitted broadness of the daily maximum and reduced transect analysis (Carbone and Tuttle, 2008), the precipitation range, and the amplitudes of leading empirical orthogonal functions (Kikuchi and Wang, 2008). For regions in which the diurnal cycle is strongly tied to non-local forcing mechanisms, it is better to use an objective time coordinate (i.e. universal time coordinate, UTC) in order to visualize diurnally propagating signals.

Many traditional diagnostics of the diurnal rainfall cycle have previously been explored in MMFs and the results have been promising. Khairoutdinov et al. (2005) showed an improvement (relative to a conventional GCM) in the simulated local time of peak precipitation over continents in the SP-CAM3.0 (Super-Parameterized Community Atmosphere Model) MMF. This improvement in diurnal peak rainfall

timing has also been documented in an independent MMF framework developed at NASA Goddard (Tao et al., 2009). Khairoutdinov et al. (2008) further demonstrated realistic relationships in SP-CAM3.0 between the diurnal variability of several stratocumulus properties (cloud liquid water, longwave cooling, vertical velocity variance, inversion height and sub-cloud vertical velocity skewness) for a single model grid point in the northeastern subtropical Pacific. DeMott et al. (2007) evaluated the simulated composite diurnal cycle of rainfall, convective available potential energy, convective inhibition, buoyancy and planetary boundary layer height, in three regional subdomains where nearby data from intense observing periods were available. Zhang et al. (2008) analyzed the amplitude and phase of the best-fit 24-hour harmonic of the July and January composite days' precipitation for the entire tropics from a 4-year SP-CAM3.0 simulation; they identified a weak bias in the 24-hour mode's precipitation amplitude during July over land, and an overall tendency for too much amplitude in the fitted 24-hour harmonic over the oceans, but otherwise reasonable agreement in the actual simulated precipitation in SP-CAM3.0. Zhang et al. (2008) also used SP-CAM3.0 cloud water distributions harvested from the nested cloud-resolving subdomain scale as input to radiative transfer code, in order to emulate and evaluate the diurnal cycle of several operational proxies of precipitation and cloudiness that are routinely derived from space based measurements of infrared brightness temperature at two discrete frequency channels. They found significant deficiencies in the diurnal variability of these simulated top-of-the-atmosphere radiative and radar signals, and attributed them to an overall excess high cloud bias in SP-CAM3.0.

Here, the simulated diurnal rainfall cycle in SP-CAM3.0 is examined in closer detail, extending the existing work to include several non-traditional metrics of composite diurnal precipitation that do not rely on curve fitting (diurnal peak broadness, reduced transect analysis, and regional animation) during DJF and JJA; results from empirical orthogonal function decomposition of the JJA diurnal

rainfall cycle were previously analyzed in Section 4.1. The aim in adding these complementary vantage points to the existing body of diurnal MMF precipitation diagnostics is to clarify where (in order to better understand why) super-parameterized climate models exhibit improved regional moist convective circulations at diurnal timescales, at high levels of scrutiny. The SP-CAM3.0 MMF is compared against its counterpart GCM (CAM3.0) which uses a conventional Arakawa-Schubert cumulus parameterization closed on undilute CAPE, and against a multi-satellite merged precipitation product.

The central United States provides a telling example, and a challenging litmus test for any model of diurnal hydrologic variability. Over the central United States, the SP-CAM significantly underestimates JJA mean precipitation relative to both CAM and observations, despite showing considerable improvement in the statistics of light vs heavy rainfall (DeMott et al., 2007).

As described in Section 2.1.3, observations indicate that the daily cycle of precipitation over the central United States is controlled by events upstream; convective initiation during the late afternoon over the sun-warmed Rockies self-organizes into mesoscale convective complexes (Carbone et al., 2002). Sustained by a favorable vertically sheared background wind environment, this organized convection is unusually long-lived, and drifts so far east that its precipitation dominates the diurnal cycle over the central United States, causing a late evening diurnal peak. This diurnal mechanism is primarily responsible for the climatological summer precipitation falling over the central United States (Carbone and Tuttle, 2008). Conventional climate models have understandable difficulty capturing this phenomenon - at coarse resolution, the topographic heating features and the low-level dynamical environment that enable such MCC propagation are not resolved (Moncrieff and Liu, 2006). In fact, DeMott et al. (2007) showed that although the Community Atmosphere Model appears to correctly simulate the seasonal scale precipitation over the central United States, it does so for the wrong reason- excess local evapo-

transpiration is produced in the land surface model's vegetative canopy as a result of mis-estimating the statistical distribution of light vs heavy rainfall.

Models, data and methods

As in the preceding section, the MMF used in this study is the SP-CAM v3.0, which is described in Khairoutdinov et al. (2005). The two simulations analyzed are four month (MJJA, NDJF) integrations of the SP-CAM in which the host CAM horizontal resolution was approximately 2.8° latitude by 2.8° longitude (T42 spectral truncation). The first month is considered as spin-up, and only results from JJA and DJF are depicted in this analysis. Within each CAM grid cell there were 32 nested CRM columns arranged zonally with a horizontal spacing of 4 km in a 128-km, laterally-periodic idealized subdomain, spanning less than half of the typical zonal extent of the host model grid points. At the large scale, SP-CAM was configured to run with a 15 minute timestep on 26 vertical levels, and the idealized embedded CRM was run with a 20 second timestep on vertical levels co-located with the 24 interior levels of CAM. In order to adequately resolve diurnal variability, model output was stored globally at three hourly increments, on both the host GCM and CRM scales. Corresponding single-summer control runs of CAM3.0 were also carried out for MJJA and NDJF as comparison.

Figure 4.4 contrasts the well documented seasonal scale biases in the JJA and DJF precipitation rates in the SP-CAM and CAM, showing that tropical seasonal precipitation biases are worse in both models (and especially the SP-CAM) during JJA than in DJF. During JJA, CAM exhibits the notorious “double ITCZ (Intertropical Convergence Zone)” problem, as well as excessive JJA orographic precipitation in the Indian Monsoon region. In the SP-CAM, the JJA double ITCZ problem is mitigated but the excessive monsoonal rainfall problem is exac-

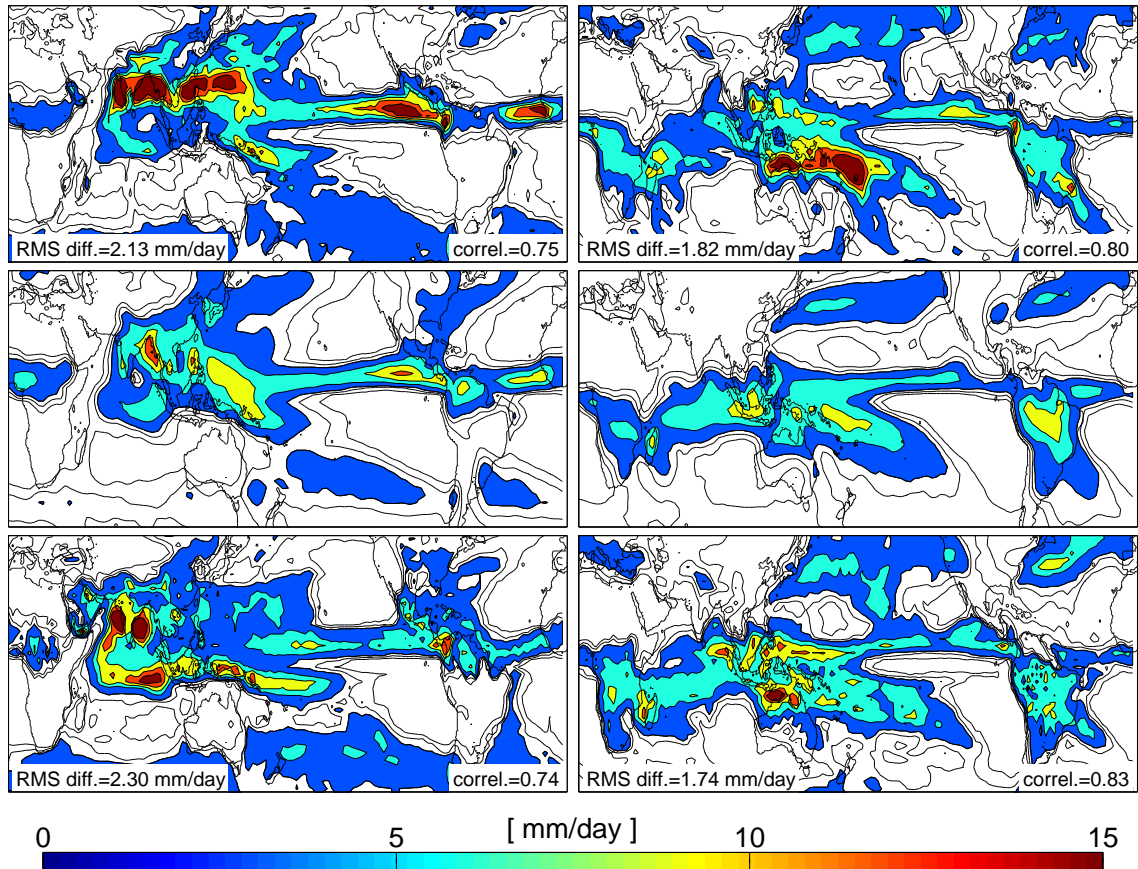


Figure 4.4: JJA (left) and DJF (right) precipitation for (top) one year simulation of SP-CAM3.0, compared to (middle) 7 years of a merged multi-satellite, multi-instrument observational product (TRMM 3B42) and (bottom) CAM3.0. The contouring interval is 1 mm/day for precipitation rates below 3 mm/day (unshaded contours) and 3 mm/day for precipitation rates greater than or equal to 3 mm/day (shaded contours). Root-mean-squared difference and pattern correlation coefficient relative to the observations are shown for the two models.

erbated and a new tropical bias arises, known as the “Great Red Spot”, i.e. far too much simulated JJA precipitation in the Western Pacific (Luo and Stephens, 2006; Khairoutdinov et al., 2005). During DJF, both models are in better agreement with the observed seasonal precipitation in the tropics, as evidenced by the RMS difference and pattern correlation values in Figure 4.4.

This has consequences for the design of an analysis of simulated diurnal variability. Given the fact that the tropical diurnal cycle amplitude is fairly strong and seasonally invariant, the seasonality of model biases described above suggests DJF is a more appropriate season to study simulated diurnal variability than JJA, at least in the tropics. For the extratropics, diurnal variability is weaker and the greater diurnal signal-to-noise ratio afforded by more summer solar forcing and less baroclinicity and storm activity make JJA a better choice to study the simulated interior and coastal diurnal circulations of the northern hemisphere continents.

To gain a comprehensive view of the diurnal cycle of precipitation in model output and satellite observations, a suite of complementary diurnal cycle diagnostics is considered. All have as their starting point a climatological composite mean seasonal day, which is constructed by averaging all available days (e.g. for JJA, 92 for each of the single-summer climate model simulations, and 644 for years 2000 to 2006 of the TRMM 3B42 rainfall product). The following diagnostics are examined:

1. *Harmonic analysis*: For each spatial location, a 24-hour sinusoid is fit to the seasonal composite day time series (transformed to local solar time) to obtain spatial maps of the two degrees of freedom in the curve fit, the phase and amplitude, which are traditionally simultaneously visualized as a vector field (e.g. Wallace 1975). Of course, this technique only provides meaningful information at locations where the sinusoidal curve fit is a reasonable approximation to (i.e. explains a significant fraction of the variance in) the raw mean summer day time series (Dai 2001).

2. *Broadness of the diurnal maximum:* A metric for the broadness, or duration, of the daily maximum in the mean summer day time series of precipitation is computed. The metric was conceived and is illustrated in (Carbone and Tuttle, 2008), hereafter CT08. Briefly, it is computed as follows: At each spatial grid point, the time of maximum precipitation in the mean summer day time series is located. Then it is computed how far in time one must march equal distances forward and backward (in time) from the time of maximum precipitation in order to encompass 68 % (i.e. $\pm 1\sigma$) of the total area under the mean summer day precipitation time series. Where the diurnal cycle has an isolated, sharp diurnal maximum this will be a relatively small measure of time whereas for multiply peaked or sinusoidal diurnal cycles it will be a larger measure; hence the CT08 diagnostic is a metric of the broadness of the precipitation maximum in the mean summer day, measured in units of time.
3. *Spatio-temporal variability in the central United States:* Animations of the mean summer day precipitation are constructed using an objective time coordinate (i.e. no transformation to local solar time) to characterize the SP-CAM's ability to simulate sea breeze precipitation and the diurnal propagation of convective precipitation initiated over the Rockies into the central United States.
4. *Reduced transect analysis:* Several transects are defined in regions of interest, for detailed regional analysis of the CT08 broadness metric, and the diurnal evolution of parameterized vs. super-parameterized convective heating and moistening.

Harmonic analysis

Figures 4.5 and 4.6 show the amplitude and phase of (color hue), and variance attributable to (color saturation), the least squares fitted 24-hour sinusoid, for the DJF and JJA composite days. Figure 4.5 shows that both models capture the observed tendency for there to be higher diurnal rainfall amplitudes over tropical land masses, tropical convergence zones, and summer hemispheric continents.

The fact that colors are overall unsaturated (i.e. closer to white) for the satellite observations in Figures 4.5 and 4.6 indicates that in nature the composite daily cycle of rainfall is not well described by a single sine wave. For CAM3.0, the opposite is true - color hues are uniformly saturated, indicating far too much diurnal variance in the 24-hour mode, a sign that its daily cycle of rainfall is too simple. For SP-CAM3.0, the results are mixed. In the high amplitude regions of diurnal variability (tropical land masses and tropical ocean convergence zones), decreased color saturation (i.e. increased whiteness) in Figure 4.5 indicates that the SP-CAM3.0 daily cycle of rainfall, like the observations, is more complicated than a simple sine wave. But outside of these most diurnally active parts of the world, for instance over most of the open ocean, the SP-CAM3.0 still simulates an overly sinusoidal diurnal rainfall cycle.

In CAM3.0 it is clear from Figure 4.6 that the diurnal cycle is highly consistent over land and ocean respectively, but that these are very different from each other, a property that the observations do not share. The SP-CAM3.0 improves in this regard- like the observations there is considerable horizontal inhomogeneity in the phase of the diurnal cycle, both over oceans and within continents. Major documented biases in the amplitude of the 24-hour harmonic in CAM3.0 in Figure 4.5, such as an overly strong diurnal rainfall cycle in the tropics, as well as over South America during JJA, and overly weak diurnal variability over the northwestern tropical Pacific (Collier and Bowman 2004), have been fixed in the SP-CAM3.0.

The seasonal scale wet biases in the SP-CAM3.0 manifest themselves as localized excessive 24-hour amplitude maxima in Figure 4.5. Near the overactive

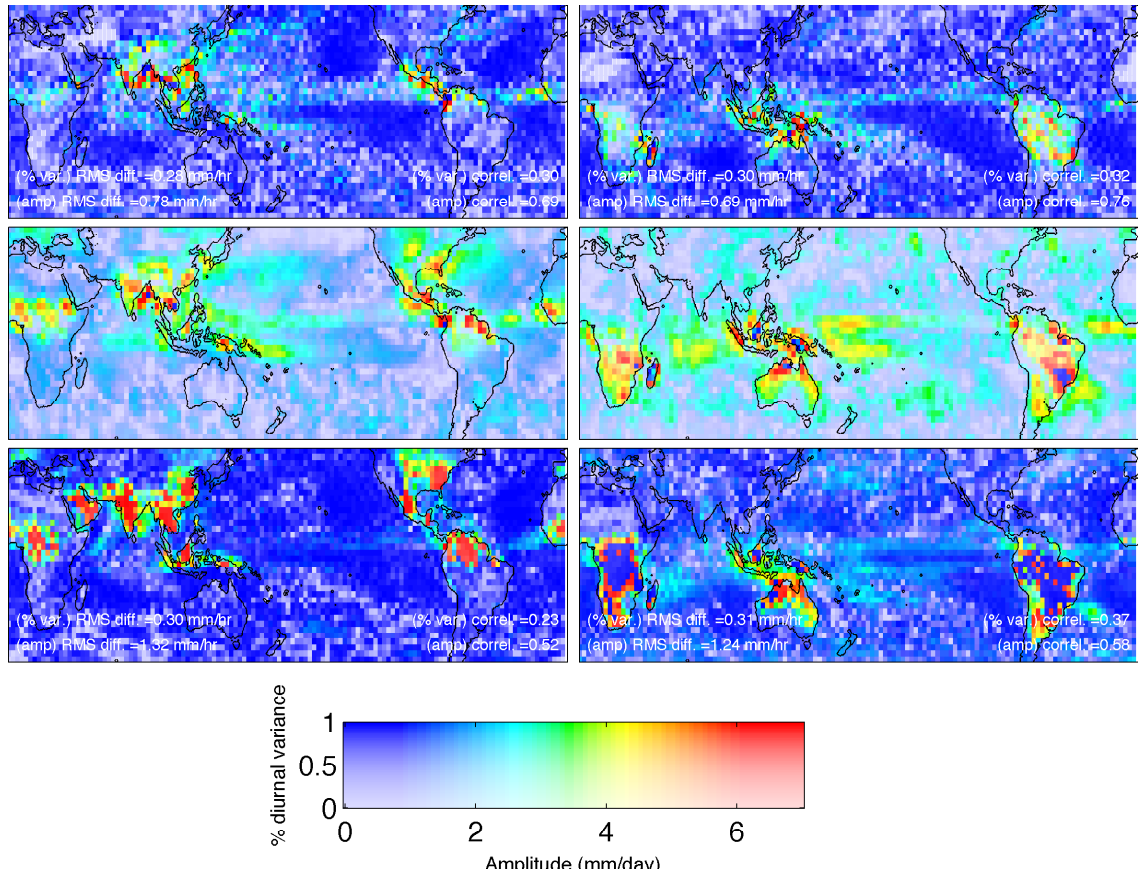


Figure 4.5: Amplitude of (color hue; mm/day), and variance attributable to (color saturation; fraction) the least squared fitted 24-hour harmonic of precipitation for (top) the SP-CAM, (middle) satellite observations and (bottom) standard CAM, during (left) JJA and (right) DJF. RMS difference and pattern correlation relative to the observations are shown for the two models.

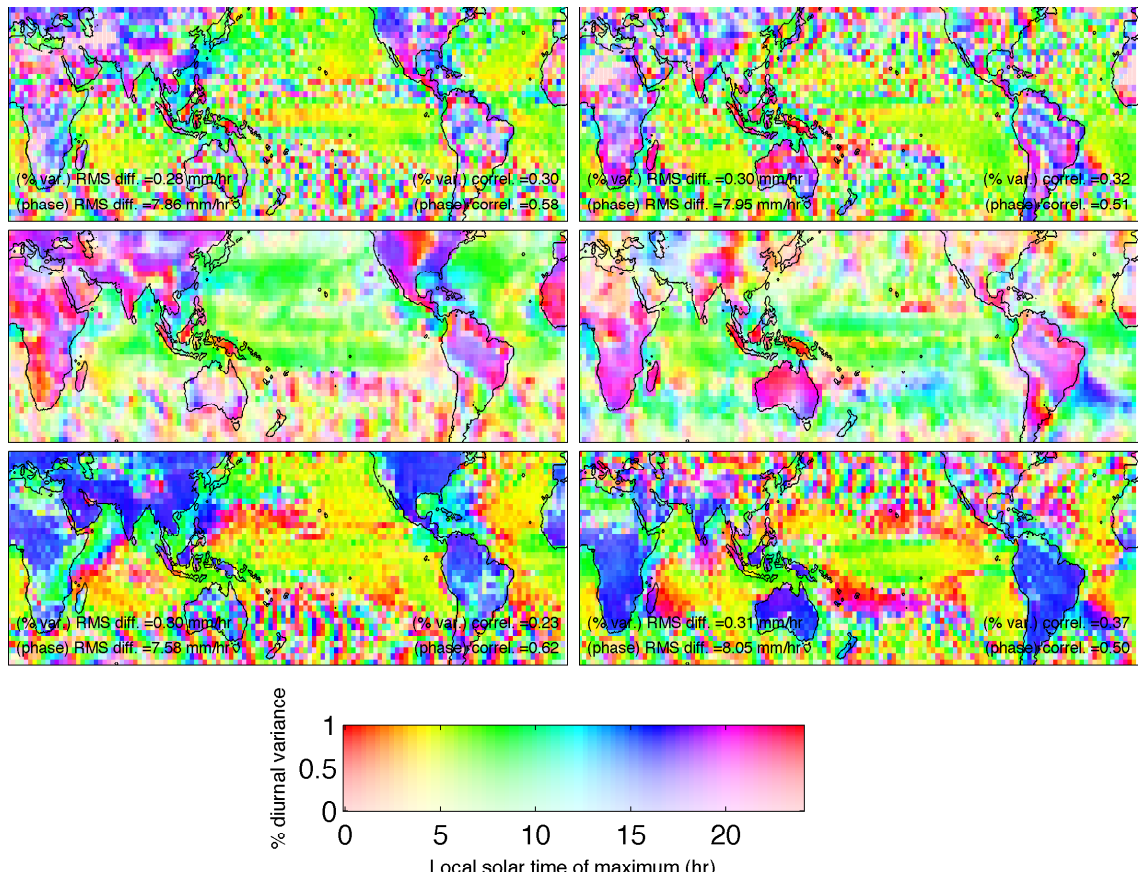


Figure 4.6: As in Figure 4.5, but for the phase, or peak timing (color hue; local hour) of the fitted 24-hour sinusoid of precipitation.

monsoon, Figure 4.6 shows that the timing of peak precipitation over the Bay of Bengal occurs too early in the SP-CAM3.0, and there is no phase propagation southwest from the Himalayas in the 24-hour mode, which is apparent in the observations. Over the Great Red Spot bias of the central Pacific, Figure 4.6 shows that the phase of the 24-hour harmonic is in relatively good agreement with observations, despite excessive amplitude.

Near the United States, Figure 4.6 also shows that the land-ocean phase inversions associated with the sea breeze diurnal cycle in the Gulf of Mexico and along the eastern seaboard are captured well by the SP-CAM3.0, marking an improvement relative to CAM3.0. Observed phase inversions of the 24-hour mode across the coast of Mexico and western Central America are similarly improved in the SP-CAM3.0. But in the western and central United States, the phase characteristics of the 24-hour mode in the SP-CAM3.0 are out of line with observations, and its amplitude is underestimated. The SP-CAM3.0 does not capture the observed nocturnal maximum over the continental interior, and the timing of peak precipitation over the Rocky Mountains occurs too early. No eastward phase propagation is evident in the 24-hour mode into the central United States.

Broadness of the daily maximum

Figure 4.7 compares the CT08 metric (color hue) of the broadness of the diurnal maximum computed from the climate model simulations against the TRMM 3B42 product, bin-averaged to the models' grid. For the models, the absolute bias in the timing of the precipitation peak is also shown (color saturation). The observations show a clear land-sea contrast in the CT08 metric, with isolated patches of narrower maxima occurring over continental interiors, particularly in the summer hemisphere. The land-sea contrast of the observed CT08 metric is also present in

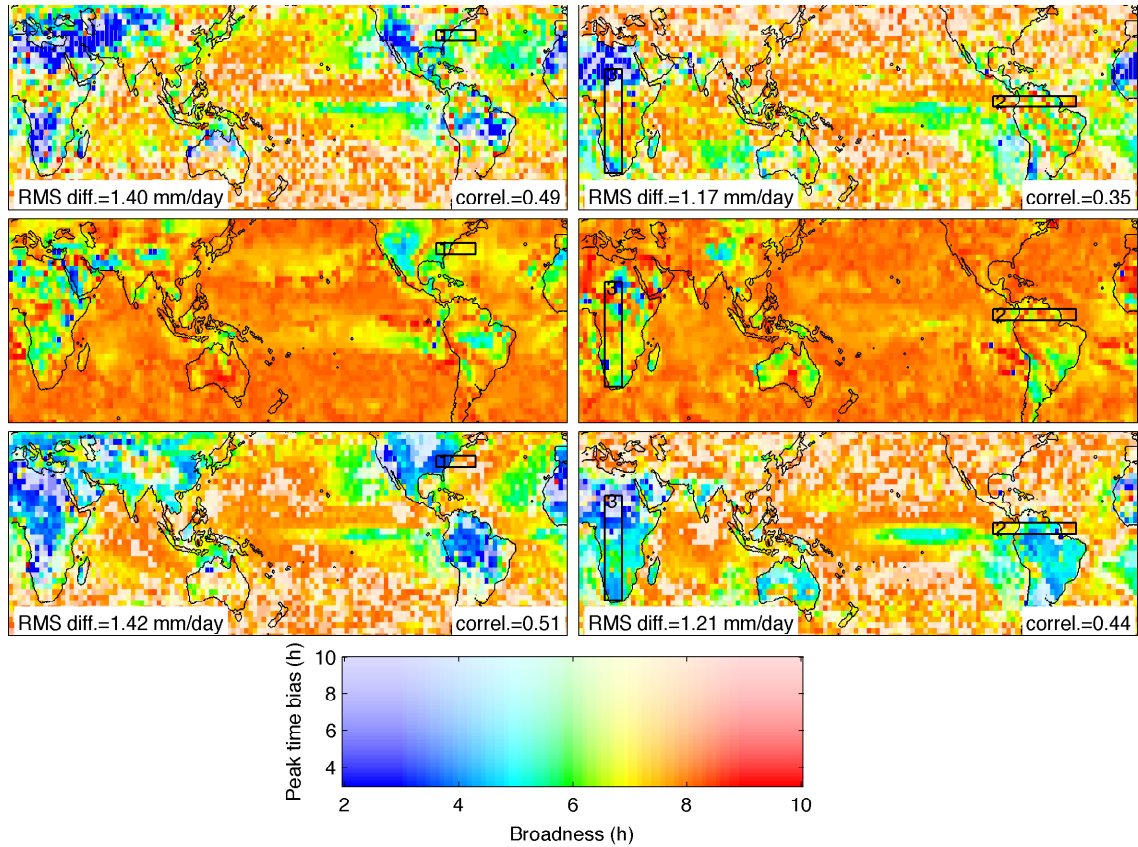


Figure 4.7: CT08 metric of the broadness of the composite day's precipitation peak (color hue) for (top) the SP-CAM, (middle) satellite observations and (bottom) standard CAM, during (left) JJA and (right) DJF. For the two models, the absolute bias in the time of peak precipitation (color saturation) is also shown. The CT08 broadness quantity is the number of hours that must be marched forward and backward from the time of maximum precipitation in order to encompass 68 % of the total area under the mean summer day precipitation time series. Cool color hues correspond to regions with tightly peaked diurnal cycles, and warm hues correspond to broad or multiply peaked composite diurnal variability.

SP-CAM3.0 and CAM3.0 but in the models these patterns are exaggerated (more so in CAM3.0), with values of the CT08 metric reaching as low as 2 hours (narrow diurnal maxima) over continental interiors (note that diurnal broadness less than the time resolution of the data is possible owing to linear interpolation between the 3-hourly data and output in calculating the CT08 metric). Although such tightly peaked diurnal cycles exist in the full resolution TRMM 3B42 data (not shown), when bin averaged to the model grid the diurnal cycle in the observations is considerably broader than the models in these regions. The observations also show that during boreal summer (JJA), the extratropical coastal ocean bordering eastern Asia and the North America exhibits a slightly narrower diurnal peak precipitation than during boreal winter (DJF); this seasonality in the CT08 broadness appears to be captured by the SP-CAM3.0 but not by CAM3.0.

Closer inspection of Figure 4.7 reveals two interesting differences between the structure of the CT08 metric in SP-CAM3.0 and CAM3.0. Firstly, within the continental interiors of North America, Africa, and equatorial South America, the broadness of the diurnal cycle in CAM3.0 appears to be homogeneously small, in the 2-5 hour range. In contrast, the SP-CAM3.0 shows much more horizontal inhomogeneity in the CT08 metric over these land surfaces; there is an east-west contrast over North America, more broadness over equatorial South America, and substantial meridional variability over central Africa. These variations in the SP-CAM3.0's diurnal cycle broadness seem more consistent with the observations, albeit exaggerated in the model in the same fashion as its overall land-sea contrast. Secondly, like the observations, the land-sea contrast of the CT08 metric across coastal ocean boundaries is less sharply defined in the SP-CAM3.0 than in CAM3.0.

Is the apparent improvement in the horizontal variability of the precipitation maximum broadness within continents and across coastal boundaries in the SP-CAM3.0 a true reflection of improved diurnal cycle variability in these regions, or a coincidence of the way in which the CT08 metric is computed? To find out, the

following figures show the spatial variability of the seasonal composite day along three transects (shown in Figure 4.7) where the variability of the CT08 scalar metric of the mean summer day's precipitation in the SP-CAM3.0 appears to be improved relative to CAM3.0. The reduced transect analysis is limited to the DJF composite for tropical transects, and to the JJA composite for extratropical transects in the northern hemisphere.

Figure 4.8 shows that the apparent improvement in the CT08 structure in the SP-CAM3.0 along Transect 1 during JJA (zonal transect straddling eastern seaboard and Gulf Stream) is indeed due to an overall improvement in its diurnal cycle of precipitation. The right panels of Figure 4.8 show the along-transect (zonal) variability in the mean summer day's precipitation in the models and observations, averaged in the cross-transect direction over the transect subdomain. For comparison, the left panels show the variability of the CT08 metric within the same transect subdomain. The along-transect variability in the CAM3.0 mean summer day is dominated by an unrealistic strongly peaked diurnal cycle at the west, over land. This is improved in the SP-CAM3.0. Offshore, the opposite occurs. The CAM3.0 diurnal cycle of precipitation is too weak over the Gulf Stream portion of the transect, and enhanced in the SP-CAM3.0.

Finally, Figure 4.10 shows that apparent improvement in the CT08 metric along Transect 3 (meridional transect through south central Africa) corresponds to real diurnal cycle improvement. In the tropics, the left panels of Figure 4.10 show that the SP-CAM3.0 captures an observed equatorial region of diurnal cycle broadness, while CAM3.0 does not. The right panels of Figure 4.10 show why this is the case; in CAM3.0, the mean summer day over equatorial Africa has a single strong peak near 1500 to 1800 UTC, whereas in the SP-CAM3.0 the mean summer day's structure is doubly peaked (0300-0600 UTC, and 1500 UTC) as are the observations (0300-0600 UTC, and 1500 UTC). The first peak occurs earlier (0300 UTC) south of the equator and later (0600 UTC) north of the equator,

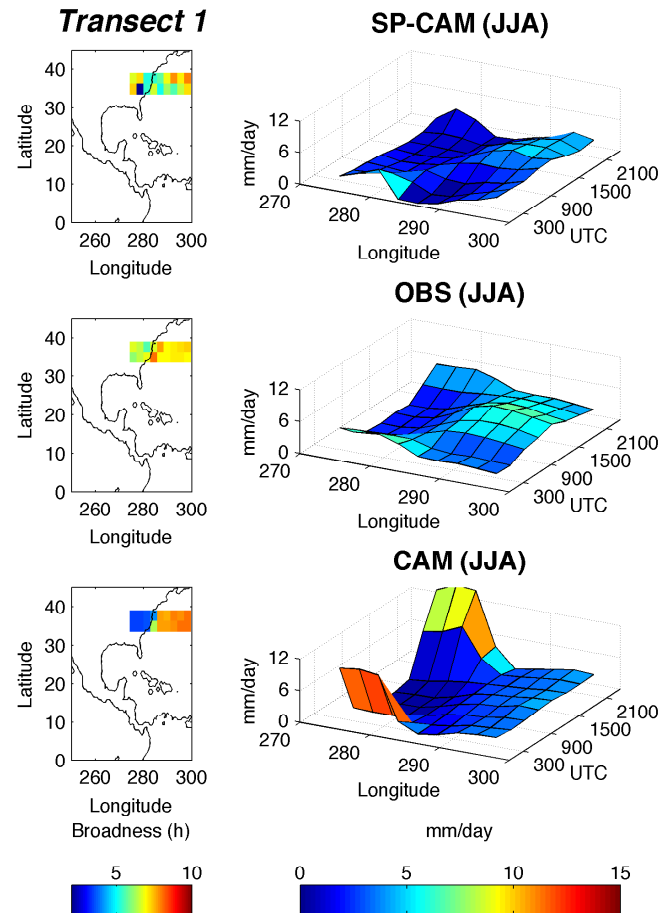


Figure 4.8: (Left) CT08 metric of the broadness of the mean JJA day’s maximum precipitation, shown in a zonal transect domain of interest over the US eastern seaboard and Gulf Stream, comparing the model simulations and the satellite observations, bin-averaged to the model grid. The along-transect structure of the time evolution in the cross-track-averaged mean summer day is shown for comparison to the right.

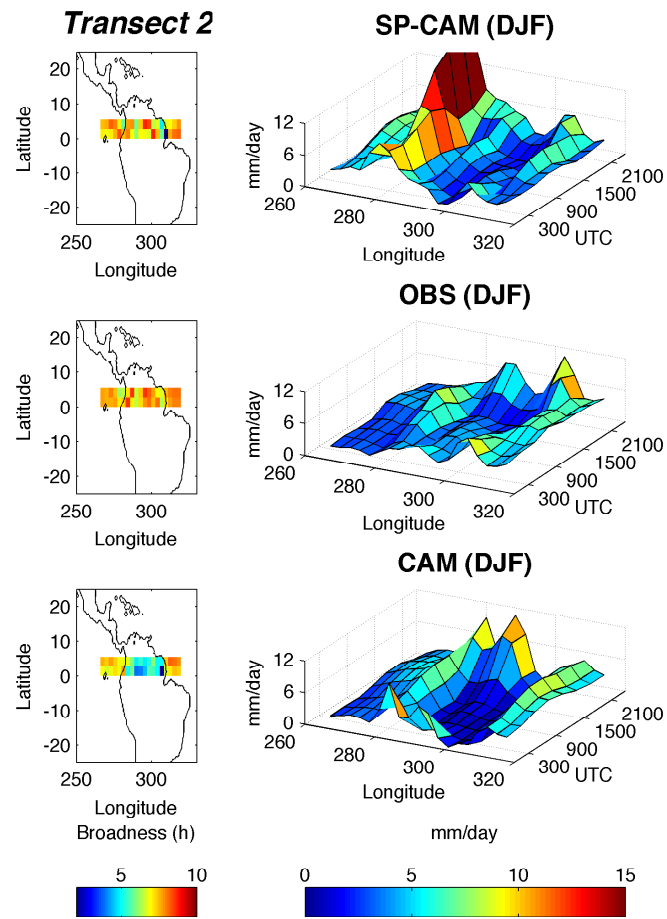


Figure 4.9: As in Figure 4.8, but for a DJF zonal transect straddling equatorial South America.

Figure 4.9 shows that the apparent improvement in the CT08 metric along Transect 2 (zonal DJF transect straddling both coastal boundaries of northern equatorial South America) corresponds to real improvement in the SP-CAM3.0 diurnal cycle at the eastern coastal boundary, but not at the west. The right panels of Figure 4.9 clearly show that CAM3.0 has an overly sharp continental peak in the central region of the transect, and does not capture the diurnal cycle phase inversion in the transition from land to sea at the eastern coast; the SP-CAM3.0 is improved in these respects. But near the western part of the transect, just interior to the Pacific coast, the SP-CAM3.0 diurnal cycle over elevated terrain is much too vigorous, and apparent improvement in the CT08 broadness metric here are misleading.

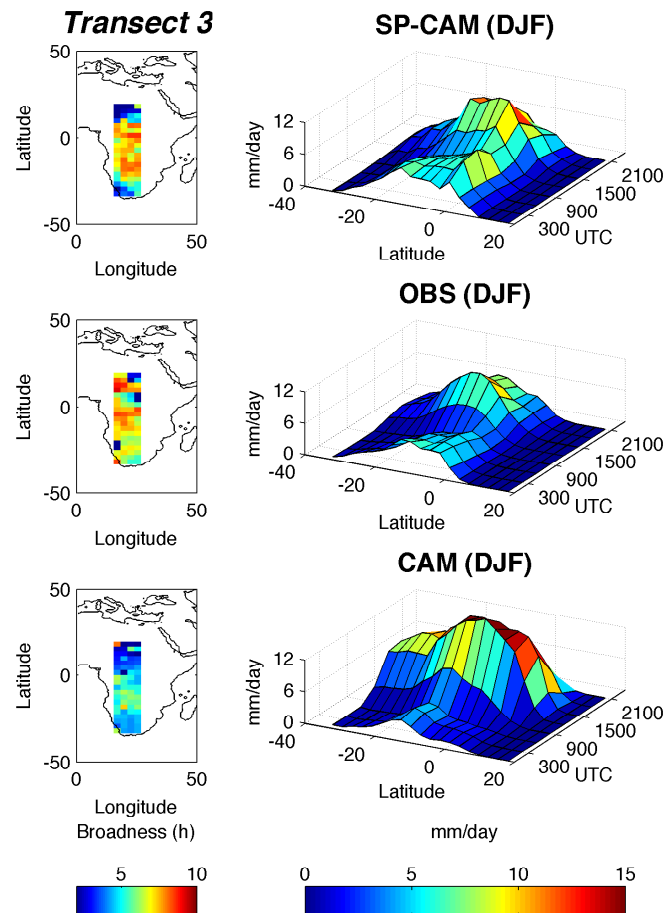


Figure 4.10: As in Figure 4.9, but for a DJF meridional transect straddling equatorial Africa.

which is also captured by the SP-CAM3.0, although it overdoes the magnitude of the latter. In the southern portion of Transect 3, only one diurnal peak is observed, whose amplitude decreases with latitude. This feature is also simulated by the SP-CAM3.0; underestimation of CT08 broadness in CAM3.0 in the southern part of Transect 3 is again due to overshooting the magnitude of the diurnal peak precipitation over land.

The CT08 metric of the broadness of the mean summer day's precipitation maximum is a difficult diagnostic to interpret, but is a useful tool for identifying features of the diurnal cycle that may not be differentiated via harmonic analysis. In the above analysis, the CT08 diagnostic identifies improvements in the SP-CAM3.0's representation of cross-coastal land-sea diurnal cycle variations near the Gulf Stream, improved tropical diurnal variability over equatorial Africa, and improved phasing across the Atlantic coast of north equatorial South America.

Spatial-temporal variability: North America

Figure 4.11 and Video S1 [PRECIP.MOV]² show the spatial and temporal variability of the composite boreal summer day over North America at the full 3-hourly resolution of the satellite product. This is the most information-rich vantage point from which to evaluate the fidelity of the simulated mean summer day's precipitation. We define the following list of the most significant events in the observations (OBS) as a useful baseline for model comparison:

1. (0600-1500 UTC; Figure 4.11 c. through f.) A flare of oceanic precipitation occurs over the Gulf Stream current, reaching peak rain rates near 7 mm/day near the midlatitude (offshore) portion of the current around 1200 UTC

²Available online at <http://james.agu.org/index.php/JAMES/article/downloadSuppFile/v1n12/S1>

(Figure 4.11 e.), and several hours later for the southern (coastal) portion of the current, peaking around 1500 UTC (Figure 4.11 f.) off the eastern coast of Florida. From 1200-1800 UTC (Figure 4.11 e. through g.) there is a southwestward shift in the location and increase in the magnitude of maximum Gulf Stream precipitation in the diurnal composite.

2. (1200-1500 UTC; Figure 4.11 e. through f.) A localized pulse of offshore precipitation over the coastal ocean borders the northern boundary of the Gulf of Mexico.
3. (1800-0000 UTC; Figure 4.11 g., h., and a.) The above is followed as it dissipates by a broad pulse of heavy continental precipitation, initiating at the southern extremity of the Florida panhandle where precipitation rates exceed 7 mm/day over a broad region, and progressing towards the continental interior, with precipitation rates diminishing towards the northwest farther inland.
4. (0000 UTC; Figure 4.11 a.) A brief pulse of convective precipitation collocated with topographic features in the Western United States, reaching rain rates of 2-3 mm/day.
5. (0300-1200 UTC; Figure 4.11 b. through e.) Eastward propagation into the central United States of a coherent precipitating feature with rain rates in the 3 mm/day to 5 mm/day range, dissipating as it progresses.

The apparent noisiness in the SP-CAM3.0 composite is a result of sporadic, localized precipitation and a relatively short (single summer) composite. When only a single summer of observations is composited (not shown) the result is similarly noisy, although the chronology of events outlined above based on the full 7-summer observation composite is still discernible in each individual summer. The noisiness in the SP-CAM3.0 precipitation actually represents an improvement relative to

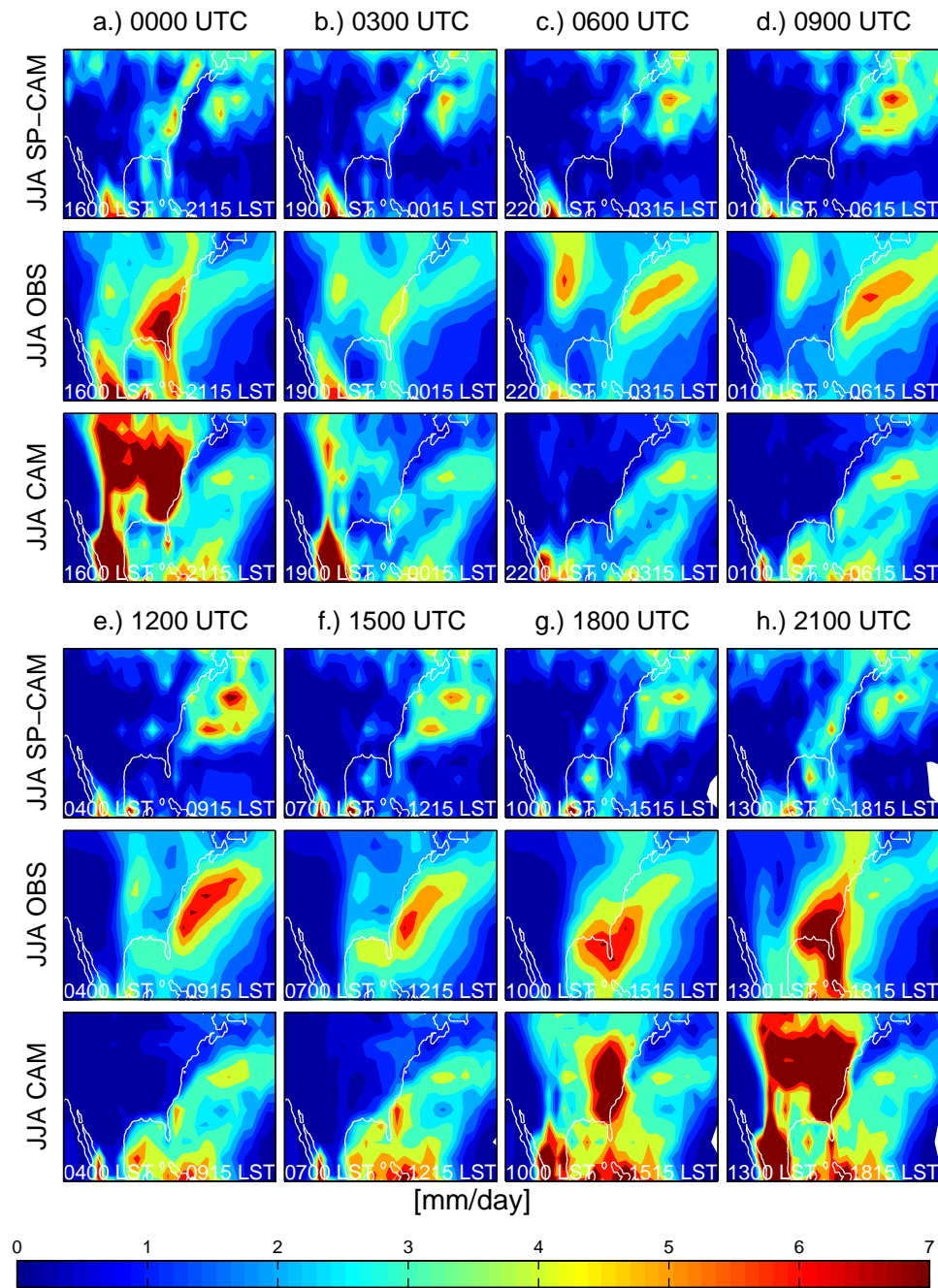


Figure 4.11: Evolution of the composite JJA day's precipitation over North America, comparing the two climate models against the satellite observations. Snapshots of the 3-hourly average precipitation rate are shown. Local solar time at the longitude axis limits is superimposed at the bottom of each subpanel in text. Note the model-observation-model comparison shown here is more intuitively absorbed in animation format; viewing the auxiliary animation file is recommended.

CAM3.0, which within the composite exhibits a too regularly repeated, and expansive, rainfall cycle and thus produces an overly smooth composite from only a single summer of output.

Looking past the noisiness caused by the single-season compositing, the SP-CAM3.0 does a strikingly better job than CAM3.0 at capturing effects (1) through (3) above, but like the CAM3.0 it misses (4) and (5). The magnitude and chronology of the diurnal cycle of precipitation over the Gulf Stream (1) are particularly impressive. Here, CAM3.0 has little diurnal variability and undiscernable phase differentiation between the phase of the diurnal cycle in the open ocean (northern) segment versus the coastal ocean (southern) portion of the Gulf Stream. With respect to (3), Figure 4.11 h.,a.,b. reveals that the pattern of southeastern continental precipitation in the SP-CAM3.0 from 2100 UTC to 0300 UTC resembles the observations fairly well, although the magnitude is underestimated; there is a fringe of high rainfall adjacent to the east coast (Figure 4.11 a.), preceded by a localized maximum near Florida (Figure 4.11 h.). In contrast, Figure 4.11 h.,a.,b., show that in the CAM3.0 mean summer composite day the entire continental interior east of the Rockies experiences a sudden pulse of unrealistically widespread, homogeneous and heavy precipitation, producing high diurnal cycle amplitudes throughout the central United States (as observed) but for the wrong reason (the pattern is incorrect).

Over the continental United States, the satellite data in Figure 4.11 a. through e. clearly show how a pulse of precipitation initiated over the mountain ranges in the western United States propagates eastward into the continental interior, causing the nocturnal maximum in rainfall. SP-CAM3.0 and CAM3.0 show markedly different diurnal variability over the continent, with respect to the observations and each other. The top panel of Figure 4.11 shows that neither model is able to capture the localized afternoon convective precipitation over high topography evident in the observations near 2100 UTC. Thus it is not surprising that subsequent

eastward propagation and central United States nocturnal maximum are also not simulated.

Discussion

The most energetic locations of diurnal rainfall in the SP-CAM3.0, over tropical land masses and the oceanic convergence zones, are not well fitted with a single 24-hour sine wave, which is an important improvement over CAM3.0. Harmonic analysis shows far too much variance attributable to the 24-hour mode in CAM3.0 globally (and in SP-CAM3.0 where the diurnal cycle of rainfall is weak) and the CT08 broadness of the CAM3.0 diurnal maximum is uniformly too narrow over land surfaces. Transect analysis shows that CAM3.0 misses the doubly peaked tropical precipitation cycle over central Africa, favoring sinusoidal variability, and the North American animation shows unrealistically homogenous pulsating diurnal precipitation over the central United States. In each of the above diagnostics, the SP-CAM3.0 diurnal variability, like the observations, appears much less sinusoidal, at least over land masses and in regions of vigorous convection. This can be explained by the fact that in CAM3.0, precipitation is rigidly tied to CAPE which like solar variability varies rather sinusoidally, whereas in the nested cloud resolving subcomponent of the SP-CAM3.0, high resolution moist boundary layer dynamics provide new degrees of freedom for more sophisticated convective activity and moisture transport, which result in a more complex daily rainfall cycle that is not well fit with a single sine wave. The overly sinusoidal weak rainfall cycle in the open ocean remains a perplexing problem in the SP-CAM3.0.

The SP-CAM3.0 approach does not admit diurnally propagating orogenic precipitation systems over the Central United States, which may explain the model's

seasonal scale dry bias in this region. It is logical to suspect³ the SP-CAM3.0 fails to resolve orogenic propagating organized precipitation due to a key design limitation, *the use of periodic boundary conditions* in the cloud-resolving subdomain. Although necessary from a technical and parallel computing perspective, the fact that CRM columns don't communicate across host GCM grid cell boundaries in the SP-CAM3.0 limits the ability for propagation of organized convection to the extent that it can be mediated via its influence on large scale motions. Although this is apparently not an obstacle for the propagation of the MJO, it likely limits the degree to which smaller-scale organized convection can propagate and sustain itself in the SP-CAM3.0, especially at the coarse T42 (300-700 km) horizontal resolution in the host GCM.

The SP-CAM3.0 appears to do a better job at capturing structural changes in the diurnal cycle of precipitation across land-sea boundaries. The North American animations also show that the SP-CAM3.0 has improved the overall progression of precipitation events over the Gulf Stream, Gulf of Mexico and southeastern continental United States. The cross-coastal contrast in the broadness of the diurnal cycle maximum is smaller in the SP-CAM3.0 than in CAM3.0, and transect analysis shows that this is due to improved representation of shifts in diurnal rainfall cycle across coastal boundaries.

It is well worth understanding the mechanisms responsible for the improved continental diurnal rainfall timing in MMF simulations. Much has been learned about the actual mechanisms that underly the continental diurnal rainfall cycle on regional scales from explicit cloud resolving simulations and mesoscale observational literature (Guichard et al., 2004; Grabowski et al., 2006; Kuang and Bretherton,

³Indeed, it was speculated that these inherent design features should prohibit Central US propagating rainfall systems in the published version of this section, Pritchard and Somerville (2009a). However, it will be shown in Chapter 6, that it is nonetheless possible for a superparameterized climate model to produce nocturnal propagating MCS in the Central US, and that this has implications for how one should think about slow- versus fast-manifold control on the nocturnal maximum of rainfall.

2006; Khairoutdinov and Randall, 2006). But the topic is still an area of active research (Zhang and Klein, 2010), and questions remain for the modeling community to address. For instance, in the purely cloud resolving modeling literature the ability of 2D CRMs to capture the transition from shallow to deep convection is still in debate (Petch et al., 2008; Wu et al., 2009). In the LES modeling community, there are controversies about the role of localized cold pool driven mesoscale organization versus bulk detrainment preconditioning in removing the entrainment barrier during the transition to deep convection (Kuang and Bretherton, 2006; Khairoutdinov and Randall, 2006). For all such studies, regarding the timing of continental convection, how much of the “answer” is built in to the forcings used to drive cloud resolving simulations (Petch et al., 2008)? Super-parameterized simulations add a novel perspective in this regard, since both the forcing on the cloud-resolving scale, and its feedback to large-scales, are independently resolved. Superparameterization also restricts the spatial scale over which fast manifold processes can operate, which provides a unique learning opportunity traditionally unavailable from limited domain CRM simulations.

The only study that has previously examined the physical mechanisms controlling the timing of continental convection in super-parameterized climate simulations was by DeMott et al. (2007). Their strategy was to apply lag (in time) - correlation analysis to document the relationships between humidity, boundary layer energy, and afternoon rainfall in three continental subregions near well instrumented field sites. As outlined above in Section 2.3.4, the authors develop a **hypothesis that explicitly resolved entrainment humidification preconditioning is the cause for the improved (delayed) diurnal rainfall maximum over land** in SP-CAM. This hypothesis is shown to be consistent with the above statistical relationships.

However, correlation is not necessarily causation, and Figure 4.12 and its ac-

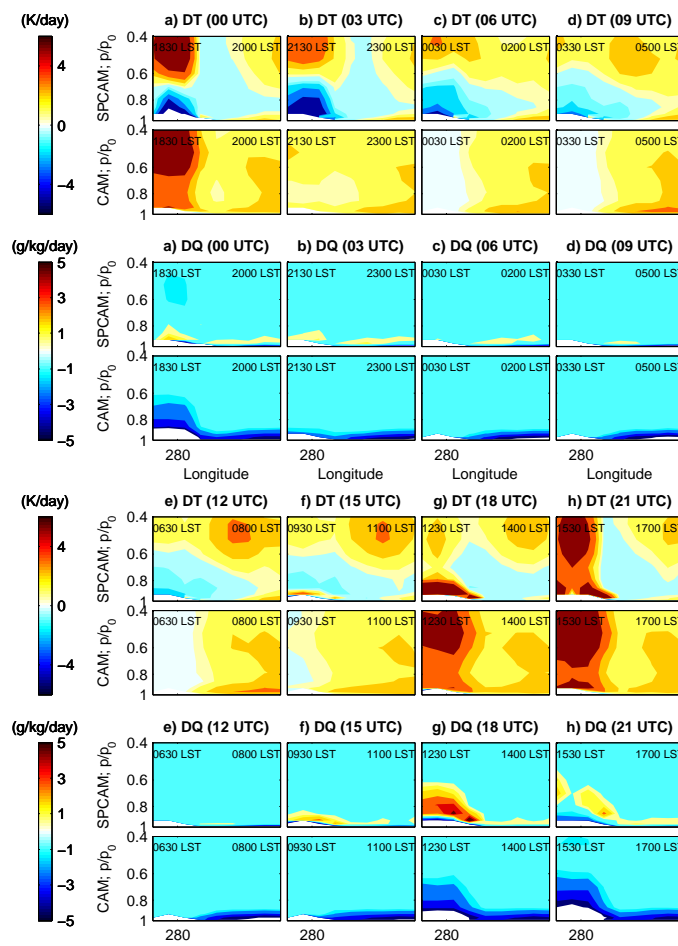


Figure 4.12: Height-longitude section contrasting the diurnal chronology of convective heating and convective moistening in the SP-CAM and the CAM, along a zonal transect straddling the Gulf Stream and eastern United States (Transect 1 in Figure 4.7). The quantities shown are tendencies exerted by convection in the physics package, i.e. by nudging towards the nested CRM in the SP-CAM and as diagnosed by conventional parameterization in CAM. The vertical coordinate is normalized pressure ($\sigma = p/1000$ hPa), and the land component at the western edge of the transect is identifiable as a blanked out region at the base of the domain. This is easiest viewed in the auxiliary animation file, Video S2 [CONVTEND.MOV].

companying animation Video S2⁴ seek an additional burden of proof be met regarding the physics underlying the continental diurnal rainfall in SP-CAM. Is the DeMott et al. (2007) hypothesis supported by unambiguously causal model diagnostics that explicitly bracket the effect of the embedded CRM on the outer model? To find out, Figure 4.12 contrasts the vertical and along-transect diurnal evolution of heating and moistening due to convection in the two models, along the Gulf Stream zonal transect discussed previously. In the case of the CAM3.0, these convective tendencies are diagnosed in the model physics package by the Zhang-McFarlane and Hack convection schemes (variables ZMDT, ZMDQ, CMFDT, CMFDT). In the case of SP-CAM3.0, all the subgrid-scale tendencies that include cloud processes but exclude radiative heating rates are computed by the embedded CRMs; details are given by Khairoutdinov et al. (2005). In Figure 4.12 the most thermodynamically significant difference between the two models' diurnal cycle is the daytime convective heating and moistening (in the SP-CAM3.0) of the lower and mid troposphere over land. In the western part of the transect, from 0630 to 0930 LST (Figure 4.12 e.,f.) vertically confined convection in the SP-CAM3.0 manifests as a shallow layer of convective heating near the surface. Above the deepening SP-CAM3.0 boundary layer the mid-troposphere is cooled and moistened by the influence of the nested CRM. This is consistent with the key role of entrainment mixing by shallow convection argued by DeMott et al. (2007), as is captured by CRMs run in full three dimensional domains (Guichard et al., 2004; Bretherton, 2007). From the perspective of internal model diagnostics, pre-conditioning of the mid troposphere appears to play a role in delaying the onset of subsequent deep convection over land in the SP-CAM3.0, resulting in the improved diurnal timing of peak diurnal rainfall, and also drastically altering the chronology and vertical structure of thermodynamic forcing on the atmospheric

⁴Available online at <http://james.agu.org/index.php/JAMES/article/downloadSuppFile/v1n12/S2>

column adjacent to the ocean, relative to CAM3.0. The same coastal land inter-model difference shown in Figure 4.12 can be seen in many other cross-coastal transects, straddling the Maritime Continent, equatorial South America, and the Gulf of Mexico (not shown).

Over the oceanic (eastern) portion of the transect, Figure 4.12 shows that CAM3.0 tends to convect deeply at all times of day, presumably because its formulation of deep convection is cast in terms of undilute CAPE and thus constantly triggered by the high surface fluxes over the Gulf Stream. In the SP-CAM3.0, most of the enhanced day-to-day variability over the Gulf Stream occurs in a shallow convective boundary layer which deepens and invigorates nocturnally (Figure 4.12a.-c.), apparently following humidification (cooling and moistening) of air atop a very thin convective layer during the day (Figure 4.12 f.-h.). Unlike the SP-CAM3.0 diurnal chronology of convective heating higher up in the atmosphere discussed below, this boundary layer cycle over the Gulf Stream in the SP-CAM3.0 occurs regularly on individual days. Further evidence that low cloud processes are involved in the enhanced SP-CAM3.0 diurnal rainfall cycle is provided by the fact peak Gulf Stream rainfall coincides with a southward extension of a broader area of high low-cloud fraction in the North Atlantic (not shown). In fact, all climatological regions of low cloud coverage exhibit more areal diurnal expansion and contraction in the SP-CAM3.0 than in the CAM3.0 (not shown).

In Figure 4.12 c.-f., the apparent eastward propagation of a mid-tropospheric convective heating signal in the SP-CAM3.0 diurnal composite near $\sigma = 0.5$ is difficult to interpret because it appears sporadically on individual days. The possibility of a free atmospheric wave mechanism linking land and coastal ocean diurnal cycles in the SP-CAM3.0 is intriguing. Although the gravity wave process implicated in the tropical study of Mapes et al. (2003) is unlikely to be resolvable by the SP-CAM3.0 (since adjacent gravity-wave-resolving CRMs cannot propagate information across host model grid boundaries), larger-scale mechanisms active in

midlatitudes, such as inertia-gravity waves, or synoptic advection of convective heating anomalies induced by the embedded CRM, could be operative in linking Gulf Stream diurnal precipitation with thermal forcing over land in the SP-CAM3.0. This issue of the Gulf Stream diurnal rainfall cycle, and the mechanisms that support it, is investigated in further detail in Section 5.3.

Section 4.2, in part, is a reprint of material as it appears in *Assessing the diurnal cycle or precipitation in a multi-scale climate model 2009*. Pritchard, Michael S., Somerville, R. C. J., *Journal of Advances in Modeling Earth Systems*, Vol. 1, Article No. 16, 2009. The dissertation author was the primary investigator and author of this paper.

4.3 Conclusions

In summary, EOF decomposition (Section 4.1) and multiple, complementary diagnostics of seasonal composite diurnal cycle of precipitation (Section 4.2) have been combined in order to characterize the performance of moist dynamics in a multi-scale modeling framework (SP-CAM3.0) and its GCM counterpart (CAM3.0) on diurnal timescales. Multi-platform merged satellite data is used as a baseline for model evaluation. Each diurnal cycle diagnostic comes with pros and cons. Traditional harmonic analysis allows an analysis of the global structure of both the strength and phase of sinusoidal diurnal cycles, but is only applicable to regions where this curve fit is a reasonable approximation. The non-traditional CT08 metric of the broadness of the peak precipitation distinguishes narrowly peaked diurnal cycles from broader, or doubly peaked diurnal cycles, without the necessity for curve fitting, but there is a degeneracy problem in that very different diurnal cycles can produce the same result. Animations or reduced dimension transects of the full spatial and temporal variability of the climatological seasonal composite day provide the most information-rich perspective for model evaluation, but must

be undertaken regionally and are difficult to summarize since their interpretation can be subjective.

Combining all of these perspectives, several common features distinguishing the diurnal rainfall cycle in the SP-CAM3.0 from CAM3.0 may be summarized, which have not been previously identified in the literature. Positive features in SP-CAM3.0 include:

- Less sinusoidal variability where diurnal rainfall is vigorous,
- Less overestimation of diurnal rainfall over tropical and summer hemispheric land masses,
- Good representation of the observed structural transitions of diurnal rainfall across coastal ocean boundaries.
- More horizontal inhomogeneity of diurnal rainfall cycles within continents and within oceans,
- Improved chronology of diurnal precipitation in the southeastern United States, western Atlantic and Gulf of Mexico diurnal composite.

Remaining negative features of the SP-CAM3.0 diurnal rainfall cycle include:

- No orogenic propagating precipitation over the central United States.
- Excessive diurnal variability associated with the overactive monsoon
- Overly sinusoidal diurnal rainfall over most of the open ocean

These findings are consistent with the more compact EOF analysis of the composite boreal diurnal cycle of rainfall discussed in Section 4.1. For instance, harmonic analysis has indicated that over the entire globe, too much of the variance in the CAM3.0 diurnal cycle could be explained by a single 24-hour harmonic, just

as EOF analysis indicates that too much of the variance in CAM3.0 is in a single EOF (Figure 4.1). Harmonic analysis also revealed excessive diurnal variability associated with the super-active Indian Monsoon in the MMF, a region in which biases are also evident in the amplitudes of the leading EOFs (Figures 4.2 and 4.3). Animation of the mean summer day indicated that the MMF is unable to capture the observed diurnal eastward propagation of organized convective precipitation over the central United States, a fact that is consistent with the presence of regional anomalies in the amplitudes of EOF₁ and EOF₂. The EOF analysis in Section 4.1 thus provides a consistent and compact framework for evaluating simulated model biases on diurnal timescales.

Epilogue: Sensitivity to arbitrary configuration options

The above analysis has distilled the major apparent diurnal rainfall benefits of super-parameterization *only in its most widely analyzed application*, i.e. at low spectral exterior resolution (T42; 400-700 km) with a zonally oriented, 4-km embedded CRM. To re-iterate, the most significant improvements under this configuration are:

1. a decrease in the goodness of fit of the 24-hour rainfall harmonic,
2. a reduction in the amplitude of the tropical land diurnal rainfall, and
3. a shift in the timing of much continental rainfall from noon to late afternoon.

As a closing question, it is important to ask – **are these beneficial effects of super-parameterization robust to arbitrary configuration choices such as exterior model resolution and CRM orientation?**

To find out, a variety of perturbed CAM and SPCAM configurations⁵ are explored from the same perspective of harmonic analysis of the boreal summer composite diurnal rainfall cycle applied above. The first is a modified version of the standard low-resolution (T42; $\sim 400\text{-}700$ km) configuration of SPCAM3.0, called SPCCSM3.0. In this model, the orientation of the 4 km resolution CRM is switched from east-west to north-south and an interactive⁶ coupled ocean model is included. A variety of higher resolution ($1.9^\circ \times 2.5^\circ$; ~ 200 km) finite volume runs are also analyzed based on the models tagged CAM3.5, SPCAM3.5, and MACM. The conventionally parameterized benchmark model CAM3.5 employs a dilution limiter in its cumulus parameterization closure, instead of closing on undilute CAPE as in CAM3.0. The SPCAM3.5 runs were also configured with higher resolution in the embedded CRMs than in SPCAM3.0 (1 km instead of 4 km), for both an east-west and north-south CRM orientation. The most recent prototype superparameterized model (MACM) is analyzed in the east-west CRM orientation configuration for direct comparison to SPCAM3.5. This model stands alone in that it includes several updates to the subgrid physics in the CRM including a higher order treatment of sub-grid turbulence, double-moment microphysics, and new degrees of freedom for convection-aerosol interactions. The performance of MACM has never before been examined on diurnal timescales.

Figures 4.13 and 4.14 show the results of harmonic decomposition of the boreal summer 24-hour day for the ensemble of superparameterized and conventionally parameterized simulations. Are the three apparent improved effects of superparameterization found previously for SPCAM3.0 and CAM3.0 robust to changes in model configuration?

The first effect, a decrease in the goodness of fit of the 24-hour rainfall sinusoid

⁵See Appendix A.

⁶The frequency of atmosphere-ocean coupling does not occur more than once a day; there is no representation of SST skin temperature effects on the lower boundary of the atmosphere in SPCCSM3.0 (Cristiana Stan, personal communication).

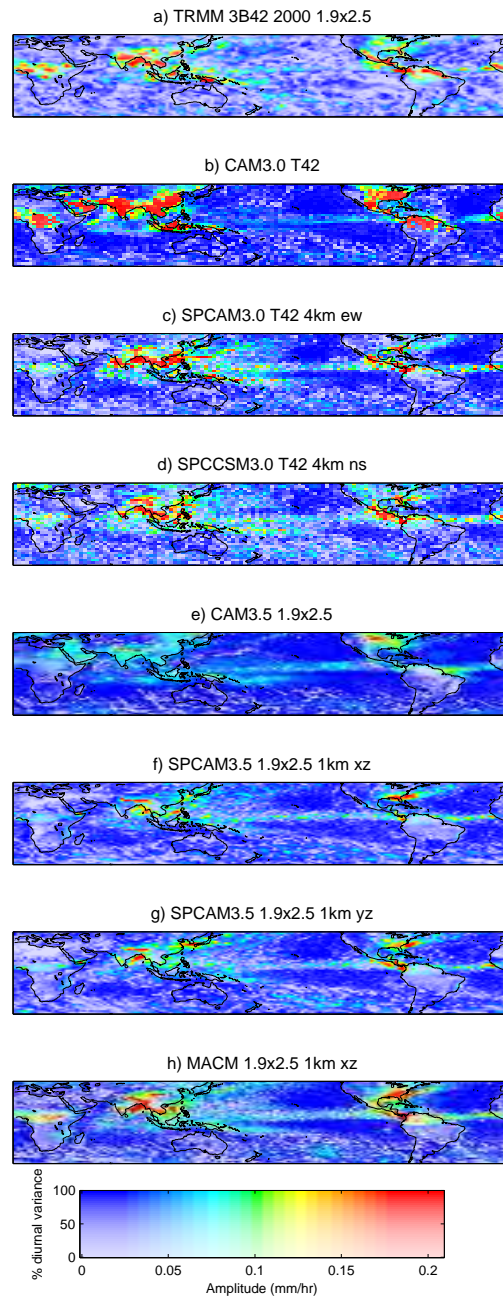


Figure 4.13: Amplitude of the fitted 24-hour diurnal harmonic of JJA composite rainfall in a) observations compared to b)-h) an ensemble of conventional and superparameterized global climate model simulations in various configurations. See text for details.

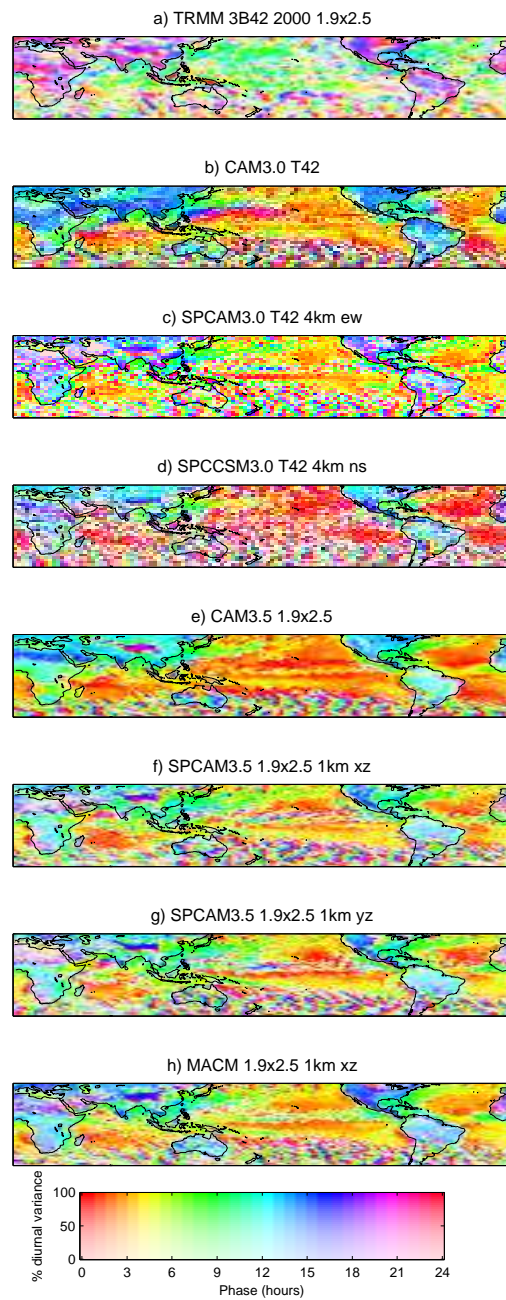


Figure 4.14: As in Figure 4.13 but for the phase (local time of maximum rainfall) of the 24-hour rainfall harmonic.

does appear to be a robust benefit of superparameterization on diurnal timescales, for all model configurations. For both the low-resolution superparameterized runs (Figure 4.13c,d) and the high resolution superparameterized runs (Figures 4.13f-h), the percent of diurnal variance explained by the 24-hour mode decreases relative to the conventionally parameterized benchmark cases (Figure 4.13b,e). Evidently, the addition of a dilution constraint into the conventional cumulus parameterization's closure in CAM3.5 did not remedy the problem of producing a simplistically sinusoidal simulated diurnal rainfall cycle in CAM3.0 (Figure 4.13b,e).

Figure 4.13 illustrates that the second effect, reducing the amplitude of the tropical land diurnal rainfall cycle, is also a robust feature of all the superparameterized simulations. However, the analysis also indicates that there are more efficient strategies than superparameterization to ameliorate this model bias. A similar tropical amplitude reduction is also achievable through the use of a conventional cumulus parameterization that has a dilution constraint incorporated in its closure (CAM3.5; Figure 4.13e vs. 4.13b). However, this strategy does not fix the problem of peak rainfall occurring too early over continents (Figure 4.14e vs. 4.14b).

Improved diurnal rainfall timing over land is evidently *not* a robust benefit of superparameterization. In the standard low-resolution implementation, when the 4 km CRM orientation is switched from zonal (Figure 4.14 b) to meridional and an interactive ocean model is coupled to the atmosphere (Figure 4.14 d), the simulated local time of peak continental rainfall reverts to occurring too early in the day, as in the conventionally parameterized models. Similarly, when the resolution at both resolved scales is increased from 400-700 km to 200 km at the exterior resolved scale, and from 4 km to 1 km in the interior resolved scale, superparameterization (Figures 4.14f-h) has very little influence on the continental daily rainfall timing (Figure 4.14e). There is more influence of superparameterization on diurnal rainfall timing in the only MMF in the ensemble that includes aerosol effects and multi-

moment cloud microphysics (MACM; Figure 4.14h) in an identical high resolution configuration (Figure 4.14f). It is possible that the apparent improved diurnal rainfall timing in SPCAM3.0 was a fortuitous coincidence somehow connected to the choice of very coarse resolution in the exterior model (400-700 km) and coarse 4 km resolution in the interior model.

In the following chapter, regional sensitivity studies focus on oceanic diurnal precipitation and the mechanisms that link it to the representation of diurnal convective heating and moistening over adjacent land in the SP-CAM3.0 (Chapter 5). The nocturnal maximum over the Central US is re-visited in Chapter 6. Inspired by the above analysis, these are aspects of the diurnal rainfall cycle where superparameterized climate simulations offer new learning opportunities.

Chapter 5

Non-local control of the marine diurnal rainfall cycle by land

Chapter 3.2 asked the following questions regarding the connection between land and the oceanic diurnal cycle:

1. **Can coarse resolution climate projection models capture observed tropical diurnal subsidence waves over the ocean?** Section 5.1 focuses on the representation of large-scale diurnal subsidence waves equatorward of the diurnal-inertial resonance latitude. Such waves have become a recent topic of interest in the literature, due to new constraints from satellite scatterometer data, which are here brought to bear to investigate climate model simulations of long-range remote control of the oceanic diurnal rainfall cycle.
2. **Does super-parameterization alter the remote control of the marine diurnal rainfall cycle by land?** Section 5.2 analyzes the effect of super-parameterization on the simulated atmospheric diurnal water budget over a large swath of tropical ocean.

3. **How do land-sea control mechanisms relate to the observed Gulf Stream diurnal rainfall pattern?** Section 5.3 seeks to understand the mechanisms supporting the observed boreal summer diurnal rainfall cycle over the Gulf Stream, which is a robust feature of JJA climate that has not received much attention in the literature. An ensemble of conventional and prototype super-parameterized climate model simulations, some of which capture the observed pattern of rainfall variability, and some of which do not, is analyzed over the Gulf Stream.

5.1 Climate model representation of tropical diurnal subsidence waves

Figure 5.1 shows a recent analysis of the observed diurnal cycle of ocean surface divergence by Wood et al. (2009). Diurnally resolved satellite surface wind retrievals are rare but were available from a brief time period during which a pair of overlapping wind scatterometer satellite missions together provided 4× daily sampling surface winds over the ocean. The fitted 24-hour diurnal cycle of surface inferred wind divergence¹ exhibits amplitude fringes extending outwards from coastlines (Figure 5.1a) and co-incident coherent diurnal phase striations (Figure 5.1b). Together, these are clear signatures of long-range remote control of the marine diurnal cycle by diurnal heating over land.

Wood et al. (2009) showed that a very high resolution (40 km) operational forecast analysis model could reproduce many of these observed subsidence wave features, but emphasized that it is unknown to what degree these features are captured by coarse resolution climate projection models.

The following analysis makes a contribution in this regard, by documenting the

¹Equivalently, through continuity, surface wind divergence represents free tropospheric subsidence.

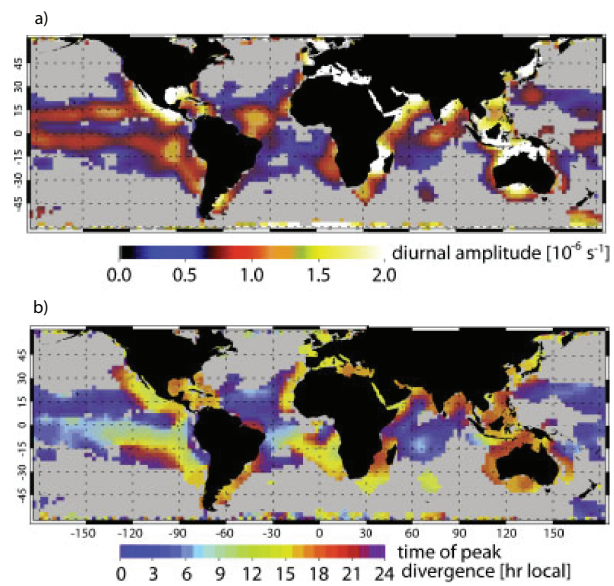


Figure 5.1: “Diurnal amplitude (a), and local time of maximum diurnal surface divergence (b) for April-September 2003 from the tandem SeaWinds data (left panels).” Reproduced from Wood et al. (2009) Figure 1.

representation of long-range subsidence waves in a conventional climate model and a prototype super-parameterized climate model. Can coarse resolution climate projection models and prototype super-parameterized climate models reproduce the diurnal remote control of surface divergence that is captured by the scatterometer data of Wood et al. (2009)?

Figure 5.2 contrasts the mean state JJA surface divergence pattern in an ensemble of super-parameterized and conventionally parameterized climate simulations, relative to the scatterometer results derived in Wood et al. (2009). All of the models capture the gross aspects of the pattern associated with the general circulation: Divergence associated with subsidence over the subtropical gyres, convergence in the ITCZ, the Warm Pool, the Indian Ocean, and over the Gulf Stream and Kuroshio Currents. Super-parameterization evidently enhances the mean state convergence over the Bay of Bengal and western tropical Pacific, co-incident with known areas of anomalous JJA rainfall biases in SPCAM3.0. The Great Red Spot JJA model bias is clearly associated with an anomalous mean state convergence zone, Figure 5.2 b), as discussed by Luo and Stephens (2006). The orientation of the embedded CRM has a large impact on the mean state convergence zones co-incident with the Great Red Spot, to the east of Asia, consistent with the findings of Khairoutdinov et al. (2005) (Figures 5.2 d,e). Interestingly, a similar sensitivity to CRM orientation is also apparent in superparameterized simulated simulations over the Gulf Stream, to the east of North America.

Figure 5.3 contrasts the amplitude of the 24-hour surface divergence harmonic in simulations and observations. All of the climate models capture amplitude fringes around the coastlines representing non-local control of the marine diurnal cycle by land. For the coarser resolution spectral models (Figure 5.3a,b) the horizontal extent of these fringes is largest and super-parameterization results in additional amplitude in the Western and equatorial Pacific, and removes amplitude to the west of Africa. For the higher resolution, finite volume models (Figure

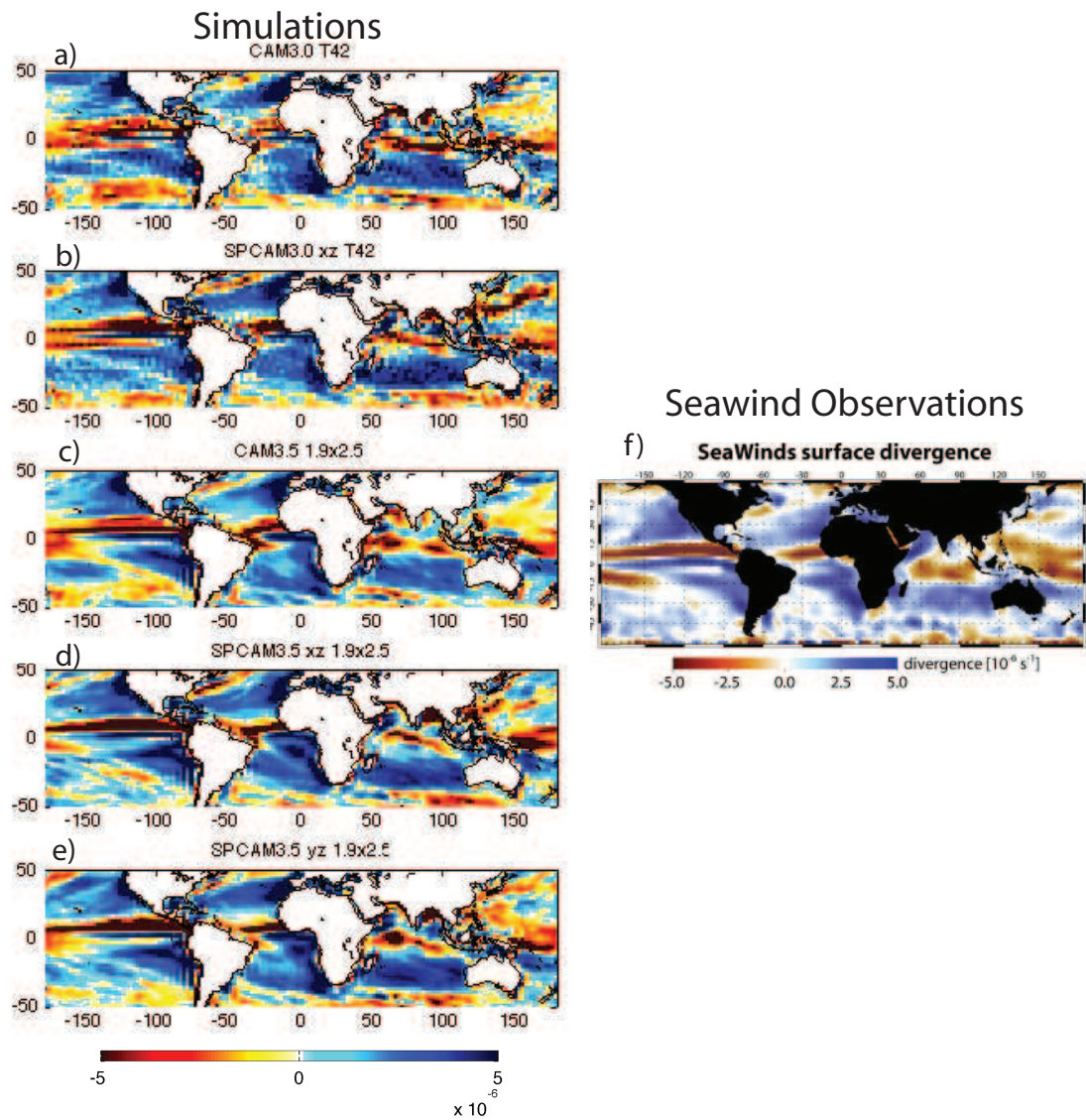


Figure 5.2: (Left) simulated JJA vs. (right) observed MJJAS composite diurnal cycle of surface divergence, contrasting an ensemble of coarse resolution climate models. The observational panel is reproduced from Wood et al. (2009).

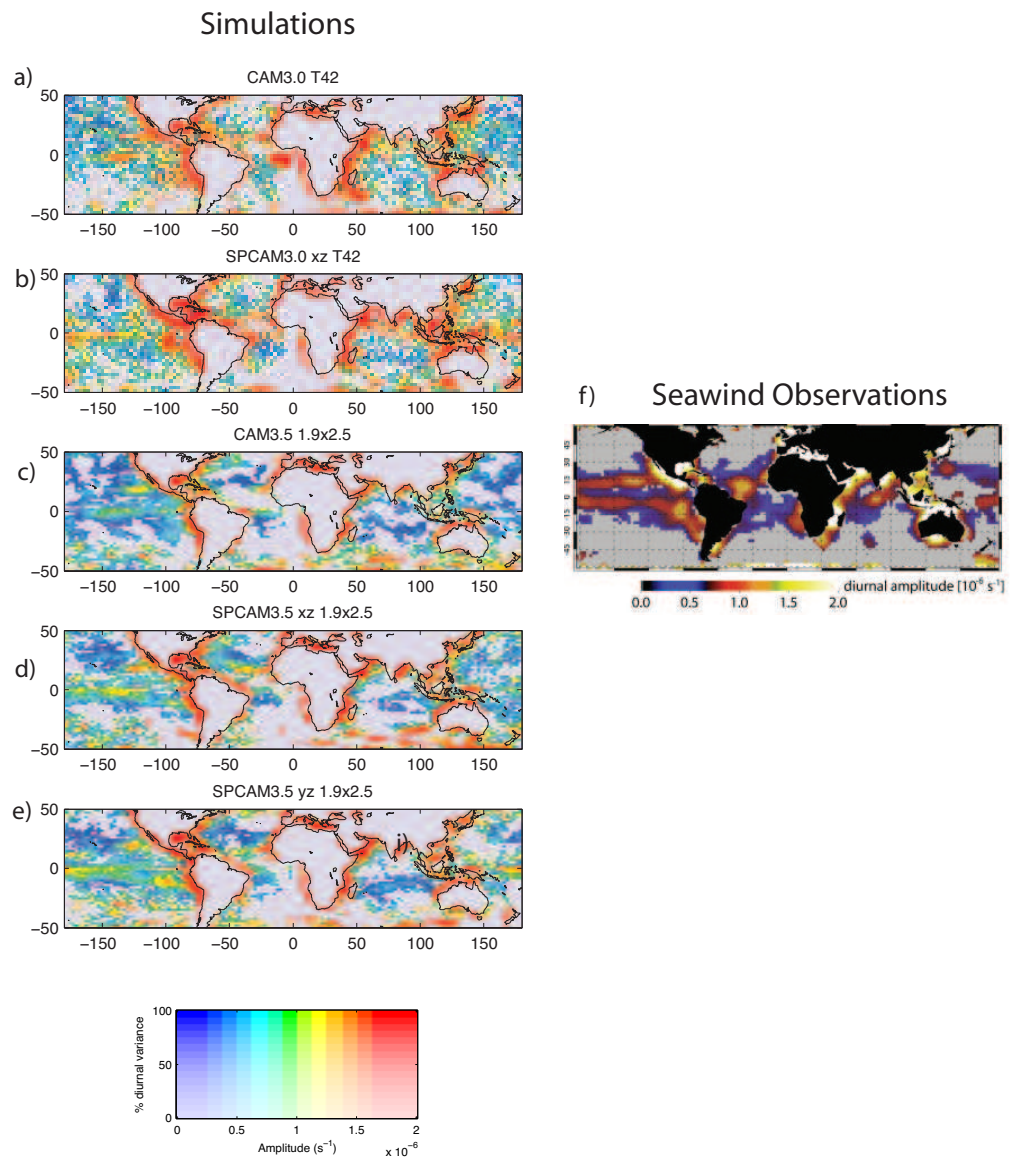


Figure 5.3: As in Figure 5.2 but for the phase of the fitted 24-hour harmonic.

5.3c-e), super-parameterization adds missing diurnal surface divergence amplitude in the Bay of Bengal, South China, and coastal waters of the Maritime Continent. In general, super-parameterization boosts the level of diurnal surface divergence amplitude over the Western and Central equatorial Pacific, with curious sensitivity to the CRM orientation (Figure 5.3b,d,e). Interestingly, none of the models capture the coherent, dual-band amplitude structure of the observed wave amplitude in the Central-Eastern Pacific immediately to the north and south of the equator.

Figure 5.4 contrasts the phase of surface divergence in the models with the scatterometer observation composite. All of the models except CAM3.0 capture the strikingly zonal phase lines associated with an Eastern equatorial Pacific diurnal subsidence wave, though the simulations appear to erroneously extend this wave feature far into the Western Pacific where it is not observed. The phase lines are more zonal in the simulations than in the observations, consistent with the description of this feature as a wave sourced from the ITCZ (Wood et al., 2009), which is also overly zonal in the mean state of most of the models (Figure 5.2). Super-parameterization appears to extend the meridional range of these simulated waves and to slow their phase speed to more realistic values. But the super-parameterized models also contain similar waves with zonally oriented phase lines where they are not observed in nature (e.g. east of S. America, west of Australia, and east of the Phillipines in Figure 5.4 d,e).

The observed long-range westward coastal propagation of a surface divergence wave through the sub-tropical stratocumulus decks west of California, South America, West Africa, and southern Africa, is not captured by the simulations. The failure of super-parameterized climate models to capture these *non-local* external influences on simulated stratocumulus variability is somewhat at odds with the realism of *local* internal stratocumulus diurnal variability documented at a single SPCAM3.0 grid-point in the sub-tropical Pacific by Khairoutdinov et al. (2008). Also, both of the conventionally parameterized simulations (Figures 5.4a,c) exhibit

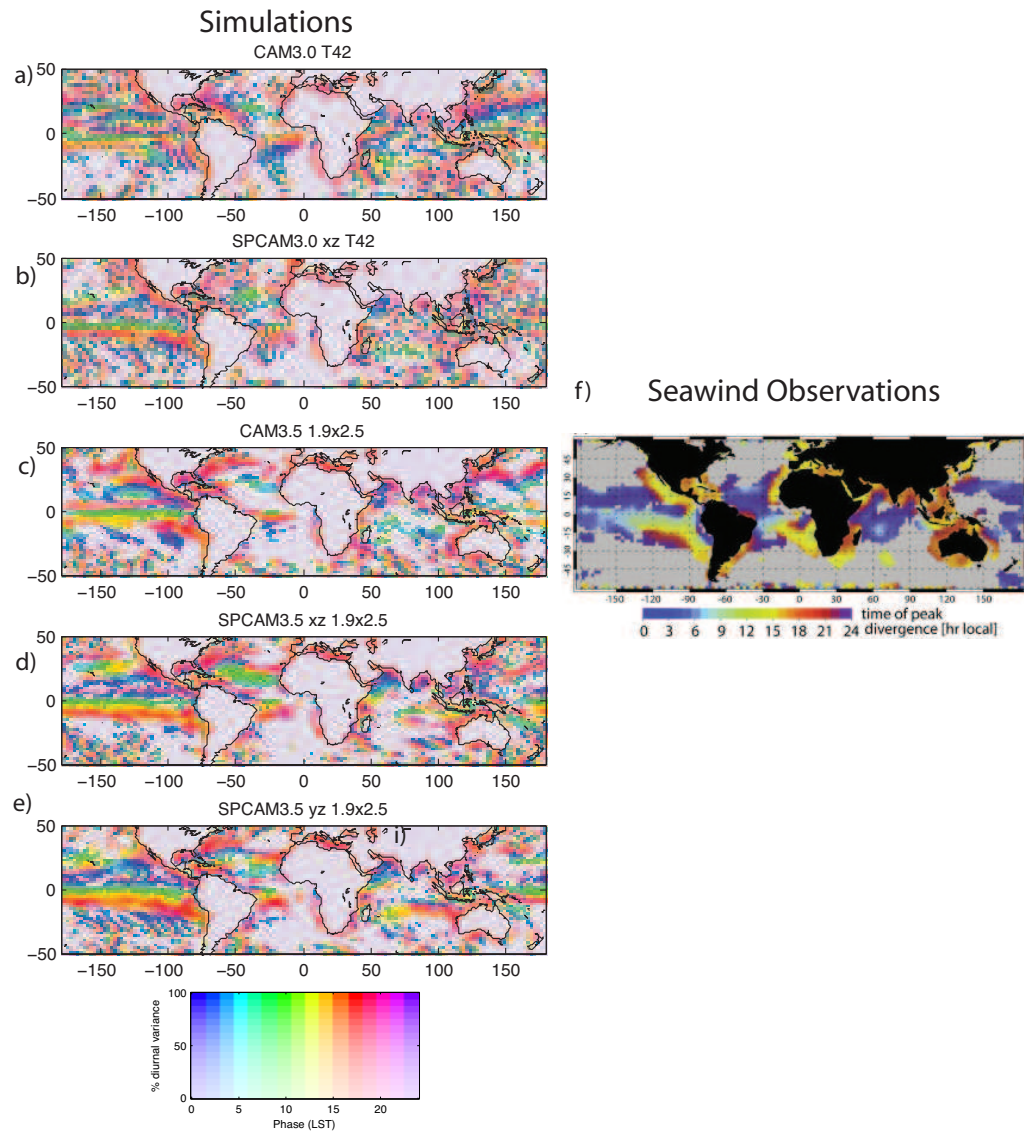


Figure 5.4: As in Figure 5.2 but for the amplitude of the fitted 24-hour harmonic.

a coherent subsidence wave band east of Japan (phase lines oriented to the north-east) that is absent in SPCAM3.5 and also not detected in the observations. It is unknown why these aspects of large scale diurnal subsidence are poorly simulated.

Of all the models, CAM3.0 alone fails to capture the zonal phase lines in the Eastern Pacific (Figure 5.4a) but instead exhibits curiously localized concentric subsidence wave phase striations emanating from South America and Africa. Evidently, super-parameterization corrects this unrealistic wave structure (SPCAM3.0; Figure 5.4b), but why? In the following analysis, CAM3.0 and SPCAM3.0 are examined from a water budget perspective to find out.

5.2 Effects of super-parameterization on the tropical ocean diurnal water budget

This section expands on previous work by analyzing the signature of long-range subsidence waves via their effect on four independent components of the vertically integrated atmospheric water budget. Philosophically, this budgetary approach emphasizes the relationship of such waves to the simulated diurnal *rainfall* cycle, the focus of this dissertation.

The budget (i.e. conservation) equation of vertically integrated water is written as follows.

$$\int \rho \frac{\partial q}{\partial t}(z) dz = - \int \nabla \cdot (\rho q \mathbf{v}_{\mathbf{H}}) dz + E - P \quad (5.1)$$

Here, $q(z)$ is the vertically varying sum of all (vapor and otherwise) water constituent concentrations in the model, expressed as a mixing ratio, E is a source² term through the base of the column due to evapotranspiration, and P is a sink term due to surface rainfall. The first term on the right hand side represents the net

²Strictly speaking, this is only *usually* a source term. Whereas evaporation is always a source of water to the atmospheric column, transpiration can produce modulating sink effects when plants inhale vapor. This is not an issue here as the budget will be applied over ocean columns.

lateral inflow or outflow of total water due to moisture convergence (divergence) associated with vapor and condensate advection by vertically varying horizontal winds $\mathbf{v}_{\mathbf{H}}(z)$. All terms are expressed in units of $\text{kg}/\text{m}^2/\text{s}$.

From this budgetary perspective, long-range oceanic diurnal surface divergence waves are indirectly connected to diurnal rainfall via the moisture storage³ budget term, and directly related via the lateral column moisture convergence budget term⁴. Both of these terms in the vertically integrated water budget can play a role in supporting the oceanic composite diurnal rainfall cycle.

Two model simulations in the above ensemble were uniquely configured to produce sufficient output to constrain four terms of the vertically integrated water budget independently. The first is CAM3.0, which uses a cumulus parameterization that rigidly depletes undilute CAPE with a 2 hour timescale. The second is SPCAM3.0, in which the cumulus parameterization is replaced with a 4km horizontal resolution, 128 km extent, zonally oriented CRM. Both models are run with identical forcings (climatological SSTs), on 26 vertical levels, with T42 spectral truncation (400-700 km effective horizontal resolution). The diurnal composite is analyzed during boreal winter (DJF) to avoid complications associated with the Great Red Spot rainfall bias in SPCAM3.0 during boreal summer (JJA).

Does super-parameterization alter the simulated diurnal water balance over the tropical ocean in climate models? On first inspection, the answer appears to be “no” (Figures 5.5 a,b). The composite diurnal rainfall cycle, and the composite cycle of all other terms in the column water budget that balance rainfall, is nearly identical in SPCAM3.0 and CAM3.0. Both models show peak ocean rainfall occurring near 3am, associated with anomalous lateral water convergence and drawdown

³This is the term on the left hand side of the budget equation. Surface divergence (convergence) is connected to free tropospheric subsidence (uplift) through the continuity equation, which is in turn associated with adiabatic cooling (warming) corresponding via the Clausius-Clapeyron relation to a decrease (increase) in moisture holding capacity.

⁴The exponential decrease with height of atmospheric water vapor implies that the *surface* divergence disproportionately dominates the net column moisture divergence.

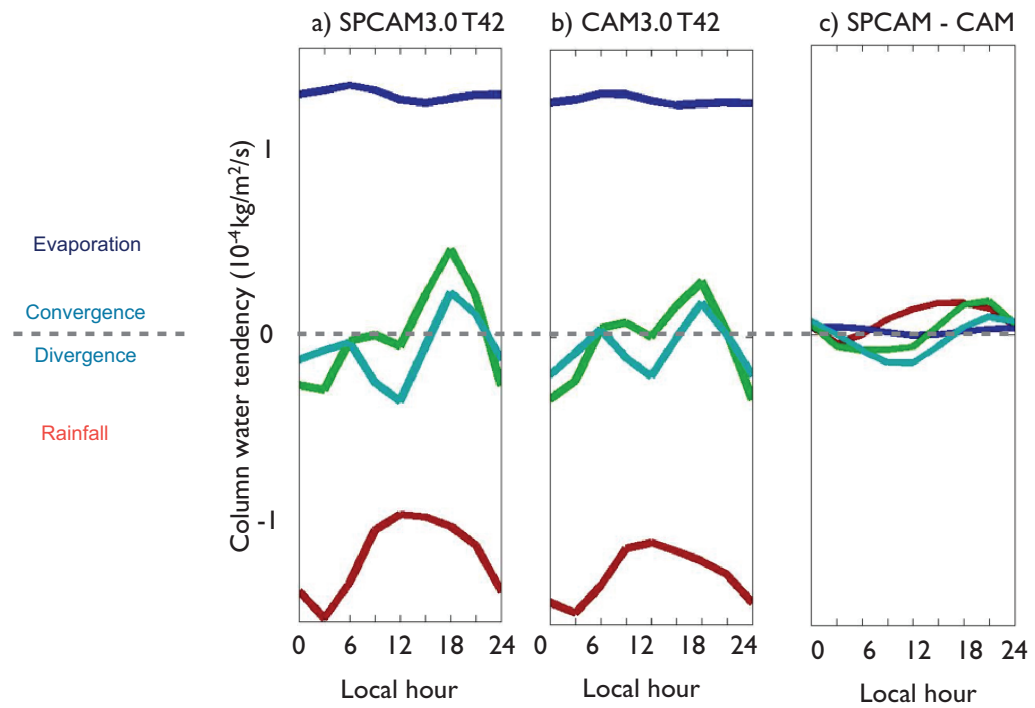


Figure 5.5: Composite DJF diurnal cycle of all components of the vertically integrated moisture budget, averaged over ocean points only within a latitude band from 10 S to 10 N, comparing (left) CAM3.0 to (right) SPCAM3.0.

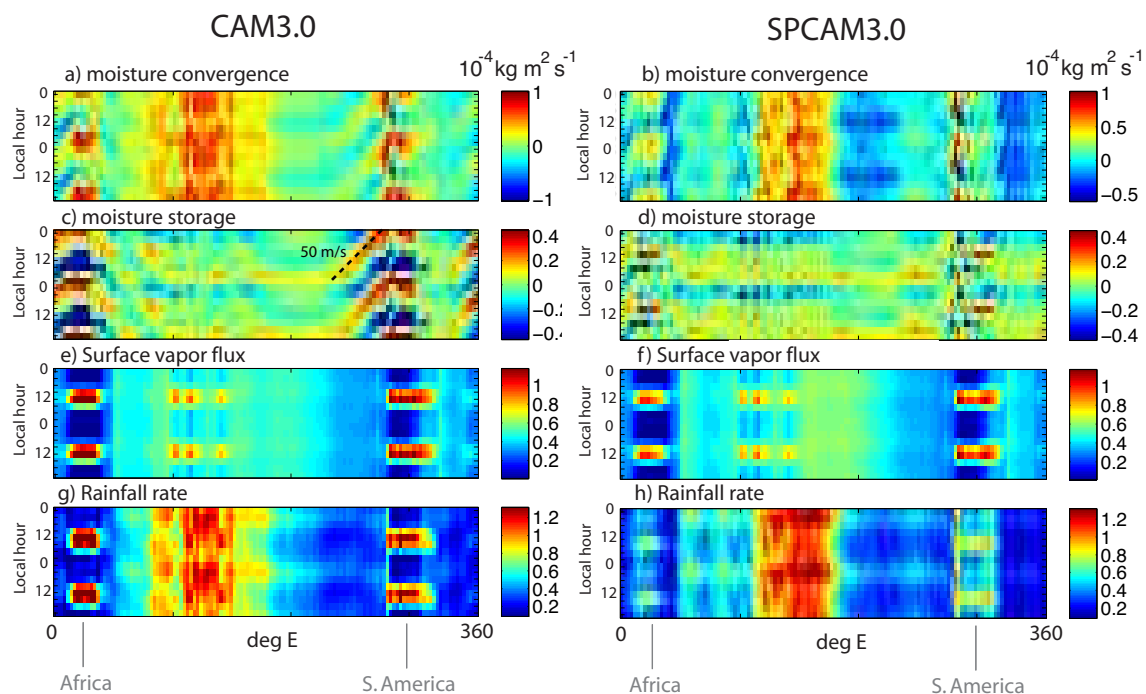


Figure 5.6: As in Figure 5.5 but unfolding the zonal variability in the composite budget, and including land points. Each descending subplot shows the local time - longitude structure for each of the four terms in the water budget, comparing (left) CAM3.0 and (right) SPCAM3.0. The composite diurnal cycle is repeated twice for clarity.

of the column reservoir. However, a curious coherence in the inter-model anomaly (Figures 5.5 c) of diurnal moisture convergence (cyan lines) and diurnal moisture storage (green lines) suggests there is more to the story.

Figure 5.6 shows that the apparently negligible water cycle differences between SPCAM3.0 and CAM3.0 ocean grid-points in the *horizontal average* are an artifact of over-compositing. Unfolding the zonal variations behind the average, a striking regional difference in the two models is revealed in the time-longitude structure of the composite diurnal cycle of water convergence (Figure 5.6a,b) and water storage (Figure 5.6c,d) in SPCAM3.0 and CAM3.0. In CAM3.0 there is an apparent large

scale westward (eastward) propagation of a diurnally initiated convergence and storage signal from equatorial South America (Africa) into the eastern Pacific (western Indian ocean)⁵.

The dramatic column moisture convergence wave in CAM3.0 is a sign of unrealistically severe remote control by tropical land on the remote atmospheric diurnal water cycle. This is evident in its horizontal scale; the signal extends 5000 km to the west of South America (45 deg E; zonal extent of fitted dashed line in Figure 5.6c), which is far too large compared to the observed extent of land-ocean phase coherence in the 10S-10N band for the scatterometer observations of surface wind convergence shown previously (Figure 5.1).

What is the source of this unrealistically severe remote control by land of the marine diurnal rainfall cycle in CAM3.0? One clue is that the propagating signal is well fit by a phase speed of approximately 50 m/s, which is consistent with a deep barotropic gravity wave⁶. The obvious nearby source of deep barotropic heating is latent heating associated with the dramatic rainfall cycle over equatorial landmasses in CAM3.0 (Figure 5.6g), which is clearly located in the source zone of the propagating disturbance.

One effect of super-parameterization is a reduction in the amplitude of the tropical land diurnal rainfall cycle. This was previously discussed in analysis of the 24-hour rainfall harmonic (Section 4.2) and attributed to entrainment humidification barriers by DeMott et al. (2007). The reduction in rainfall amplitude can also be seen in Figure 5.6h).

Evidently, one counter-intuitive non-local benefit of tempering the diurnal latent heating cycle over tropical landmasses using super-parameterization is the

⁵The absence of this diurnal wavelike convergence and storage feature in SPCAM3.0 underlies the over-ocean coherent budgetary differences noted in Figure 5.5.

⁶Recall from Equation 2.2, the gravity wave phase speed $c_g = N/m$. Substituting for the vertical wavenumber $m \equiv 2\pi/H$ where $H = 12km$, corresponding to a heating throughout the depth of the troposphere, and Brunt-Väisälä frequency $N = 0.013$ consistent with a tropical moist adiabatic lapse rate, yields $c_g \approx 50$ m/s.

elimination of an unrealistically large-scale remote control mechanism on the atmospheric diurnal water balance over the ocean. The overly strong offshore propagation in CAM is due to an overly intense diurnal heating cycle over land, emphasizing how important realistic simulation of diurnal rainfall and convection is.

5.3 A model-informed explanation for the Gulf Stream diurnal rainfall pattern

Several published studies have remarked tangentially on the regionally anomalous⁷ observed diurnal convection cycle over the Gulf Stream (Meisner and Arkin, 1987; Schmetz and Liu, 1988; Kondragunta and Gruber, 1996; Janowiak et al., 2007; Carbone and Tuttle, 2008) but the causes and mechanisms that support its observed composite regional structure are a matter of ongoing debate.

Some studies have speculated on the possible physics that could explain the observed pattern. For instance, regarding the southwestern section of the Gulf Stream where rainfall is in range of coastal radar near Carolina, Carbone and Tuttle (2008) hypothesized that local surface fluxes associated with warm Gulf Stream waters play a key role:

Nocturnal rainfall is quite frequent and extensive off of the Carolina coasts ... Because of its frequency, persistence, and relatively distant offshore maximum, the bulk of this rainfall occurrence is likely associated with lower boundary forcing from warmer Gulf Stream waters. [(Carbone and Tuttle, 2008)]

Janowiak et al. (2007) wondered if organized orographic convective systems generated non-locally upstream over Appalachian topography are responsible for an

⁷In many parts of the world, regions of anomalously large mean convection are also regions of enhanced diurnal variance (Bergman and Salby, 1996). The Gulf Stream is no exception in this regard.

interesting change in the local timing of maximum rainfall within the Gulf Stream region with distance offshore:

.... an early morning maximum in [oceanic] precipitation near the eastern [US] Atlantic coast ... occurs later in the day to the east of that region. This feature is likely the result of two factors: one being the formation of convective systems near midday over the Appalachians that advect to the east and the other being the re-amplification of some of those systems and formation of new systems at night and in the early morning when the Gulf Stream becomes a source for atmospheric instability and rising motion.[citetJanDagKou07]

Two studies have offered more than speculation, invoking numerical models to determine mechanisms relevant to the regional composite structure of Gulf Stream diurnal rainfall (Alliss and Raman, 1995a; Ruane, 2010). Alliss and Raman (1995a) focused only on the coastal Carolina region of the Gulf Stream. Their analysis of the statistical relationship of high cloud diurnal frequency from infrared observations and an operational analysis estimation of boundary layer convergence and advection from land led them to conclude “that atmospheric dynamics play a significant role in the diurnal cycle of high cloudiness [over the Gulf Stream]”. In examining the internal statistical relationships between various components of the water cycle within a state of the art regional reanalysis model, the North American Regional Reanalysis, Ruane (2010) found that:

...precipitation in the warm and nearly saturated air over the ... Gulf Stream ... reacts strongly to diurnal variations in moisture flux convergence. [Ruane (2010)]

In summary, existing work suggests atmospheric dynamics and local moisture convergence are key to the Gulf Stream diurnal rainfall pattern. But a clear explanation of how these two factors interplay to produce the observed pattern of diurnal rainfall is lacking in the literature.

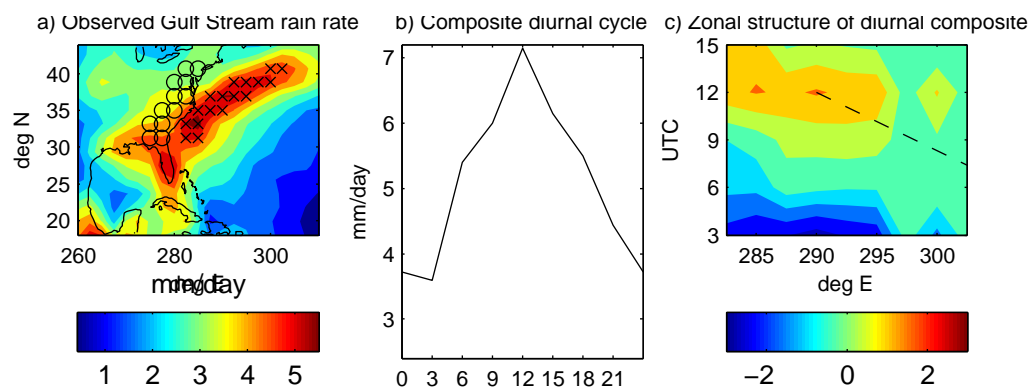


Figure 5.7: a) JJA mean 2000-2006 rainfall rate from the TRMM 3B42 observations bin averaged to a 1.9×2.5 model grid, defining coastal land and Gulf stream regions of interest (grid points marked ‘O’ and ‘X’, respectively). b) Horizontally averaged composite rainfall cycle in the Gulf stream region. c) As in b) but retaining the zonal variability in the composite and focusing only on the nocturnal (rainiest) times. The dashed line corresponds to constant local solar time.

The following work aims to contribute to this gap. An ensemble of conventional and super-parameterized simulations that use different techniques to represent sub-grid convection are analyzed over the Gulf Stream. Simulations that produce a realistic pattern of Gulf Stream rainfall diurnal evolution provide an opportunity to diagnose in more detail the mechanisms supporting Gulf Stream rainfall physics from unobservable vantage points. Comparing the realism of ensemble members with well characterized differences in their treatment of sub-grid convection provides additional clues as to the relevant physics of Gulf Stream diurnal rainfall.

Results

Figure 5.7 shows that the Gulf Stream diurnal rainfall cycle is a well defined feature of JJA climatology in the TRMM 3B42 observations, which does not appear

to be well explained by insolation timing. Two horizontal averaging regions are defined for process analysis, one for coastal land, and another in an oceanic transect oriented northeastward over the localized Gulf Stream rainfall feature.

Figure 5.7 b) shows the observed composite diurnal cycle in the Gulf Stream averaging region, which peaks at 12 Z (approximately 8 am local time). Figure 5.7c) retains the longitudinal variability in the diurnal composite, showing the peak time varies as a function of longitude⁸, and that the largest regional contributor to the horizontal average diurnal variability is in the coastal waters adjacent to Carolina. The dashed line in Figure 5.7 c) shows the diurnal phase speed associated with the passage of the sun, emphasizing that at the different endpoints of the transect, the peak rainfall occurs at different *local times*. The local time of maximum precipitation is 0530 LST at the northeastern (most offshore) transect terminus compared to 1000 LT the southwestern (most coastal) terminus. Clearly, something more complicated than a simple local day-night difference in insolation or radiative cooling controls the diurnal rainfall timing in this Gulf Stream region. But what?

How well can a suite of climate models capture the salient features of Gulf Stream diurnal rainfall variability discussed above? Figures 5.8 and 5.9 contrast simulations of diurnal rainfall across an ensemble of coarse resolution climate models that treat sub-grid convection differently (see Appendix A for a description of the models). Although the models exhibit wildly different mean rainfall rates over the Gulf Stream region⁹ (Figure 5.8a), all but one model (CAM3.0 T42) captures the observed morning maximum (Figure 5.8b). Furthermore, when zonal variabil-

⁸Janowiak et al. (2007) also point this out.

⁹There are many possible reasons for inter-model mean state and diurnal variance differences. It is worth mentioning that a perfect match to observations cannot be expected in an uncontrolled inter-comparison such as this. For instance, the sea surface temperatures used to drive the models are not the same that occurred in nature. Also, many of the models are prototypes that have not had their mean energy balance “tuned”. Especially in the superparameterized models, significant cloud biases can distort the energy balance. Of concern here however is the *timing* of peak diurnal rainfall, changes in timing along the Gulf Stream transect, and the mechanisms supporting this.

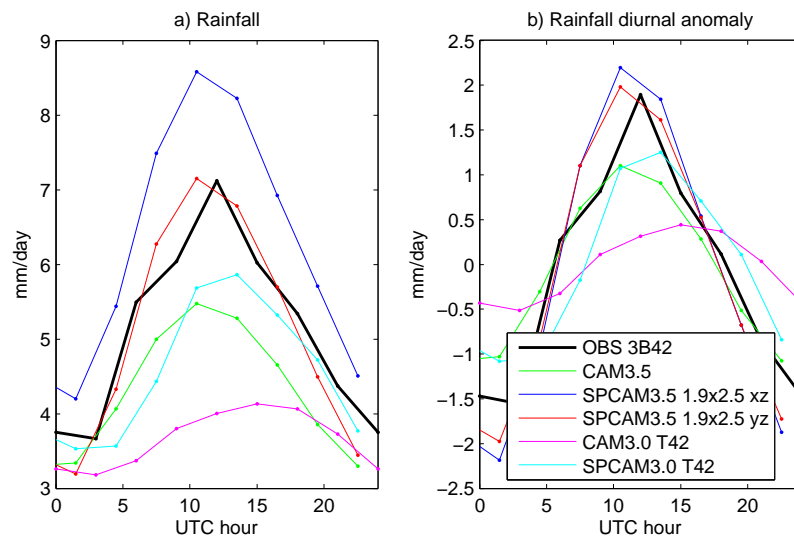


Figure 5.8: Multi-model comparison of the observed (solid black line) and simulated (colored lines) horizontal mean Gulf Stream JJA composite diurnal rainfall variability in the transect defined in Figure 5.7a, for an ensemble of models that treat sub-grid convection differently.

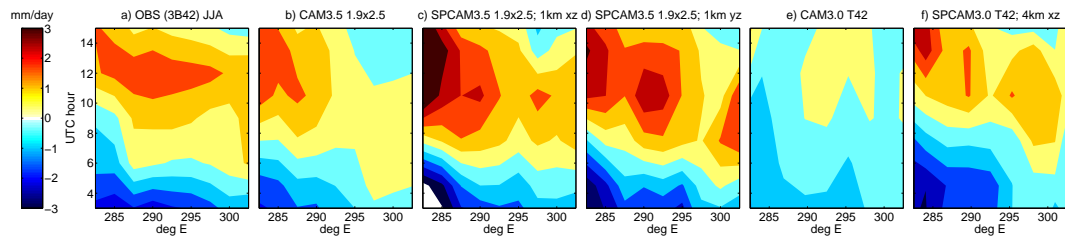


Figure 5.9: As in 5.8 but showing the zonal structure of the a) observed versus b)-f) simulated diurnal anomalous rainfall.

ity is retained in the diurnal composite, all but one model also realistically captures the change in local timing of maximum precipitation with distance offshore (Figure 5.9).

Interestingly, the only model that does not capture these basic aspects of the observed diurnal rainfall chronology is CAM3.0 T42, which unlike all other models uses an undilute CAPE-based closure in its sub-grid cumulus parameterization. This model alone produces an overly weak Gulf Stream diurnal rainfall cycle, with a modest afternoon maximum (Figure 5.8b, magenta line) and does not capture the coherent change in peak rainfall timing along the Gulf Stream transect (Figure 5.9e). Since it is well known that mass flux parameterizations closed on undilute CAPE are under-sensitive to free atmosphere humidity (Guichard et al., 2004; Grabowski et al., 2006), this may be interpreted as a hint that free tropospheric diurnal moisture variations play a role in the observed pattern of Gulf Stream rainfall variability, as also suggested by Ruane (2010).

Analysis of the vertically integrated water budget within the models also suggests that diurnal fluctuations of free tropospheric moisture are important to the observed pattern of Gulf Stream diurnal rainfall (Figure 5.10). From a column water budget perspective, Gulf Stream precipitation represents a sink (blue line) that must be balanced by sources, such as surface latent fluxes (black line) and vertically integrated horizontal vapor convergence (red line), as well as other terms captured by the budget residual (dashed line)¹⁰. A symmetry in the diurnal variation suggests that tropospheric diurnal moisture variations may be important to the simulated pattern of Gulf Stream diurnal precipitation. A similar internal balance between rainfall and low-level moisture convergence was hinted at in the correlation budget analysis of a modern regional reanalysis product by Ruane (2010).

¹⁰Here, the residual represents the net effect of other processes that are not explicitly discernable from the simulation output, such as storage and depletion of the total column water, and horizontal convergence of non-vapor water species.

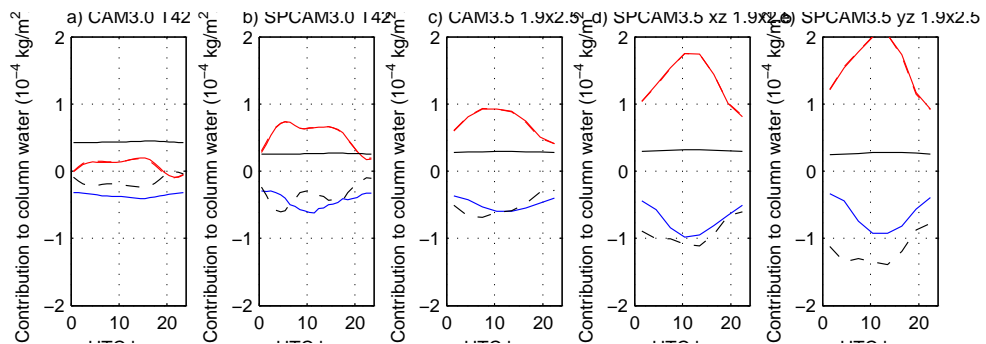


Figure 5.10: The simulated Gulf Stream diurnal cycle of JJA precipitation (blue line), expressed as a sink to the column water budget, compared to two balancing source terms, latent fluxes (black line) and vertically integrated moisture convergence (red line). The dashed red line shows the effect of diurnal wind variations on the vertically integrated moisture convergence (see text for details). The only model that does not simulate realistic Gulf Stream rainfall a) has a dominant balance between precipitation and latent heat fluxes whereas the other models b)-f) suggest diurnal variations of moisture convergence play an important role in balancing the Gulf Stream rainfall cycle..

To summarize findings thusfar, two key features of the pattern of Gulf Stream diurnal rainfall (morning maximum in the average, and-along transect variability in the local timing) are captured by all but one member of an ensemble of climate models. Two lines of evidence in turn suggest *free tropospheric moisture variations* as a mechanistic link to the Gulf Stream diurnal rainfall pattern:

1. The only climate model that did not capture the pattern is well known to be convectively under-sensitive to free tropospheric moisture fluctuations.
2. The climate models that do capture the pattern exhibit a diurnal water budget balance between column moisture convergence and diurnal rainfall.

Of course, cause and effect are difficult to untangle from composite budget analysis and balances therein. But this motivates the question: Is there a plausible mechanism involving moisture convergence that could explain the difference in local timing of maximum rainfall at the northeastern versus southwestern ends of the Gulf Stream transect?

First, it is important to determine whether the diurnal variability of the vertically integrated moisture convergence term,

$$M = - \int \nabla \cdot (\mathbf{v}_H q_v) \frac{dp}{g}, \quad (5.2)$$

is primarily due to diurnal fluctuations in horizontal winds, \mathbf{v}_H , or in vapor concentration, q_v , or a combination of both. Observations of column water vapor suggest q_v has a weak diurnal variability (Dai et al., 2002; Li et al., 2008), so it is reasonable to expect that diurnal wind fluctuations dominate M , but this is important to verify in the models. One way to find out is to expand the water vapor concentration q_v into the sum of a daily mean and diurnal anomaly component, i.e. $q_v = \overline{q_v} + q'_v$, such that

$$M = - \int \nabla \cdot (\mathbf{v}_H \cdot \overline{q_v}) \frac{dp}{g} + \int \nabla \cdot (\mathbf{v}_H \cdot q'_v) \frac{dp}{g}. \quad (5.3)$$

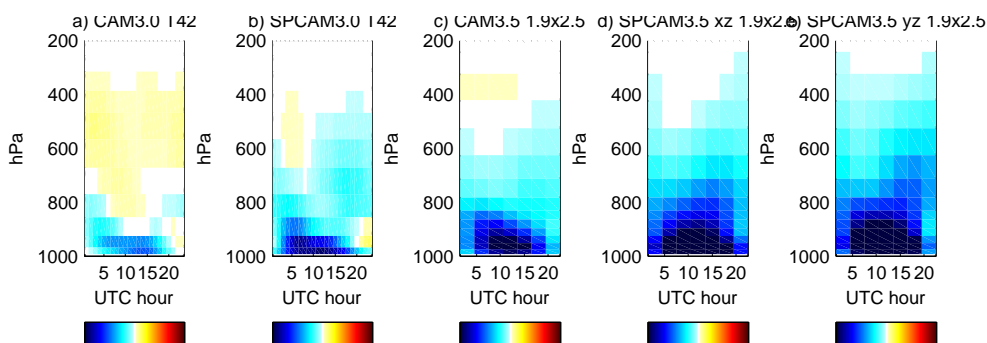


Figure 5.11: Height-time section unfolding the vertical structure of the diurnal moisture convergence column water budget term (red line in Figure 5.10) expressed as a layer mass-weighted contribution to the total column tendency.

The dashed red line in Figure 5.10 corresponds to the first term on the right hand side of Eq. 5.3, which is evidently a very good approximation to the total moisture convergence M (i.e. it is nearly indistinguishable from the solid red line on the figure). This suggests that, more fundamental to moisture convergence are diurnal *horizontal wind fluctuations* over the Gulf Stream, and that their interaction with the mean vapor distribution is what provides a key balance to diurnal rainfall in the models.

It is logical to expect that, since moisture content is higher in the lower atmosphere, it is in fact the diurnal variation of *low-level winds* that mediates the majority of the diurnal moisture convergence signal. Figure 5.11 shows that indeed this is the case. For all of the models the majority of the column vapor convergence diurnal variation is contributed beneath the 800 hPa pressure surface. Thus, in searching for a mechanism that explains the along-transect change in local timing of peak rainfall, it is necessary to understand the diurnal pattern of low-level wind variations.

What is the origin of low-level diurnal wind variations over the Gulf Stream? Figure 5.12 shows a regional map of the amplitude of the fitted 24 hour harmonic

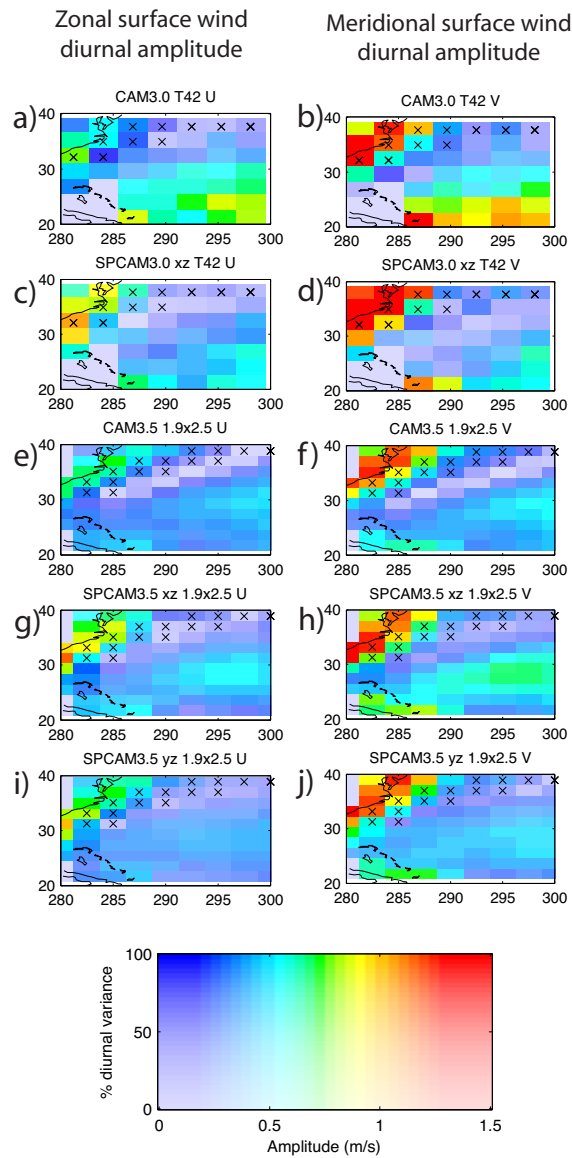


Figure 5.12: Amplitude of the fitted JJA composite 24-hour diurnal harmonic of (left) zonal versus (right) meridional wind on the lowest model level, for the ensemble of climate models in Appendix A.

of surface winds in the region. All models exhibit a diurnal wind amplitude fringe that extends from the land into the ocean, suggestive of a large scale sea breeze circulation, i.e. non-local control of the marine diurnal cycle by circulations set up by more vigorous land heating/cooling (see Section 2.1.2).

Figure 5.13 shows that the diurnal phase of the surface winds is consistent with a large scale land-sea breeze circulation. The local time of most southerly (onshore) winds is at the end of the day (6pm-9pm), i.e. after land has been maximally heated by daytime insolation and the surface pressure gradient force is thus onshore. Conversely, the local time of most westerly (offshore) winds is the end of the evening (3am-6pm), i.e. after land has been cumulatively cooled by nocturnal infrared cooling, and the surface pressure gradient force is offshore.

Together, Figures 5.12 and 5.13 demonstrate that in all models the diurnal low-level wind fluctuations over a distance of several hundred kilometers offshore are coherently linked to land forcing.

Discussion and Conclusions

To summarize the above analysis,

- Model intercomparison and model budget analysis suggest free tropospheric moisture variations help support the pattern of Gulf Stream diurnal rainfall.
- Diurnal low-level wind variations are suggested to dominate the column moisture convergence.
- Harmonic analysis shows the diurnal wind phase is coherently linked to land via. what looks like a giant sea-breeze circulation.

In other words, the model intercomparison suggests that a large-scale sea breeze circulation, and its associated diurnal perturbations to column humidity may be

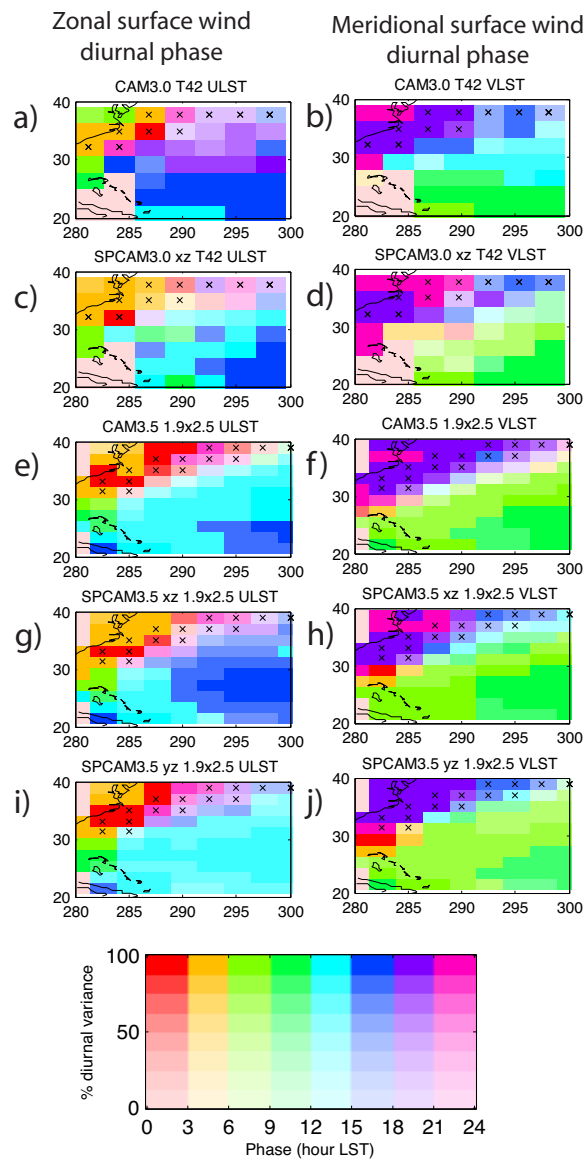


Figure 5.13: As in Figure 5.13, but for the phase (local time of maximum diurnal anomaly).

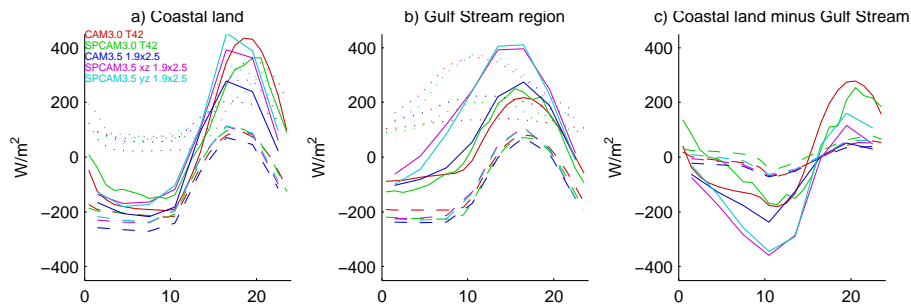


Figure 5.14: Comparison of the (a) coastal land versus (b) Gulf Stream horizontal average column (dashed lines) radiative heating, (dotted lines) convective heating and (solid lines) their sum. The right panel c) shows that the land-ocean contrast in radiative heating (dashed lines) is amplified by the convective heating (solid lines; radiative plus convective heating).

responsible for the difference in local timing of Gulf Stream diurnal rainfall with distance offshore. This is an alternative explanation to the advective mechanism speculated by Janowiak et al. (2007) but is consistent with the results of Ruane (2010) supported by internal budget diagnostics from regional reanalyses.

It is interesting to note that differences in the diurnal phasing of convective heating over land versus ocean can act dynamically as a positive feedback to sustain an especially large scale and deep sea breeze circulation in this region, by convectively amplifying the diurnally reversing land-sea radiative contrast (Christopher Bretherton, personal communication). Figure 5.14 illustrates this effect in the model output through an analysis of the column energetics for the coastal land and Gulf Stream averaging areas defined previously in Figure 5.7a. The horizontally averaged diurnal cycles of column radiative heating (dashed lines), vs. convective heating (dotted lines) and their net (solid lines) are shown for the coastal land and Gulf Stream regions in Figures 5.14 a,b respectively. Evidently, the land-ocean *contrast* (difference; Figure 5.14c) of radiative heating (dashed lines) is greatly amplified by the latent heating (solid lines; radiative+convective heating). This

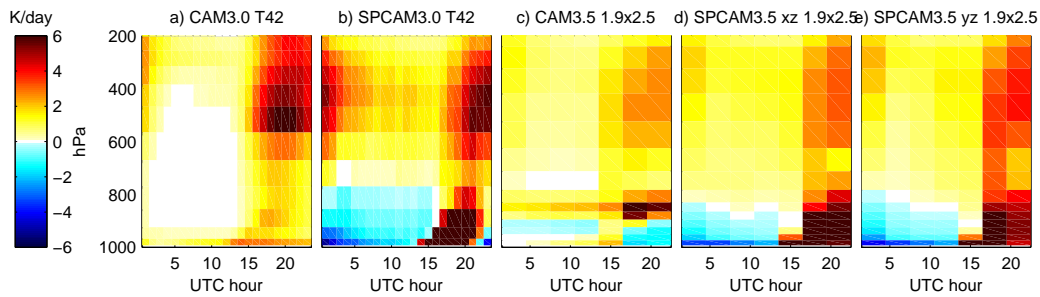


Figure 5.15: Pressure-time sections comparing the structure of the simulated composite diurnal cycle of convective heating over the coastal land horizontal averaging region (gridpoints marked ‘o’ in Figure 5.7a).

effect is quite clear in all the models.

One interpretation of the inability of a single ensemble member - CAM3.0 T42 - to capture the Gulf Stream diurnal rainfall pattern is that the sub-grid convection schemes in climate models must be sufficiently sensitive to free tropospheric moisture variations to capture the diurnal rainfall cycle over the Gulf Stream. CAM3.0 T42, which uses an Akarawa-Schubert mass flux cumulus parameterization variant closed on *undilute* CAPE, does not reproduce the water budget balance or rainfall pattern. Modifications in CAM3.5 that introduced *dilution* in the mass flux scheme’s closure, and super-parameterized versions of CAM, both improve the simulation of Gulf Stream diurnal rainfall.

Another interpretation of the inability of the CAM3.0 T42 ensemble member to simulate the Gulf Stream diurnal rainfall cycle has to do with the nature of the convective heating structures set up over coastal land grid points, and associated teleconnective wave implications. Figure 5.15 compares the simulated height-time diurnal structure of the horizontally averaged coastal land convective heating. Convection in all the models acts to spread the radiative surface heating into the mid-troposphere during the afternoon and evening, but in the later stages the vertical structure in CAM3.0 lacks a baroclinic component associated

with surface cooling. This low-level convective cooling is especially apparent in the superparameterized simulations, in which it represents the later stages of explicitly resolved deep convection, which contain strong evaporatively cooled downdrafts. Mapes (1993) has shown the first baroclinic convective heating mode in the tropics is associated with a 20 m/s wave of low-level convergence. It is possible that such a baroclinic wave component excited over coastal land could play a role in instigating the low-level moisture convergence seen to balance Gulf Stream diurnal rainfall in the other models (Christopher Bretherton, personal communication); consistently, the required travel time to connect land to ocean is approximately 6 hours (400 km).

The idea of land controlling the oceanic diurnal cycle is not new, but these results lend weight¹¹ and add new regional detail to speculations by Dai and Deser (1999) and Dai (2001) based on sparse marine station data, that the composite early morning maximum of oceanic diurnal rainfall may be a remote response to land forcing:

The [global] diurnal phase patterns of surface wind divergence (Dai and Deser, 1999) suggest that there exists a large-scale diurnal circulation in which surface air converges and rises over continents (except for the innermost parts) and diverges and sinks over large nearby oceanic areas in the afternoon and early evening and opposite occurs in the early morning. This thermally driven land-ocean diurnal circulation may contribute to the general pattern of afternoon rainfall maxima over land areas and early morning rainfall maxima over the adjacent oceans. [(Dai, 2001)]

Refinements here added to this picture over the Gulf Stream region include the strong coupling of the radiatively driven sea breeze circulation to convective heating, and the possible role of convectively excited baroclinic gravity waves on the

¹¹There is some uncertainty about the conclusions drawn in Dai and Deser (1999) due to the way they reduce noise associated with sampling issues in the marine surface station data (Wood et al., 2009)

coast in mediating the required convective phase lag for amplification via low level moisture convergence.

One limitation of the above column water budget analysis is that it contained a significant residual that also plays a role in balancing diurnal moisture convergence. Unfortunately sufficient model output was not available to satisfactorily close the budget. One logical speculation is that moisture storage decreases (increases) associated with sea breeze related adiabatic uplift cooling (subsidence warming) over the Gulf Stream are also important to the water budget. Further analysis is required to explore this issue.

Evidently, in super-parameterized models the nature of the sea breeze circulation is sensitive to the arbitrary choice of orientation of the embedded CRM (Figure 5.9c,d). It is unknown why this is the case. One interpretation is that wind shear-convection couplings can act to feed back on the simulated circulation; which dimension of the shear is transmitted to the CRM (i.e. in which plane it is oriented) would therefore matter. Consistent with this view, there is a modest increase in the amplitude of diurnal zonal wind variations when the CRM is oriented zonally as opposed to meridionally (Figure 5.12 g,i). Another factor is the interaction of the diurnal cycle with an unrealistically enhanced mean state convergence zone over the Gulf Stream when the embedded CRM is in a zonal configuration (Figure 5.2 d,e) as also occurs to the east of Asia (i.e in the Great Red Spot model bias) for unknown reasons.

Finally, it could be argued that it is somewhat unsatisfactory to draw conclusions about nature from free-running coarse resolution global model simulations¹² that have not been constrained by data. From this perspective, there is a need to extend the above analysis to see if the proposed mechanism is borne out in best-estimates of the atmospheric state, i.e. optimal combinations of models and

¹²It could also be argued that the above model-intercomparison strategy fulfils a useful secondary objective of characterizing the representation of the Gulf Stream diurnal mode for the purpose of evaluating the realism of several climate projection models.

data, and in high resolution simulations that treat convection explicitly. Such work is beyond the scope of this dissertation, but is an obvious avenue for future work. In the meantime, the proposed mechanism should be cautiously viewed as a model-informed hypothesis for why the boreal summer Gulf Stream diurnal rainfall pattern looks the way it does.

Chapter 6

Evidence for slow-manifold control of the Central US nocturnal rainfall maximum

Climate projections of future rainfall by current generation global climate models (GCMs) are especially uncertain in the Central US, as well as other continental interiors during the warm season. The 2007 Fourth Assessment Report (AR4) of the Intergovernmental Panel on Climate Change (IPCC) shows that the ensemble of conventional GCMs cannot even agree on the sign of rainfall changes in these heavily populated parts of the world.

A fundamental reason for this inadequacy is that conventional GCMs cannot capture the physics of diurnally propagating organized mesoscale convective systems (MCSs). In nature, such systems deliver much of the warm seasonal mean rainfall to the continental interior in the lee of topography (Laing and Fritsch, 1997). In the Central United States as much as half of summer rain is linked to these eastward propagating systems originating over the Rockies (Jiang et al., 2006). But in atmospheric climate models MCSs are below the affordable grid res-

olution for climate-scale integration and are not properly represented by statistical cumulus parameterization schemes (Moncrieff and Liu, 2006). These parameterizations are generally cast rigidly in terms of a local buildup (usually within intervals of 15 to 60 minutes) of instability metrics like convective available potential energy (CAPE). Thus they cannot admit non-local diurnal convective physics governing MCS organization and propagation in nature, which take place over several hours, and involve non-equilibrium, often non-local physics. As a result, the ensemble members of the AR4 GCMs do not simulate propagating episodes of convection and disagree wildly about precipitation trends in the lee of mountains, such that there is low confidence in long term projections of seasonal-to-climate scale rainfall variations over continents around the world.

The above issues associated with convective parameterization in climate models are in stark contrast to the successful simulation of MCS-type organization afforded by (nonhydrostatic) cloud-system resolving models (CRMs) with a computational mesh of about 1 km. This success is summarized in the review paper on MCSs by Houze (2004), and on cloud-system models by Tao and Moncrieff (2009). In particular, Moncrieff and Liu (2006) showed that MCS initiated over the Continental Divide and their subsequent eastward travel were reliably simulated by a cloud resolving model, as comparisons of simulated precipitation with radar measurements indicated.

This chapter asks, **is it possible for the multi-scale global climate modeling approach to admit the physics of propagating diurnal convection in continental interiors?** Section 3.3 described how asking this question is useful in the context of an ongoing controversy in the literature regarding “fast-manifold” vs. “slow manifold” control over the propagation of organized convection in the lee of the Rockies. Analysis in Chapter 4 showed no indication of propagating diurnal surface precipitation in the central United States in global diagnostics of the diurnal rainfall mode, despite broad improvements in simulated diurnal rainfall

variability overall. However in this work, the MMF model was configured with a coarse horizontal spectral resolution at the exterior scale, and 4 km cloud-system resolving model horizontal resolution in the interior (SPCAM3.0). At this early stage of multi-scale modeling research it is not known whether the lack of propagating US convective systems represents a tunable deficiency due to this particular model configuration, or a fundamental restriction of the physics admitted by the idealizations in the multi-scale approach as argued by Ovtchinnikov et al. (2006).

This chapter demonstrates that indeed, under a slightly different configuration than was employed in Chapter 4, propagating Central US organized convection can be represented in a multi-scale global model. Evidence of the signal emerges when the exterior model is upgraded to a finite-volume dynamical core at $1.9^\circ \times 2.5^\circ$ resolution, and the embedded cloud-system resolving model resolution is increased from 4 km to 1 km. To investigate the realism of the propagating convective signal in this configuration, simulated storm propagation and genesis characteristics are analyzed, and the effects of the superparameterization approach on regionally relevant diurnal circulations and mean thermodynamics are explored.

Section 6.1 describes the conventional and multi-scale versions of the global climate model that are analyzed and their configuration. In Section 6.2 the Central US diurnal convection signal is evaluated in the models, and the phase speed statistics of propagating events in the multi-scale model are analyzed. In Section 6.3, simulated thermodynamics and orographic diurnal circulations are compared in the model with and without the embedded explicit convection and evaluated against observations. In Section 6.4, the simulated orogenesis mechanism, dynamical evolution, and multi-scale structure of an individual organized propagation event is evaluated. In Section 6.5, the simulated physics are discussed in light of established analytic theory, and a conceptual framework is developed to illustrate potential multi-grid convective propagation pathways in the multi-scale model.

6.1 Models, observations and simulation design

Two heavily composited dynamically consistent best estimates of the observed atmospheric state, the Rapid Update Cycle (RUC) operational data assimilation model and the European Centre for Medium-ranged Weather Forecast (ECMWF) analyses, are used as a baseline for model evaluation.

The two climate models compared in this study are identical in every respect other than their treatment of sub-grid convection and boundary layer effects. One is a standard global climate model (GCM), the NCAR Community Atmosphere Model (CAM). The other is a Multiscale Modeling Framework (MMF), called Super-Parameterized CAM (SP-CAM). In CAM, sub-grid convection is handled diagnostically by statistical cumulus parameterizations and boundary layer schemes (Zhang and McFarlane, 1995; Collins et al., 2004) while in SP-CAM these modules are replaced by an embedded, interactive, prognostic idealized cloud-system resolving model.

Previous publications that document diurnal rainfall in “SP-CAM” simulations have been based on an implementation of the Khairoutdinov and Randall cloud-system resolving model (Khairoutdinov and Randall, 2003) embedded in an older version of CAM3.0 that used a semi-Lagrangian global spectral dynamical core at T42 resolution (Khairoutdinov et al., 2005; McFarlane et al., 2007; DeMott et al., 2007; Khairoutdinov et al., 2008). Hereafter, this original implementation is tagged SP-CAM3.0. In Chapter 4, analysis of the diurnal cycle of surface rainfall in SP-CAM3.0 at T42 horizontal truncation (approximately 350 to 700 km effective horizontal resolution) indicated no evidence of propagating precipitation systems in the central United States (Pritchard and Somerville, 2009b,a).

In this chapter an updated version of SP-CAM is analyzed, in which essentially the same cloud-system model is embedded in a more recent development version of CAM (development software tag CAM3.5.32), hereafter called SP-CAM3.5. A key

advantage of SP-CAM3.5 over SP-CAM3.0 is that the exterior model dynamics are formulated as a finite volume dynamical core, such that the sub-grid response (including collective cloud-resolving model effects) is not smeared out by spectral dynamics. Furthermore, the conventional convection parameterization in CAM 3.0 was updated in CAM3.5 to include effects of convective momentum transport and dilution of convective plumes by increased entrainment (see Section 2.2.2).

SP-CAM3.5 and CAM3.5 are configured at $1.9^\circ \times 2.5^\circ$ horizontal resolution (approximately $230 \text{ km} \times 230 \text{ km}$ at 40° N), with 30 vertical levels. In SP-CAM3.5, the inner cloud-system resolving model domain is two dimensional (height-longitude), on a vertical grid co-located with the outer model's interior 28 levels. The GCM time-step (which is also the multi-scale coupling interval) is 30 minutes.

CAM3.5 and SP-CAM3.5 are driven identically, with a prescribed climatological sea surface temperature annual cycle and modern orbital and greenhouse gas parameters. The model runs freely, i.e. no data assimilation is applied. Simulations were initialized on May 1, and the first month considered a spin-up period. Three months' output are analyzed (JJA), which are sufficient to statistically characterize the key features of warm season central US diurnal variability that distinguish the two models from each other and from observations.

6.2 Propagating diurnal convection

Figure 6.1 shows the classic “reduced transect” signature of propagating rainfall systems in the central US in SP-CAM3.5. The time-longitude structure of the mid-tropospheric heating rate due to sub-grid physics for CAM3.5 and SP-CAM3.5 (a model convection proxy) is compared against an independent observational convection proxy (IR brightness temperature at 11 microns observed from geosynchronous orbit during an arbitrary summer, 2005). In nature (Figure 6.1a) convective phase lines are tilted, evidence of eastward diurnal convective propaga-

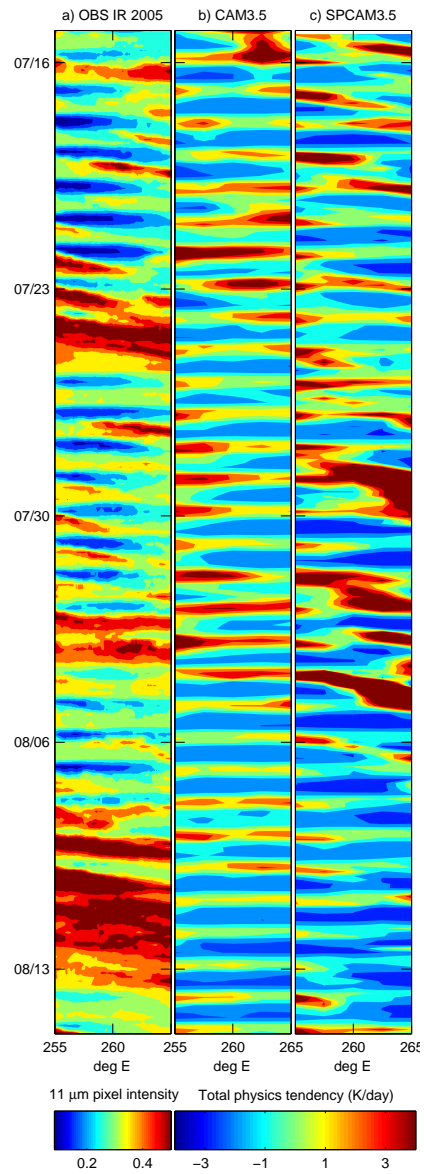


Figure 6.1: Reduced transect comparison of the time-longitude structure of warm season diurnal convective activity in the lee of the Rocky Mountains between 35-45N a) as observed in 2005 from spaceborne infrared imagers, and b) as diagnosed from the total physics package temperature tendency averaged between 350 hPa and 750 hPa in the free-running CAM3.5 and c) SP-CAM3.5 simulations.

tion in the Central US. This observed propagation signal is modulated on synoptic timescales, with consecutive packets of enhanced propagating diurnal convection occurring in intermittent episodes. While both models simulate intermittent periods of enhanced diurnal US convection on synoptic timescales, only in SP-CAM3.5 are these episodes composed of consecutive, coherent, nocturnally persistent, diurnally propagating convective events. In SP-CAM3.5, convective phase lines are tilted but in CAM3.5 they are flat (Figure 6.1b,c). The diurnal convection signal in CAM3.5 is sun-synchronous, short-lived, and does not propagate. The embedded explicit convection model in SP-CAM3.5 improved the space-time structure of the Central US diurnal convection cycle.

The phase and propagation speeds of simulated organized convection in the lee of the Rockies in SP-CAM3.5 are derived from analysis of the standard deviation of the physics package temperature tendency across tropospheric model levels (hereafter called ζ). Due to the characteristically intense vertical dipole heating-atop-cooling structure of these organized convective systems (see Section 6), ζ is a convenient model proxy for the simulated storm location. Long-lived propagating convective systems in a sheared environment are a product of interaction between environmental shear and dipole-like latent heating, formed by latent heat released in mesoscale slantwise ascent and the evaporation of precipitation in mesoscale descent as described in the review paper of Moncrieff (2010, in press).

Figure 6.2 shows Hovmöller maps of ζ for each simulated nocturnal storm in SP-CAM3.5 at the latitude of its maximum convective heating. The zonal phase speed c_x (slope of white line) was estimated for each propagation event by numerically fitting a phase line segment Gaussian envelope function of the form

$$F(x, t) = \exp\left(\frac{(x - x_0 - c_x t)^2}{\sigma}\right)$$

where $\sigma \approx 65$ km and (x_0, c_x) were constrained using Monte Carlo variation and optimal pattern correlation of the assumed form F . This approach is similar

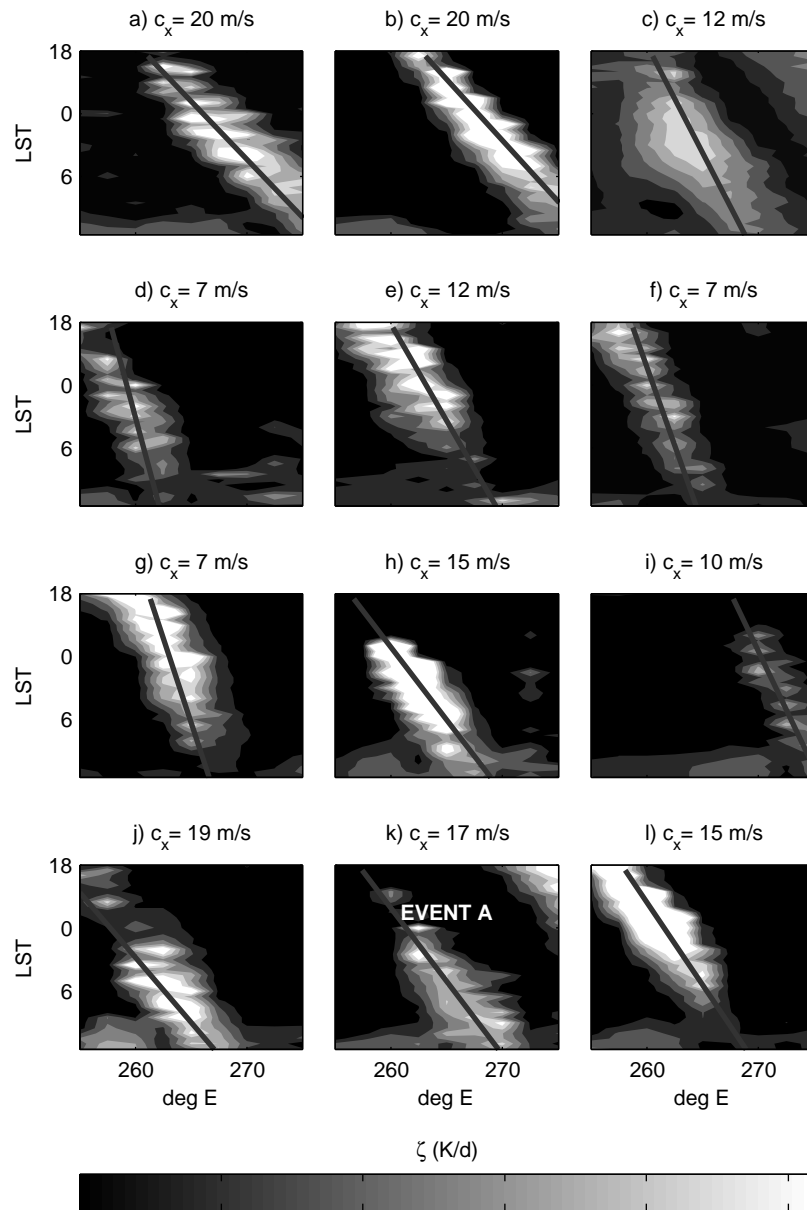


Figure 6.2: Time-longitude section showing the standard deviation across tropospheric model levels of the physics package temperature tendency (a storm location proxy) and fitted zonal phase speed (overlain line) for 12 of 13 propagating convective events simulated by SP-CAM3.5 in the lee of the Rockies.

to that applied in Matsui et al. (2010).

Figure 6.3a.) shows that the ensemble of simulated orogenic convective events in SP-CAM3.5 travel eastward at speeds in the range of 7 to 20 m/s. Reassuringly, this is within the range of the observed zonal speed of orogenic mesoscale convective systems in the lee of the Rockies, determined from radar reflectivity data to range from 7 to 30 m/s (Carbone et al., 2002).

In nature the travel speed of mesoscale convective systems involves both an advective and a propagating component (i.e. the systems are not simply advected by the mass- and/or buoyancy-weighted mean tropospheric flow; Carbone et al. (2002); Moncrieff (1981)). The zonal *propagation speed*, $c_x - \bar{u}$ of the simulated orogenic convective events in SP-CAM3.5 was determined by subtracting the mass-weighted mean tropospheric zonal wind $\bar{u} = \frac{\int_{p_0}^{p_{TTL}} u dp}{\int_{p_0}^{p_{TTL}} dp}$ from the zonal speed, where u was averaged horizontally in space and in time along the lines overlain in Figure 6.2.

Figure 6.3b.) shows a histogram of $c_x - \bar{u}$. Most of the simulated convective systems exhibit a zonal propagation in excess of 2 m/s relative to the tropospheric background flow, typically propagating in the direction of the ambient westerlies. As in Carbone et al. (2002), the median implied steering level (height at which the travel speed equals the environmental flow) for the simulated events is in the range of 400-500 hPa (Figure 6.3c.))

6.3 Regional flows, thermodynamics, and synoptics

Observations indicate that episodes of orogenic propagating diurnal convection in the lee of the Rockies are associated with conditions of synoptic uplift, zonal geostrophic flow aloft, low-level shear, and higher than usual regional water vapor

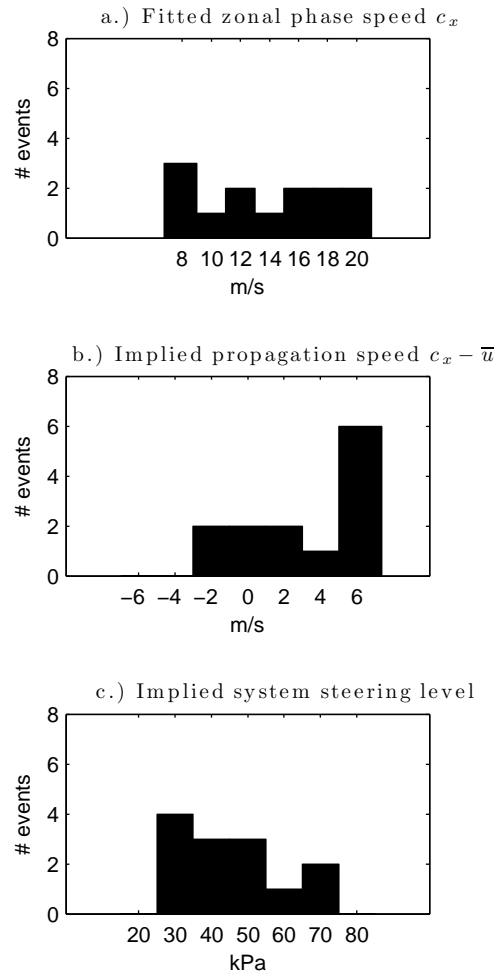


Figure 6.3: Histograms across the ensemble of simulated propagating convection events showing a.) the distribution of c_x , the fitted zonal phase speed from Figure 6.2, b.) the implied storm propagation speed relative to the mean mass-weighted background flow, $c_x - \bar{u}$, and c.) the implied storm steering level.

content (e.g., Maddox, 1983; Laing and Fritsch, 2000; Jirak and Cotton, 2007). Carbone and Tuttle (2008) describe how two aspects of the composite regional diurnal dynamics in the lee of the Rockies – the Great Plains Low-Level Jet (LLJ) and mountain-plains solenoid (MPS) – “conspire” to promote a dynamical environment conducive to the upscale development and nocturnal enhancement of propagating convective systems initiated upstream over the Continental Divide. In this section, these thermodynamic and dynamic aspects of CAM and SP-CAM behavior are evaluated against baseline RUC analyses.

Figure 6.4 contrasts the climatological warm season thermodynamic state in the two global models against the RUC observational analysis over the Central United States. In CAM3.5 the warm season atmosphere is too dry (precipitable water bias ranging from -2 mm to -10 mm). In SP-CAM3.5, there is more moisture available to feed convection (+2 to +4 mm). It is conceivable that the propagating convective signal in SP-CAM3.5 is related to this improvement in summertime US climate. But offline sensitivity tests rule this out: even when constrained to follow SP-CAM3.5’s climate trajectory on inter-diurnal timescales, CAM3.5 does not admit a propagating convective signal (not shown).

Figure 6.5 contrasts the upward branch of the simulated composite mountain-plains solenoidal (MPS) circulation in CAM3.5 and SP-CAM3.5 with the baseline representation in the operational Rapid Update Cycle data assimilation model. As described in Carbone and Tuttle (2008), the thermally driven nocturnal reversal of the solenoid, from daytime conditions of strong ascent during the day over the Continental Divide and broad subsidence over the Central Plains (Fig 6.5 a.), to strong descent over the Continental Divide and weak ascent over the Plains (Fig 6.5b.) corresponds to a Plains uplift environment favorable for sustaining nocturnal mesoscale convective systems. The western, upward branch of the solenoidal circulation is only weakly simulated by both climate models, perhaps due to the coarse model resolution (smooth low orography) inhibiting local topographically

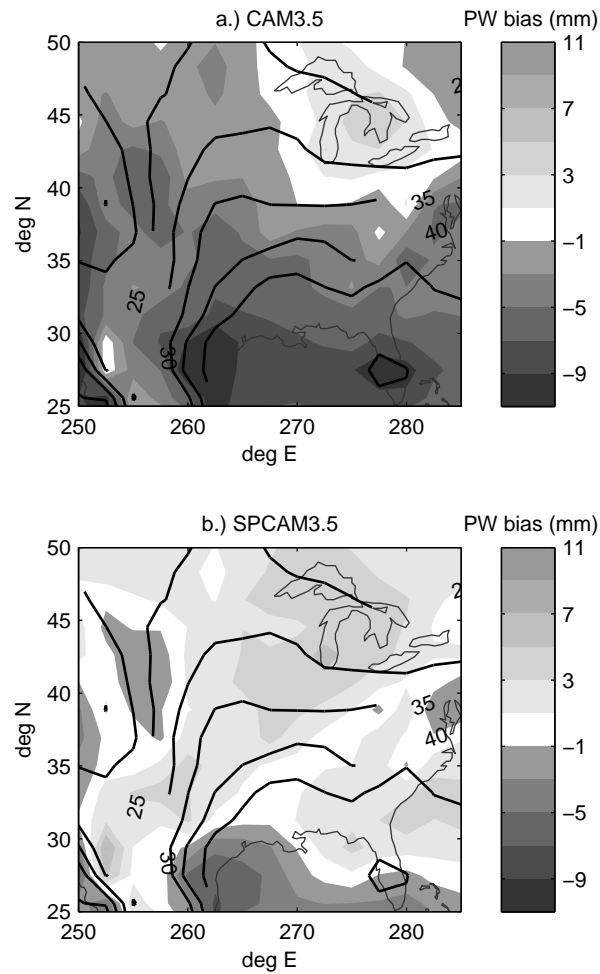


Figure 6.4: JJA climatological precipitable water anomaly at 0000 UTC (shading; mm) for the single-season a) SP-CAM3.5 and b.) CAM3.5 simulations, relative to the Rapid Update Cycle 2003 analysis (contours; interval of 5 mm)

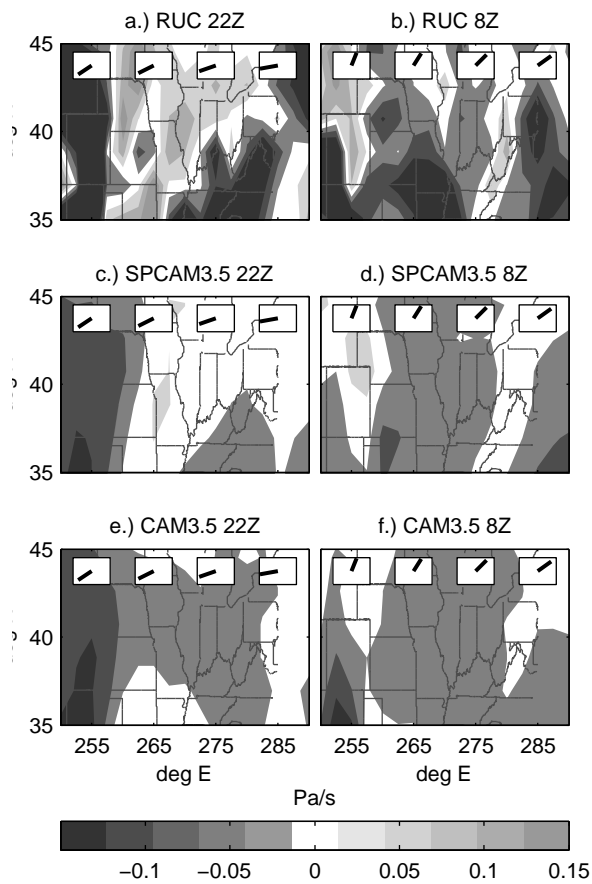


Figure 6.5: 3-hour average vertical pressure velocity centered at (left) 22Z and (right) 8Z comparing the upward branch of the Central US solenoidal diurnal mountain-plains circulation in (top) the Rapid Update Cycle analysis during JJA 2003, to JJA averages of the single-season (middle) SP-CAM3.5 and (bottom) CAM3.5 simulations. Local time of day is depicted on 24-hour clock icons.

driven convection associated with this uplift regime (Lee et al., 2008). However, the non-local daytime Plains descent phase of the MPS is better represented in SP-CAM3.5. (Fig. 6.5c. vs. Fig. 6.5e.). A similar non-local improvement occurs in SP-CAM3.5 in a descending circulation adjacent to the Appalachian mountain chain.

In nature the descent phase of the mountain-plains solenoid produces a subsidence inversion (barrier to convective ascent) over the Great Plains, which traps daytime surface buoyancy over a vast area (Carbone and Tuttle, 2008). As a result, the CAPE generated by daytime surface heating accumulates and is focused into a narrow leeside zone by easterly upslope surface density flows (Dirks, 1969; Tripoli and Cotton, 1989a). Mountain generated cumulonimbus advecting off the Rockies can tap into this concentrated potential buoyancy reservoir, which in the presence of deep zonal shear, can produce rapid upscale growth into mesoscale convection systems (Tripoli and Cotton, 1989a). Figure 6.6 shows that the strength of the capping inversion is too weak in CAM3.5, but is strengthened using the embedded explicit convection approach in SP-CAM3.5. This is consistent with SP-CAM3.5's improved representation of the daytime descent phase of the solenoidal circulation discussed above, and suggests SP-CAM3.5 more readily concentrates accumulated Plains CAPE in the leeside convergence zone.

The northern terminus and eastern flanks of the low-level jet circulation are important sources of localized low-level nocturnal moisture convergence, temperature advection, and low-level vertical shear, which help sustain organized convective systems into the night along distinct latitude "corridors" (Tuttle and Davis, 2006; Trier et al., 2006; Jirak and Cotton, 2007; Trier et al., 2010). Figure 6.7 evaluates the warm season composite nocturnal evolution of the 850 hPa moisture convergence zones associated with the low-level jet circulation in the two models against diurnally composited Rapid Update Cycle data. The analyses show a broad zone of moisture convergence from 265-270E and 38-45N, which intensifies from 10pm

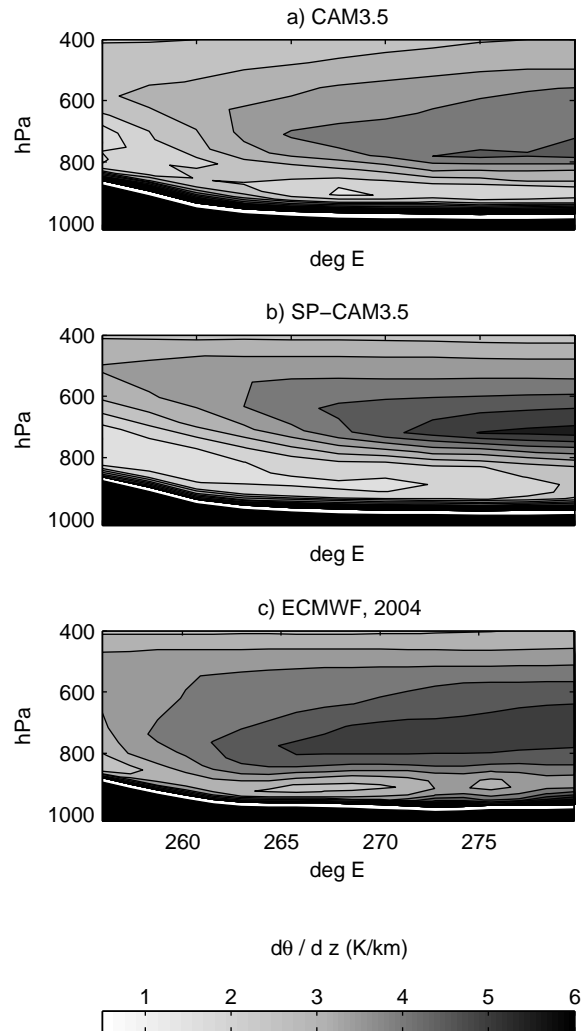


Figure 6.6: Pressure-longitude section showing JJA climatological static stability ($\partial\theta/\partial z$) averaged from 35-45N in the lee of the Rockies for a) CAM3.5, b.) SP-CAM3.5 and c.) a year of ECMWF interim reanalysis. Surface topography is shown in black.

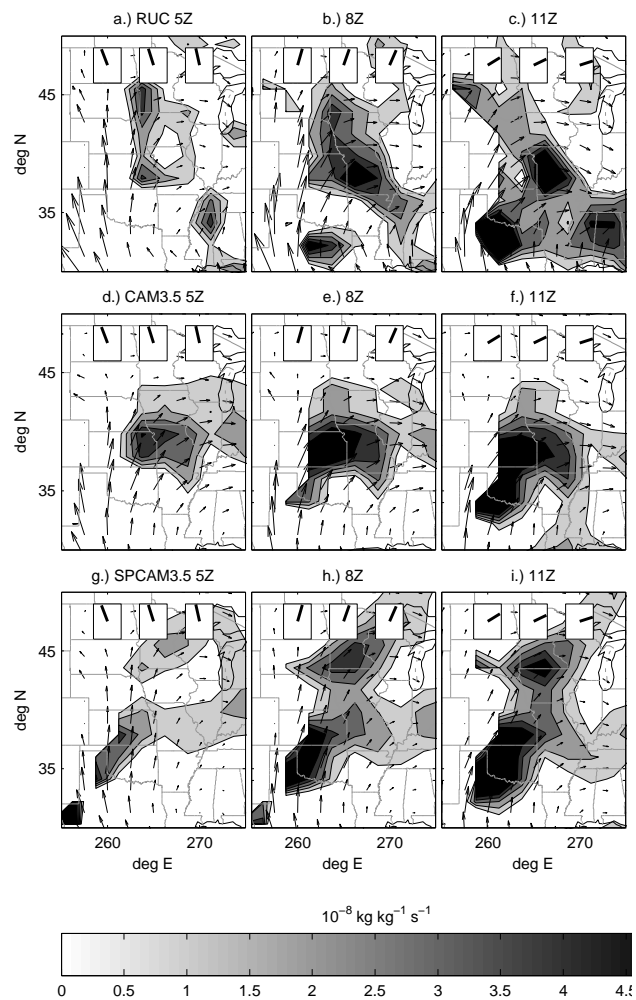


Figure 6.7: Maps over the central United States comparing the nocturnal evolution of the 850 hPa vapor transport (vector field; $q\mathbf{V}_H$) showing the Great Plains Low Level Jet (LLJ) and its associated moisture convergence (shading; $\nabla \cdot (q\mathbf{V}_H)$) in (top) the 2003 Rapid Update Cycle analysis, compared to global simulations using (middle) CAM3.5 and (bottom) SP-CAM3.5.

(5Z) to 4am (11Z) local time (Figure 6.7a.-c.), tracking the northeastern terminus of the evolving low-level jet circulation as it veers increasingly eastward throughout the night. Dual local vapor convergence maxima emerge in the early morning hours of the composite RUC data, centered at 32-34N / 262E and 38-40N / 270E (Figure 6.7c.). The northernmost of these maxima has previously been linked to a corridor of preferred MCS propagation at 40N (Tuttle and Davis 2006).

Like most coarse resolution climate models, the resolved physics of SP-CAM3.5 and CAM3.5 admit the essential ingredients for thermally driven orographic low-level jet dynamics (Ghan et al., 1996). However the chronology and structure of the associated 850 hPa moisture convergence zones are different in the two models. In CAM3.5 there is only a single broad zone of nocturnal maximum convergence in the nocturnal composite (Fig. 6.7d.-f.). In contrast, SP-CAM3.5 exhibits a dual maximum nocturnal moisture convergence structure, as in the data (Fig. 6.7g.-i.). In SP-CAM3.5, LLJ vapor transport and the northern convergence maximum extend farther north than in CAM3.5 and observations. The preferred latitude of orogenic convective complexes in SP-CAM3.5 coincides with the northernmost moisture convergence maximum at 45N.

Figure 6.8 contrasts the shear characteristics of the low-level jet circulation in the observations and models. Wind shear below 3 km is an important organizing influence for MCS generation in nature, and is modulated diurnally by the low-level jet. In the RUC data, maximum anomalous low-level shear occurs near local midnight (7Z) in a compact zone between 30N and 40N, and weakens into the morning. Both climate models reproduce this aspect of the LLJ, but in SP-CAM3.5 the zone of enhanced nocturnal shear extends farther north, to almost 50N. Although low-level shear cannot influence convection by design of the cumulus parameterization in CAM3.5 (except through convective momentum transport, which reduces the shear), its zonal component is an organizing influence on 2D convection in the embedded cloud resolving model arrays in SP-CAM3.5.

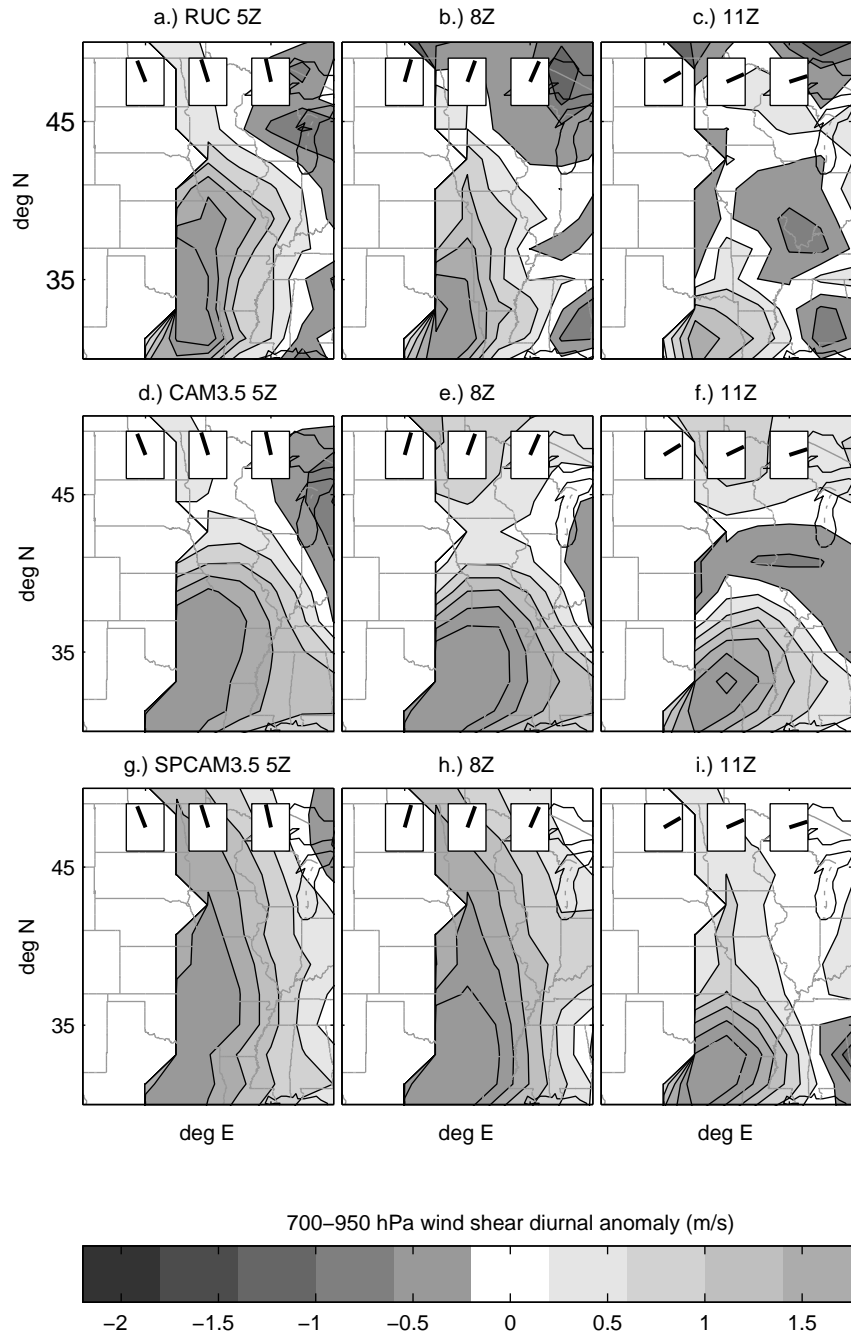


Figure 6.8: As in Figure 6.7 but showing the diurnal anomaly of low-level wind shear magnitude (700 hPa minus 950 hPa) associated with the Great Plains Low Level Jet (LLJ) in (top) the 2003 Rapid Update Cycle analysis, (middle) CAM3.5 and (bottom) SP-CAM3.5.

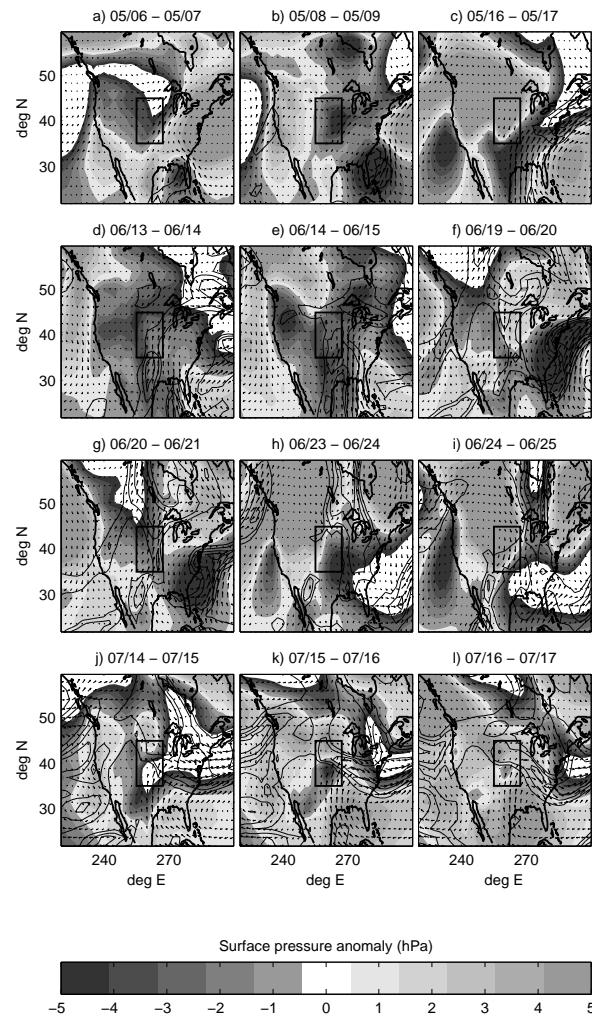


Figure 6.9: Composite anomaly maps over the central US showing the deviation of surface pressure (shading; hPa), positive column water vapor mass anomalies (contour interval of 4 g/m²) and column water vapor transport (vector field) during 12 propagating convection events in SP-CAM3.5, relative to its simulated seasonal JJA climatology.

Reassuringly, similar synoptic conditions accompany simulated propagating diurnal convection events in SP-CAM3.5 as are observed in nature. Figure 6.9 shows the anomalous (with respect to warm season model climatology) sea level pressure, precipitable water and vertically integrated water vapor transport, $q \cdot \mathbf{V}$ for 12 propagation episodes that took place during the single-summer SP-CAM3.5 simulation. Most of the propagation events occur during periods of synoptic uplift (anomalously low surface pressure) in the lee of the Rockies (Fig 6.9 a,b,d,e,g,h,j). The remaining events occur during conditions of anomalously high precipitable water (Figure 6.9 c,f,i,k,l). The signature of a southerly jet structure in the anomalous water vapor transport vector field for several events (Fig. 6.9 d,e,f,g,j,k,l) further suggests that enhanced moisture convergence and wind shear due to low-level jet flow into the Great Plains also plays a role in generating organized propagating nocturnal convection in SP-CAM3.5.

6.4 Genesis and multi-scale structure of a propagating event

This section focuses on a specific simulated propagation event (hereafter Event A; the topmost tilted phase band in 6.1c) for additional physical process analysis. Event A was chosen for in depth analysis because the weather state in SP-CAM3.5 over the central US was dominated by abnormally zonal geostrophic flow aloft, due to the positioning of a synoptic long-wave pattern (Figure 6.10). This is an ideal environment to test the model's unsteady orogenesis mechanism against a classic conceptual dynamical model developed by Tripoli and Cotton (1989a) (hereafter TC89) around a historical case study of observed mesoscale convective system orogenesis that took place in a similar weather state.

Figure 6.11 shows the evolution of condensate and large scale horizontal winds

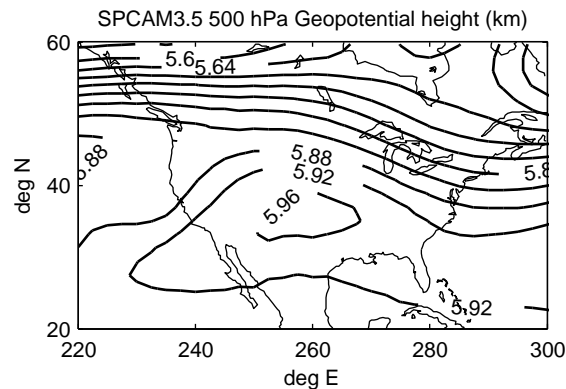


Figure 6.10: SP-CAM3.5 500 hPa geopotential height (km) showing the synoptic state during a simulated 3-day packet of consecutive diurnal orogenic convection propagation.

during Event A. Initially (Fig. 6 a), two condensate structures (contours) are visible. The westernmost is Event A, near 250 E, an organized convective system that has just begun to form. The easternmost (270 E) is a mature convective system that was generated 24 hours prior near 250E, but has since traveled twenty degrees (1700 km) to the east, at about 20 m/s. The formation of Event A occurs during conditions in which the zonal westerlies are deeply sheared and a shallow easterly upslope surface wind layer converges near 260E (Fig. 6 a.,c.,e.,g.). As in the TC89 model, condensate is first produced by locally forced deep mountain convection at 2030Z (Fig. 6a,b; contours). Upscale development occurs around 0000Z when the system reaches the leeside convergence zone (Fig. 6 c.). Convection weakens at 0430Z and re-intensifies by 1130Z, where it coincides with the LLJ inflow. A northerly wind component near 500 hPa develops along the western flank of the organized convective system, suggesting flow balance on the large scale grid. Such balance is clearly evident for the mature organized convective system generated the previous day (Fig. 6.11b.,d.,f.), which exhibits a classic stacked cyclone-anticyclone signature.

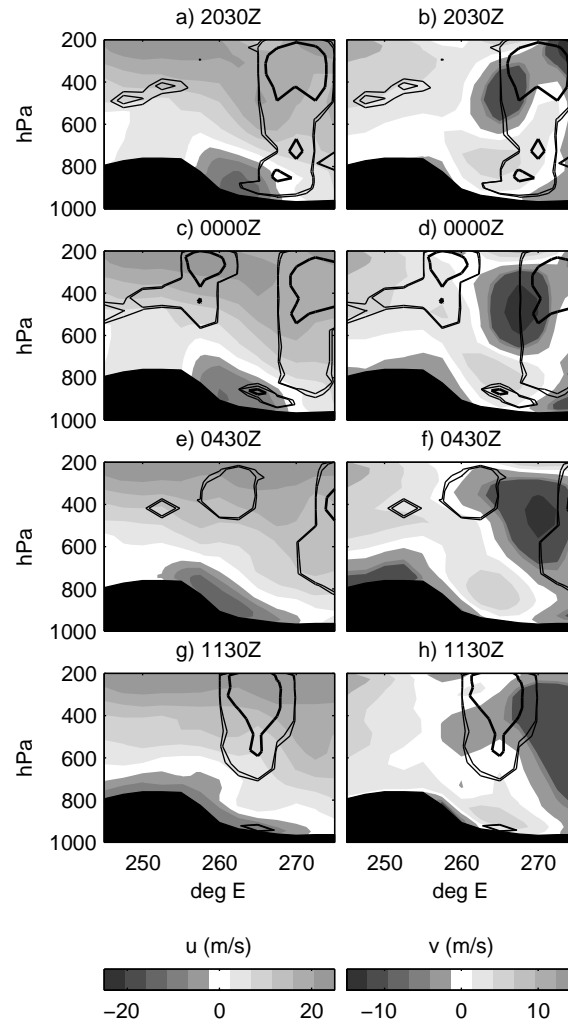


Figure 6.11: Height-longitude structure at 40 N showing the time evolution of (left) zonal and (right) meridional wind during Event A. Condensate concentration contours are superimposed for values of (0.005, 0.01, 0.1, 1) g/kg.

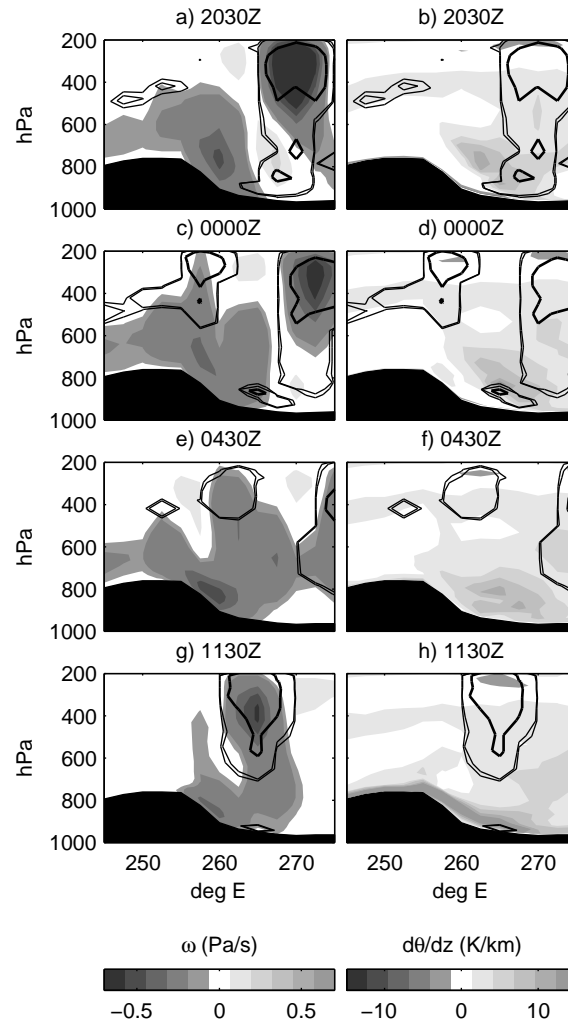


Figure 6.12: As in Figure 6.11, but for (left) vertical pressure velocity and (right) $d\theta/dz$.

Figure 6.12 shows the vertical velocity and stability during the same period. At 2030Z, the Plains inversion traps locally generated surface instability in a thin boundary layer. To the west the cloud topped afternoon boundary layer is deep. The leeside convergence zone causes upward motion near 260E (Figure 6.12 a.). This plume supplies zonally converged, inversion-trapped Plains instability upwards and feeds convection expansion. Convective heating aloft is straddled by mesoscale downdrafts (Figure 6.12 e.; 255E, 270E at 300 hPa). In the mature phase, deep vertical velocity associated with convective heating produces local breaks in the capping inversion (Figure 6.12c., d.; 275E at 800 hPa).

Figure 6.13 visualizes both resolved grids in SP-CAM3.5 simultaneously during the propagation event the day before Event A, showing evidence of multi-grid convection-dynamics interactions across the two resolved scales. Propagating 3D condensate meta-structures transcend individual embedded explicit convection subdomains but exhibit morphology on larger scales that is reminiscent of observed mesoscale convective systems (deep precipitating system “core”, leading ice/virga anvil). The condensate structure of the embedded cloud resolving model states show distinct organization resulting from 2D shear and cold pool effects. The fact that the system coherently propagates across many embedded cloud model subdomains while retaining its meta-structure emphasizes interaction between the two resolved physical scales.

6.5 Discussion

Dynamical considerations

Theoretical investigations have shown that as well as the convective available

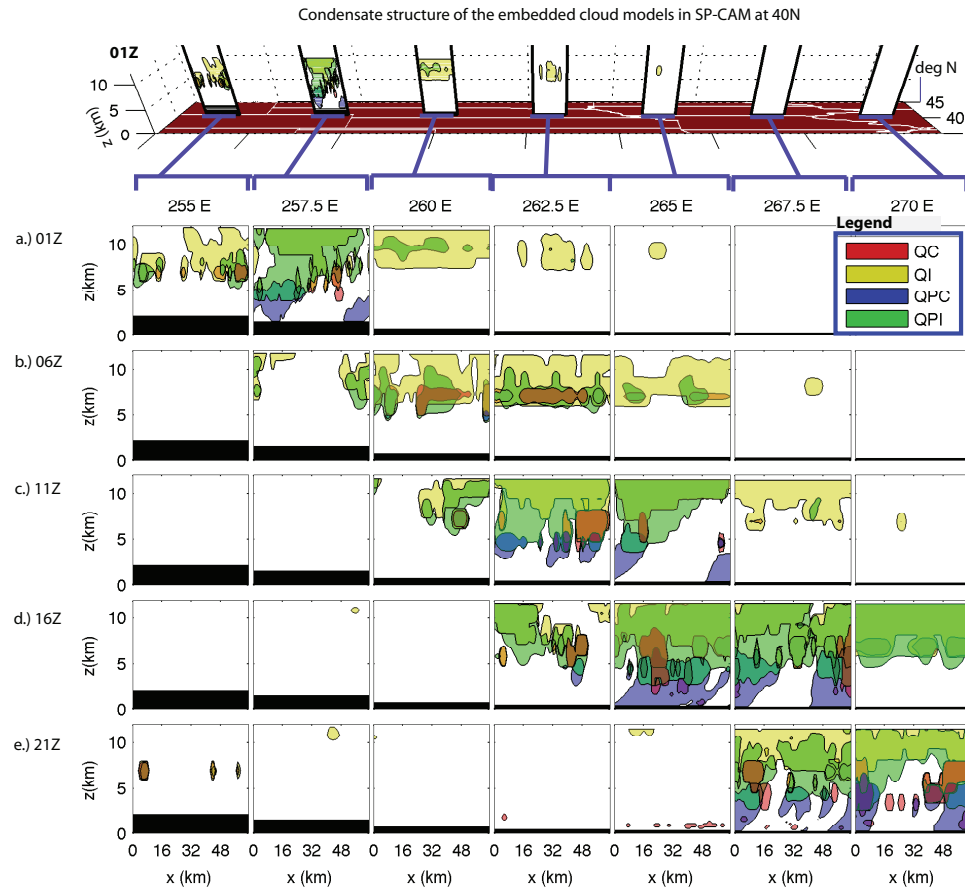


Figure 6.13: Time-longitude matrix of height-longitude sections showing snapshots of condensate within adjacent cloud resolving models at 40N in SP-CAM3.5 during a simulated organized propagation episode, at five hour intervals from top to bottom. Shaded transparent contours outline the 0.01 g/kg threshold for non-precipitating cloud water (red; QC), non-precipitating cloud ice (yellow; QI), precipitating cloud water (blue; QPC) and precipitating cloud ice (green; QPI) within the embedded explicit convection model subdomains shown above. Surface orography is shown in black.

potential energy (CAPE) normally associated with deep convection, the highly organized mesoscale convective system (MCS) is partly sustained by the mean-flow kinetic energy and the work done by the horizontal pressure gradient. These dynamical forms of energy are fundamental to the convective organization process and the interaction of environmental shear with latent heating atop evaporative cooling (see review by Moncrieff 2010). This dipole-like heating projects onto the first baroclinic gravity wave mode and is important for injecting kinetic energy upscale (Pandya and Durran, 1996; Moncrieff and Liu, 2006; Correia et al., 2008). The mesoscale circulations occur as distinctive regimes of organized airflow (Moncrieff, 1981). The simplest possible (i.e., archetypal) dynamical model distinguishes the following regimes of slantwise MCS-type convective overturning: i) a purely propagating system where the relative inflow derives entirely from ahead of the system; ii) a symmetric system where the updraft and downdraft have comparable depth; iii) a system that contains hydraulic jump-like ascent in the cooling region (Moncrieff 1992; their Fig. 2). These three regimes are distinguished by a measure of dynamical efficiency, i.e., the quotient of the work done by the horizontal pressure gradient and the kinetic energy available from shear. None of these slantwise circulations is present in CAM (or any standard climate model) because, firstly, traditional convective parameterizations do not represent the salient dynamics of convective organization and, secondly, the horizontal resolution of the model is insufficient to explicitly simulate these circulations.

The above analysis has shown that organized circulations occur in SP-CAM3.5. A salient question concerns their realism. Figure 6.14 shows the dipole-like heating for a dozen propagating events in SP-CAM3.5, and the zonal component of airflow relative to the traveling systems, i.e., $(u', \omega) = (u - c_x, \omega)$. In most of the events a distinctive overturning solenoidal circulation exists ahead of the system (e.g. Figure 14 g; rotational relative circulation centered near 270 E and 500 hPa), in broad agreement with TC89. However, the depth of the surface east-

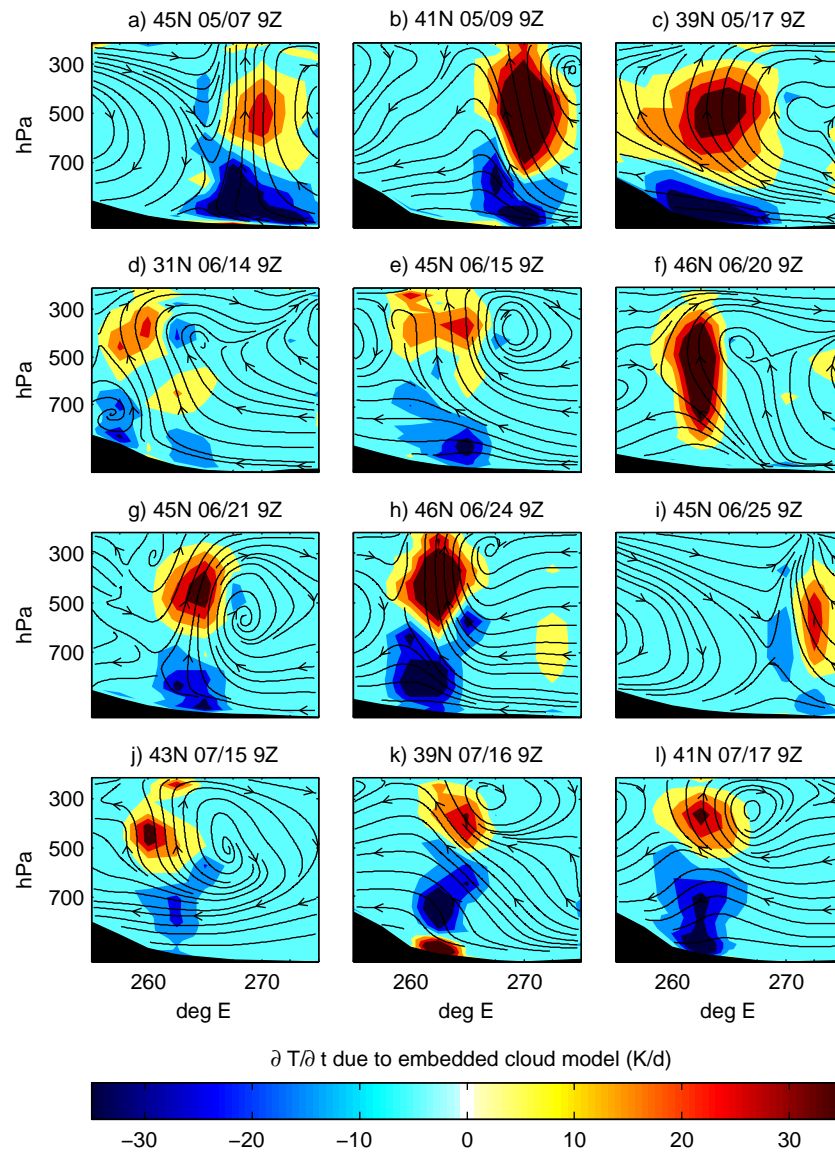


Figure 6.14: Pressure-longitude sections at 2am local time, showing storm-relative zonal flow (solid streamlines) atop the convective heating structure (temperature tendency due to the embedded CRM; thin contours at 10 K/day increments, negative contours dotted; light shading for $\partial T/\partial t > +15$ K/day, dark shading for $\partial T/\partial t < -15$ K/day) for 12 separate instances of MCS propagation in the lee of the Rockies in SP-CAM3.5.

erly inflow is unusually deep, ranging from 4 km to 7 km (Figure 6.14 b,e,k,l). A prevalent feature of this inflow is the up-down circulation that traverses the system front-to-rear, sometimes featuring deep vertical displacement (e.g., Figure 6.14 b,k), consistent with the above archetypal hydraulic jump regime. This regime contrasts with orogenic propagating MCSs over the continental US continent simulated by Moncrieff and Liu (2006) and Trier et al. (2006) and verified against a continental-scale radar network. Those simulations are consistent with the symmetric archetypal regime. It is not understood why the SP-CAM3.5 convective systems tend to have a prevalent jump-like morphology. Among possible explanations is that evaporative cooling (associated with the cloud-microphysical parameterization in the embedded explicit convection with emphasis on the stratiform region and mesoscale downdrafts) is too strong. In summary, the morphology of the airflow organization simulated by SP-CAM3.5 differs from the natural world, and also from cloud-system simulations, e.g. Grabowski and Moncrieff (2001), and the above dynamical efficiency with emphasis on the simulated horizontal pressure gradient. A basic study of these important aspects while necessary is beyond the scope of this dissertation.

Role of dipole-heating in shear-flow compared to cold-pool triggering

It was argued above that the basic reason why SP-CAM3.5 generates organized propagating convection is that the embedded cloud-system resolving models produce the dipole heating required for mesoscale convective organization in shear flow. The upper-tropospheric latent heating overlies a deep evaporative cooling layer that typically extends from the surface to 600 hPa in the model. As explained above, the dipole-like diabatic heating is linked to the propagation physics of MCS in shear flow *on the coarse SP-CAM3.5 outer grid*. The convective heating

profiles associated with the mesoscale convective systems project favorably onto first baroclinic gravity wave modes. Such a slow-manifold control of the propagating systems in SP-CAM3.5 is evidenced by the dynamical balance in Figure 6.11. This property is consistent with the convectively generated potential vorticity propagation mechanism of Raymond and Jiang (1990) and Li and Smith (2010). Indeed, convectively generated diurnal potential vorticity anomalies are routinely spawned by the organized convective events in SP-CAM3.5 (not shown).

On the other hand, cold-pools in the form of density currents generated by convective downdrafts impinging on the underlying surface and/or convectively generated gravity-waves have an important local effect *on the fine-scale cloud-system resolving grid*. The density currents continually trigger fresh cumulonimbus, which in a sheared environment, organize upscale into mesoscale convective systems (e.g., Thorpe et al., 1980; Rotunno et al., 1988a; Lafore and Moncrieff, 1989). However, contrary to the implications of Carbone et al. (2002); Carbone and Tuttle (2008) and others, neither cold pools nor gravity waves can explain the propagating MCS simulated by SP-CAM3.5. The periodic lateral boundary conditions imposed on the cloud-system resolving model, a key aspect of the MMF approach that makes it scalable for massively parallel climate modeling, trap the density-currents within each fine-scale domain, hence precluding long-range interaction on the coarse grid.

Multi-grid propagation of organized convection across scales

Figure 6.15 is a framework for how convective signals can propagate over many GCM grid-boxes in a multi-scale model despite the restriction of lateral periodicity in the embedded cloud-system resolving models. Consider a thought experiment in which (1) the resolved tendency in the outer (large-scale; LS) model of SP-CAM has just produced organized convection in the embedded explicit convection

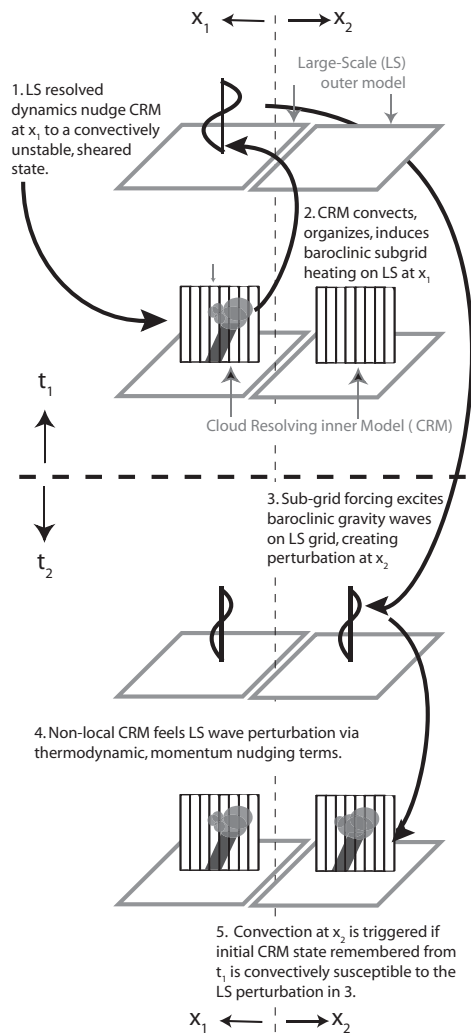
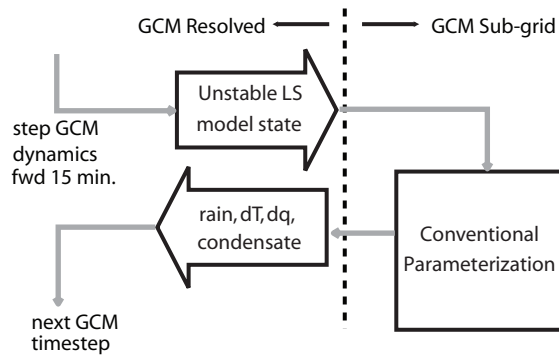


Figure 6.15: Conceptual schematic illustrating how multi-grid propagation of convective signals can occur across the two resolved scales, (top) interior Cloud Resolving Model (CRM) and (bottom) exterior Large Scale (LS), contained in SP-CAM3.5. A sequence of events is shown at adjacent LS grid columns x_1 (left) and x_2 (right), straddling the transition from (above dashed line) LS timestep t_1 to the subsequent LS timestep t_2 . Since the CRMs are laterally periodic, convective propagation can only occur as mediated by the LS model.

model at horizontal location x_1 . Consequently, (2) the CRM induces a convective heating typical of organized convection (i.e. containing a deep stratiform cooling layer) onto the LS model at x_1 . This sub-grid diabatic forcing projects onto first baroclinic LS waves, such that on the following LS timestep, (3) resolved convection information at x_1 propagates, as mediated by resolved LS wave dynamics, to an adjacent horizontal location x_2 . The LS model at x_2 (4) transmits received wave-induced perturbations of temperature, momentum, and shear to its embedded CRM via the nudging terms that link the LS to the CRM. Provided the CRM at x_2 is initially in a state that is susceptible to convecting in response to such perturbations, non-local convection propagation can occur, despite the fact that the CRMs are isolated and periodic. The limiting timescale for the communication of convective information between the two scales is the large-scale model timestep. When it is less than the lifetime of individual cumulus elements or organized 2D cumulus systems, as in the simulation here (30 min), stages of the horizontal mean plume lifecycle in the CRM can interact with dynamical modes resolved by the large-scale model.

Figure 6.16 shows how the scale interface in SP-CAM3.5 was re-designed via the embedded explicit convection approach, emphasizing the introduction of sub-grid memory. The inclusion of a *prognostic convective system lifecycle* is a crucial extra degree of freedom that allows sub-grid heating profiles in SP-CAM3.5 to respond to organizing environmental influences such as wind shear or convectively-generated organized flows. In CAM3.5, sub-grid convective heating is slave to the resolved dynamical tendency of a single instability metric accumulated during a single GCM time step. On the other hand, in SP-CAM3.5, resolved tendencies of temperature, water, momentum, and condensate are instead applied as a forcing on a prognostic embedded explicit convection integration. The consequent heating profile adjustment is determined by the cloud-system resolving model under this forcing. Being an integration rather than a diagnostic calculation, the explicit cloud-

a.) The GCM scale interaction is self contained in space and time



b.) The MMF scale interaction is not self contained in time.

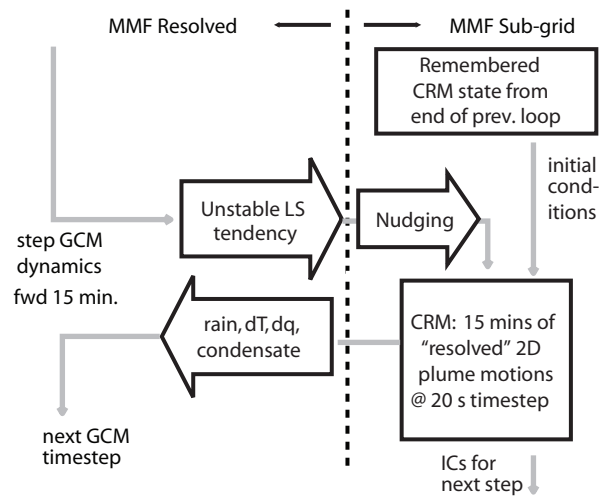


Figure 6.16: Schematic illustrating how the scale interface in (top) GCMs is re-engineered in (bottom) the Multi-scale Modeling Framework (MMF) approach to global climate modeling. Light grey arrows define the code flow, and the vertical dashed line separates the resolved and sub-grid scales. In the MMF approach, “memory” at the inner resolved scale plays a role in the sub-grid response to large-scale forcing.

system resolving model physics is, in part, determined by the initial conditions. In other words, memory exists at the smallest resolved scale in the multi-scale modeling framework. As such, if instability is generated by large-scale temperature and moisture advection and shear, the CRM will tend to develop organized convection, i.e. propagating mesoscale convective systems. In a separate context, organization memory was recently introduced in the sub-grid convection package of a conventional global model in Mapes and Neale (2011), who also demonstrate improvements on diurnal timescales.

Role of the dynamical core in the outer model

Chapter 4 showed no evidence of propagating systems in the central US in a previous version of SP-CAM (SP-CAM3.0), which was run using a slightly different multi-scale model configuration. At that time, this deficiency was attributed to the assumption of periodicity in the embedded cloud-system resolving models. Revisiting these results (not shown), some evidence of propagating convective heating signatures is found in SPCAM3.0, but nothing close to that reported herein for SP-CAM3.5. This is likely in part a resolution issue: in offline resolution sensitivity tests with SP-CAM3.0 at higher spectral resolution (T85, or 175-350 km) evidence of propagating convective heating (latent heat release) is apparent in the lee of the Rockies, but no propagating rainfall signatures (not shown).

The further improvement reported here using SP-CAM3.5 in finite volume mode at comparable horizontal resolution (approximately 250 km) highlights the importance of the choice of dynamical core in the outer model. The grids on which large-scale and cloud resolving model effects were computed in SP-CAM3.0 were inconsistent. Physics tendencies computed on the non-aliasing Gaussian grid in SP-CAM3.0 are not fully recognized by the spectral dynamics, which has fewer

degrees of freedom. This may prevent latent heating that is barely resolved on the grid from realistically interacting with the spectral dynamics (David Randall, personal communication).

Figure 6.17 illustrates this effect visually: A compact, localized 400 hPa diabatic heating anomaly induced by the embedded CRMs during Event A in SP-CAM3.5 is horizontally interpolated using spectral routines to a 128×256 Gaussian grid, using triangular (T85) truncation. Although the Gaussian grid has higher “resolution” than the $1.9^\circ \times 2.5^\circ$ finite volume grid, the resulting heating anomaly is more diffuse, emphasizing that a spectral dynamical core cannot support the small-scale waves excited by localized heating anomalies in the finite volume model. Whilst Figure 6.15 depicts the cloud resolving and large-scale models on an equivalent horizontal grid, this is only true for SP-CAM3.5 as a result of the finite volume dynamical core.

It is unknown to what extent the propagating signal in SP-CAM3.5 was enabled due to increasing the horizontal resolution of the embedded CRM from 4 km to 1 km. Existing documentation of the sensitivity of MMF simulations to varying the CRM grid spacing is insufficient to anticipate the effect of quadrupling CRM resolution on deep nocturnal US convection. Marchand and Ackerman (2010) examine only low cloud mean sensitivities to CRM resolution, and Khairoutdinov and Randall (2001) smooth their results with a 12 hour filter. In the face of limited computing resources for this analysis, an interior model resolution of 1 km was chosen to optimally admit key physics of 2D squall line organization based on the explicit CRM experience of Lafore and Moncrieff (1989) and Moncrieff and Liu (2006). The sensitivity of the result to this CRM resolution choice remains to be determined.

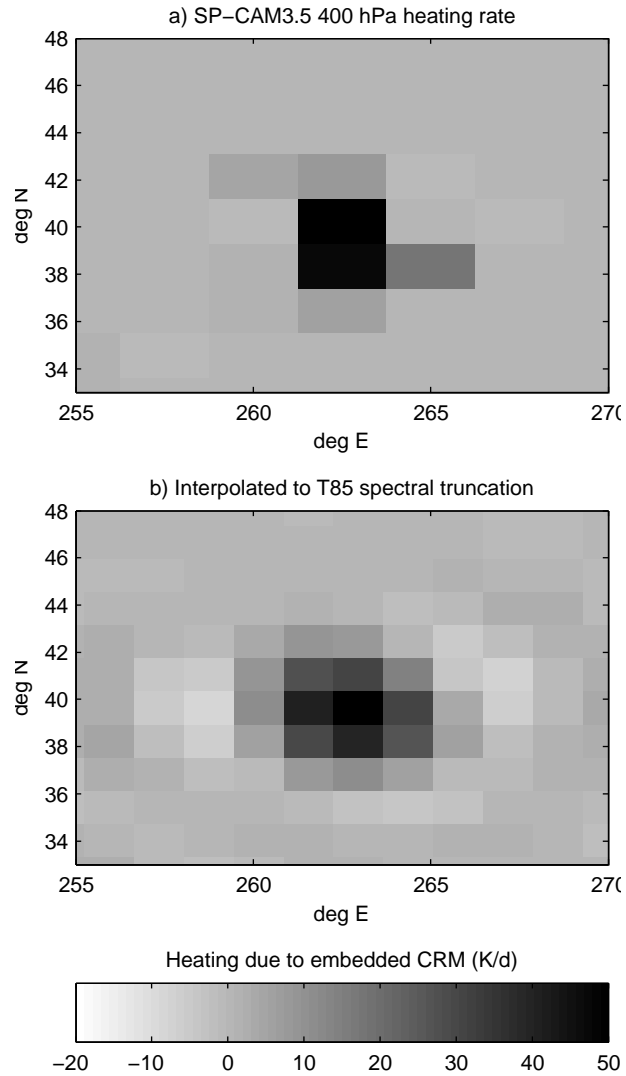


Figure 6.17: a) A snapshot showing the horizontal extent of the 400 hPa SP-CAM3.5 heating signature during a nocturnal propagating convective event on its $1.9^\circ \times 2.5^\circ$ finite volume horizontal grid. b) Diffuse representation of the same field after spectral horizontal interpolation to triangular truncation at T85.

6.6 Conclusion

Current generation global climate model projections of future hydrologic changes are especially uncertain in the lee of mountain chains due to deficiencies in conventional convective parameterization that were not designed to represent organized convective systems. This is strikingly apparent in the Central US, where such systems account for much of the warm season climatological rainfall.

The above analysis documents nocturnally persistent orogenic midlatitude warm season convection in the lee of the Rockies in a coarse resolution global climate model that uses the embedded explicit convection approach to represent sub-grid convection (i.e., a multiscale modeling framework). Analysis shows that the simulated propagating events in terms of propagation speed, synoptic forcing, and characteristic scale of the simulated events are within the observed range. Mean moisture content, stability of the Great Plains capping inversion, and mountain-plains solenoidal circulation are concurrently improved due to the embedded cloud resolving model approach. Storm-relative flow is realistically solenoidal at mid-tropospheric levels ahead of the simulated systems, but the simulated low-level penetrative easterly inflow is two to four times too deep.

In nature, propagating diurnal convective systems are also observed to occur over Africa, Indonesia and South America, among other places. It is currently unknown if SPCAM3.5 can produce such tropical organized propagating diurnal convection - due to the substantial data volume of the inner model, output for the simulation reported here was restricted to a North American subregion. Global output from the older spectral version of SP-CAM3.0 does not appear to contain propagating convection west of Colombia, or around the Indonesian islands, at either T42 or T85 horizontal resolution (not shown). But since SP-CAM3.0 also did not admit significant Central US propagating convection, which has since turned out to exist in SP-CAM3.5, the question is still open for the time being: Can

the multi-scale modeling approach admit propagating orogenic diurnal convection in the tropics, where geostrophic dynamics have less control on scale interactions between the cloud resolving model and large-scale grids?

Other issues associated with the simulated organization of airflow in the evaporatively cooled (mesoscale) downdraft region remain to be understood. Follow-on sensitivity studies of the nocturnal organized US convection documented herein would be useful to clarify the convective propagation mechanisms across the two resolved scales in the multi-scale modeling approach. This chapter has advocated that cloud-system resolving simulations of organized convective heating project onto first baroclinic gravity wave modes in the large scale model, which in turn mediate dynamically consistent convective lifecycle responses in non-local cloud resolving models. However, other propagation mechanisms may exist within the possible multi-grid degrees of freedom in multi-scale modeling frameworks (e.g. large scale advection of condensate or vapor anomalies impacting non-local cloud resolving model behavior via its total water equation). Further testing is needed that can discriminate between such mechanisms (for instance with dual-grid water and energy budget calculations at the time resolution of scale coupling).

Limitations of the scope of this study open important new research questions in regard to the multi-scale modeling approach, for example:

- Did the zonal orientation of the two dimensional cloud-system resolving models in this simulation optimize the ability for SP-CAM3.5 to respond to the all-important effects of zonal shear in the lee of the Rockies on the propagating systems?
- To what extent would multi-grid propagation have occurred if the 2D cloud-system resolving models had been oriented meridionally?
- Should the fixed cloud-system resolving model orientation be relaxed in MMFs, for example, through a random rotation of the 2D array to represent

the 3D effects of large scale wind shear on convective organization?

- Should the alignment be chosen in terms of dynamical criteria, such as the mean vertical shear direction?
- To what extent was the propagating signal enabled by the increase in the horizontal resolution of the embedded explicit convection grid from 4 km to 1 km?

A fundamental issue is the role of momentum transport by organized convection which differs from the convective momentum transport parameterized in CAM3.5 as a mixing process that decreases shear. Organized convective momentum transport has the opposite effect – it can increase vertical shear in certain atmospheric layers, e.g., low-level shear which is basic to mesoscale convective systems and their scale-interaction properties.

In the meantime, the broader implication of this chapter is that multi-scale modeling frameworks admit some of the missing diurnal physics of orogenic organized propagating convection over continents that are conspicuously absent from contemporary global climate models. Crucially, this occurs *despite the fact that fast-manifold processes are artificially restricted and cannot have a long-range effect* in the superparameterization approach. This is consistent with a slow-manifold interpretation of the dynamics that control the eastward traveling organized convection signal in the Central US (Tripoli and Cotton, 1989a; Raymond and Jiang, 1990; Li and Smith, 2010). The result is also a glimmer of hope that with additional understanding and refinement the multi-scale approach to climate modeling may help improve longer term hydrologic climate forecasts in heavily populated parts of the world where diurnal physics project onto climate timescales and conventional climate model projections disagree.

Chapter 6, in part, is a reprint of material as it appears in Orographic propagating precipitation systems over the US in a global climate model with embedded explicit

convection 2011. Pritchard, Michael S., Moncrieff, M. W., and Somerville, R. C. J., *Journal of the Atmospheric Sciences*, in press. The dissertation author was the primary investigator and author of this paper.

Chapter 7

Summary

The work in this dissertation is motivated by the problem that cloud processes are poorly represented in global climate projection models, to the point where even the most simply forced mode of convective variability – the diurnal rainfall cycle – is not well simulated. Distortion of a fundamental mode of simulated convective variability in *current climate* erodes faith in model projections of how cloud processes may feedback on *future climate* change, a key problem for society. Furthermore, it prevents the application of global climate models to better understand the physical mechanisms underlying unresolved aspects of the observed climatological diurnal rainfall pattern, where simulations might otherwise provide scientific insight.

This dissertation has first sought to clarify to what extent distorted simulation of global diurnal rainfall in climate projection models may be remedied through the use of a new technique for handling cloud processes – cloud superparameterization. Superparameterized climate models (i.e. MMFs) deploy thousands of embedded high resolution models of explicit convection inside a coarse resolution global climate model, replacing conventional statistical “parameterizations” for the effects of sub-grid cloud processes. Unlike fully global cloud resolving mod-

els, prototype MMFs are already computationally affordable for the problem of climate projection, but are also still in their infancy such that their performance and appropriateness for this application has not been completely evaluated.

Chapter 4 (Pritchard and Somerville, 2009b,a) evaluates the effect of superparameterization on the simulated diurnal rainfall mode from a number of diagnostic perspectives not previously explored in the literature, using a recent multi-satellite rainfall data product as a baseline. This is intended not only as a contribution to the community assessment of the MMF technology's potential for reducing cloud-related uncertainties for the problem of future climate projection, but also to identify regions where the technique may already offer new opportunities for understanding unresolved aspects of the observed diurnal rainfall cycle.

The results affirm a previous finding that in its typical configuration¹ simulated peak rainfall timing over most continents is favorably shifted from noon to late afternoon as a result of superparameterization. Several previously unappreciated improvements of diurnal rainfall due to super-parameterization are discovered: It becomes less well fit by a simple 24-hour sinusoid over the most energetic diurnal rainfall regimes, more horizontally inhomogeneous within continents and oceans, and more faithful to observed structural transitions across coastlines than the conventional climate model. A multi-model intercomparison of several recent SP-CAM variants suggests that while improved diurnal timing over land is not a robust effect of superparameterization, the other main improvements outlined above are. Regional deficiencies of overly vigorous diurnal rainfall are found in the superparameterized model associated with the Andean topography, and mean state rainfall biases during boreal summer in the Western Pacific. The space-time variability of the diurnal rainfall over the Gulf Stream look particularly realistic. Empirical orthogonal function decomposition of the diurnal composite is found to be a particularly compact diagnostic technique for summarizing many of the above

¹In other words, at a coarse exterior (interior) horizontal resolution of 400 km (4 km).

effects.

A second objective of this dissertation is to seek insight from superparameterized simulations towards understanding unresolved diurnal rainfall mechanisms in nature, in two regimes where the approach can offer new insight. The first is over the ocean, where remote control by circulations set up over land are thought to play a role in the observed oceanic diurnal rainfall pattern, which is not completely understood. The unique ability of superparameterized simulations to handle convection explicitly while still treating global scales provides a useful perspective. The second is over the Central US, where trade-offs in the superparameterization approach situate it conveniently in the midst of a debate about the role of small-scale vs. large-scale dynamics in underpinning a regional nocturnal rainfall maximum.

Chapter 5 focuses on the diurnal rainfall cycle over oceanic regimes where gauge data are sparse, and trustworthy satellite constraints on the space-time structure of rainfall have only recently provided adequate sampling. In the subtropics and tropics, several aspects of diurnal remote control by land are poorly simulated in an ensemble of conventional and superparameterized climate projection models. For the worst performing conventional climate projection model, superparameterization appears to offer some benefits by removing an unrealistic deep barotropic gravity wave emanating from land. The source of this wave is shown to be unrealistically extreme diurnal latent heating over tropical landmasses, a consequence of using an undilute CAPE closure in implementing the Arakawa-Schubert cumulus parameterization.

In the extratropics, model analysis over the boreal summer Gulf Stream diurnal rainfall regime suggests that diurnal moisture convergence associated with an especially large scale sea breeze circulation provides a key budgetary balance to the observed rainfall pattern. The observed pattern is well simulated by all but one model, for which it is argued that under-sensitivity of the cumulus parameter-

ization to free tropospheric humidity, and distortions in the vertical structure of convective heating over coastal land, play joint roles in suppressing Gulf Stream diurnal rainfall. Column energetics indicate a strong convective amplification of the land-sea radiative contrast that drives the sea breeze circulation in the simulations. This dynamical coupling to deep convection may help explain the fact that the Gulf Stream regime is a regionally anomalous feature of the boreal summer climatological diurnal rainfall composite.

Finally, Chapter 6 addresses the issue of the Central US warm season nocturnal rainfall maximum, itself a symptom of long range propagating organized convection traveling eastward from the Rockies. The rate of eastward travel, which situates the rainfall maximum where it exists in nature, is in debate in that it can arguably be controlled either by fast manifold processes (density currents, gust fronts) or slow manifold processes (regional semi-geostrophic circulations, potential vorticity advection, large scale gravity wave dynamics) or some combination thereof. Chapter 6 presents new evidence supporting the slow-manifold view, in that a superparameterized simulation – which artificially restricts the spatial scale of fast manifold processes – is shown to capture the essence of the observed signal. This result is surprising in that it has been previously argued that the assumption of periodic boundary conditions in the embedded cloud model should prohibit propagating nocturnal Central US convective systems in superparameterized simulations (Ovtchinnikov et al., 2006). A conceptual model is thus developed describing how new pathways are available in the re-engineered subgrid interface of MMFs to mediate such diurnal propagation that are not available in conventionally parameterized climate models. An argument is proposed, drawing on ideas from the literature, suggesting that the propagating convection signal in superparameterized simulations may be mediated by large-scale first-baroclinic gravity wave interactions with a prognostic organization lifecycle, emphasizing the physical importance of preserving convective “memory” at the inner resolved scale.

Appendix A

Model nomenclature

These are the conventionally parameterized and superparameterized (SP) versions of the Community Atmosphere Model (CAM) and Community Climate System Model (CCSM)¹ that are analyzed in this dissertation:

¹CCSM means CAM coupled to an interactive ocean model.

Acronym	Horizontal resolution	Dynamical core	Convection scheme
CAM3.0	T42 ($\sim 300\text{-}700$ km)	Spectral; semi-Lagrangian	Conventional parameterization; Zhang-McFarlane closed on <i>undilute</i> CAPE.
SPCAM3.0	T42 ($\sim 300\text{-}700$ km)	Spectral; semi-Lagrangian	Super-parameterization; 32 CRM columns 4 km apart, arranged east-west.
SPCCSM3.0	T42 ($\sim 300\text{-}700$ km)	Spectral; semi-Lagrangian	Super-parameterization; 32 CRM columns 4 km apart, arranged east-west.
CAM3.5	$1.9^\circ \times 2.5^\circ$ (~ 250 km)	Finite-volume	Conventional parameterization; Zhang-McFarlane closed on <i>dilute</i> CAPE.
SPCAM3.5	$1.9^\circ \times 2.5^\circ$ (~ 250 km)	Finite-volume	Super-parameterization; 64 CRM columns 1 km apart, arranged either east-west (xz) or north-south (yz).

Bibliography

- Albright, M. D., E. E. Recker, and R. J. Reed, 1985: The diurnal variation of deep convection and inferred precipitation in the central tropical Pacific during January–February 1979. *Monthly Weather Review*, **113**, 1663–1680.
- Alliss, J. R. and S. Raman, 1995a: Diurnal variations in cloud frequency over the Gulf Stream locale. *Journal of Applied Meteorology*, **34**, 1578–1594.
- Alliss, R. and S. Raman, 1995b: Diurnal variations in cloud frequency over the gulf stream locale. *Journal of Applied Meteorology*, **34** (7), 1578–1594.
- Arakawa, A., 2004: The cumulus parameterization problem: Past, present, and future. *Journal of Climate*, **17** (13), 2493–2525.
- Arakawa, A. and W. Schubert, 1974: Interaction of a cumulus cloud ensemble with large-scale environment. *Journal of the Atmospheric Sciences*, **31** (3), 674–701.
- Arkin, P. A. and B. N. Meisner, 1987: The relationship between large-scale convective rainfall and cold cloud over the western hemisphere during 1982–1984. *Monthly Weather Review*, **115**, 51–74.
- Ashley, W., T. Mote, and M. Bentley, 2007: The extensive episode of derecho-producing convective systems in the United States during May and June 1998: A multi-scale analysis and review. *Meteorological Applications*, **14** (3), 227–244.
- Bergman, J. and M. Salby, 1996: Diurnal variations of cloud cover and their relationship to climatological conditions. *Journal of climate*, **9** (11), 2802–2820.
- Bergman, J. W. and M. L. Salby, 1997: The role of cloud diurnal variations in the time-mean energy budget. *Journal of Climate*, **10** (5), 1114–1124.
- Bernardet, L. R. and W. R. Cotton, 1998: Multi-scale evolution of a derecho-producing MCS. *Monthly Weather Review*, **126**, 2991–3015.

- Betts, A. K. and C. Jakob, 2002: Evaluation of the diurnal cycle of precipitation, surface thermodynamics and surface fluxes in the ECMWF model using LBA data. *Journal of Geophysical Research*, **107 (D20)**, 8045.
- Blackadar, A., 1957: Boundary layer wind maxima and their significance for the growth of nocturnal inversions. *Bulletin of the American Meteorological Society*, **38 (5)**, 283–290.
- Bony, S. and J. Dufresne, 2005: Marine boundary layer clouds at the heart of tropical cloud feedback uncertainties in climate models. *Geophysical Research Letters*, **32 (20)**.
- Bretherton, C. S., 2007: Challenges in numerical modeling of tropical circulations. *The global circulation of the atmosphere*, T. Schneider and A. Sobel, Eds., Princeton University Press, 302–330.
- Bretherton, C. S. and P. K. Smolarkiewicz, 1989: Gravity waves, compensating subsidence and detrainment around cumulus clouds. *Journal of the Atmospheric Sciences*, **46 (6)**, 740–759.
- Brier, G. W. and J. Simpson, 1969: Tropical cloudiness and rainfall related to pressure and tidal variations. *Quarterly Journal of the Royal Meteorological Society*, **95**, 120–147.
- Buajatti, K. and A. K. Blackadar, 1957: Theoretical studies of diurnal wind-structure variations in the planetary boundary layer. *Quarterly Journal of the Royal Meteorological Society*, **83 (358)**, 486–500.
- Byers, H. R. and L. J. Battan, 1949: Some effects of vertical shear on thunderstorm structure. *Bulletin of the American Meteorological Society*, **30**, 168–175.
- Carbone, R. E. and J. D. Tuttle, 2008: Rainfall occurrence in the United States warm season: The diurnal cycle. *Journal of Climate*, **21 (16)**, 4132–4146.
- Carbone, R. E., J. D. Tuttle, D. Ahijevych, and S. B. Trier, 2002: Inferences of predictability associated with warm season precipitation episodes. *Journal of the Atmospheric Sciences*, **59 (2033–2056)**.
- Chang, A., L. Chiu, and G. Yang, 1995: Diurnal cycle of oceanic precipitation from SS/MI data. *Monthly Weather Review*, **123 (11)**, 3371–3380.

- Cole, J. N. S., H. W. Barker, W. O'Hirok, E. E. Clothiaux, M. F. Khairoutdinov, and D. A. Randall, 2005a: Atmospheric radiative transfer through global arrays of 2D clouds. *Geophysical Research Letters*, **32** (L19817).
- Cole, J. N. S., H. W. Barker, D. A. Randall, M. F. Khairoutdinov, and E. E. Clothiaux, 2005b: Global consequences of interactions between clouds and radiation at scales unresolved by global climate models. *Geophysical Research Letters*, **32** (L06703).
- Collier, J. C. and K. P. Bowman, 2004: Diurnal cycle of tropical precipitation in a general circulation model. *Journal of Geophysical Research - Atmospheres*, **109** (D17).
- Collins, W., et al., 2004: Description of the NCAR community atmosphere model (CAM 3.0). *NCAR Tech. Note NCAR/TN-464+ STR*.
- Collins, W., et al., 2006: The formulation and atmospheric simulation of the Community Atmosphere Model version 3 (CAM3). *Journal of Climate*, **19** (11), 2144–2161.
- Correia, J., R. W. Arritt, and C. J. Anderson, 2008: Idealized mesoscale convective system structure and propagation using convective parameterization. *Monthly Weather Review*, **136**, 2422–2442.
- Cotton, W. R. and R. A. Anthes, 1989: *Storm and Cloud Dynamics*. Academic Press.
- Dai, A. and C. Deser, 1999: Diurnal and semidiurnal variations in global surface wind and divergence fields. *Journal of Geophysical Research*, **104** (31), 109–131.
- Dai, A., J. Wang, R. Ware, and T. Van Hove, 2002: Diurnal variation in water vapor over North America and its implications for sampling errors in radiosonde humidity. *Journal of Geophysical Research - Atmospheres*, **107** (D10).
- Dai, A. G., 2001: Global precipitation and thunderstorm frequencies. Part II: Diurnal variations. *Journal of Climate*, **14**, 1112–1128.
- Dai, A. G., F. Giorgi, and K. E. Trenberth, 1999: Observed and model-simulated diurnal cycles of precipitation over the contiguous United States. *Journal of Geophysical Research - Atmospheres*, **104** (D6), 6377–6402.

- Dai, A. G., X. Lin, and K. L. Hsu, 2007: The frequency, intensity, and diurnal cycle of precipitation in surface and satellite observations over low- and mid-latitudes. *Climate Dynamics*, **29** (7–8), 727–744.
- Dai, A. G. and K. E. Trenberth, 2004: The diurnal cycle and its depiction in the Community Climate System Model. *Journal of Climate*, **17** (5), 930–951.
- DeMott, C. A., D. A. Randall, and M. Khairoutdinov, 2007: Convective precipitation variability as a tool for general circulation model analysis. *Journal of Climate*, **20** (1), 91–112.
- Dirks, R. A., 1969: A theoretical investigation of convective patterns in the lee of the Rockies. Ph.D. thesis, Colorado State University.
- Fingerhut, W. A., 1978: A numerical model of a diurnally varying tropical cloud cluster disturbance. *Monthly Weather Review*, **106**, 255–264.
- Fritsch, J., R. Kane, and C. Chelius, 1986: The contribution of mesoscale convective weather systems to the warm-season precipitation in the United States. *Journal of Applied Meteorology*, **25**, 1333–1345.
- Fu, R., A. D. Genio, and W. B. Rossow, 1990: Behavior of deep convective clouds in the tropical Pacific deduced from ISCCP radiance. *Journal of Climate*, **3** (1129–1152).
- Ghan, S., X. Bian, and L. Corsetti, 1996: Simulation of the great plains low-level jet and associated clouds by general circulation models. *Monthly Weather Review*, **124** (7), 1388–1408.
- Gille, S., S. Smith, and S. Lee, 2003: Measuring the sea breeze from QuikSCAT scatterometry. *Geophys. Res. Lett.*, **30** (3), 1114.
- Gille, S., S. Smith, and N. Statom, 2005: Global observations of the land breeze. *Geophys. Res. Lett.*, **32** (5).
- Grabowski, W., et al., 2006: Daytime convective development over land: A model intercomparison based on LBA observations. *Quarterly Journal of the Royal Meteorological Society*, **132** (615), 317–344.
- Grabowski, W. W., 2001: Coupling cloud processes with the large-scale dynamics using the cloud-resolving convection parameterization (CRCP). *Journal of the Atmospheric Sciences*, **58** (9), 978–997.

- Grabowski, W. W. and M. W. Moncrieff, 2001: Large-scale organization of tropical convection in two-dimensional explicit numerical simulations. *Quarterly Journal of the Royal Meteorological Society*, **127** (572), 445–468.
- Grabowski, W. W. and P. K. Smolarkiewicz, 1999: A cloud resolving convective parameterization for modeling the tropical convective atmosphere. *Physica D*, **133**, 171–178.
- Gray, W. and R. Jacobson, 1977: Diurnal variation of deep cumulus convection. *Monthly Weather Review*, **105** (9), 1171–1188.
- Guichard, F., et al., 2004: Modelling the diurnal cycle of deep precipitating convection over land with cloud-resolving models and single-column models. *Quarterly Journal of the Royal Meteorological Society*, **130** (604), 3139–3172.
- Hann, J., 1901: *Lehrbuch der Meteorologie, 1st ed.*, 338–346. Leipzig, Chr. Herm. Tauchnitz.
- Hendon, H. H. and K. Woodberry, 1993: The diurnal cycle of tropical convection. *Journal of Geophysical Research*, **98** (16), 16 623–16 637.
- Higgins, R. W., J. E. Janowiak, and Y.-P. Yao, 1996: A gridded hourly precipitation database for the United States (1963-1993). *NCEP/Climate Prediction Center ATLAS No. 1*, U. S. Department of Commerce, Washington, D. C.
- Hirose, M. and K. Nakamura, 2005: Spatial and diurnal variation of precipitation systems over Asia observed by the TRMM precipitation radar. *Journal of Geophysical Research*, **110**.
- Hirose, M., R. Oki, S. Shimizu, M. Kachi, and T. Higashiuwatoko, 2008: Finescale diurnal rainfall statistics refined from eight years of TRMM PR data. *Journal of Applied Meteorology and Climatology*, **47** (2), 544–561.
- Holton, J., 1967: The diurnal boundary layer wind oscillation above sloping terrain. *Tellus*, **19** (2), 199–205.
- Houze, R., 2004: Mesoscale convective systems. *Reviews of Geophysics*, **42** (4).
- Huffman, G., et al., 2007: The TRMM multisatellite precipitation analysis (TMPA): Quasi-global, multiyear, combined-sensor precipitation estimates at fine scales. *Journal of Hydrometeorology*, **8** (1), 38–55.

- Huffman, G. J., R. F. Adler, B. Rudolf, U. Schneider, and P. R. Keehn, 1995: Global precipitation estimates based on a technique for combining satellite-based estimates, rain gauge analysis, and NWP model precipitation information. *Journal of Climate*, **8** (78), 1284–1295.
- IPCC, 2007: *Climate Change 2007 - The Physical Science Basis: Working Group I Contribution to the Fourth Assessment Report of the IPCC (Climate Change 2007)*. Cambridge University Press.
- Janowiak, J., V. Dagostaro, V. Kousky, and R. Joyce, 2007: An examination of precipitation in observations and model forecasts during name with emphasis on the diurnal cycle. *Journal of climate*, **20** (9), 1680–1692.
- Janowiak, J. E., P. A. Arkin, and M. Morrissey, 1994: An examination of the diurnal cycle in oceanic tropical rainfall using satellite and in situ data. *Monthly Weather Review*, **122**, 2296–2311.
- Jiang, X., N.-C. Lau, and S. A. Klein, 2006: Role of eastward propagating convection systems in the diurnal cycle and seasonal mean of summertime rainfall over the U.S. Great Plains. *Geophysical Research Letters*, **33** (19).
- Jirak, I. L. and W. R. Cotton, 2007: Observational analysis of the predictability of mesoscale convective systems. *Weather Forecasting*, **22**, 813–838.
- Jones, T. R. and D. A. Randall, 2011: Quantifying the limits of convective parameterizations. *Journal of Geophysical Research - Atmospheres*, **116**, D08 210.
- Joyce, R. and P. A. Arkin, 1997: Improved estimates of tropical and subtropical precipitation using the GOES precipitation index. *Journal of Atmospheric and Oceanic Technology*, **14**, 997–1011.
- Khairoutdinov, M., C. DeMott, and D. Randall, 2008: Evaluation of the simulated interannual and subseasonal variability in an AMIP-style simulation using the CSU multi-scale modeling framework. *Journal of Climate*, **21** (3), 413–431.
- Khairoutdinov, M. and D. Randall, 2006: High-resolution simulation of shallow-to-deep convection transition over land. *Journal of the Atmospheric Sciences*, **63** (12), 3421–3436.
- Khairoutdinov, M., D. Randall, and C. DeMott, 2005: Simulations of the atmospheric general circulation using a cloud-resolving model as a superparameterization of physical processes. *Journal of the Atmospheric Sciences*, **62** (7), 2136–2154.

- Khairoutdinov, M. F. and D. A. Randall, 2001: A cloud resolving model as a cloud parameterization in the NCAR Community Climate System Model. *Geophysical Research Letters*, **28** (3617–3620).
- Khairoutdinov, M. F. and D. A. Randall, 2003: Cloud resolving modeling of the ARM summer 1997 IOP: Model formulation, results, uncertainties, and sensitivities. *Journal of the Atmospheric Sciences*, **60** (4), 607–625.
- Kidd, C., 2001: Satellite rainfall climatology: A review. *International Journal of Climatology*, **21** (9), 1041–1066.
- Kidd, C. and E. C. Barrett, 1990: The use of passive microwave imagery in rainfall monitoring. *Remote Sensing Reviews*, **4**, 415–450.
- Kikuchi, K. and B. Wang, 2008: Diurnal precipitation regimes in the global tropics. *Journal of Climate*, **21** (11), 2680–2696.
- Kincer, J. B., 1916: Daytime and nighttime precipitation and their economic significance. *Monthly Weather Review*, **44**, 628–633.
- Kingsmill, D. E. and R. A. Houze, 1999: Kinematic characteristics of air flowing into and out of precipitating convection over the west Pacific warm pool: An airborne Doppler radar survey. *Quarterly Journal of the Royal Meteorological Society*, **125**, 1165–1207.
- Knierel, J., D. Ahijevych, and K. Manning, 2004: Using temporal modes of rainfall to evaluate the performance of a numerical weather prediction model. *Monthly weather review*, **132** (12), 2995–3009.
- Kondragunta, C. and A. Gruber, 1996: Seasonal and annual variability of the diurnal cycle of clouds. *Journal of geophysical research*, **101** (D16), 21 377–21.
- Kraus, E. B., 1963: The diurnal precipitation change over the sea. *Journal of the Atmospheric Sciences*, **20**, 551–556.
- Kuang, Z. and C. S. Bretherton, 2006: A mass-flux scheme view of a high-resolution simulation of a transition from shallow to deep cumulus convection. *Journal of the Atmospheric Sciences*, **63** (7), 1895–1909.
- Kummerow, C., W. Barnes, T. Kozu, J. Shiue, and J. Simpson, 1998: The Tropical Rainfall Measuring Mission (TRMM) sensor package. *Journal of Atmospheric and Oceanic Technology*, **15**, 908–817.

- Lafore, J. and M. Moncrieff, 1989: A numerical investigation of the organization and interaction of the convective and stratiform regions of tropical squall lines. *Journal of the Atmospheric Sciences*, **46** (4), 521–544.
- Laing, A. G. and J. M. Fritsch, 1997: The global population of mesoscale convective complexes. *Quarterly Journal of the Royal Meteorological Society*, **123** (538), 389–405.
- Laing, A. G. and J. M. Fritsch, 2000: The large-scale environments of the global populations of mesoscale convective complexes. *Monthly Weather Review*, **128**, 2756–2776.
- Lang, T., D. Ahijevych, S. Nesbitt, R. Carbone, S. Rutledge, and R. Cifelli, 2007: Radar-observed characteristics of precipitating systems during NAME 2004. *Journal of climate*, **20** (9), 1713–1733.
- Lee, M.-I., S. D. Schubert, M. J. Suarez, J.-K. E. Schemm, H.-L. Pan, J. Han, and S.-Y. Yoo, 2008: Role of convection triggers in the simulation of the diurnal cycle of precipitation over the United States Great Plains in a general circulation model. *Journal of Geophysical Research - Atmospheres*, **113** (D2), D02111.
- Li, G., F. Kimura, T. Sato, and D. Huang, 2008: A composite analysis of diurnal cycle of GPS precipitable water vapor in central Japan during Calm Summer Days. *Theoretical and applied climatology*, **92** (1-2), 15–29.
- Li, X., 2004: Cloud modeling in the tropical deep convective regime. *Observation, theory, and modeling of atmospheric variability*, World Scientific Publishing Co. Pte. Ltd.
- Li, Y. and R. B. Smith, 2010: The detection and significance of diurnal pressure and potential vorticity anomalies east of the rockies. *Journal of the Atmospheric Sciences*, **67** (9), 2734–2751.
- Liebmann, B. and C. A. Smith, 1996: Description of a complete (interpolated) outgoing longwave radiation dataset. *Bulletin of the American Meteorological Society*, **77**, 1275–1277.
- Lin, M., 1986: The evolution and structure of composite meso- α -scale convective complexes. Ph.D. thesis, Colorado State University.

- Lin, X., D. A. Randall, and L. D. Fowler, 2000: Diurnal variability of the hydrologic cycle and radiative fluxes: Comparisons between observations and a GCM. *Journal of Climate*, **13**, 4159–4179.
- Lindzen, R. S., 1978: Effect of daily variations of cumulonimbus activity on the atmospheric semidiurnal tide. *Monthly Weather Review*, **106**, 526–533.
- Liu, C. and M. W. Moncrieff, 1998: A numerical study of the diurnal cycle of tropical oceanic convection. *Journal of the Atmospheric Sciences*, **55** (13), 2329–2344.
- Luo, Z. Z. and G. L. Stephens, 2006: An enhanced convection-wind-evaporation feedback in a superparameterization GCM (SP-GCM) depiction of the Asian summer monsoon. *Geophysical Research Letters*, **33** (6), Art. No. L06 707.
- Maddox, R. A., 1980: Mesoscale convective complexes. *Bulletin of the American Meteorological Society*, **61**, 1374–1387.
- Maddox, R. A., 1981: The structure and life-cycle of midlatitude mesoscale convective complexes. Tech. Rep. Atmospheric Science Paper No. 336, Dept. of Atmos. Sci., Colorado State University.
- Maddox, R. A., 1983: Large scale meteorological conditions associated with midlatitude, mesoscale convective complexes. *Monthly Weather Review*, **111**, 126–140.
- Malkus, J. S., 1964: Convective processes in the tropics. *Proceedings of the Symposium of Tropical Meteorology*, Rotorua, New Zealand, 247–277.
- Mapes, B., 1993: Gregarious tropical convection. *Journal of the atmospheric sciences*, **50** (13), 2026–2037.
- Mapes, B., T. Warner, M. Xu, and A. Negri, 2003: Diurnal patterns of rainfall in northwestern South America. Part I: Observations and context. *Monthly Weather Review*, **131** (5), 799–812.
- Mapes, B. E. and R. B. Neale, 2011: Parameterizing convective organization. *Submitted to Journal of Advances in Modeling Earth Systems*, **3**, M06 004.
- Mapes, B. E., T. T. Warner, and M. Xu, 2003: Diurnal patterns of rainfall in northwestern South America. Part III: Diurnal gravity waves and nocturnal convection offshore. *Monthly Weather Review*, **131** (5), 830–844.

- Marchand, R. and T. Ackerman, 2010: An analysis of cloud cover in multiscale modeling framework global climate model simulations using 4 and 1 km horizontal grids. *Journal of Geophysical Research - Atmospheres*, **115**.
- Marchand, R., N. Beagley, and T. P. Ackerman, 2009a: Evaluation of hydrometeor occurrence profiles in the multiscale modeling framework climate model using atmospheric classification. *Journal of Climate*, **22**, 4557–4573.
- Marchand, R., J. Haynes, G. Mace, T. Ackerman, and G. Stephens, 2009b: A comparison of simulated cloud radar output from the multiscale modeling framework global climate model with CloudSat cloud radar observations. *Journal of Geophysical Research*, **114** (8).
- Matsui, T., D. Mocko, M.-I. Lee, W.-K. Tao, M. J. Suarez, and R. A. P. Sr., 2010: Ten-year climatology of summertime diurnal rainfall rate over the conterminous u.s. *Geophysical Research Letters*, **37** (L13807).
- McBride, J. L. and W. M. Gray, 1980: Mass divergence in tropical weather systems. Paper I: Diurnal variation. *Quarterly Journal of the Royal Meteorological Society*, **106**, 501–506.
- McFarlane, S., J. Mather, and T. Ackerman, 2007: Analysis of tropical radiative heating profiles: A comparison of models and observations. *J. Geophys. Res.*, **112**, D14218.
- Meisner, B. and P. Arkin, 1987: Spatial and annual variations in the diurnal cycle of large-scale tropical convective cloudiness and precipitation. *Monthly weather review*, **115** (9), 2009–2032.
- Moncrieff, M. W., 1981: A theory of organized steady convection and its transport-properties. *Quarterly Journal of the Royal Meteorological Society*, **107** (451), 29–50.
- Moncrieff, M. W., 1992: Organized convective systems: Archetypal dynamical models, mass and momentum flux theory, and parametrization. *Quarterly Journal of the Royal Meteorological Society*, **118** (507), 819–850.
- Moncrieff, M. W., 2010, in press: The multiscale organization of moist convection and the intersection of weather and climate. Chapter 1: Why does climate vary? *American Geophysical Union Publication Series*, D. Sun, Ed., American Geophysical Union.

- Moncrieff, M. W. and C. H. Liu, 2006: Representing convective organization in prediction models by a hybrid strategy. *Journal of the Atmospheric Sciences*, **63** (12), 3404–3420.
- Munoz, R., 2008: Diurnal cycle of surface winds over the subtropical southeast pacific. *J. Geophys. Res*, **113**, D13 107.
- Neale, R., 2007: CAM3.5 model changes. *Proceedings of the 12th annual Community Climate System Model Annual Workshop*.
- Newton, C. W., 1950: Structure and mechanism of the prefrontal squall line. *Journal of meteorology*, **7**, 210–222.
- North, G. R., T. L. Bell, R. F. Cahalan, and F. J. Moeng, 1982: Sampling errors in the estimation of empirical orthogonal functions. *Monthly Weather Review*, **110** (7), 699–7606.
- Ovtchinnikov, M., T. Ackerman, R. Marchand, and M. Khairoutdinov, 2006: Evaluation of the multiscale modeling framework using data from the atmospheric radiation measurement program. *Journal of Climate*, **19** (9), 1716–1729.
- Pandya, R. E. and D. R. Durran, 1996: The influence of convectively generated thermal forcing on the mesoscale circulation around squall lines. *Journal of the Atmospheric Sciences*, **53** (20), 2924–2951.
- Petch, J. C., P. N. Blossey, and C. S. Bretherton, 2008: Differences in the lower troposphere in two- and three-dimensional cloud-resolving model simulations of deep convection. *Quarterly Journal of the Royal Meteorological Society*, **134** (636, Part A), 1941–1946.
- Petty, G. W., 1995: The status of satellite-based rainfall estimation over land. *Remote Sensing of the Environment*, **51**, 125–137.
- Pielke, R., 2002: *Mesoscale meteorological modeling*. International geophysics series, Academic Press.
- Pritchard, M. S., M. W. Moncrieff, and R. C. J. Somerville, 2011: Orographic propagating precipitation systems over the us in a global climate model with embedded explicit convection. *Journal of the Atmospheric Sciences*, **68**, 1821–1840.
- Pritchard, M. S. and R. C. J. Somerville, 2009a: Assessing the diurnal cycle of precipitation in a multi-scale climate model. *Journal of Advances in Modeling Earth Systems*, **1**, Art. No. 16.

- Pritchard, M. S. and R. C. J. Somerville, 2009b: Empirical orthogonal function analysis of the diurnal cycle of precipitation in a multi-scale climate model. *Geophysical Research Letters*, **35** (5), L05 812.
- Randall, Ding, and Pan, 1997: *The Arakawa-Schubert parameterization*, chap. 11, 281–296. Kluwer Academic Publishers.
- Randall, D., M. Khairoutdinov, A. Arakawa, and W. Grabowski, 2003: Breaking the cloud parameterization deadlock. *Bulletin of the American Meteorological Society*, **84** (11), 1547–1562.
- Randall, D. A., Harshvardhan, and D. A. Dazlich, 1991: Diurnal variability of the hydrologic-cycle in a general-circulation model. *Journal of the Atmospheric Sciences*, **48** (1), 40–62.
- Raymond, D. and A. Blyth, 1992: Extension of the stochastic mixing model to cumulonimbus clouds. *Journal of the Atmospheric Sciences*, **49** (21).
- Raymond, D. and H. Jiang, 1990: A theory for long-lived mesoscale convective systems. *Journal of the Atmospheric Sciences*, **47** (24), 3067–3077.
- Rotunno, R., 1983: On the linear theory of the land and sea breeze. *Journal of the Atmospheric Sciences*, **40** (8), 1999–2009.
- Rotunno, R., J. Klemp, and M. Weisman, 1988a: A theory for strong, long-lived squall lines. *Journal of the Atmospheric Sciences*, **45** (3), 463–485.
- Rotunno, R., J. B. Klemp, and M. L. Weisman, 1988b: A theory for long-lived squall lines. *Journal of the Atmospheric Sciences*, **45** (3), 463–485.
- Ruane, A. C., 2010: NARR’s Atmospheric Water Cycle Components. Part II: Summertime Mean and Diurnal Interactions. *Journal of Hydrometeorology*, **11** (6), 1220–1233.
- Schmetz, J. and Q. Liu, 1988: Outgoing longwave radiation and its diurnal variation at regional scales derived from meteosat. *Journal of Geophysical Research*, **93** (D9), 11 192–11.
- Schumacher, C., R. Houze Jr, and I. Kraucunas, 2004: The tropical dynamical response to latent heating estimates derived from the TRMM precipitation radar. *Journal of the Atmospheric Sciences*, **61** (12), 1341–1358.

- Schumacher, R. and R. Johnson, 2005: Organization and environmental properties of extreme-rain-producing mesoscale convective systems. *Monthly weather review*, **133** (4), 961–976.
- Simpson, J. E., D. A. Mansfield, and J. R. Milford, 1977: Inland penetration of sea-breeze fronts. *Quarterly Journal of the Royal Meteorological Society*, **103** (435), 47–76.
- Sobel, A. H., J. Nilsson, and L. M. Polvani, 2001: The weak temperature gradient approximation and balanced tropical moisture waves. *Journal of the Atmospheric Sciences*, **58**, 3650–3665.
- Soden, B. J., 2000: The diurnal cycle of convection, clouds, and water vapor in the tropical upper troposphere. *Geophysical Research Letters*, **27** (15), 2173–2176.
- Soden, B. J. and F. P. Bretherton, 1993: Upper tropospheric relative humidity from the GOES 6.7 μm channel: Method and climatology for July 1987. *Journal of Geophysical Research*, **98** (16), 16 669–16 688.
- Stan, C., M. Khairoutdinov, C. A. DeMott, V. Krishnamurthy, D. M. Straus, D. A. Randall, J. L. Kinter, and J. Shukla, 2010: An ocean-atmosphere climate simulation with an embedded cloud resolving model. *Geophysical Research Letters*, **37**, L01 702.
- Stensrud, D. J., 1996: Importance of low-level jets to climate: A review. *Journal of Climate*, **9** (8), 1698–1711.
- Stephens, G. L., et al., 2002: The Cloudsat mission and the A-Train – A new dimension of space-based observations of clouds and precipitation. *Bulletin of the American Meteorological Society*, **83** (12), 1771–1790.
- Sui, C.-H., K.-M. Lau, Y. N. Takayabu, and D. A. Short, 1997: Diurnal variations in tropical oceanic cumulus convection during toga coare. *Journal of the Atmospheric Sciences*, **54** (5), 639–655.
- Sui, C.-H., X. Li, and K.-M. Lau, 1998: Radiative-convective processes in simulated diurnal variations of tropical oceanic convection. *Journal of the Atmospheric Sciences*, **55**, 2345–2357.
- Sun, Y., S. Solomon, A. Dai, and R. Portmann, 2006: How often does it rain? *Journal of climate*, **19** (6), 916–934.

- Tao, W. and M. Moncrieff, 2009: Multiscale cloud system modeling. *Reviews of Geophysics*, **47** (4).
- Tao, W. K., J. Lang, C.-H. Simpson, B. S. Ferrier, and M.-D. Chou, 1996: Mechanisms of cloud-radiation interaction in the tropics and midlatitude. *Journal of the Atmospheric Sciences*, **53**, 2624–2651.
- Tao, W.-K., et al., 2009: A multiscale modeling system - developments, applications, and critical issues. *Bulletin of the American Meteorological Society*, **90** (4), 515+.
- Thorpe, A., M. Miller, and M. Moncrieff, 1980: Dynamical models of two-dimensional downdraughts. *Quarterly Journal of the Royal Meteorological Society*, **106** (449), 463–484.
- Tian, B., I. Held, N. Lau, and B. Soden, 2005: Diurnal cycle of summertime deep convection over North America: A satellite perspective. *J. Geophys. Res.*, **110**, D10 108.
- Tian, B., B. J. Soden, and X. Wu, 2004: Diurnal cycle of convection, clouds, and water vapor in the tropical upper troposphere: Satellites versus a general circulation model. *Journal of Geophysical Research*, **109** (D10101).
- Trenberth, K., A. Dai, R. Rasmussen, and D. Parsons, 2003: The changing character of precipitation. *Bulletin of the American Meteorological Society*, **84** (9), 1205–1217.
- Trier, S. B., C. A. Davis, and D. A. Ahijevych, 2010: Environmental controls on the simulated diurnal cycle of warm-season precipitation in the central united states. *Journal of the Atmospheric Sciences*, **67** (4), 1066–1090.
- Trier, S. B., C. A. Davis, D. A. Ahijevych, M. L. Weisman, and G. H. Bryan, 2006: Mechanisms supporting long-lived episodes of propagating nocturnal convection within a 7-day wrf model simulation. *Journal of the Atmospheric Sciences*, **63**, 2437–2461.
- Trier, S. B. and D. B. Parsons, 1993: Evolution of environmental conditions preceding the development of a nocturnal mesoscale convective complex. *Monthly Weather Review*, **121**, 1078–1098.

- Tripoli, G. J. and W. R. Cotton, 1989a: Numerical study of an observed orogenic mesoscale convective system. Part 1: Simulated genesis and comparison with observations. *Monthly Weather Review*, **117** (2), 273–304.
- Tripoli, G. J. and W. R. Cotton, 1989b: Numerical study of an observed orogenic mesoscale convective system. Part 2: Analysis of governing dynamics. *Monthly Weather Review*, **117** (2), 305–328.
- Tuttle, J. and R. Carbone, 2004: Coherent regeneration and the role of water vapor and shear in a long-lived convective episode. *Monthly weather review*, **132** (1), 192–208.
- Tuttle, J. D. and C. A. Davis, 2006: Corridors of warm season precipitation in the central United States. *Monthly Weather Review*, **134** (9), 2297–2317.
- UCAR, 2009: How models produce clouds and precipitation. The source of this material is the COMET[®] Website at {http://www.meted.ucar.edu/nwp/model_precipandclouds/} of the University Corporation for Atmospheric Research (UCAR), sponsored in part through cooperative agreement(s) with the National Oceanic and Atmospheric Administration (NOAA), U.S. Department of Commerce (DOC). [®] 1997–2011 University Corporation for Atmospheric Research. All Rights Reserved.
- Wakimoto, R. M. and N. T. Atkins, 1994: Observations of the sea-breeze front during CaPE. Part I: Single-doppler, satellite, and cloud photogrammetry analysis. *Monthly Weather Review*, **122**, 1092–1114.
- Wallace, J. M., 1975: Diurnal-variations in precipitation and thunderstorm frequency over conterminous United States. *Monthly Weather Review*, **103** (5), 406–419.
- Wallace, J. M., C. Smith, and C. S. Bretherton, 1992: Singular value decomposition of wintertime sea-surface temperature and 500-mb height anomalies. *Journal of Climate*, **5** (6), 561–576.
- Weckwerth, T. and D. Parsons, 2006: A review of convection initiation and motivation for IHOP 2002. *Monthly weather review*, **134** (1), 5–22.
- Wexler, H., 1961: A boundary layer interpretation of the low-level jet. *Tellus*, **13** (3), 368–378.

- Wilson, C. and J. Mitchell, 1986: Diurnal variation and cloud in a general circulation model. *Quarterly Journal of the Royal Meteorological Society*, **112** (472), 347–369.
- Wilson, J. and R. Roberts, 2006: Summary of convective storm initiation and evolution during IHOP: Observational and modeling perspective. *Monthly weather review*, **134** (1), 23–47.
- Wolyn, P. G. and T. B. McKee, 1994: The mountain-plains circulation east of a 2-km-high north-south barrier. *Monthly Weather Review*, **122** (7), 1490–1508.
- Wood, R., M. Köhler, R. Bennartz, and C. O’Dell, 2009: The diurnal cycle of surface divergence over the global oceans. *Quarterly Journal of the Royal Meteorological Society*, **135** (643), 1484–1493.
- Woodruff, S. D., S. J. Lubker, S. J. Worley, and J. D. Elms, 1993: Comprehensive ocean-atmosphere data set (COADS) release 1a: 1980-1992. *Earth System Monitoring*, **4**, 1–8.
- Wu, C., B. Stevens, and A. Arakawa, 2009: What controls the transition from shallow to deep convection? *Journal of the Atmospheric Sciences*, **66** (6), 1793–1806.
- Xie, P. and P. A. Arkin, 1995: An intercomparison of gauge observations and satellite estimates of monthly precipitation. *Journal of Applied meteorology*, **34**, 1143–60.
- Xie, P. and P. A. Arkin, 1997: Global Precipitation: A 17 year monthly analysis based on gauge observations, satellite estimates, and numerical model predictions. *Bulletin of the American Meteorological Society*.
- Yamamoto, M. K., F. A. Furuzawa, A. Higuchi, and K. Nakamura, 2008: Comparison of diurnal variations in precipitation systems observed by TRMM PR, TMI, and VIRS. *Journal of Climate*, **21**, 4011–4028.
- Yan, H. and R. Anthes, 1987: The effect of latitude on the sea breeze. *Monthly Weather Review*, **115** (5), 936–956.
- Yang, G. Y. and J. Slingo, 2001: The diurnal cycle in the Tropics. *Monthly Weather Review*, **129** (4), 784–801.

- Yang, S. and E. A. Smith, 2006: Mechanisms for diurnal variability of global tropical rainfall observed from TRMM. *Journal of Climate*, **19** (20), 5190–5226.
- Yang, S. and E. A. Smith, 2008: Convective-stratiform precipitation variability at seasonal scale from eight years of TRMM observations: Implications for multiple modes of diurnal variability. *Journal of Climate*, **21** (16), 4087–4114.
- Zhang, G. J., 2002: Convective quasi-equilibrium in midlatitude continental environment and its effect on convective parameterization. *Journal of Geophysical Research - Atmospheres*, **108** (D19), 4592.
- Zhang, G. J. and N. A. McFarlane, 1995: Sensitivity of climate simulations to the parameterization of cumulus convection in the Canadian Climate Centre general circulation model. *Atmosphere-Ocean*, **33**, 407–446.
- Zhang, Y. and S. A. Klein, 2010: Mechanisms Affecting the Transition from Shallow to Deep Convection over Land: Inferences from Observations of the Diurnal Cycle Collected at the ARM Southern Great Plains Site. *Journal of the Atmospheric Sciences*, **67** (9), 2943–2959.
- Zhang, Y., S. A. Klein, J. Boyle, and G. G. Mace, 2010: Evaluation of tropical cloud and precipitation statistics of Community Atmosphere Model version 3 using CloudSat and CALIPSO data. *Journal of Geophysical Research*, **115** (D12205).
- Zhang, Y., et al., 2008: On the diurnal cycle of deep convection, high-level cloud, upper troposphere water vapor in the Multiscale Modeling Framework. *Journal of Geophysical Research - Atmospheres*, **113** (D16), D16 105.